SOME STUDIES ON NANO-PARTICLES DOPED ALTERNATIVE FUELS IN UNMODIFIED CI ENGINE

A thesis submitted to the Delhi Technological University, Delhi in fulfillment of the requirements for the award of the degree of

DOCTOR OF PHILOSOPHY

in

Mechanical Engineering

by

MUKUL TOMAR
(2K17/PhD/ME/02)

Under the supervision of

Dr. NAVEEN KUMAR
(Professor)

Mechanical Engineering Department
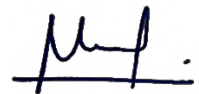## Delhi Technological University
Shahbad Daulatpur Bawana Road
Delhi – 110042, INDIA
June 2021

DECLARATION

I hereby declare that the thesis entitled "**SOME STUDIES ON NANO-PARTICLES DOPED ALTERNATIVE FUELS IN UNMODIFIED CI ENGINE**" is an original work carried out by me under the supervision of Dr. Naveen Kumar, Professor, Mechanical Engineering Department, Delhi Technological University, Delhi. This thesis has been prepared in conformity with the rules and regulations of the Delhi Technological University, Delhi. The research work reported, and results presented in the thesis have not been submitted either in part or full to any other university or institute for the award of any other degree or diploma.

(Mukul Tomar)
2K17/PhD/ME/02
Research Scholar
Mechanical Engineering Department
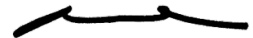Delhi Technological University
Delhi-110042

Date: 27.04.2021

Place: Delhi

CERTIFICATE

This is to certify that the work embodied in the thesis entitled "**SOME STUDIES ON NANO-PARTICLES DOPED ALTERNATIVE FUELS IN UNMODIFIED CI ENGINE**" by **Mukul Tomar**, (Roll No.-**2K17/PhD/ME/02**) in partial fulfilment of requirements for the award of Degree of **DOCTOR OF PHILOSOPHY in Mechanical Engineering**, is an authentic record of student's own work carried by him under my supervision.

This is also certified that this work has not been submitted to any other University or Institute for the award of any other diploma or degree.

(Dr. Naveen Kumar)
Professor
Mechanical Engineering Department
Delhi Technological University
Delhi-110042

Dedicated to my

parents

&

wife

ACKNOWLEDGEMENT

To my friends, Rohan Tomar, Siddhartha Tyagi, Harshit Negi and Mayank Maan thank you all for your well-wishes, phone calls, texts, visits, offering me advice and being there whenever I need a support. Also, special appreciation to the present and former CASRAE members Srishti Mishra, Adeel Ahmad, Harshil Kathpalia, Rohit Thakur, Abhinav Malaiya, Shikhar Jain, Aakriti Bagla, Sandeep Baranwal, Vaibhav Singh, Devanshu Jain and Rohan Brella for helping in experimental measurements, scientific discussion and for all the fun we had in the lab.

Besides, this journey would not have been possible without the blessings and support of my family. I am especially grateful to my parents, who have supported me emotionally and financially. Thank you for teaching me that my job in life was to learn, be happy, and know and understand myself; only then could I know and understand others. I am also indebted to my brother-in-law Ankur Sirohi who always extended help whenever required. My sincere respect and gratitude to parents-in-law as well for showering their blessings on me forever.

Finally, I am falling short of words to express my deepest gratitude towards my wife, Dr. Anshu Sirohi. Affection, motivation, guidance and moral support extended by her at every step of this journey is unforgettable; hence, I owe much to her. I know how beholden to you I am for not giving due attention and time during my Ph.D. journey.

In addition, there are many more person who knowingly and unknowingly contributed in making my work easier and a real success. I take this opportunity to express word of thanks to all of them.

Last but not least, I praise and thank the Almighty for his shower of blessings, providing me self-motivation, focus, enthusiasm and patience to complete the research work successfully.

(Mukul Tomar)

ABSTRACT

Diesel fleets, the most efficient prime mover, plays a transformative role in powering the world economy. However, the undue reliance on petrodiesel, coupled with alarming environmental concerns, are severely threatening its existence. Across all, agriculture will be the sector most vulnerable to the transition of existing diesel engine technology. These engines fulfill more than 60% of the total energy demand of the farmlands worldwide. Biodiesel derived from inedible sources can be a productive approach, especially for an agricultural-driven economy like India, rich in biodiversity and has more than 47,000 oil-bearing plants. It can revolutionize the agriculture sector to a whole new level by imparting new life to the millions of existing diesel engines. In view of this, the present study highlights the potential of underutilized inedible oil biodiesel, *Schleichera oleosa*, as a promising renewable fuel for stationary light-duty agricultural engines.

However, despite interest in sustainable energy resources is growing sharply, the popularity of the biodiesel economy is relatively low. Several reasons, particularly poor flow properties, lower calorific value, sensitivity to cold weather conditions, inadequate shelf life, engine incompatibility and higher NO_x emission, are accountable for this cause, which requires attention. Therefore, in order to encounter the critical issues and stimulate the engine performance of biodiesel blends, the properties of two different nanoparticles, alumina and MWCNT, in the form of additives, have been investigated and utilized in the present research.

The primary objective is to identify a propitious fuel borne nano-additive that can simultaneously improve the performance and regulate the harmful emissions associated with the operation of *Schleichera oleosa* biodiesel blends in farmland-based CI engine. In light of the above, the research effort has been broadly divided into three major sections. In the initial phase of work, the selection and production of biodiesel and nanoparticles were carried out.

Subsequently, the biodiesel and nanoparticles produced were characterized with the aid of Gas Chromatography-Mass Spectroscopy (GC-MS), Scanning Electron Microscopy (SEM) and X-ray diffraction (XRD) spectroscopy techniques, respectively. The first phase of research ended up by preparing different nano-fuel blends containing (25, 50, 75, 100 and 125) ppm dosage level of nanoparticles. The dispersion of nanoparticles in the base fuel (diesel-biodiesel blend) was achieved with the aid of ultrasonication and addition of arrogate surfactant (Sodium Dodecyl Sulfate).

In the second phase of work, the prepared blends of nano-fuels underwent a short/ long-term stability test known as zeta potential measurement and visual inspection to ensure the test fuels were free from agglomeration. The MWCNT dispersed test fuels showed a higher value of zeta potentials than alumina, thus signifying the higher stability of MWCNT nanoparticles in the base fuel and were only considered for further analysis. Also, the visual inspection result of six-month duration showed that nano-fuel blend containing 125 ppm dosage showed aggregation at a lower temperature (10^oC). Thereafter, the physico-chemical properties of the nano-fuel blends such as density, viscosity, calorific value, cetane index, etc. were evaluated as per relevant ASTM standard methods. The properties of nano-fuel blends were well-within range and comparable to neat diesel; the value of calorific value, cetane index, flash point, and cold flow properties were higher than diesel-biodiesel blend (D80B20).

The final phase of work includes evaluation of ignition probability, spray and engine characteristics of nano-fuels by undergoing trials on hot-plate, Malvern spraytec and 3.5 kW Kirloskar make single-cylinder, direct injection CI engine setup. The results obtained were compared with the biodiesel blend (D80B20) and neat diesel (D100). Due to increase in thermal conductivity with respect to temperature and shorter wavelength of nanoparticles, the nano-fuel blends showed higher ignition probability among all the fuels. Interestingly, the droplet size of nano-fuels was also comparable to neat diesel and smaller than diesel-biodiesel

blend with D80B20C75S3 exhibiting the lowest sauter mean diameter i.e., (15.1µm) among all the nano-fuel blends. The engine performance also showed an overall increase of upto 6.7% in brake thermal efficiency and upto 10.2% reduction in brake specific energy consumption with the addition of 75 ppm dosage of MWCNT nanoparticles as compared to D80B20 blend. Moreover, due to efficient atomization, excellent reactivity and thermal properties, the combustion characteristics of all the nano-fuel were also significantly improved. The ignition delay was reduced to 7.9º for D80B20C75S3 from 14.1º for D80B20 blend whereas the peak heat release rate showed upto 11% rise for D80B20C75S3 as compared to D80B20 blend. The exhaust emissions were also found to be (5-45%) lower when engine was operated with nano-fuel blends, most importantly NO_x emission showing an overall decrease of upto 22.8% with the addition of 125 ppm dosage of MWCNT nanoparticles in D80B20 blend. Lastly, as the consequence of exhaustive experimental results, RSM based multi-objective model was constructed to calculate the optimal dosage of MWCNT nanoparticle to be dispersed in the base fuel.

Thus, findings from the present research confirm that utilizing nanoparticles' strength as a fuel additive for biodiesel blends can be a great leap forward in the fuel reformulation realm. As, it can play a decisive role in preserving the existing diesel engine technology in certain ways.

LIST OF CONTENTS

LIST OF FIGURES

Some studies on nano-particles doped alternative fuels in Unmodified CI Engine

LIST OF PLATES

S. No.	Caption	Page No.
Plate 3.1.	Plate 3.1: *Schleichera oleosa*; **A**: Dense evergreen tree; **B**: Kernels.	49
Plate 3.2.	*Schleichera oleosa* oil Biodiesel production; **A:** separation of glycerol layer; **B,** removing moisture from biodiesel heating at 100ºC	54
Plate 3.3.	Physical appearance of neat diesel, *S.oleosa* biodiesel and their blend	56
Plate 3.4.	Synthesized aluminium oxide nanopowder	59
Plate 3.5.	Synthesized multi-walled carbon nanotube nanoparticles	61
Plate 3.6.	Demonstration of ultrasonication process	65
Plate 3.7.	Prepared nano-fuel samples	66
Plate 3.8.	Viscometer	71
Plate 3.9.	Density Meter	71
Plate 3.10.	Flash point tester	71
Plate 3.11.	Distillation setup	71
Plate 3.12.	Bomb Calorimeter	74
Plate 3.13.	CHNS/O Elemental Analyzer	74
Plate 3.14.	Carbon Residue tester	74
Plate 3.15.	Copper Strip Corrosion tester	74
Plate 3.16.	Cold filter plugging point apparatus	76
Plate 3.17.	Cloud point and Pour point apparatus	76
Plate 3.18.	Actual representation of diesel engine test bench	83
Plate 3.19.	AVL Exhaust gas analyzer and smoke meter	84
Plate 4.1.	Visual Inspection of nano-fuel samples at different temperature ranges	102

LIST OF TABLES

NOMENCLATURE

aBDC	After Bottom Dead Centre
aTDC	After Top Dead Centre
ANOVA	Analysis of Variance
ASTM	American Society for Testing and Materials
B20	20% biodiesel/80% Diesel
bBDC	Before Bottom Dead Centre
bTDC	Before Top Dead Centre
BHA	Butylated hydroxyanisole
BHT	Butylated hydroxytoluene
BMEP	Brake Mean Effective Pressure
B.P	Brake Power
BSEC	Brake Specific Energy Consumption
BSFC	Brake Specific Fuel Consumption
BT	Bluetooth
BTE	Brake Thermal Efficiency
BS-VI	Bharat Stage Emission Standards
cc	cubic centimetre
cSt	Centistokes
cm	Centimetre
CA	Crank Angle
CFPP	Cold Filter Plugging Point
C.P	Cloud Point
CI	Compression Ignition
CO	Carbon Monoxide
CO_2	Carbon Dioxide
CV	Calorific Value
DI	Direct Injection
eq	Equation
ECU	Electronic Control Unit
EHN	2-ethylhexyl Nitrate
EN	European Union Standard
EPS	Expanded Polystyrene
ft	Feet
gm	Gram
g/kWh	Gram per kilowatt hour
GC-MS	Gas Chromatography Mass Spectrometry
HC	Hydrocarbon
HP	Horsepower
hr	Hour
IAAI	Indian Agriculture and Allied Industries
IBEF	India Brand Equity Foundation
IC	Internal Combustion
IEA	International Energy Agency

J	Joule
J/kgK	Joule per kelvin per kilogram
kg	Kilogram
kW	Kilo Watt
kHz	Kilohertz
KJ/Kg	Kilojoule per kilogram
ltr	Litre
ml	Millilitre
mm	Millimetre
ms	Millisecond
mV	Millivolt
1M or mol	1 Mole
MICO	Motor Industries Co. Ltd.
Mtoe	Million tonnes of oil equivalent
MJ/kg	Megajoules per kilogram
mgI_2	Milligram Iodine
nm	Nanometer
NI	National Instrument
NPs	Nanoparticles
NO_x	Oxides of Nitrogen
NO	Nitric Oxide
NO_2	Nitrogen dioxide
PID	Proportional-Integral-Derivative
PM	Particulate Matter
P.P	Pour Point
P-Ɵ	Pressure-Crank Angle
ppm	Parts per million
rpm	Revolutions per minute
RSM	Response Surface Methodology
SDS	Sodium dodecyl sulfate
SOC	Start of Combustion
SOI	Start of Ignition
SOME	Schleichera oleosa methyl ester
SMD	Sauter Mean Diameter
TBHQ	Tertiary butylhydroquinone
TDC	Top Dead Centre
vol.	Volume
UBHC	Unburnt Hydrocarbon
v/v	Volume by Volume
wt	Weight
w/w	Weight by Weight
@	At the rate
ºC	Degree Celsius

μg/m³	Micrograms per Cubic Mete
μmol/L	Micromole per litre
μl	Microliter
μm	Micrometre
η	Efficiency

1.1. Motivation for the present research

Diesel engines significantly contribute to the ever-growing concerns of energy security, climate variations and perturbation in crude prices; however, it persists the technology of choice primarily for running the transportation and agricultural farm machinery. There are millions of on/off-road engines in India that heavily rely on diesel fuel and a relatively similar scenario prevails in American farmlands where these engines contribute 2/3rd of share in meeting the energy requirement [1]. The higher efficiency, fuel economy, better credibility and fidelity, together with their lower operational cost, make diesel engines the workhorse in the global economy. Among the alternatives to petroleum diesel scouted till date, biodiesel had shown promising results regarding their renewable origin and cleaner combustion. Besides, being a potential drop-in fuel, insufficient feedstock availability, lower calorific value, and several long-run operational issues are grave concerns to biodiesel sustainability [2]. In view of this, the present thesis showcases the state-of-the-art fuel reformulation technique, which aims to utilize the characteristics of nanoparticles as a fuel-borne additive for diesel-biodiesel blend.

1.2. World Energy Outlook

Energy consumption per capita of any country is gauged based on its economic and sustainable growth. The world's energy demand is escalating every year at a pace of 1% and will witness a critical juncture by 2040 [3]. Petroleum-derived fuels and their products (coal, oil and natural gas) share a major chunk in the global energy supply chain, with China surpassing the USA in the leading consumer of primary energy fuels followed by India, according to the 'Statista' report published on Jun 23, 2020 [4]. **Figure 1.1.** highlights the

world's consumption of different energy sources in Mtoe and the top ten leading primary energy-consuming countries. The energy trend clearly justifies that despite of the significant increase in renewable energy sources since the year 2000, primary sources' consumption rate showed no significant reduction in their demand until 2040. If the excessive consumption continues with the same growth rate, the per-day demand for petroleum will surge upto 109.4 million barrels by 2040, showing the diesel fuel demand highest, i.e., 5.7 million barrels [5]. Therefore, considering the current petroleum fuels depletion rates, which is more than 4 billion tonnes/year, the day will not be far when fossil fuels will eliminate, flattening the global economic development curve. The ever-rising dependency on fossil-based fuels, on another note, is also leading cause of the most pressing current generation issues, including climate change, air pollution, and oil spills [6].
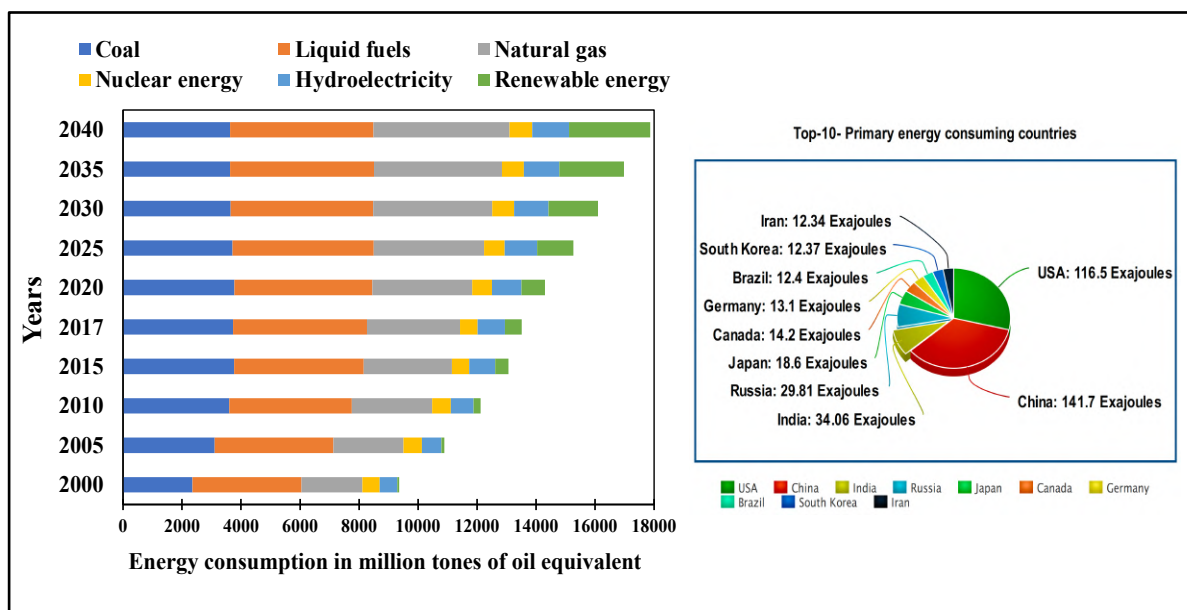
Figure 1.1. World's energy consumption and leading primary (oil, coal and natural gas) energy consuming countries, 2020 [BP statistical reviews of world energy, 2020]

1.2.1. Indian Energy Scenario

India is one of the few fastest-growing economies and, at the same time, among the major consumer of petroleum fuels to fulfill their energy requirement. The doughnut chart in **Figure**

1.2. shows India's energy consumption from different sources with coal and petroleum fuel share is maximum. The rising concerns of environmental degradation, crude reserves depletion and perturbation in their price are more intense in India than the other developing nations. Unfortunately, India stands nowhere among the top ten largest oil (including crude, petroleum and biofuels) producing countries. In contrast, it grabs a third place in the largest oil consumers in the year 2017 [7-9]. Therefore, undoubtedly highlighting the insufficient crude oil reserves and at the same time the over-dependency of nation on non-renewable energy sources. Moreover, the country spends its colossal portion of the exchequer on crude oil imports by fulfilling more than 85% of its petroleum requirement from the middle east countries. According to the report published in January 2019, India stands the second-largest Iranian importer after China, procuring 230004 barrels of crude oil per day [10,11]. The percentage import of Iranian oil by the top seven countries in barrels per day is shown in **figure 1.2**.
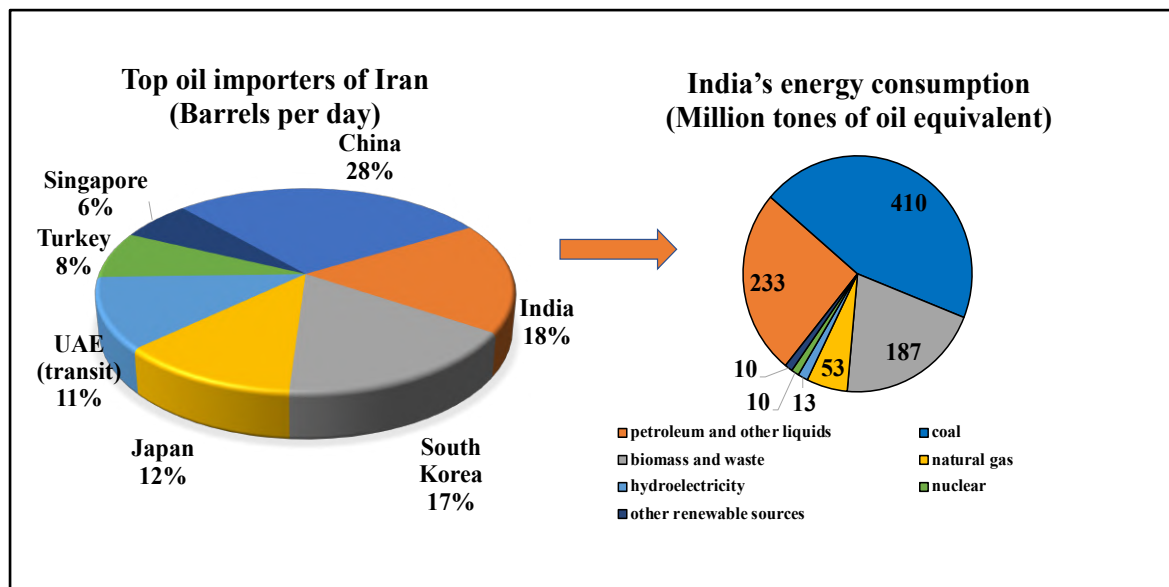
Figure 1.2. World's leading importers of oil from Iran [BP Statistical Review of World Energy 2018] and total primary energy consumption of India in terms of different fuel types, 2019 [IEA world energy outlook, 2019]

Apart from dependency on oil import, the harmful pollutants associated with petrodiesel fuel combustion are also the major troublesome. At present, the air quality index of India has

reached an alarming level, which can be clearly assessed based on the world's air quality report of 2019, listing India's 21 big cities as the world's polluted out of 30 [12,13]. Therefore, to maintain the momentum of economic development by causing minimum harm to the environment, there are urgent requirements of alternatives to petroleum fuels in the energy system that can result in cleaner combustion and improve the nation's self-sustainability.

1.3. Diesel engines and its economic relevance

Diesel engines, the heart of millions on-road and off-road vehicles, are considered the backbone of global economic expansion. Due to lower running costs, higher torque and better fuel efficiency than gasoline engines, it is the technology of choice, especially for running heavy-duty commercial transportation, stationary engines for power backups, railroads, marine and agricultural machines [14]. Life without the diesel engine is hard to imagine; it powers about 75% of the farm machinery/equipment, 90% of the agricultural products' transportation in the United States. These engines' role becomes more significant for a country like India, where 58% of the total population livelihood is dependent on agriculture source [15,16]. **Figure 1.3** shows the significance and bright future perspective of Indian agricultural economy as per Indian Agriculture and Allied Industries Report of IBEF [17]. However, on the counterpart, the harmful emissions of carbon monoxide (CO), oxides of nitrogen (NOx), unburnt hydrocarbon particles and particulates associated with diesel use fuel are causing severe environmental threats in the form of acid rain, ozone-depletion and climatic uncertainties. Driven by the increasing energy crisis, ecological problems and health risks involved with the diesel fuel, the governments are introducing stringent emission standards and new mandates. The implementation of BS-VI norms from April 1, 2020, in India is one such fine example, forcing the auto companies to remold, bringing the diesel engines technology on the back foot [18, 19]. Among all the society's major sectors, the consequences of diesel engine

technology disruption will have the worst hit back on the agricultural industry, where hundreds of thousands of these engines empowers the economy. In this regard, researchers worldwide are probing into different alternative technologies searching for potential drop-in fuel, which could compromise the diesel demand [20-22]. The electrification of road transportation has shown some brighter future prospects by reducing the burden on crude reserves. Electric vehicle fleets are expanding promptly and are expected to capture 50% of the world's auto market in the next two decades. However, finding a sustainable solution for the processing of millions of lithium-ion batteries dumped into the open environment is still a big challenge and a real future threat [23-25]. Also, dependency on a single energy source for powering the wider economy sections will be big chaos soon alike fossil-based economy. Thus, to obtain an optimum balance in the energy supply chain, multiple renewable energy sources should be identified; only then the world can be made a better place to live for the future generation.
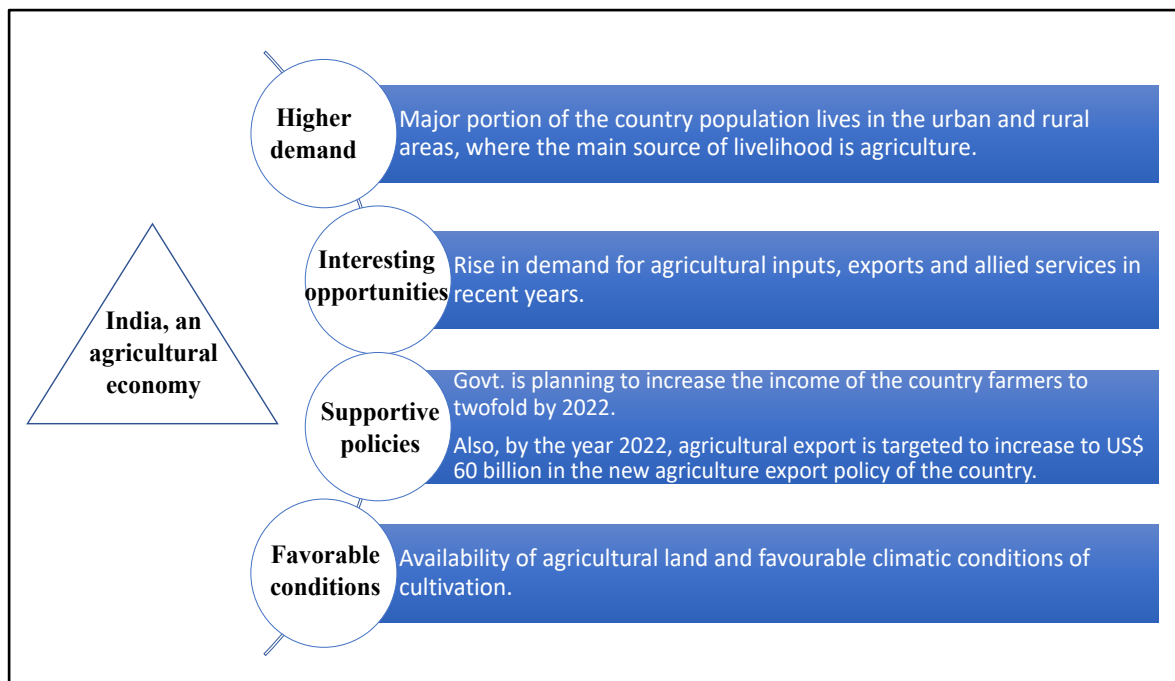
Figure 1.3. India's agricultural sector present and future scenario [IBEF, IAAI report, 2020]

1.4. Biodiesel economy- Current status and Future prospects

Biodiesel, the product of a wide variety of edible, non-edible and waste biomass, is considered the foremost alternative liquid fuel which can lease a new impetus to the millions of existing diesel engines. Owing to its carbon-neutrality, biodegradability, compatibility, safer handling and excellent lube properties in CI engines, it has gained substantial attention in recent years [26,27]. As per the affirmation of several recent studies, around 3 kg of CO_2 emission is curtailed for every 1 kg of biodiesel combustion, illustrating its importance in the energy supply chain [28]. Countries like the USA, Brazil and parts of the European nations are already leading their way by following low carbon fuel standard models. Authorities in the United States have set a target of achieving at least 36 billion gallons of biofuel blending with transportation fuel by 2022 under the Renewable Fuel Standard program [29]. Likewise, the Indian Government is also planning to cut down its crude demand by 10% by 2022 by setting an objective to meet 20% of the country's diesel demand by biodiesel [30,31].
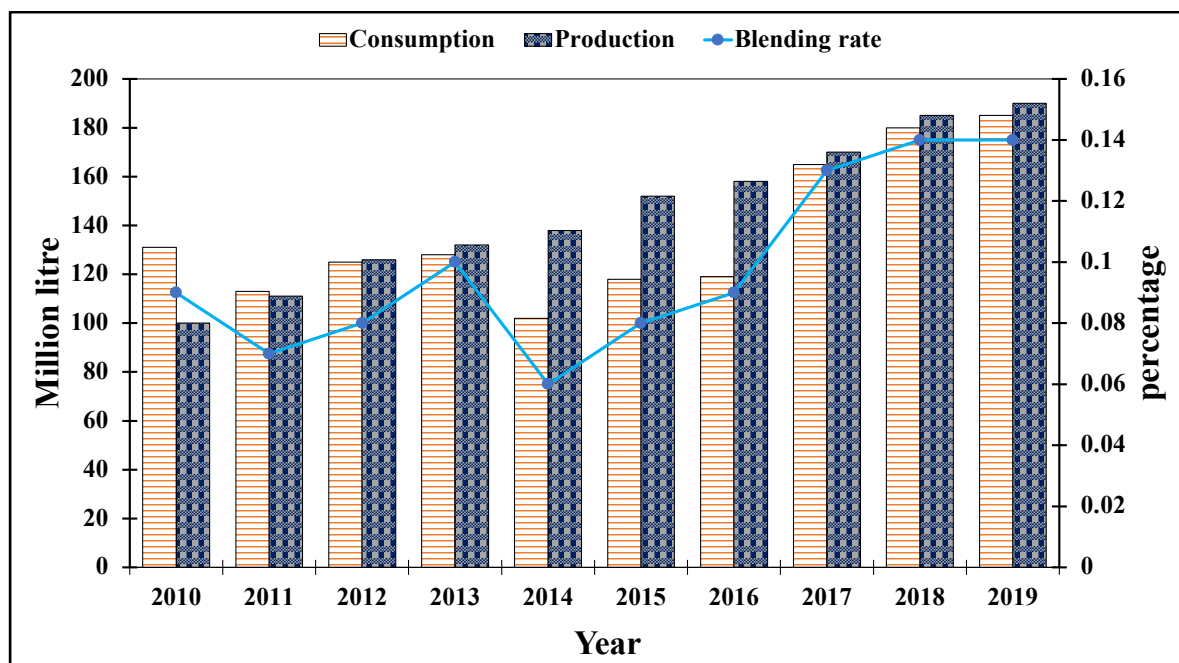
Figure 1.4. Variation in production, Consumption and blending rate of biodiesel in the Indian economy since 2010-19 [31]

However, the current status of biofuels – biodiesel economy, in particular, indicates that regardless of the sustainable origin and countless benefits, it is losing its importance from the world-wide market by each passing year. Several reasons are countable for this loss, including the shortage of land resulting in feedstock's unavailability, higher production rates, deficient engine performance, and higher NO_x emissions [32,33]. The problems associated with the biodiesel feedstock is more common for a densely populated country like India, which is short of barren land and import around 15 million tons of edible oils to complete its food requirement. Therefore, taking into consideration the growing concerns of food versus fuel in India, the biodiesel blending ratio is reduced to not more than 5% in 2019 biofuel policy reforms [31]. **Figure 1.4**. shows the last ten years data of change in blending percentage, consumption and production of biodiesel in India economy. It can be observed that the blending percentage remains muted to 0.14% between 2018-19, along with consumption and production rate, also showing a slower growth rate. This is the direct consequence of limited feedstock, engine operational issues and lack of indicated and dedicated government policies. Similarly, within a time frame of 2018-19, biodiesel industries in the United States have also recorded an overall loss of 132 million gallons in their production rates due to biodiesel fuel's poor stability, engine clogging, lower heating value and evaporation rate [3].

However, with the world's rapid transition towards sustainable energy, biodiesel is the need for current times, especially for powering the agricultural sector, dominated by diesel engine technology. India, a rich bio-diverse country, has more than 47,000 species of oil-bearing plants and trees in its 70% of the geographical area surveyed till now. There is an extensive population of inedible oil trees such as Karanja (*Pongamia pinnata*), Mahua (*Madhuca indica*), Moringa (*Moringa oleifera*), Neem (*Azadirachta indica*) and Kusum (*Schleichera oleosa*), having good oil content and can be utilized for energy production [34,35]. However, due to the poor infrastructure, lack of government funding and inadequate policies, the majority of

inedible feedstocks are still unexplored to their full production potentials [36]. Secondly, the other grave matter is the usability of pure biodiesel and its blends require special handling and may sometimes require retrofits in existing CI engines [37]. Hence, considering the future biodiesel prospects, the on-going biodiesel economy trends demand an economical feedstock and persistent fuel reformulation approach to mitigate the challenges in the road map of its commercialization. Although researchers are striving hard and working on different retro fitment and fuel reformulation approaches to improve biodiesel's compatibility and blends in CI engines, finding an optimum solution is still underway. According to the Indian economy perspective, dwelling towards fuel modification is much more significant when it comes to cost-effectiveness and existing engine survival. One such fuel-modification concept is nano-fuels, which is descriptively explained in the next section.

1.5. Nanoparticles for energy sustainability- Nanofuels

In recent years, nanotechnologies have achieved a substantial breakthrough in every scientific field by synthesizing nanoparticles of utmost importance. The exclusive properties of nanomaterials not only stimulate the existing technologies but also penetrates those areas of interest where bulk-materials fall short. Nanomaterials are solid crystalline particles, size ranging from 1-100nm has a remarkable surface to volume ratio, physico-chemical properties, chemical reactivity and enhanced heat and mass transfer properties offering ample opportunity to fix the problems related with conventional technologies. In this context, utilizing nanoparticle characteristics in the fuel reformulation technique is no exception, as it can serve the multiple purposes of regulating environmental challenges and improving biodiesel sustainability as well [38].

Mixing/Doping of specific nanoparticles (also known as nano-additive) with diesel, biodiesel, and blends aiming to improve their properties and performance is known as Nano-fuels [39].

During the CI engine operation, different physical, chemical and thermal processes take place, which governs the combustion, performance, and emission characteristics. The role of nanoparticles and its dosage level is unique in every process; however, based on some earlier and present current investigations, its acting mechanisms can be broadly categorized as:

> **Cold-flow operability improver-** Polymeric-like structure nanoparticles especially carbon-based nanoparticles act as potential pour point depressants by altering the morphology of wax crystals.

> **Efficient fuel-air mixing-** Higher force of collision between surfactant encapsulated nanoparticles suspended in the base fuel, resulting in micro explosion and promoting secondary atomization.

> **Promoting combustion-** Tendency to donate extra oxygen atom from the lattice cite of nanoparticles in combustion chain reaction.

> **Exhaust gases absorbent-** Higher surface ratio promoting chemical reactivity, the nanoparticles can easily react with combust products such as NO, CO, HC and carbon present in the soot.

> **Regulating combustion chamber temperature-** Nanoparticles act as a heat sink due to the higher thermal diffusivity and conductivity, resulting in lower in-cylinder temperature and controlling the NOx formation mechanism.
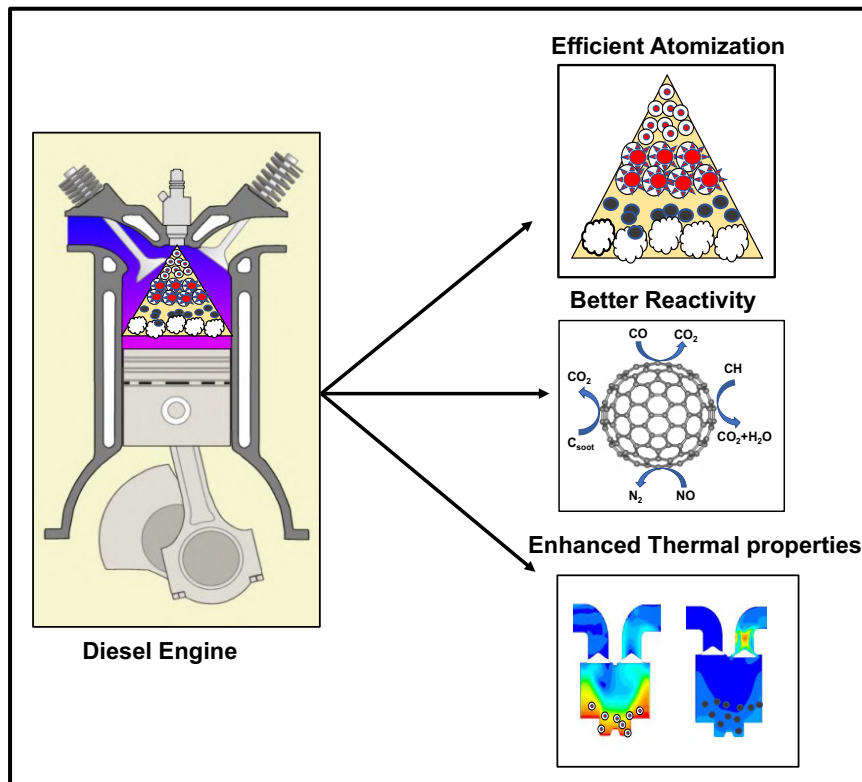
Figure 1.5. Graphical summary stating the different acting mechanism of nanoparticles in diesel engine [40]

1.6.   Structure of Thesis

The thesis has been structured to contain five chapters and the essence of each chapter is detailed below:

CHAPTER 1: INTRODUCTION – This chapter highlights the overview of present research. It starts with the motivation for choosing the topic of interest, present outlook of world energy, Indian energy scenario, diesel engines and their economic relevance. Subsequent section describes the significance of alternative fuels in particular the present status of biodiesel economy and its future prospects. This is further continued with a detailed discussion on role of nanotechnology in energy sustainability. Chapter 1 closes by introducing the nano-fuels concept and their acting mechanism on different operations occurring inside the diesel engine.

CHAPTER 2: LITERATURE REVIEW - This chapter provide a detailed literature survey, which includes an overview of physico-chemical properties, performance, combustion and

emissions of diesel, biodiesel and diesel-biodiesel blends with nano-additives. The review of the results associated with the literature mentioned here is focused on challenges associated with the usability of biodiesel and its blend in CI engine. The extensive literature survey also highlights the studies which precisely focus on nanoparticles synthesis, characterization and stability aspects.

CHAPTER 3: SYSTEM DEVELOPMENT AND METHODOLOGY - This chapter explains the procedure for *schleichera oleosa* biodiesel production. The detailed procedure for synthesis of alumina nanoparticles and multi-walled carbon nanotubes including their characterization by using SEM and XRD analysis are also discussed. Instrumentation and techniques used for preparation of stable and homogenous nanofuel blends is described. The methodology preferred for evaluation of physico-chemical properties and stability analysis of different test fuels prepared are also shown in detail. Also, the system development for calculating the ignition probability, spray characteristics and engine trials has been portrayed thoroughly. Finally, yet importantly, the accuracy and uncertainty of various instruments and measurements are also elaborated in this chapter.

CHAPTER 4: RESULTS AND DISCUSSION - This chapter contain detailed analysis of the results obtained from the experimentation task, statistical calculations and characterization techniques used in the current study. The discussion is based on the elaborate argument and scrutiny of the findings drawn from the experimental work besides comparing them with the results of the previous findings shown in the literature review. Moreover, to determine the optimum dosage of nanoparticle to be mixed with the fuel blend, the RSM based optimization study is also shown in the subsequent section.

CHAPTER 5: CONCLUSION - It is the closing chapter of the thesis which includes the summary, and salient points drawn from the present research. Some logical outcomes

formulated on the basis of facts and figures obtained in the present work are also stated with outlining the recommendation for the future work.

Last but not least, the detailed references and appendices, related to the present research work are listed at the end of the thesis.

2.1. Introduction

As discussed in the previous chapter, the contribution of diesel/compressed ignition engines in the global economy are of paramount significance. However, the ever-rising dependency and environmental degradation are worrisome for its existence. The integration of biodiesel economy is the most feasible solution that can be a life saviour to the millions of existing diesel engines if its usability can be upgraded. Nano-fuels, a surrogate fuel formulation concept is one such solution that can improve the engine characteristics of biodiesel and its blend in the CI engine.

Therefore, the present chapter gives an overview of diesel engine working by explaining the processes occurring inside it and the mechanism of different exhaust emission associated with it. After that, the detailed review of the combustion, performance, and emission characteristics of the CI engine fuelled with diesel, biodiesel, and blends are shown. The chapter also enumerates the fuel additive concept and different additive's role in a CI engine. The literature review further focuses on various methods applied to prepare nanoparticles and techniques for investigating nanoparticles characteristics. The studies highlighting the engine characteristics of different nano-fuel blends are also listed. The outcome gathered from the exhaustive literature survey is pointed out subsequently. At the end, the gaps, research statements and objectives of the present research are shown in the chapter.

2.2. Overview of CI engine operations

Broadly, the diesel engine operation is based on three different processes [41,42]:

- ➢ Fuel Injection

- ➢ Atomization

> ➢ Combustion

2.2.1. Fuel injection

The fuel injection phenomenon inside the CI engine takes place after the air has been sucked inside the engine cylinder. The fuel with a high pressure and velocity is injected in a high-temperature region just before the piston reaches the Top Dead Centre (TDC) in the compression stroke. It is the primary and most influencing process, which regulates the subsequent fuel atomization, and combustion phenomenon. The event of injection is governed by different parameters which includes injection timing, duration, pressure, rate of injection and spray characteristics. Furthermore, these parameters are significantly influenced by the fuel composition and its properties, type of injection system, geometry, and engine operation [43,44]. However, in the case of fuel reformulation research, the injection system, composition and properties of the fuel are of much greater importance than others. In former CI engines, equipped with a manual fuel injection system, the fuel injection rate should be as low as possible to prevent the formation of NOx and smoke emissions. On the other side, the emissions in modern engines are significantly lower due to electronically controlled injection and the overall injection process can be precisely controlled by ECU [45,46]. However, the injection timing is a critical parameter as the more advanced is the timing, the higher the fuel accumulation, which will give rise to incomplete combustion. On the contrary, the retardation in timing will lead to the burning of major fuel-air mixture portions in the second phase of combustion and resulting in the higher combustion temperature and, analogously, NOx formation [47]. Therefore, the fuel injection event should start at an optimum crank angle position for obtaining efficient engine characteristics.

2.2.2. Atomization

Atomization is the breakdown of injected fuel droplets into finer particles so that it can be mixed with air and then vaporized easily. It is a complex phenomenon, and the whole process,

i.e., starting from the breakdown of fuel particles to the fuel-air mixing, occurs in three different steps: (i) Ejection of fuel (ii) Primary atomization (ii) Secondary atomization as shown in **Figure 2.1** [48]. As soon as the fuel droplet crosses the injector nozzle periphery, the deformation or breakdown starts and grows further with respect to space and time, known as primary atomization. Furthermore, the distortion and disintegration of the fuel droplets will continue until the fuel droplet's surface tension forces are powerful enough to restrain the cohesion forces. This procedure of stable droplet formation is termed as secondary atomization [49]. The spray characteristics are invariably dependent on the fuel's flow properties such as density, viscosity, and surface tension. Besides, the injector nozzle geometry, temperature and pressure of the domain in which the fuel is sprayed also plays a dominating role. Therefore, considering these governing factors, the fuel spray characteristics are categorized as microscopic and macroscopic properties. The spray head penetration, cone angle, breakup length of spray, and surface area of the fuel droplet are sorted under macroscopic properties. In contrast, fuel droplet size or sauter mean diameter (SMD) and fuel velocity spray are the microscopic properties [50].

During the atomization process, the SMD of the spray plume is the crucial property, which is also a subject of interest for several underlying research. In actual, the atomization is a rapid process, and particles sprayed out of the injector are non-uniform, due to which particle size is distinguished based on Sauter Mean Diameter (SMD). It is equal to the average sum of liquid droplets' diameter ejected from the nozzle for a specific time duration. The smaller the SMD, the better the fuel droplet's evaporation and the more efficient will be the mixing and fuel-burning rate [51]. However, there exists a critical range of SMD for achieving better combustion characteristics. The significance of particle size becomes more significant when the fuel blends or the influence of fuel additives on spray characteristics are considered for

examination. Therefore, similar circumstances prevail in the present study and spray characteristics were examined via—Malvern spraytec instrument.
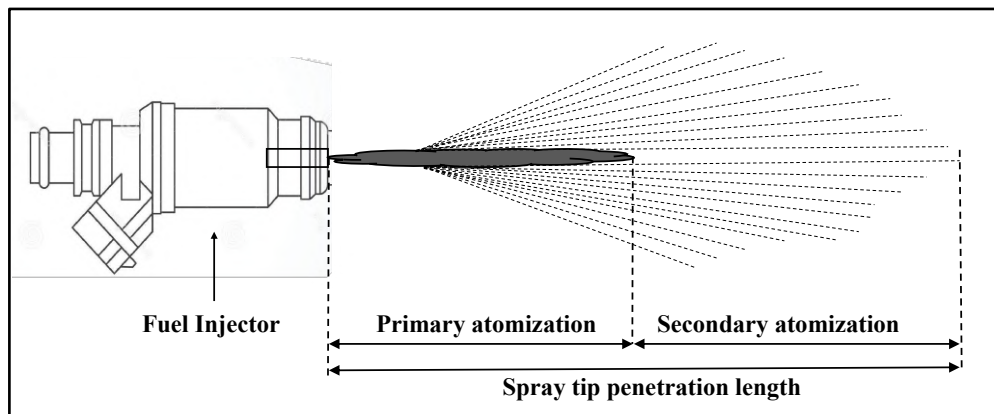
Figure 2.1. Demonstration of fuel atomization process [52]

2.2.3. Combustion

In a simple term, the combustion can be defined as a chemical process wherein a substance reacts promptly with an oxygen source and emanates heat. Concerning the I.C engine working, the substance is the fuel and air acts as the oxidizer. In CI engines, the combustion process is generally divided into four different stages, i.e., ignition delay, premixed or uncontrolled combustion, diffusion or controlled combustion, and later combustion phase [52]. The amount of heat emanating during the burning of fuel at different combustion stages is of paramount significance and is strongly influenced by the fuel-air mixing phenomenon. It determines the important combustion parameters such as delay in the ignition, starting and ending of burning and fuel mass burnt at different crank angle positions [53]. **Figure 2.2.** demonstrates the rate of heat emanated during different phases of combustion with premixed phase showing highest peak followed by diffusion and later combustion phase.

As soon as the injected fuel droplets get atomized, it starts evaporating by exchanging heat with the nearby surrounding air, known as the fuel-air mixing stage. However, in actual, the burning will not begin till the fuel reaches its auto-ignition point; this difference between the injection time and start off burning is termed as delay in ignition [54]. The physico-chemical

properties of the fuel, especially cetane index, density, viscosity and volatility, significantly affect the ignition delay. For the same injection timing, the higher cetane index value fuel will result in a lower delay. However, in biodiesel fuel, usually having higher viscosity and density, the delay is more.

Furthermore, the premixing is an instantaneous process and is marked with a maximum rise of peaks in the heat release rate curve, signifying the mixture's rapid burning. The point on the HRR vs. crank angle curve where the heat release rate becomes positive is termed as the start of combustion [55]. The diffusion is a slow and controlled process and usually, a stagnant peak is observed in this phase of burning. Almost 90% of the mixture is burned in this stage. Also, the heat released during the diffusion combustion phase is directly dissipated in the engine exhaust as a waste, due to its incapability to convert into useful work [56]. Therefore, the higher the amount of heat release in the second phase of combustion, the greater the NO_x formation chances. The heat emanation continues in the expansion stroke as well due to the availability of rich-fuel regions. However, the rate of occurrence is prolonged. This slow kinetic phenomenon, where around 10-20% of the mass fraction burning occurs, is known as the late combustion phase.
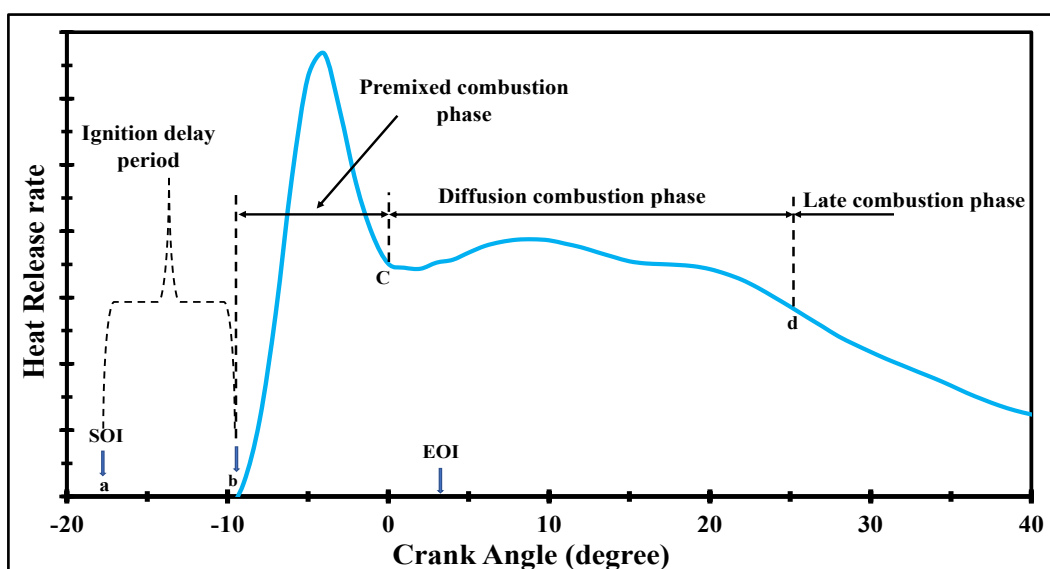
Figure 2.2. Demonstration of different combustion phases via. heat release rate curve [54]

2.3. Emissions associated with CI engine combustion

The impacts of climate change and air pollution are hitting harder and sooner than speculated. The increased amount of greenhouse gases such as carbon dioxide, carbon monoxide, nitrous oxide, methane and chlorofluorocarbons into the atmosphere are responsible for changing the earth's climate. Among all the CO_2 emitting sources, the global transportation sector mainly driven by petrol and diesel alone accounts for more than 20% share of total emissions across all the major countries of the world [3]. In India, the situation seems to worsen where the CO_2 emission growth rate had shown a steep rise of 4.8% during the year 2017-2018 [57,58]. Even though the contribution of hydrocarbons and oxides of nitrogen emissions in environmental pollution counts less, their growth rate has also doubled in the last ten years, which cannot be overlooked by the fact. **Figure 2.3.** contribution of different sources responsible for air pollution (PM10 and PM2.5) in India [59]. The doughnut chart indicates that the percentage of the transportation sector and diesel generator sets alone accounts for 22% of PM10 and 28% of PM2.5 emissions. Several studies conducted in the past have shown that diesel exhaust gases contribute primarily to the ground-level ozone, poor air quality and human health causing lung diseases and respiratory disorders. Alarming levels of air pollution in India alone accounts for 67,000 deaths annually [60,61]. According to a report on the Global Burden of Disease Study of 2017 published by Lancet, about 76.8% of the Indian population is exposed to PM emission critical limit, i.e., above 40 μg/m³ (set by the air pollution control board of country). The report also envisioned that the country's average life would increase to 1.7 years if the exposure rate to PM emission can be brought down to the critical limit of exposure [62]. **Table 2.1.** listed below shows the adverse effect of different pollutants on human health. Ideally, the complete combustion of diesel fuel would result only H_2O and CO_2 as the end product. However, in actual the combustion of fuel in diesel engine is dependent on different

parameters (as discussed in the above section) which affects the rate of burning and result in formation of harmful emissions such as CO, HC, NOx and smoke/soot.
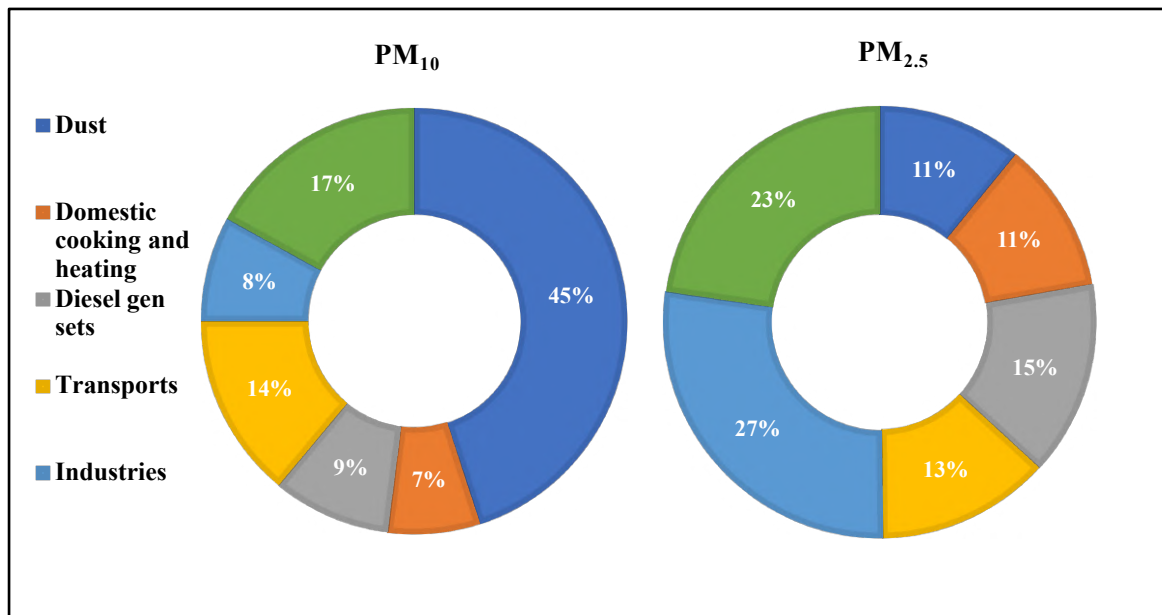
Figure 2.3. Share of different air polluting sources in Indian cities [59]

Table 2.1. List of different pollutants and health problems associated with them [60, 63,64]

Pollutants	Health Problems
Carbon Monoxide (CO)	Obstruct the amount of oxygen required for the body organs and tissues; facilitates heart diseases, chest pain and other critical disorders in the body (asphyxiation).
Oxides of Nitrogen (NO$_x$)	Increased proneness to respiratory illnesses (influenza), smog formation in atmosphere, visibility impairment.
Oxides of Sulfur (SO$_x$)	Risk of Asthma, wheezing, cheat tightness, breathing shortness, respiratory disorder on prolonged exposure
Ozone (O$_3$)	Reduces lung function, coughing and breathing shortness, premature mortality.
Particulate Matter (PM)	Premature death, lung cancer, building soiling, visibility reduction, loss in agricultural productivity, other cardiovascular diseases in humans.
Volatile Organic Compounds (VOCs)	Respiratory tract irritation, Provoke lung diseases, respiratory infection.

2.3.1. Nitrogen Oxides (NO$_x$)

The NOx accounts for almost 30% share in the diesel exhaust emissions. It is the constituent of nitrogen dioxide (NO$_2$) and nitric oxide (NO), out of which the contribution of NO$_2$ is only 5 to 10% and NO is predominant. Moreover, several recent studies have also reported that the formation mechanism of NO$_2$ depends on pre-existing NO [65]. Due to higher temperature

combustion chain reactions (around 1500°C), the NO_x emissions are higher in CI engines compared to gasoline. The oxides of nitrogen formation mechanism during combustion are divided into Thermal NO_x (Zeldovich mechanism), Fuel NO_x and Prompt NO_x (Fenimore mechanism). The constitution of thermal NO_x is dependent on the local temperature inside the cylinder during combustion, presence of oxygen-rich regions and residence time of high-temperature chemical reactions [66]. The chemical reactions involved in the formation of thermal NO_x via Zeldovich mechanism is portrayed in equation **2.1, 2.2 and 2.3** [67]**.**

$$N + NO \leftrightarrow N_2 + O \hspace{4cm} \textbf{(2.1)}$$

$$N + O_2 \leftrightarrow NO + O \hspace{4cm} \textbf{(2.2)}$$

$$N + OH \leftrightarrow NO + H \hspace{4cm} \textbf{(2.3)}$$

On the other hand, the prompt nitrogen oxide is insuppressible and is formed when atmospheric nitrogen reacts with combust products in the fuel-rich flame zone. The chemical reaction involved in the formation of prompt NO_x (via Fenimore mechanism) is listed in equation 2.4.

$$fuel\ radical\ CH_n + N_2 \longrightarrow prompt\ NOx \hspace{2cm} \textbf{(2.4)}$$
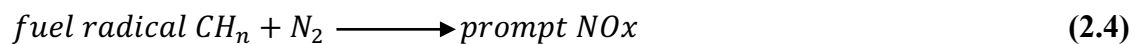
Also, the nitrogen that is chemically bonded in the fuel is responsible for developing fuel NO_x. However, the primary reason for NO formation in diesel engines is the high temperature-dependent chemical reaction referred to as the extended Zeldovich mechanism [68]. Researchers are dwelling into different techniques which can regulate NO_x emissions from CI engines. Most widely preferred are Exhaust gas recirculation (EGR) and selective catalytic and non-catalytic reduction (SCR); however, these techniques too have certain limitations associated with them [69].

2.3.2. Carbon Monoxide (CO)

The carbon monoxide formation in the CI engine is mainly the product of incomplete combustion. Some of the major factors responsible for the incomplete combustion are the deficiency of oxygen (leading to partial oxidation), improper fuel-air mixing, prolonged delay

in the ignition, etc. Petrodiesel fuel having insufficient oxygen content and lower cetane index contributes substantially to the CO emissions. Generally, during the start and sudden accelerating the engine, the probability of CO emission is higher due to the disproportionate fuel-air mixture [60].

2.3.3. Unburnt hydrocarbons (UBHC)

The fuel particles left unburnt after completion of the combustion process are known as Unburnt hydrocarbons. It is the direct measure of the combustion quality of the engine. UHC is of numerous varieties, including aromatics, alkanes and alkenes, and its content is usually indicated in terms of CH_4. Identically the CO emissions formation, the UHC is also the result of inadequate availability of oxygen and temperature, the presence of rich fuel-zones inside the combustion chamber and improper flame speed. Besides, fuel type, engine design, erratic engine operating conditions and poor maintenance resulting in frowzy injection, needle bounce and improper atomization can significantly affect the quality of combustion, resulting in the dissipation of unburnt fuel in the engine exhaust [70]. Apart, numerous studies in the past have also highlighted that oxygen traces and higher temperatures (>600°C) in exhaust tailpipe also favours the formation of UBHC emissions [52]. This is why sometimes the UBHC formation leaving the cylinder is lower than it is in the engine exhaust. Usually, diesel engines emit fewer UBHC emissions; however, at lower loads when the mixture is lean, the chances of emissions are maximum due to the irregular flame speed.

2.3.4. Diesel Particulate Matter (PM)

The formation of particulate matter is the result of the complex combustion process. The tiny gases particles of unburnt fuel and lube oil, traces of fuel ash, sulphates and water vapour agglomerated together are known as diesel particulate matter. On a broader scale, PM emission can be classified as soot and soluble/insoluble organic fraction. However, the soot emission alone accounts for more than 50% of the total PM [71,72]. Soot is a carbon-rich PM and is

generally originated due to the continuous supply of rich fuel-air mixture. In contrast, opacity is the measurement quantity of smoke, i.e., the degree to which the smoke can obstruct the path of light. Besides, the higher aromatic content in the fuel, insufficient controlling of fuel injection rate during acceleration of the engine, also promotes soot emission. The appearance of black smoke in the diesel engine signifies the higher content of soot. The study carried out by Aggarwal [73] on PM constituents also showed that the percentage of carbon, unburnt fuel, unburnt lube oil, sulphates and moisture is about 31%, 7%, 40% and 14%, respectively. The chances of soot formation during the second phase of combustion are higher than the premixed phase. However, due to ignition delay, the supply is rich fuel mixture in premixed combustion, sometimes facilitates soot emission formation. Compared to gasoline, which operates at a stoichiometric ratio, the soot formation is less than CI engine.

2.4. Engine characteristics of neat diesel, biodiesel and their blends

For a long time, diesel is considered as the most preferred fuel of choice. However, with the amendment of stringent emissions norms due to rising environmental pollution, the life of millions of existing CI engines is at stake. Extensive studies were conducted in the past, in search of a potential drop-in fuel substitute for diesel. As a neat or in the form of blend with diesel, biodiesel is the most widely explored alternative that had shown some promising results [74]. A wide variety of edible/inedible oils as a biodiesel feedstock has been tested in CI engines in last couple of years. **Table 2.2.** gives an insightful review of the several past studies highlighting the variation in physico-chemical properties of neat diesel, different biodiesel fuel and their blends.

Table 2.2. Physico-chemical properties of diesel, biodiesel and blends

Fuel/Fuel blends	Viscosity at 40°C (cSt)	Density at 15°C (kg/m³)	Calorific value (MJ/kg)	Cetane Index	Flash point	Cloud Point (ºC)	Pour Point (ºC)
Diesel (D100) [Devan and Mahalaxmi, 2009; Ruhul et al., 2017]	2.9	831.5	45	48	79	6	-10
Calophyllum	5.5	878.5	39.5	59.6	162.5	2	2

Some studies on nano-particles doped alternative fuels in Unmodified CI Engine

Inophyllum biodiesel (CI100) [Ong et al., 2014; Atabani et al., 2013]							
Calophyllum Inophyllum Biodiesel blend (CI20) [Silitonga et al., 2016; How et al., 2018]	4.02	863.9	41.9	53.1	140.0	0	0
Ceiba pentandra biodiesel (C100) [Jamaluddin et al., 2019; Silitonga et al., 2014]	4.16	876.9	40.4	---	156.5	3	2.5
Ceiba pentandra Biodiesel blend (C20) [Khan et al., 2014; Ong et al., 2014]	3.7	857.9	44	51.7	91.5	5	3
Moringa oleifera biodiesel (M100) [Esmaeili et al., 2019; Wakil et al., 2015;]	4.7	880	---	---	166	0	-1
Moringa oleifera biodiesel blend (P20) [Rashed et al., 2016; Teoh et al., 2019]	3.67	846.6	44.1	---	82.5	8	6
Jatropha Curcas biodiesel (J100) [Mazumdar et al., 2012; Kouame, 2011]	5.68	850	40.1	52	120	8	2
Jatropha Curcas biodiesel blend (J20) [Rajak et al., 2020; Sahoo and Das, 2009]	3.96	844.7	42	48.4	108.4	6.9	3.3
Rubber seed biodiesel (RS100) [Dhawane et al., 2016; Morshed et al., 2011]	4.85	870	38.7	51	155	3.4	-2
Rubber seed biodiesel blend (RS20) [Devi et al., 2012; Vishal et al., 2020]	4.0	856	40.1	---	137	2	-2.2
Schleichera oleosa biodiesel (SO100) [Kumar and Tomar, 2019; Yadav et al., 2016; Yadav and Sharma 2018]	4.26	860.3	38.3	47.2	139	-2.5	-10.8
Schleichera oleosa biodiesel blend (SO20) [Pali and Kumar, 2016]	3.56	846	42.2	53.3	69	---	---
Karanja oil biodiesel (K100) [Shukla et al., 2015; Kamath et al., 2011]	4.41	881	37.9	50.8	168	---	---
Karanja oil biodiesel blend (K20) [Shrivastava et al., 2020; Aggarwal et al., 2015 [55]]	3.18	842.4	41.7	48.8	---	---	---
Linseed oil biodiesel (L100) [Demirbas, 2009; Puhan et al., 2010]	4.1	890	37	55	192	---	---
Linseed oil biodiesel blend (L20) [Veinblat et al. 2018]	3.23	841	42.2	---	---	---	---

Some studies on nano-particles doped alternative fuels in Unmodified CI Engine

Rice Bran oil biodiesel (R100) [Dharmaraja et al., 2019; Musthafa et al., 2011]	4.46	876	42.2	55.7	213		-4
Rice Bran oil biodiesel blend (R20) [Ahmad et al., 2011]	4.2	886.4	---	---	75	-9	-10
Neem oil biodiesel (N100) [Das et al., 2018; Kannan et al., 2020]	4.5	860	41	51	152	---	---
Neem oil biodiesel blend (N20) [Kattimani et al., 2015]	4.3	826.8	44.8	---	77.4	---	---
Waste cooking oil biodiesel (B100) [Yilmaz et al., 2017; Silva et al. 2017]	4.5	855	40.5	52.2	126	---	0
Waste cooking oil biodiesel blend (B20) [Yildizhan et al., 2017]	3.18	847	44.3	53	93	---	---

Widespread studies were also conducted in the past, focusing on performance, combustion, and emission characteristics of various CI engines fuelled with different vegetable oils, diesel, and blends. The findings of several investigations are listed further. Das et al. [115] conducted engine testing on single cylinder four stroke, DI, diesel engine by using (5%,10% and 20%) blend of castor oil biodiesel. The combustion starts early for diesel-biodiesel blends and the rate of pressure rise was also quicker in premixed combustion than neat diesel. Besides, the biodiesel blends showed slightly higher brake thermal efficiency and increased NOx emissions at peak load compared to diesel. A comparative assessment of spray and engine characteristics of diesel (D100), Karanja biodiesel (B100) and their blends (B5, B10, B15, B20, B25 and B50) were conducted by Lahane and Subramanian [116]. Due to higher viscosity, density and surface tension, the Sauter mean diameter of neat biodiesel and blends were significantly higher than diesel. The ignition delay starts decreasing with the increase in biodiesel blends, whereas combustion duration showed a vice-versa trend. As compared to diesel, the rate of pressure rise, brake thermal efficiency, CO, HC and smoke emissions were lower in biodiesel blends. However, BSEC and NO_X were significantly higher with the increase in biodiesel blends. Lower ignition delay and shorter combustion duration were observed when direct ignition,

turbocharged CI engine, is operated by neat Karanja biodiesel (Anand et al. [117]). The HC and smoke emissions were also significantly lower. However, engine efficiency and carbon monoxide emission showed marginal improvement, whereas NO emission of neat biodiesel was higher than diesel. An investigation conducted by Jose and Anand [118] on biodiesel's long-term stability showed that the utilization of aged biodiesel fuels degrades the engine characteristics. Due to higher unsaturated fatty acid content, the stability of vegetable oils is deficient. The study also highlighted that blending or mixing fuel additive methods are the two prominent methods that can improve the engine characteristics and shelf life of methyl esters over time. Similarly, experiments conducted on agriculture purpose diesel engines by Raman et al. [119] showed that using 25% by volume of rapeseed oil biodiesel blend can be used as a substitute for neat diesel without undergoing any retro fitments. The results also showed the lowest BTE, higher BSEC, NOx and smoke emissions for neat biodiesel among all the test fuels.

Limited studies were also conducted in the past on exploring the possibility of underutilized *schleichera oleosa* biodiesel blends as an alternative fuel for light and medium-duty CI engines. Fuelling multi-cylinder diesel engine with (5%, 10%, 15% and 20%) blend of *schleichera oleosa* biodiesel showed up to 15% reduction in CO, HC and smoke emissions as compared to neat diesel (Yadav et al. [120]). However, fuel consumption and NO_x emissions were significantly higher for higher percentage blends. Also, the pressure rise rate and premixed combustion peak were observed to be lower in biodiesel blends as compared to diesel. Likewise, experiments were also carried out on stationary agricultural engine by Pali et al. [121] using higher blends of (10%, 20%, 30% and 40%) *schleichera oleosa* biodiesel. Due to poor atomization, the biodiesel blends showed lower engine performance as compared to diesel. Also, the NOx emissions were observed 4-20% higher with the increase in biodiesel percentage. However, the HC, CO and soot % were lower than neat diesel.

Several long run experiments were also carried out on a variety of biodiesel feedstocks. The majority of studies revealed that due to methyl esters' excellent lubricant properties, the carbon deposit and wear of engine parts were considerably less than that of running diesel fuel [122-124]. Due to the oxygenated nature and low content of aromatic compounds in biodiesel, the PM emission is also lower compared to neat diesel. Despite having renewable nature and potential substitutes of diesel, studies had also reported some long run operating issues that decrease the popularity of biodiesel fuel. Loss in engine power, higher fuel consumption, reduced engine efficiency, lower calorific value and various low temperature operating difficulties such as wax and deposit formation, chocking of engine parts, higher NO_x formation, etc. are some of the severe challenges stated in the majority of engine trials [125-128].

However, researchers are dwelling into different engine retro fitment and fuel reformulation techniques, which can improve the compatibility of biodiesel fuel in diesel engines. Amongst of all, the modification of biodiesel properties and engine working characteristics by using fuel additives can be break-through for millions of existing diesel engines running all around the globe (Imdadul et al. [129]). Additives on the basis of their origin, size, and properties are classified into various types. Many researchers in the past have employed the assets of additives to improve the biodiesel properties and engine characteristics. A comprehensive review on the types of additive and their effect on the diesel engine performance, combustion and emission characteristics are discussed in depth in the subsequent sections.

2.5. Fuel additives, types and their role in CI engine

Additives are the chemicals, or the foreign substances added to the base fuel to improve its properties and engine performance. It plays a significant role in meeting up the strict emission norms and enhancing the fuel's physio-chemical properties. Additives can reduce the dependency on conventional fuel by resolving the challenges associated with the wide-reaching utilization of biodiesel fuel in the diesel engine. The additives are being utilized in the oil

industries since the early '90s. Therefore, some of the common obstacles that could be circumvented using additives are: (i) Protect the fuel line, petroleum tank, and engine parts' corrosion. (ii) Improvement in Cold flow properties and promote biodiesel blending with diesel. (iii) Reduced harmful emissions from engine combustion. (iv) Enhances the combustion process and performance characteristics. (v) Promote storage stability for a longer duration throughout the operating conditions [130-132]. The dosage of additives added in the base fuel depends on the mixture's chemistry and chemical composition of the base fuels. However, the optimum dosage to be blended with the fuel is identified by undergoing different experimental analysis. As already discussed, the additives can be classified into wide variety based on their origination, size, chemical compound and state (solid or liquid). Therefore, the selection of appropriate additive to be mixed with biodiesel or its blend is a critical step and are dependent on different factors such as economic feasibility, fuel blending property, toxicity, additive solubility, the flashpoint of the blend, viscosity of the blend, water solubility in the resultant blend, and water partitioning of the additive (Abe et al. [133]). Hence, according to the availabilities of additives in the world market, they are primarily classified into different categories, as shown in **Figure 2.4** [134-136].
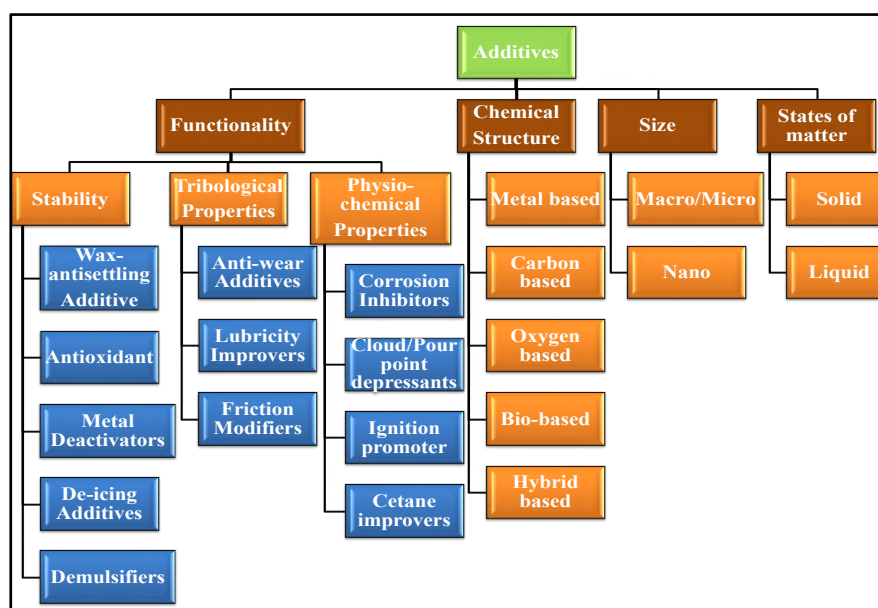
Figure 2.4. Categorization of fuel additives

Some studies on nano-particles doped alternative fuels in Unmodified CI Engine

Below is listed the summary of several literature findings focusing the effect on fuel properties, engine performance and emission characteristics by the addition of a wide variety of additives. Also, the constraints and demerits associated with macro/micro fuel additives are also illustrated further. The presence of unsaturated fatty acids in biodiesel decreases its oxidation stability with time, thus affecting the engine performance. In regard to this, dosing small amount of antioxidants such as Butylated-hydroxytoluene (BHT), alkyl/aryl-aminophenol, 2,6-di-tert-butyl-phenol (2,6-dtbp), alkyl/aryl-phenylenediamine, neem extract (collected from crushing of neem leaves), 2,4-dimethyl-6-tert-butyl-phenol and ethylene-diamine in biodiesel blends can improve the oxidation stability of biodiesel fuels considerably, studies conducted by Borsato et al. [137] and Sindhi et al. [138]. Similarly there are certain additives which can resolve the wax settling, corrosion of engine parts and inner lines of the combustion cylinder issues arising after a certain period of time when engine is operated with bio-based fuel in the colder conditions. Metal deactivators N,N- disalicylidine 1,2- propane-diamine available in the market can serve as a remedy and deactivate the upper surface of metal parts for oxidation and improves the oxidation and overall life of the diesel engine (Sorate and Bhale [139]; Srivyas and Charoo [140]). In the same way, to get rid of poor ignition delay, lower calorific value issues the addition of bio-based co-polymer of 2-ethy-hexylmethacrylate and dimethyl aminoethyl methacrylate can work wonders, according to the study performed by Fangsuwannarak et al. [141]. A series of engine trials were conducted with/without adding additive on B10 to B100 fuels. The result showed that among all the test fuels, B40 and 0.1 gm additive is the optimum concentration which showed better combustion, performance and emission characteristics as compared to diesel. Members of alcohol group such as ethanol, n-butanol, diethyl ether and methanol obtained from biological sources containing higher oxygen content can be added to the smaller quantity in the blends of biodiesel. The higher volatility, latent heat of vaporization, and higher flammability can serve as a potential fuel additive for

diesel-biodiesel blends, thus improving the cold flow properties of biodiesel in colder condition by enhancing the combustion rate in the cylinder [142].

The favourable outcomes obtained from past researches had proved metal, alcohols and copolymers based additives as excellent cold flow property improver of methyl esters. The effect of magnesium-based additive on the pour point of biodiesel of chicken fat methyl ester was examined by Guru et al. [143]. The findings of the study reported that on increasing the concentration of an additive in the fuel blend from 0 to 16mmol/l, the pour point was reduced to 7°C. Similarly, Cao et al. [144] examined the effect of Ethylene Vinyl Acetate Copolymer (EVAC) additive on Waste Cooking Oil Methyl Ester (WCOME) used for running the unmodified diesel engine. The authors found that on adding 0.04 wt.% of EVAC in the blend of biodiesel and diesel B20 (20 vol.% biodiesel + 80 vol.% diesel), there was notable reductions in the values of cold flow properties i.e. 8°C in cloud point, 11°C in CFPP, 10°C in pour point while compared with the neat diesel the values were 8°C in cloud point, 10°C in CFPP, and 10°C in pour point respectively. The effect of ethanol and kerosene (5%, 10%, 15%, and 20%) and Lubrizol 7671 (0.5%, 1%, 1.5% 2%, 2.5%, 3%, 3.5% and 4%) on pumping and injecting of biodiesel in C.I engine was also assessed by Bhale et al. [145]. The results showed that at 20% ethanol concentration the cloud point of Mahua Methyl Ester (MME) was reduced i.e. from 18°C to 8°C and further reduction i.e. upto 5°C was observed for 20% dosing level of kerosene. In addition to this, reduction of 11°C in the value of pour point for 20% ethanol and a reduction of 15°C in pour point value for 20% kerosene blended with biodiesel was observed. Moreover, an overall reduction in the Cloud Point value by 4-5°C, Pour Point values by 3-4°C, and CFPP values by 3°C respectively was observed when Ethyl Levulinate (EL) a bio-based fuel additive was mixed with Cotton Seed Methyl Ester and Poultry Fat Methyl Ester biodiesel [146].

2.5.1. Review on the effect of fuel additives on CI engine combustion

The combustion characteristics of any fuel are usually governed by its chemical composition. One of the important combustion parameter is how quickly the air-fuel mixture will ignite inside the engine within the optimum time. As the ignition of fuel is a radical-driven reaction therefore, the optimum dosage of fuel additives have a considerable impact on ignition properties i.e., by enhancing or retarding the ability for ignition. Sivalakshmi and Balusamy [147] investigated the effect of bio-based additive on the combustion characteristics of neem oil biodiesel. The experiment was carried out on naturally aspirated, 1-cylinder four-stroke direct injection diesel engine fuelled with biodiesel derived from neem oil containing ethanol as an additive and diesel fuel. The findings reported that as the concentration of ethanol increases in the fuel blends, the peak pressure of the engine cylinder becomes higher. However, no significant change in ignition delay was observed for BE5 (5% ethanol in biodiesel) and BE10 blends when compared with neat biodiesel. Apart from the analysis done on single cylinder diesel engines, Kivevele et al. [148] successfully tested 4 cylinders turbocharged direct injection diesel engine in order to find out the effect of using antioxidant additives namely 2-tert butyl-4-methoxy phenol (Butylated Hydroxyanisole, BHA), 3, 4, 5-tri hydroxybenzoic acid (Propyl Gallate, PG) and 1, 2, 3 tri-hydroxy benzene (Pyrogallol, PY) in biodiesel derived from croton megalocarpus oil. The results revealed that at ideal condition, no major change in the value of peak pressure was observed with the addition of additives in the fuel blend as compared to neat diesel. However, at higher loads, the peak pressure recorded higher value for fuel blends containing additives. Moreover, the addition of additives in the B20 fuel blend showed maximum rise in peak of heat release rate as compared to the other test fuels. Musthafa et al. [149] carried out an experiment on single-cylinder four-stroke water-cooled compression ignition engine fuelled with a blend of palm oil-derived biodiesel, di-tert-butyl peroxide (DTBP) cetane index improver additive 1% by volume, and mineral diesel in order to find out

the effect of additive on combustion phenomenon occurring inside the engine cylinder. The results concluded that maximum engine cylinder pressure was reduced when additive is mixed in the B20 blend as compared to mineral diesel fuel. Similarly, the heat release rate was also maximum when the additive was added in the fuel blend as compared to the D100 (neat diesel).

2.5.2. Review on effect of fuel additives on CI engine performance and emission

Many research had been carried out in the past on wide variety of biodiesel feedstocks by incorporating different kinds of additives in order to improve the performance and emissions characteristics of the C.I engines. But the selection of suitable additives should be chosen wisely. Sathiyamoorthi and Sankaranarayanan [150] performed an experiment on CRDI compression ignition (DICI) engine using biodiesel derived from lemongrass oil. The Butylated hydroxyanisole (BHA) and Butylated hydroxytoluene (BHT) was used as antioxidant additives for the analysis. The authors found that on increasing the amount of BHA in the fuel blend LGO25 (25% lemongrass oil derived biodiesel + 75% diesel), the Brake Specific Fuel Consumption (BSFC) value was reduced significantly. An almost similar trend of BSFC was observed in the case of adding BHT additive in the fuel blend. Also, rise in curve of brake thermal efficiency trend was observed with increasing the content of antioxidant additives in the LGO25. The emission results showed that, CO formation were increased by 5.8% at 500ppm, 10.1% at 1000ppm, 14.8% at 2000ppm with the addition of BHA antioxidant in LGO25 fuel blend. Similarly, for BHT antioxidant additive, the CO emissions were increased by 8.5% at 500ppm, 13.2% at 1000ppm, and 16.60% at 2000ppm at full load condition. This can be justified due to the decrease in ignition delay of fuel blends with the addition of anti-oxidant additives and thereby encouraging the formation of CO emissions. The similar trend is observed for unburnt hydrocarbon emissions, which were also found to be slightly higher with the adding the antioxidants in the LGO25 fuel blend. However, the percentage of NOx emissions were slightly lower by the usage of antioxidants additives.

The effect of fuel stabilizing additive namely acetone on the performance of HATZ 2-cylinder direct injection (DI) diesel engine fuelled with diesel and biodiesel derived from castor oil by adding recycled Expanded Polystyrene (EPS) was successfully examined by Calder et al. [151]. The result showed that at all engine conditions, a higher concentration of biodiesel with EPS and acetone has a better BSEC than petroleum-derived diesel fuel. Also, for all blends of biodiesel, EPS and acetone showed higher BTE than diesel. Therefore, the highest value of BTE was recorded for B50 (50% castor oil biodiesel + 50% diesel) with EPS and acetone additives. The results also illustrated that, EPS-dissolved in B50 blends with or without using acetone generates more smoke emissions as compared to diesel.

2.5.3. Challenges associated with the macro/micro scale fuel additives

As categorized above, based on the size, the additives are broadly classified as Macro, Micro and Nano-additives. If the particle size of additives is above 100 micrometres, it is termed as Macro-additives, followed by micro-additives whose size lies in between the range of 100 micrometres to 100 nanometres in diameter [152]. However, challenges such as sedimentation, particles conglomeration arising with the usage of macro and micro additives prohibit their mixing with biodiesel fuel especially with the methyl esters having poor flow properties [153]. Several recent studies conducted in the past on amalgamation of fuel additive in diesel, biodiesel and their blends have highlighted certain challenges and limitations associated with them. Despite of improving the fuel consumption rate of biodiesel fuel, the utilization of oxygenated fuel additives most commonly lower alcohols had resulted in retarded injection timing, lower temperature and consequently incomplete combustion [154]. This can be attributed to the lower cetane index of alcohol fuels. Moreover, the exhaustive review conducted by Kumar et al. [155] to investigate the suitability of organic additives in diesel engines had also reported several issues of phase separation, higher fuel consumption as well as NO_x emissions.

Similarly, there exists a trade-off between NO_x and CO emission when antioxidant nature fuel additive is mixed with biodiesel blends. Additives such as TBHQ, BHA, BHT and EHN are considered as excellent shelf life enhancer of biodiesel fuel. In addition these chemicals also prevent the formation of free radical by reacting with the aromatic amines, thus restricting the NOx formation. However, due to reduction in the oxidation rate of carbon promoted by antioxidants, the CO and HC emissions are significantly higher [156]. Polymer based additives had also shown their potential in the form of fuel stabilizers. However, the inferior flow properties of polymers resulting in poor fuel atomization, the utilization of these additives are usually avoided [157]. Water-in-diesel emulsion strategies were also adopted by various researchers in order to improve the micro-explosion phenomenon, resulting in better fuel atomization. The presence of water in fuel also regulates the local combustion temperature, thus bringing simultaneous reduction the NOx, PM and soot emissions. However, numerous studies had showed that using water-diesel emulsion concept had several disadvantages in terms of incomplete combustion, higher ignition delay due to too early reduction in temperature and higher engine noise as well [158]. Beside water-oil stability is another complicated issue associated with this concept [159].

Thus, the exhaustive literatures survey showed that the "Cure All" perception cannot be achieved with macro/micro fuel additive due to their limited penetration. Apart from this challenges such as sedimentation and particles conglomeration arising with their usage is another major issue which decrease their popularity. Hence, the addition of larger size additives is limited, upto a critical concentration in the base fluid. Therefore, setting a new benchmarks in the field of sciences, transition towards nano-sized particles size having diameter below 100 nm can be easily significant step ahead in the field of fuel additives.

2.6. Review on nanoparticles synthesis and characterization methods

2.6.1. Sol-gel Process

The sol-gel is a popular, economical and versatile chemical method of synthesis that can produce nanoparticles of lower density, porous and fragile nature. It is usually preferred for the preparation of metal oxides, composite materials of viscous nature. Generally, on a broad level the process is completed in four different steps, including hydrolysis and condensation of precursor-solution followed by aging and drying [40]. The end processes again and drying are usually performed by evaporation, heating, or in some cases calcinating at higher temperatures, i.e. (600-800°C). Radhakrishnan et al. [160] and Venu and Madhavan [161] prepared Al_2O_3 nanoparticles by adopting the sol-gel process. Initially, the precursor (0.5M aluminum nitrate solution $Al(NO_3)_3 \cdot 9H_2O$) was continuously stirred at 22°C. After that, chelating agents i.e., 0.05M urea solution followed by adding a 0.1M NaOH solution until the gel formation occurs. In the second and final stage, the gel formed is first dried for 10 hr at 150°C temperature. Lastly, the dried gel was calcinated for 2hr at 300°C to obtain Al_2O_3 NPs. In another sol-gel process adopted for silver oxide NPs, Kumar and Manisha [162] preferred silver nitrate as a precursor and citric acid as the chelate. Hence, the literature outcomes showed that the sol-gel technique allows operating at a low-temperature range providing rigorous control over stoichiometry. Thus, the nanomaterials of high purity, mono-size can be obtained at a low production cost.

2.6.2. Hydrothermal & Solvothermal Process

The hydrothermal and solvothermal process is generally preferred for the preparation of metallic and metallic oxide nanoparticles of varied morphologies. The procedure occurs at high temperature and pressure involving two major steps including hydrolysis of metallic salt solution (precursor) and metallic hydroxide condensation. The time of reaction and temperature are important parameters which controls the morphology of end products generated. Nanoparticles of well-organized structure can be synthesized easily by hydrothermal and solvothermal process. Both the process are similar except in solvothermal process the primary solvent is organic compound in place of water [163]. Therefore, solvothermal process has an

edge of more precise control on shape and crystallinity. Ettefaghi et al. [164] prepared carbon quantum dots (Cqd) by using powdered orange peel as precursor. The precursor was hydrolysed with dH_2O and the solution was placed in an autoclave for 12hr at 180°C. In the next step the autoclave was cooled at room temperature and precipitates were separated by centrifugating the solution at 5000 rpm. Lastly, the precipitates were dried out around 80°C to obtained NPs of Cqd. Similar process was adopted by Vairamuthu et al. [165] for preparation of cerium oxide nanoparticles. The cerium chloride was used as precursor, ammonium hydroxide as the solvent and NaOH (sodium hydroxide) as the pH controller.

Abdollahifar et al. [166] preferred solvothermal process for preparation of aluminium oxyhydroxide (AlOOH) NPs. The precursor used was aluminium nitrate nonahydrate, $Al(NO_3)_3 \cdot 9H_2O$ dissolved in EtOH, acting as the refluxing agent. NaOH solution was used as pH controller. Thereafter, the similar steps of formation was carried out as was adopted in hydrothermal process to obtain finer and specific crystalline nanoparticles of AlOOH.

2.6.3. Co-precipitation Process

It is the well-known and economical method which uses salt and alkaline solution to prepare metallic oxide NPs. In the process of co-precipitation, the alkalines such as NH_4OH, NaOH and KOH are added to the chloride, sulphates or nitrates. Thereafter, the next step involves formation of precipitates under the action of robust stirring. The precipitates formed are washed with hard water or EtOH solution to get rid of agglomeration. Lastly, the process of drying and calcination is carried out at the temperature range of 400-600°C. Phiwdang et al. [167] prepared copper oxide nanoparticles by following Co-precipitation process. A solution of copper chloride and copper nitrate trihydrate was used as the precursor and NaOH as the alkaline solution. The NaOH solution act as pH controller and was added drop by drop till the value of pH reaches to 14. Thereafter, the black precipitates of copper oxide formed is washed with hard water followed by EtOH solution and then dried for 16hr at 80°C temperature. Finally, the

process of calcination was carried out for 4 hr at 500ºC. Thus, the merits of adopting co-precipitation is that the process is less complex, efficient and economical. However, due to inadequacy to control size distribution and shape of produced nanoparticles, the process is under-utilized [168].

2.6.4. Chemical Vapour Deposition (CVD) Method

It is the most-cost effective process for production of nanoparticles especially of carbon nature at mass-scale. The catalyst plays an influential role in controlling the shape, size and properties of nanoparticles synthesized in CVD process. In CVD process, the surface of the substrate is exposed to the volatile nature precursor which react and deposits on the substrate to produce desired product. The by-products formed after the surface reaction is carried away by forced convection mechanism. On the basis of operating pressure and nature the CVD is further classified as: atmospheric pressure, low pressure, plasma enhanced, photochemical, thermal CVD. The previous literature survey highlighted that CVD is most commonly preferred method for preparation of MWCNT and SWCNT nanoparticles. José-Yacamán et al. [169] synthesized MWCNT nanoparticles by using acetylene as a carbon source and Fe nanoparticles as the substrate. The temperature range of 700ºC was chosen for the reaction. The utilization of alkanes as carbon source can improve the production efficiency of MWCNT nanoparticles, study conducted by Plata et al. [170]. The authors used hydrocarbon, ethylene and hydrogen as the precursor. Similarly, Hata et al. [171] produces distinctive and high purity SWCNT nanoparticles by using silicon as a substrate and water assisted ethylene as the precursor. The study also showed the amorphous tendency of carbon can be reduced by controlling the water vapour supply in the reaction chamber. Thus, the outcome obtained from the multiple literature showed that mass scale chiral CNT of high purity, high carbon source rate with easier control and low cost can be prepared by using chemical vapour deposition technique.

2.6.5. Flame spray pyrolysis (FPS) Method

It is a gas phase combustion process which is most versatile, rapid and most promising technique of nanoparticle preparation in which spray act as the precursor. The one step process of flame pyrolysis method produces unique nanomaterials having core-shell structure, pure metals or metal oxide and even nanorods of high surface area can be easily synthesized [172]. The precursors generally used are low cost metals such as nitrates, organometals and carboxylic acid salts. The precursors are dissolved or mixed in organic solvents such as alcohols and aromatics. The prepared samples are combusted to a temperature of 3000ºC in the presence of oxygen. The nanoparticles generated are collected on the filter paper in the form of dry powder. Due to the presence of excess oxygen and higher temperature range, the particles collected in the FPS method are highly crystalline and fully oxidized. Jolly and Bhattacharya [173] synthesized alumina NPs by adopting the process of FPS. Aluminium nitrate nonahydrate mixed with deionized water was used as the precursor. The process was carried out in a flame spray pyrolysis setup which is equipped with three different gases. The liquified petroleum gas (LPG) was used as fuel, oxygen was used for combustion and nitrogen was used as carried gas to transport atomized droplets to the flame zone. The result showed that particles of alumina were of spherical morphology and were also un-agglomerated. Thus, the study showed that properties of nanoparticles such as size, crystalline phase, agglomeration, surface area and porosity can be easily controlled by FPS process.

2.6.6. Physical (Arc Discharge & Ball milling) method

The arc discharge method is generally used for the synthesis of metals, metal oxide and carbon based nanoparticles. It is based on the principle of high potential difference generated between two high voltage electrode kept in a gas or liquid submerged medium. The anode is filled with a catalyst and precursor and the cathode having larger diameter than anode act as the collector. The arc generated due to the potential difference vaporizes the electrode surface and the solvent is condensed on to the cathode to form NPs [40]. The main advantage of the arc discharge

process is the simplicity, lower operating cost and single step production. However, the uncontrol on shape, size and property of nanoparticles, lower yield are some of its major drawbacks. Ando et al. [174] used graphite rod electrodes for the preparation of SWCNT nanoparticles. The electric arc is generated between the anode containing metal catalyst Iron, Cobalt and graphite cathode. Thus, the SWCNT nanoparticles are collected in the form of soot on the cathode.

The ball milling is a mechanical process in which collision takes place between the ball and the powder. The properties and the morphology of nanoparticles to be synthesize is highly dependent on the medium of milling, rotation speed, duration, weight of balls, type of milling and atmosphere inside the milling medium. It is the easier and inexpensive method also the product form is free from any kind of contamination [175]. B_2O_3 nanoparticles were obtained conducting the milling process for about 5 hr at 500 rpm speed by Alizadeh et al [176]. The weight ratio of ball to powder was 10:1. The ball used for milling was made of chromium carbide and the process was carried out in an argon rich atmosphere. Similarly, graphite nanoparticles were prepared by León et al. [177] when Exfoliate graphite and 2,4,6- triamine-1,3,5-triazine (melanine) were deformed using ball-milling process. The process was conducted in the nitrogen atmosphere at an rpm of 100-350 for about 1 hr in a planetary mill. The nanoparticles and their popular method of synthetization in summarized format is shown in **Figure 2.5.**

Top-down	**Arc discharge** **[Al, SWCNT, MWCNT]**
	Ball milling **[B$_2$O$_3$, Graphite, Fe, ZnO,Rice husk]**
Bottom-up	**Sol-gel** **[Ag$_2$O, Al$_2$O$_3$, CuO, SiO$_2$ & TiO$_2$]**
	Chemical vapour deposition **[SWCNT, MWCNT, Ag]**
	Hydrothermal **[CeO$_2$, Cqd, Co$_3$O$_4$]**
	Solvothermal **[Ag, AlOOH]**
	Pyrolysis **[ZnO, Al$_2$O$_3$, SiO$_2$, TiO$_2$, Mn$_2$O$_3$]**
	Co-precipitation **[CuO, γFe$_2$O$_3$, Fe$_3$O$_4$]**
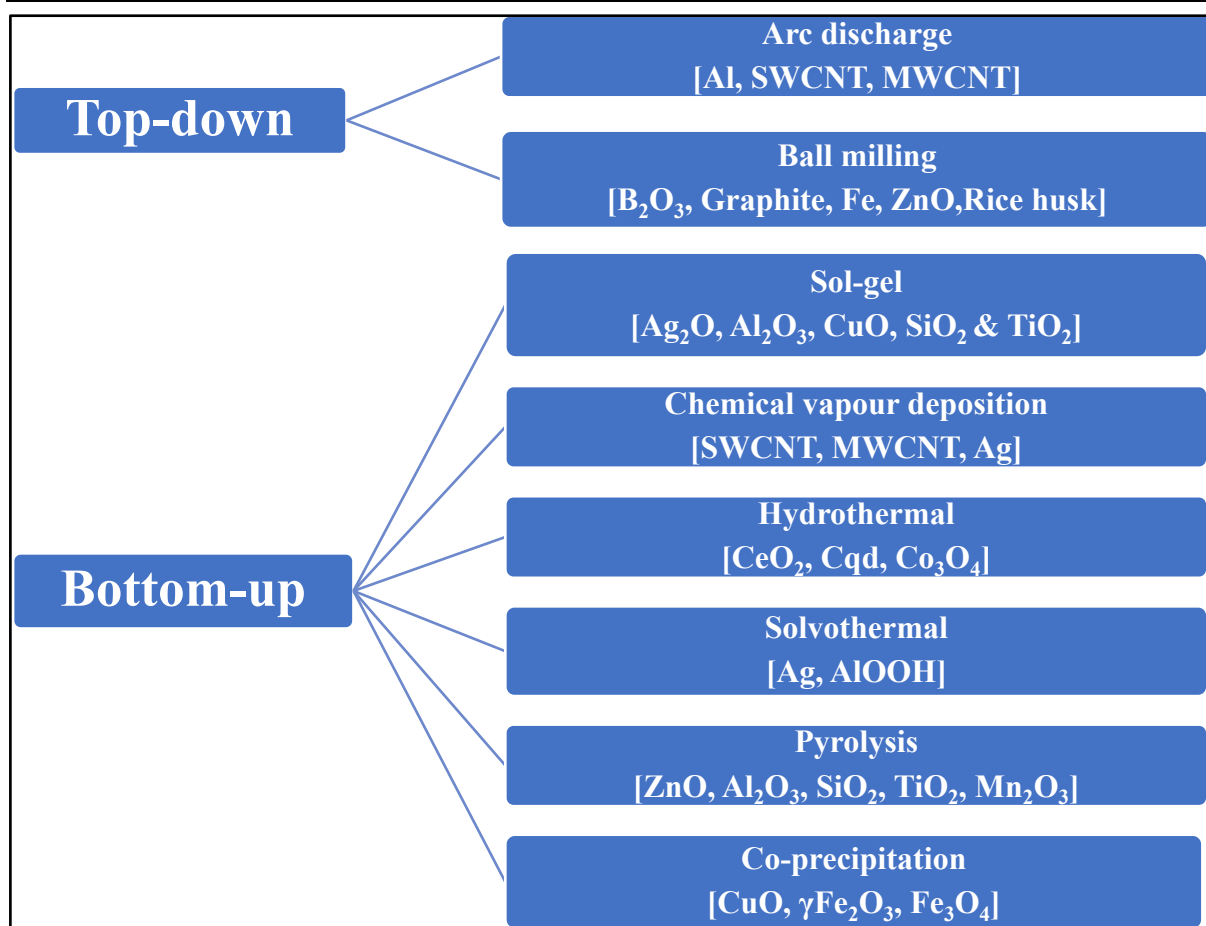
Figure 2.5. Commonly preferred method of nanoparticles synthesis

2.7. Review on physico-chemical properties and engine characteristics of different nano-fuel blends

Nanoparticles having remarkable physico-chemical properties such as higher surface to volume ratio, thermal diffusivity, catalytic activity and better stability (due to nano-size and Brownian motion) than conventional fuel additives can substantially improve the ignition, fuel atomization, performance and emission characteristics of existing CI engines [178]. The outcomes gained from several studies conducted in the past on metallic oxides, non-metallic and ferromagnetic NPs have shown some promising results.

Aalam et al. [179] studied the effect of alumina nanoparticles on the fuel properties and performance of CI engine fuelled with diesel-*Ziziphus jujuba* biodiesel blends. The nanoparticles were dosage of 25 and 50 ppm dosage were added in the base fuel. The nano-

fuel blends showed significant increase in the calorific value and flash point. The brake thermal efficiency was also 20% higher as compared to diesel-biodiesel blend. Sajith et al. [180] showed that dispersion of 40 and 80ppm dosage of cerium oxide nanoparticles increases the flash point and viscosity of the neat jatropha oil biodiesel. However, the cold flow properties remained unchanged. The collective effect of alumina and cerium oxide nanoparticles was also studied by Prabhu [181]. The result showed 30% decrease in NO_x, 60%, 44% and 38% reduction in CO, HC and smoke opacity as compared to neat biodiesel.

Some investigations of nano-fuels were also conducted in the past to overcome the challenges of prolonged ignition delay in CI engines. A comparative study was carried out by Somandepalli et al. [182] on various flammable and combustible liquids to analyse the ignition probability. Authors used hot-plate ignition setup in their investigation. The results showed that addition of alumina nanoparticles reduces the ignition lag by boosting up the initiation temperature. Later, Shams and Moghiman [183] also studied the hot-plate ignition characteristics of neat diesel with or without adding nanoparticles. The outcome showed that metal oxide nanoparticles exhibit higher ignition probability compared to neat diesel. As discussed in the (section 2.2.) evaporation rate of fuel droplet plays a significant role during the combustion process. In order to overcome the detrimental effect of higher viscosity and lower calorific value on fuel evaporation rate Khond and Kirplani [184] doped CNT nanoparticles in neem oil biodiesel. The result showed 86.9% reduction in evaporation time with the addition of 100ppm CNT nanoparticles.

The higher NO_x emission is a major issue especially with utilization of biodiesel and its blends. Even the challenges of increased NO_x emissions is also reflected in various studies performed in the past on nanoparticles as fuel additives especially metal oxides. Roy et al. [185] conducted an experimental study on single cylinder CI engine fuelled with waste cooking oil biodiesel blends and alumina nano-additives. The result showed that presence of oxygen enriched Al_2O_3

NPs facilitates the formation of NOx emission. Similarly, 3.2% increase in NOx emission was observed when light duty 3.7kW diesel engine is operated with nano-fuel blend containing 50ppm CuO, 20%, 80% (by vol.) of Mahua oil biodiesel and diesel respectively Chandrasekaran et al. [186]. Nevertheless, HC, CO and smoke emission were 5.33%, 33% and 12.5% lower as compared to diesel-20% biodiesel blend. The investigation by Nayak et al. [187] on addition of 25 and 50 ppm silver nanoparticles to neat Pongamia biodiesel also showed that NOx emissions were higher as compared to neat diesel and biodiesel. Considering the higher NOx issue researchers probed into different techniques. Based on which, Anchupogu et al. [188] coupled exhaust gas recirculation technique (EGR) and concept of nano-fuel together in their investigation on *Calophyllum inophyllum* biodiesel blends. The engine testing was done on stationary agricultural purpose CI engine and Al_2O_3 was used as nanoparticles. Interestingly, the study showed 35% reduction in NOx emission at 20% EGR rate and 40ppm dosage level of nanoparticles in diesel-biodiesel blend. However, EGR showed no net effect on other harmful emissions and also the overall operational cost were also higher.

Few recent literature had also highlighted that addition of nanoparticles having enhanced heat transfer characteristics (such as ferrocene, ferrofluid (Fe_3O_4) , graphene oxide and CNTs) can significantly encounter the issue of higher NOx emission associated with diesel-biodiesel blends. An overall reduction of 9.04% in NOx emission was observed when 1% by volume of ferrofluid and 0.3% surfactant is added to biodiesel as compared to neat mahua oil biodiesel Devarajan et al. [189]. However, the study also showed that due to the corroding tendency of ferrofluids its dosage is to be limited to only $\leq 1\%$ by volume in the base fuel. Nagaraja et al. [190] investigated the potentials of graphene oxide nanoparticles as a fuel additive for rice bran oil biodiesel blends. As compared to neat diesel, the 5% and 15% blend of biodiesel showed about 60% in NOx emission at ignition timing of 23º and 25º. Similarly, in the investigation on addition of 250mg/lt. and 300mg/lt. of ferrocene nano-additives in diesel and diesel-

biodiesel blend, respectively showed significant reduction in NO_x emission as compared to D100 and B30 blend (Elwardany et al. [191]). Carbon nanotube NPs such as single walled and multiwalled are among the greatest discovery of present times. These compounds are known for their extreme light weight, higher strength and excellent heat transfer properties. Even studies conducted in the past on CNT nanoparticles had proved the potentials as an excellent absorbent of nitric oxide, carbon dioxide and sulphur dioxide [192, 193]. Also their flexible and cheaper production have made increased their popularity in the world-wide market. Considering this, CNTs can be a promising fuel additive for CI engine. Handful of studies have also highlighted their potentials. El-Sessy et al. [194] examined the effect of dispersing 20mg/litre of MWCNT in diesel-biodiesel blend. The result showed 35% reduction in NO emission followed by 50% in CO and 60% in HC respectively. Also, 7% and 4% improvement in cylinder pressure and neat heat release rate was also observed. However, study has highlighted poor stability due to agglomeration tendency of MWCNT in the base fuel. In another study on CNT by Sadik and Basha [195] the surfactant tween 80 and span 80 added in order to improve the stability of biodiesel blends. The results of the stability analysis showed no phase separation sign for 1 month. Also, the study showed greater influence on reduction of NO_x emissions. The effect of addition of different kind of additives with on the diesel engine characteristics are summarized in **Table 2.3.**

Table 2.3. Variation of performance and emission characteristics of CI Engine fuelled with diesel/biodiesel/blends and additives of dissimilar types

Fuel/Fuel blend/additive	Additive Conc.	Engine specs	Test conditions	Performance characteristics (full load)		Emission characteristics (full load)		
				BTE	BSFC	CO	HC	NOx
B20+BHA, B20+BTA compared with **B20** (Fattah et al. [196])	2000ppm	4-cylinder, 55kW, 2500cc	Variable speed	*↑	*↓	↑	↑	↓
				↑	↓	↑	↑	↓
B100+PY compared with **B100** (Kivevele et al. [197])	1000ppm	4-cylinder, 66kW, 1896cc	Different loads	↑	↓	NC	↑	↑

Some studies on nano-particles doped alternative fuels in Unmodified CI Engine

Study	Dosage	Engine	Test condition					
B20+DPPD compared with B20 (Varatharajan and Cheralathan [198])	1000ppm	1-cylinder, Kirloskar TAF-1, 4.4 kW, 2500cc	Different B.P condition	S.I	----	↑	↑	↑
B100+DPPD compared with B100 (Varatharajan and Cheralathan [198])	2000ppm			S.I	----	↑	↑	↓
B100+Ethanol compared with B100 (Bhale et al. [145])	20 %vol.	1-cylinder, water-cooled, 17.5:1	Different bmep	↑	----	↓	↑	↓
B98+P2, B95+P5, B90+P10 and B85P15 compared with B100 (Kuzhiyil and Kong [199])	2, 5, 10, 15% (by wt.)	4-cylinder, 4500cc	Steady state	----	↑	S.I	S.I	↑
				----	↑	S.I	S.I	↑
				----	↑	↑	↑	↑
				----	↓	↑	↑	NC
B95+W compared with B100 (Debnath et al. [200])	5% (by vol.)	1-cylinder, 3.5 kW, 661cc	Different loads	↑	↓	↓	↑	↓
B90+W10, B90+W10A5 compared with B100 (Lin and Lin [201])	10 (wt.%) water and 5 (wt. %) aqueous ammonia	4-cylinder, 3856cc	Variable speed	----	↑	↑	----	↓
B100+TBHQ compared with B100 (Ryu [202])	300, 500, 1000 and 2000ppm	4-cylinder, 2607cc	Different loads	----	↓	NC	↓	↑
AN20+ 1,4-dioxane compared with AN20 (Ramaligam et al. [203])	5, 10ml	1-cylinder, 5.9kW	Different B.P	↑	↓	↓	↓	↓
B100+FeCl₃ (metal-based np's) compared with B100 (Kannan et al. [204])	(20 μmol/L)	1-cylinder, 5.2 kW, 661cc	Different bmep	↑	↓	↓	↓	↑
B20+Ce (metal oxide np's) compared with B20 and B100 (Dhinesh et al. [205])	10, 20 and 30ppm	1-cylinder, 5.2 kW, 661cc	Different load	↑	↓	↓	↓	↓
B100+ZnO & B100+TiO₂ compared with B100 (Nanthagopal et al. [206])	50, 100 ppm	2-cylinder, 21kW	Different bmep	↑	↓	↓	↓	↓
B100+CNT compared with B100 (Balaji and Cheralathan [207])	100, 200 and 300 ppm	1-cylinder, 3.5kW	Different B.P	↑	↓	↓	↓	↓
D100+Ce, D100+CNT compared with D100 (Zhang et al. [208])	Ce:25, 50 CNT:40	4-cylinder, heavy duty cummins ISB4.5	Different Load	----	----	↑	↑	↑
D100+Ce compared with D100CNT (Zhang et al. [208])			Different Load	----	----	↑	↑	↑

*PY: Pyrogallol, BHA: Butylated Hydroxyanisole, BTA: Butylated Hydroxytoluene, DPPD: N,N′-diphenyl-1,4-phenylenediamine, P: Polystyrene, W: Water, A: Aqueous ammonia, TBHQ: tert-Butylhydroquinone, FeCl₃:Ferric Chloride, Ce: Cerium oxide, AN: Annona biodiesel, ZnO: Zinc oxide, TiO₂: Titanium oxide, CNT: Carbon nanotubes, B100: Neat biodiesel, D100: Neat diesel, S.I: Slightly increase, NC: No change, , ↑↓: increase/decrease.

Some studies on nano-particles doped alternative fuels in Unmodified CI Engine

2.8.   Outcomes of Exhaustive literature review

After undergoing the exhaustive literature review, the critical findings are drawn, which are listed below:

➢ Diesel engines are the lifeline of millions of on-road and off-road vehicles, and also the backbone of global economic expansion.

➢ Despite the immense availability of seeds and higher oil content, the utilization of *schleichera oleosa* oil biodiesel continues to be underutilized.

➢ Regardless of the sustainable origin, the biodiesel economy is losing its importance. Primary matter of concern is its deficient long-run operability in CI engines.

➢ Direct utilization of higher biodiesel blends (≥30% by vol.) requires certain engine retro-fitments to prevent engine deposits, clogging of parts, injector chocking, etc.

➢ The state-of-the-art surrogate fuel reformulation concept of nano-fuels can serve the dual purpose of regulating environmental challenges and stimulating the biodiesel performance in CI engine.

➢ Nano-size fuel additives can fix those areas of interest where bulk-size additives fail to penetrate and serve as a "Cure-all additive" role in existing CI engines.

➢ Physico-chemical properties of nanofuel blends are comparable to neat diesel and significantly higher than neat biodiesel.

➢ Although the dispersion of metal oxide nanoparticles with biodiesel blends showed better stability and improved engine performance, NO_x emission remains a major challenge due to their oxygen-enriched nature.

➢ The surfactant act as a stability enhancer for nano-fuel blends as its dispersion can prevent the agglomeration tendency of nanoparticles to a greater extent.

➢ The combined effect of EGR and nanofuel concept or utilization of nanoparticles with enhanced heat transfer properties can significantly regulate the rate of NO_x emission from the CI engine.

2.9. Research gap analysis

In consideration of the literature survey and outcomes discussed in the preceding sections, the following research gaps were established:

➢ So far, limited investigations were conducted on engine characteristics of *schleichera oleosa* biodiesel and its blend.

➢ Nanoparticles synthesis and characterization process plays a major role in preparation of nano-fuel blends. However, very few literature are available which highlights the production and characterization processes of nanoparticles.

➢ Agglomeration of nanoparticles over time is a critical challenge while working with nano-fuel blends. The studies highlighting the storage stability lacks profound research.

➢ Work focussing on the ignition characteristics and evaporation time of nanoparticle dispersed fuels are very limited.

➢ Influence of nanoparticles on macro and micro spray characteristics of diesel-biodiesel blends still remains uncharted.

➢ Despite of excellent pour point depressant and also the sorbent of NO, CO and SO_2, the utilization of CNT nanoparticles as fuel additive is not actively explored.

➢ The majority of literature doesn't clearly illustrate the mechanism behind the improvement in different engine characteristics by adding nanoparticle.

➢ Limited studies have been found in which optimum dosage level of nanoparticles to be dispersed in the base fuel (diesel, biodiesel and blends) is determined.

2.10. Problem Statement

After carrying out the exhaustive literature survey on different aspects, it was observed that nanoparticles and their dosage level have greater influence on the diesel engine's physico-chemical properties and engine characteristics. Even though a decent amount of research was done on nano-fuels, identifying potential additive in terms of economical production cost, stability with the base fuel, and delivering the optimum level of engine performance lacks profound research. Many literatures have reported that the addition of nanoparticles triggers the cetane number and calorific value of the biodiesel and their blends. A detailed discussion on the heat transfer mechanism of nanofluids which helps in improving the ignition characteristics still requires deeper penetration. In addition, as already stated in the earlier sections that smaller is the droplet size of the fuel better will be the evaporation rate resulting in improved combustion. However, the influence of adding nanoparticles on spray characteristics is still an uncharted area of research.

Furthermore, for a country like India where there are hundreds and thousands of existing agricultural engines, the immense availability of *Schleichera oleosa* in the country can be promising biodiesel feedstock. Therefore, the prime motive of the present study is to improve the operability (performance, combustion and emission characteristics) of *Schleichera oleosa* biodiesel blend as an alternative fuel for farmland engines by utilizing the advantages of alumina and MWCNT nanoparticles.

2.11. Research objective

The objective proposed for the accomplishment of the present work are as follows:

- ➢ Selection, preparation and characterization of arrogate nano-particles which can serve the purpose of "Cure all additive" for CI engine.
- ➢ Production and Characterization of Biodiesel.
- ➢ Doping of nano-particles in diesel-biodiesel blend in desired proportion.

➢ Analyze the short/long-term stability of all nano fuels at different environmental conditions.

➢ Determination of physico-chemical properties of all test fuel in accordance with relevant standards and compare the results with petroleum diesel.

➢ To evaluate the Ignition probability of the test fuels.

➢ To study the spray characteristics of different fuels using Malvern spraytec.

➢ Selection of the diesel engine test rig for experimental trial.

➢ Experimental evaluation of combustion characteristics of different test fuels with the help of P-θ and heat release rate diagrams.

➢ Analysis of nano-fuel blends performance and emissions characteristics at different engine loading conditions and comparing the outcomes with biodiesel blend & petroleum diesel fuel taking it as base line data.

➢ Optimization of nano-particles dosage level and engine operating condition at which optimum performance and emission characteristics can be achieved.

SYSTEM DEVELOPMENT AND METHODOLOGY

3.1. Introduction

This chapter gives an in-depth description of the entire research work and also the procedures followed to accomplish the objectives discussed in the problem statement section of the previous chapter. The flowchart in **figure 3.1** gives the summary of the research methodology adopted in the current study.
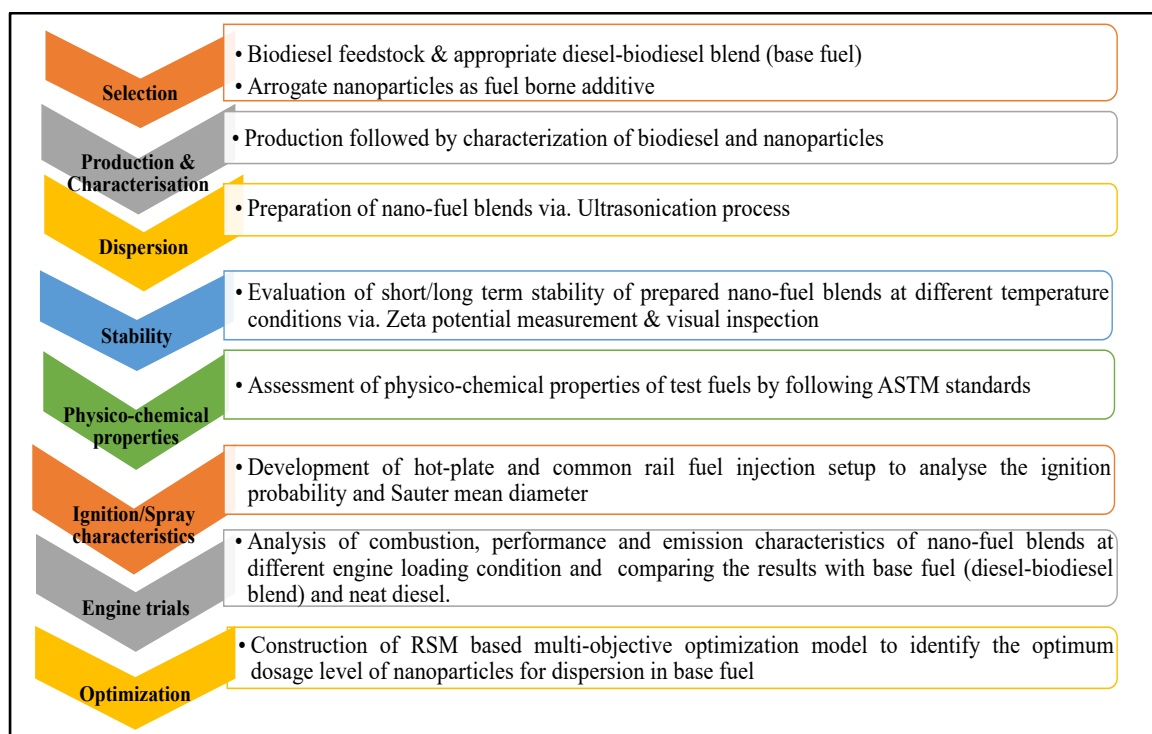
Figure 3.1. Research methodology process flow

In the present study, the selection of potential inedible oil biodiesel feedstock and nano-additives were carried out taking into consideration the results reported in previously available literatures on diesel-biodiesel blends. The chapter also describes the step by step process followed for the selection and preparation of test fuels required for conducting the experimental work. The production and characterization of biodiesel and nano-additives are also explained in detail. The long-term stability at different environmental conditions has been discussed to

make sure the prepared nano-fuels are stable and colloidal. Moreover, the fuel properties such as density, flash point, fire point, kinematic viscosity, calorific value, and cetane index, etc. of test-fuels were evaluated using relevant ASTM standards. The development of hot-plate test-setup, common rail unit for analyzing the sauter mean diameter and engine test rig for determining the engine characteristics of test fuels have been described in detail. The chapter also explains all the procedures and instruments used for calculating the combustion, performance and emission parameters. In the end, the accuracy and uncertainty associated with all the measurement performed are also described.

3.2. Selection of feedstock and production of Biodiesel

The cheaper and continuous availability of feedstock is a major challenge in the road to the commercialization of biodiesel industries. In view of this, non-edible oil seed plant Kusum oil (local name) or *Schleichera oleosa* (Botanical name) was selected as a feedstock for the biodiesel production. *Schleichera oleosa* is a dense evergreen tree, member of Sapindaceae family with 35-50 ft tall in height and size of the kernels ranging about 1.5cm long and brown in colour as shown in **plate 3.1.**

Plate 3.1: *Schleichera oleosa***; A: Dense evergreen tree; B: Kernels.**

The seeds of *Schleichera oleosa (S.oleosa)* tree are enriched with higher oil content (35-40%), 4-6% moisture and 22% protein. However, the higher free fatty acid content (5-11%), iodine value ranging between 215-220 mg I_2/100gm of oil and the presence of unsaturated fatty acids

namely Palmitoleic, Palmitelaidic, Oleic and Elaidic etc. all together limits its use for human consumption. In addition, the multiple literatures in the past had also reported the existence of about 0.03-0.05% of cyanolipids (exists as hydrogen cyanide) in the kernels of the *S.oleosa*, conforms its toxicity and inedible nature [209]. The Asian countries, mainly sub-continents and central regions of India have a vast availability of *S.oleosa* trees. With the annual production potential of more than 25,000 tonnes of *S.oleosa* oil in India, only one-fourth is utilized while rest is used for fuelwood, charcoal production or left abandoned [210]. Therefore, creating a promising gateway for production for biodiesel production in the Indian context.

3.2.1. *Schleichera oleosa* biodiesel production

Due to high viscosity, low oxidation stability and poor combustion and performance, the utilization of straight vegetable oil in the CI engine is not recommended. Various techniques had been investigated in the past to mitigate these severe issues. These involve pyrolysis, catalytic cracking, transesterification and formation of microemulsion or blends with diesel [211]. Amongst all, the transesterification of vegetable oil is the most efficient way to improve the usability of vegetable oils.

Therefore, biodiesel of *S.oleosa* oil was prepared by adopting the process of transesterification. This process involves a reaction between glyceride (oil) and alcohol (usually methanol and ethanol) in the presence of an alkaline catalyst, producing esters and glycerol as the final product. However, the *S.oleosa* oil contains undesirable constituents in its structure, which leads to higher free fatty acid (FFA) content in the oil. The result of which direct transesterification might result in saponification instead of ester formation. Considering this, the primary step of biodiesel formation involves the determination and reduction of free fatty acid content before proceeding directly on to the transesterification reaction. The procedure for acid value and free fatty acid measurement measuring is explained in the next section.

3.2.1.1. Determination of Acid number and Free Fatty Acid (FFA) Content

The acid number is defined as the amount of sodium or potassium hydroxide (in milligram) required to neutralize the free fatty acids present in 1gm of oil. It is an indirect measurement of the FFA content present in the oil sample. In the present study, the acid number was calculated by preparing a solution of 1gm filtered *S.oleosa* oil and 10ml of methanol in a burette, further followed by the addition of two phenolphthalein drops in the solution, which act as an indicator. Later, the solution is titrated with drop by drop of (0.1N) potassium hydroxide (KOH) filled in the burette. The process is continued until the solution turns and remains into pale pink colour for more than 30 seconds. Lastly, the amount of potassium hydroxide consumed is noted down by reading the mark on the burette. Thus, the acid number and fatty acid content are calculated by using the following formula:

$$\text{Acid number} = \frac{Mol.W(alkali) * V * N}{W} \quad\quad\quad (3.1)$$

Where,

Mol.W(alkali) = molecular weight of KOH; V= Volume of KOH consumed in milligrams; N= Normality of KOH solution; W= Weight of the oil sample (grams)

After measuring the acid number by using the above given formula, the FFA of the *S.oleosa* oil sample was determined by:

$$\text{FFA} = \frac{Mol.W(Oleic\ acid) * V * N}{W} \qu\quad\quad (3.2)$$

Where,

Mol.W(Oleic acid) = molecular weight of Oleic acid in 1 ml N/10 KOH; V= Volume of KOH consumed in milligrams; N= Normality of KOH solution; W= Weight of the oil sample (grams)

3.2.1.2. Esterification of *Schleichera oleosa*

The FFA content in the *S.oleosa* oil was found to be more than 2%, which might result in the saponification of free fatty acids during transesterification of oil. Therefore, the next step includes the reduction of FFA content by using the esterification reaction. In the esterification

Some studies on nano-particles doped alternative fuels in Unmodified CI Engine

process, the *S.oleosa* oil reacts with alcohol in the presence of an acid as a catalyst. The reaction was conducted in a three-neck round bottom flask, alcohol used was methanol and PTSA (p-Toluenesulfonic acid) as an acid catalyst. Out of three-neck, one was connected to the water-cooled condenser, which helps in the recovery of methanol vapours. The thermometer was installed on the other neck, which measures the temperature of the flask. The remaining neck was used for adding the chemical or collecting the sample and is covered with an airtight rubber cork.

Also, before proceeding on to esterification reaction, the oil was preheated for about 30-40min at 120°C, to boil off the water content. After removing the moisture or water content, it is again allowed to cool down to 60°C before starting the next step. In the acid catalyst esterification reaction, the solution of oil and methanol is heated on a hotplate magnetic stirrer for about 120 minutes, 1000rpm at 60°C. The alcohol to oil ratio was taken as 6:1 and concentration of catalyst as 0.5(%w/w). The end product obtained after completion of the reaction is esterified oil, surplus methanol, catalyst and water. The esterification reaction is shown in equation 3.3.

$$R\text{-}COOH + CH_3OH \quad \rightarrow \quad R\text{-}COOCH_3 + H_2O \tag{3.3}$$
$$\textbf{(Fatty acid)} \quad \textbf{(Alcohol)} \qquad \textbf{(Ester)} \qquad \textbf{(Water)}$$

The presence of water, alcohol or any other impurities in the esterified *S.oleosa* oil might affect the transesterification process and is required to be removed. Therefore, to get rid of traces of any moisture content or alcohol in the oil, the mixture was poured and then heated again at 100°C temperature for 1 hr in a rotary evaporator under vaccum conditions. After that, the FFA content of oil was rechecked and was found well within a specified range i.e. (1.8%). However, in case if the fatty acid content is still above a critical limit, the process can be repeated again until the value of FFA is reduced.

3.2.1.3. Transesterification of *Schleichera oleosa*

The esterified *S.oleosa* oil having lower FFA content was converted into fatty acid methyl esters in the presence of a strong base catalyst. The end product produced during this process

is fatty acid alkyl esters (also known as biodiesel), and glycerol and the reaction is known as transesterification. The layer of glycerol formed is further separated from alkyl ester by using the gravity separation technique. **The transesterification reaction is shown below:**

(Triglyceride) **(Alcohol)** **(Alkyl Esters)** **(Glycerol)**
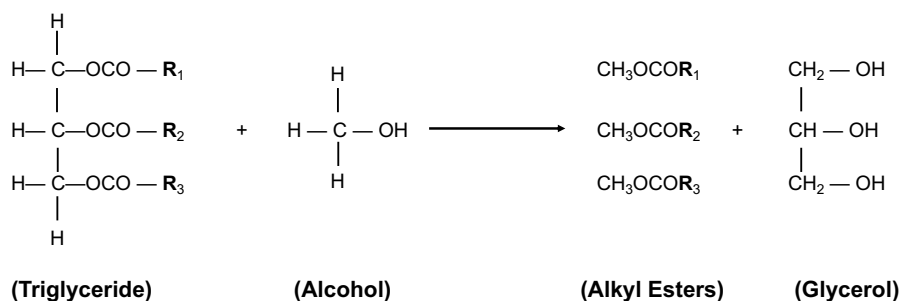
Figure 3.2. Mechanism of transesterification route

The catalyst and alcohol chosen for the present study were potassium hydroxide and methanol, respectively. Also, all the chemicals used for the current reaction were 99% pure. Thus, the primary step involves the preparation of catalyst and alcohol mixture in a small beaker. A 6:1 molar ratio of methanol to oil and catalyst concentration of (1% w/w) was considered for complete triglyceride conversion. The mixture was heated and mixed on a stirrer equipped hotplate at 60°C temperature for 100 minutes. To ensure efficient mixing of methanol with oil, the stirrer was kept constant at 1200 rpm throughout the process. Depending on the characteristics of *S. oleosa* oil, the reaction was allowed to run for 90 minutes. Later, the mixture was poured and kept undisturbed for 24 hr in the separating funnel, after completion of the transesterification process. Thereafter, the layer of glycerol was separated, and the biodiesel obtained was undergone hot water washing to remove any traces of catalyst, excess alcohol and glycerol left inside. The water washing continued until the clean layer of water was formed on the lower side of the separating funnel. In the end, the biodiesel is heated at 100°C to boil off any traces of water content left behind in the water washing step as shown in **Plate 3.2.** The schematic of step by step biodiesel formation from *S.oleosa* oil is shown in **Figure 3.3.**
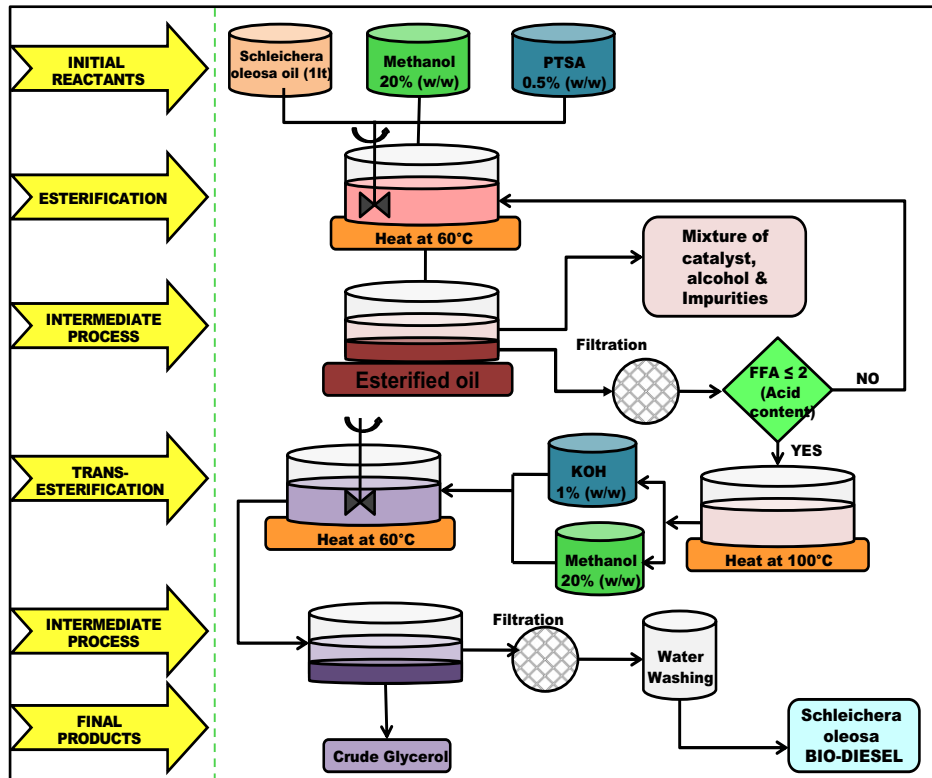
Figure 3.3. Schematic of *Schleichera oleosa* oil biodiesel production using two-step transesterification process
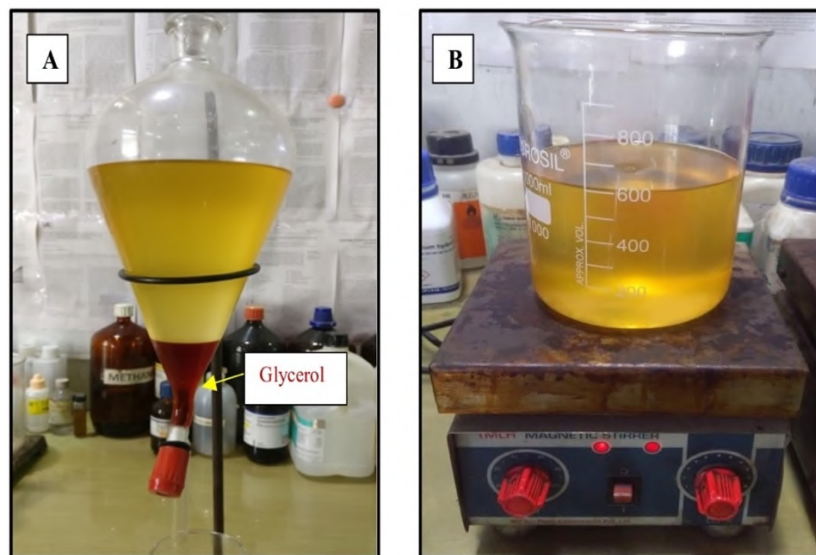
Plate 3.2. *Schleichera oleosa* oil Biodiesel production; **A:** separation of glycerol layer; **B,** removing moisture from biodiesel heating at 100ºC

3.2.2. Characterization of *S.oleosa* Oil Methyl Ester (SOME) compounds

The analysis of Gas Chromatography and Mass Spectroscopy (GC-MS) was performed on (Shimadzu, Japan, Model/Serial Number GCMSQP2010 PLUS) equipped with a flame

Some studies on nano-particles doped alternative fuels in Unmodified CI Engine

ionization spotter and Agilent DB-2887 column (10m × 0.53mm × 3.0μm). The Agilent DB-2887 column is a flow-through tube within which different constituents present inside the sample is passed at varying rates by means of a carrier gas. The passing rate of sample constituents is dependent on their physico-chemical properties and also their behaviour with the distinct column filling, also known as stationary phase. As soon as the constituents exit the column filling, they are captured and spotted via electronic means. The stationary phase serves the function to separate different constituents/compounds by triggering each one to leave the column separately at different time also known as retention time. In case of mass spectroscopy, the gas is transformed into ions.

In the present study, to investigate the GC-MS profile, a pre-weighed 0.1μl, sample of *schleichera oleosa* (*S.oleosa* oil) methyl ester was inserted into the GC column with the spotter and temperature of the injector is retained at 350°C. The inert nitrogen was used as a carrier gas for transporting the liquid sample. The GC oven temperature was controlled programmably in a manner that it increases 15°C/min after every step. Thus, GC-MS analysis provides the information regarding the composition and types of different fatty acid compounds present in the oil, which further helps in predicting the nature of different physico-chemical properties of biodiesel.

3.3. Selection of optimum diesel-biodiesel blend (Base fuel)

The primary target of the present research is to identify the optimum dosage of diesel and *S.oleosa* biodiesel blend which can be preferred as a base fuel for dispersing the nano-particles. As already discussed in chapter 2, the higher viscosity, inferior calorific value and formation of crystals at lower temperatures resulting in clogging of fuel filters, etc., are some of the major drawbacks, restricting the utilization of biodiesel as a complete replacement fuel. In view of this, blending of diesel fuel with methyl esters of vegetable oils is currently the best-known form of biodiesel. There have been countless reports available in the past that considerable

improvement in engine performance and emission reduction are obtained with blends of biodiesel primarily lower blending percentage (i.e. ≤ 20 % by volume). The most popular ratio is 80% diesel fuel (D) and 20% methyl ester, also termed B20, indicating the 20% level of biodiesel. The physico-chemical properties of D80B20 blends were stated to be well within the comparable range of neat diesel. Also, the large-scale testing of D80B20 blend showed no adverse impact on engine life, thus eliminating engine retro fitments [212,116]. Thus, considering the above viewpoints D80B20 was selected as the base fuel.

Another advantage of biodiesel blend is the simplicity of fuel preparation, which only requires mixing of the components. An economical splash blending method was adopted for mixing of diesel and biodiesel. It involves mixing of fuel precisely for a particular period of time to obtain a homogenous mixture. The physical appearance of the neat diesel, biodiesel and prepared diesel-biodiesel blends is shown in **Plate 3.3**. The physio-chemical properties such as density, viscosity, calorific value and cetane index of the prepared test fuels were also evaluated using relevant ASTM standards.

Plate 3.3. Physical appearance of neat diesel, *S.oleosa* biodiesel and their blend

3.4. Selection of arrogate nano-additives and their dosage level

Every chemical or foreign substance serving the role of fuel additive should possess some unique features or functionality for which it is being mixed with the base fuel. In fuel industries, the additives are mainly differentiated based on their role/function or remedies they are offering

to the engines. Apart from this, factors including economic feasibility, availability, toxicity, additive stability and physio-chemical properties of the fuel are also important.

Based on the literature review, it was observed that the oxidation of biodiesel over a period leads to poor performance and emission and secondly, the release of harmful NO_x emission is also the major concern of biodiesel usability. In view of this, aluminium oxide (Al_2O_3) and multi-walled carbon nanotube (MWCNT) nanoparticles were selected as an additive on account to encounter the problems and difficulties associated with biodiesel and its blend in CI engines. The doping of oxygenated aluminium oxide or alumina with biodiesel and its blend can be a breakthrough in improving the shelf life of biodiesel. The availability of extra oxygen in the fuel imparts efficient burning of fuel mixture, improved performance and reduction of soot formation. On the other side, MWCNT having exceptional thermal conductivity, low density and ideal absorbent of gases such as NO, SO_2 and CO_2 can play a significant role in eliminating the problems of harmful NO_x emissions associated with the combustion of biodiesel and its blends. The dosage of additives to be added in the fuel is a complex phenomenon. It is mainly dependent on the mixture's chemistry, chemical composition and stability of foreign substance (additive) in the base fuels. A detailed discussion on the dosage of nano-additives opted for doping in the present research is explained further in the stability section of the thesis.

3.4.1. Synthesization of Nanoparticles

3.4.1.1. Aluminium Oxide or Alumina (Al_2O_3) Nanoparticles

Aluminium oxide is the member of metal oxide nanoparticles (NPs) family. In the present study, the alumina (NPs) were prepared by adopting the cost-effective and controlled 'Sol-Gel' method. It is a wet-chemical technique, wherein gel (integrated network) is prepared with the aid of either a chemical solution or colloidal particles, titled as a sol. Usually, for synthesization of metal oxide nanoparticles, metal alkoxides and metal chlorides are utilized as precursors.

Therefore, advancing ahead, the precursor goes through the process of polycondensation or hydrolysis to develop a colloid (nanoparticles dispersed in a solvent as known as sol). The sol developed is then kept undisturbed for about 48 hrs to obtain a gel (liquid phase). Thereafter, in the next step, the drying of gel is carried out to split up the liquid part and lastly it is calcinating further to obtain the final product.

The chemicals used for the preparation were purchased from 'AVS Biochemicals' and are of AR grade. **Figure 3.4.** shows the schematic of alumina np's production. The Ethylenediaminetetraacetic acid (EDTA) served the purpose of chelating agent during the synthesis process. The role of the chelate is to react with metal ions and forms a stable solution. In addition, it also facilitates in isolating the metal ions. The synthesis was carried into two stages. The initial step involves formation of primary gel by adding 24 gm of aluminium chloride in 100 ml of ethanol and stirring the solution for 3 hrs. Later, EDTA chelate in a specified quantity i.e. 12 ml was added and stirred continuously for another 3 hours until the zerogel formation intervenes. The gel thus obtained is collected and dried in the oven, operating at a temperature of 100°C and kept untouched for about 48 hrs to separate the liquid part. The secondary step of synthesis involves solid mass formation. The zerogel obtained was sintered in a hot-furnace at 900-1000°C for approximately 2 hrs to shape stable alpha aluminium oxide. Thus, the final product obtained is fragile and porous in nature with low density. Later, to obtain fine white powder of aluminium oxide, the sintered bulk material is placed in a ball milling machine for about 6 hrs at the speed of 350 rpm. The high-speed collisions force between the balls breaks down the solid mass and the desired nanoparticles were prepared **(Plate 3.4).**
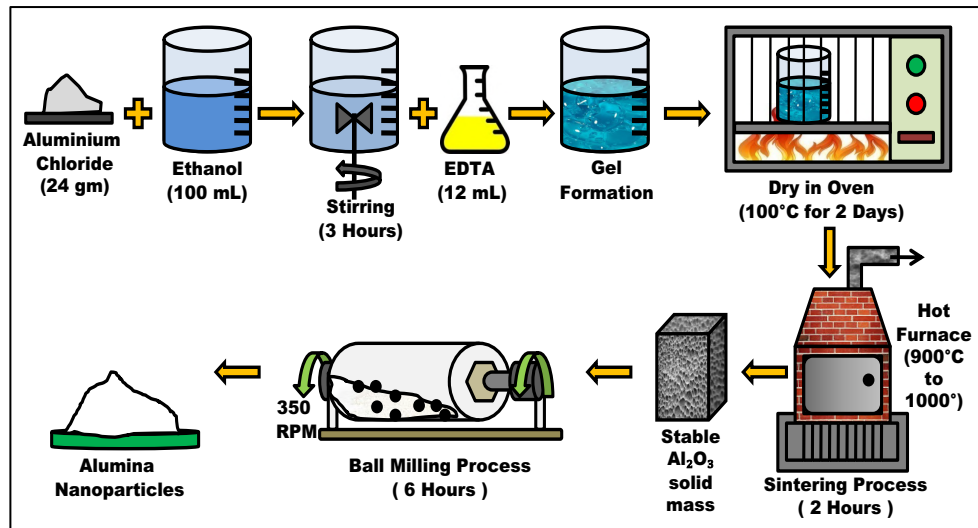
Figure 3.4. Schematic of alumina nanoparticles synthesis using sol-gel process

Plate 3.4. Synthesized aluminium oxide nanopowder

3.4.1.2. Multi-Walled Carbon Nanotubes (MWCNT) Nanoparticles

MWCNT belongs to the fullerene structural family having thickness equals 1 to 2 nm and diameter of less than 100 nm. In the present study, The synthesis of MWCNT in the present study was synthesized by adopting the most preferred and economical method known as Thermal chemical vapour deposition (TCVD). The process includes breakdown of hydrocarbon at sufficiently high temperatures in a tube-shaped reactor with the aid of an activated metal catalyst. The methane, ethylene, acetylene, and benzene are commonly preferred as the hydrocarbon sources. The schematic of TCVD is illustrated in **Figure 3.5**. In the present research, benzene was used as a source of hydrocarbon. The first step involves heating of hydrocarbon in a round bottom flask to about 80ºC and analogously purging the

inert gas into the system. Nitrogen is used as the inert gas. It serves the dual purpose of acting as a medium to transfer the vapours of hydrocarbons into the reaction zone and secondly, reduces the oxygen concentration inside the reactor to prevent the formation of any ignitable mixture. Thereafter, the break-down of hydrocarbon vapours took place in the next step. The vapours of benzene were permitted to pass continuously on to the catalyst material via. tubular type reactor for about 1 hr duration. The temperature of catalyst was maintained at 700ºC to facilitate the breakdown process. The nanoparticles of Iron served the role of catalyst during the experiment due to the higher solubility and diffusion rate of carbon in Iron. The moment benzene vapours comes in close contact with the hot catalyst, it at once decomposes the hydrocarbon into carbon and hydrogen. The carbon gets diffused into the metal nanoparticles (Iron) and hydrogen flutters away. Later, as soon as the diffused carbon reaches its solubility at that particular temperature, it gets precipitated on the top. **Plate 3.5** portrays the photograph of synthesized MWCNT NPs. The crystallization of carbon atoms chain packed closely starts in the shape of a cylindrical network. The crystal formation is a continuous process where subsequent deposition of benzene hydrocarbon takes place on the top surface of the metal until the concentration gradient prevails in the metal catalyst, which permits carbon diffusion.
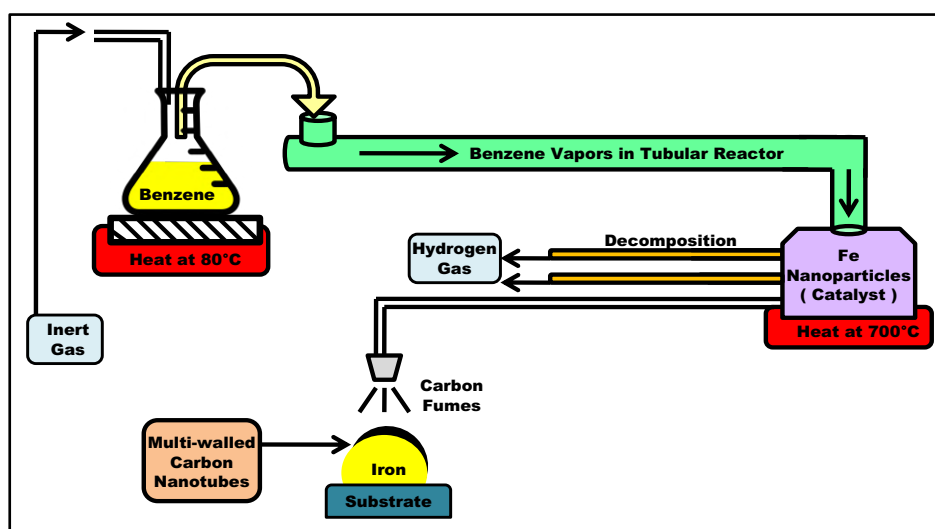
Figure 3.5. Schematic of MWCNT synthesis using TCVD process

Plate 3.5. Synthesized multi-walled carbon nanotube nanoparticles

3.4.2. Characterization of Alumina and MWCNT nanoparticles

The study of nanoparticles features including its structure, pattern, topology and crystallinity signifies its characteristics. The prepared nanoparticles can be in any form such as spherical, tubular or irregular shape and it may exist in any form fused, agglomerated and aggregated. Therefore, in the present research two different techniques i.e., Scanning Electron Microscopy (SEM) and X-ray Diffraction spectroscopy (XRD) were used to identify and confirm the formation of desired nanoparticles.

SEM works on the principle of electron beam and magnifies object upto 15,000 times more compared to light microscope. As compared to light beam, the wavelength of electron beam is much shorter thus resulting in higher resolution of the image. It is capable of generating 3-dimensional view of any specimen which is being measured. The beam of electron is produced with the help of electron gun at the tip of the microscope. Also, to avoid any obstruction in the path of beam, it is held within a vacuum. The beam following the vertical path is focused to strike on the sample by passing it through electromagnetic field and lenses. As soon as the electron beam strike the sample, the electrons and X-rays are scattered out from the sample which are further collected through detector. Finally, the signals received from the detector are processed and displayed on the screen as shown in **Figure 3.6**.
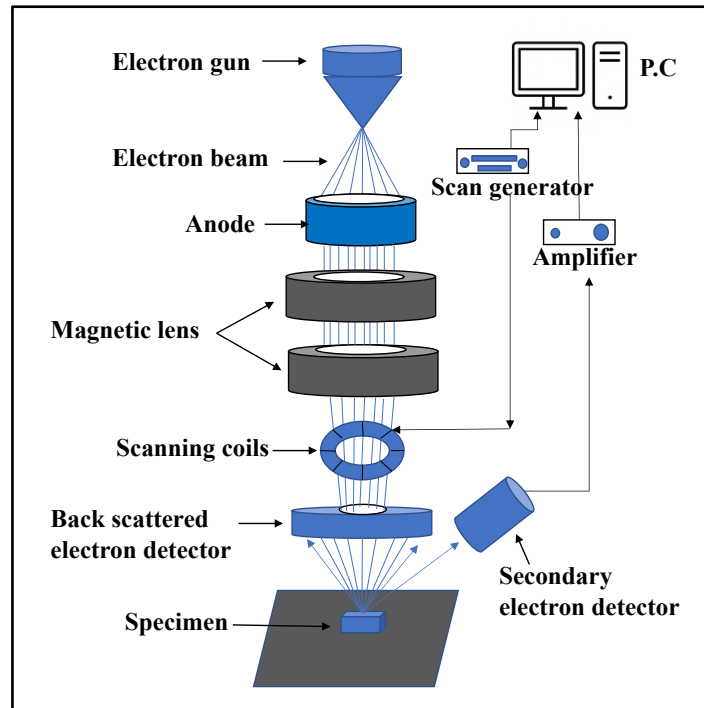
Figure 3.6. Demonstration of Scanning Electron Microscopy (SEM)

On the other side, the XRD is amongst the classical method used for identification of solid crystalline samples. It is works on the principle of X-rays diffracted by the sample in various directions. The wavelengths which are comparable to the lattice structure of the crystalline sample are vigorously scattered as illustrated in **Figure 3.7**. There are basically two approaches which are used for calculation of the crystallite size, stress and lattice strain [40]. The first is Bragg's equation:

$$n\lambda = 2d.sin\theta \tag{3.4}$$

Where n= 1,2,3…..; λ is the wavelength of X-ray; d= distance b/w interlayer; θ= scattering angle.

This equation is generally preferred for determination of interlayer distance inside the crystalline sample.

The second equation is based on Debye-Sherrer principle which is used to calculate the coherent diffracted region and is considered equal to crystalline size. The equation is as follows:

$$D = K \lambda / \beta \cos \theta \qquad\qquad\qquad (3.5)$$

where D is the size of crystal, λ is the wavelength of radiation, K is generally taken as 0.89, θ is the angle of diffraction and β is the width of line at maximum height. In the present study, Scherer method is used for determination of average crystallite size of the nanoparticles.
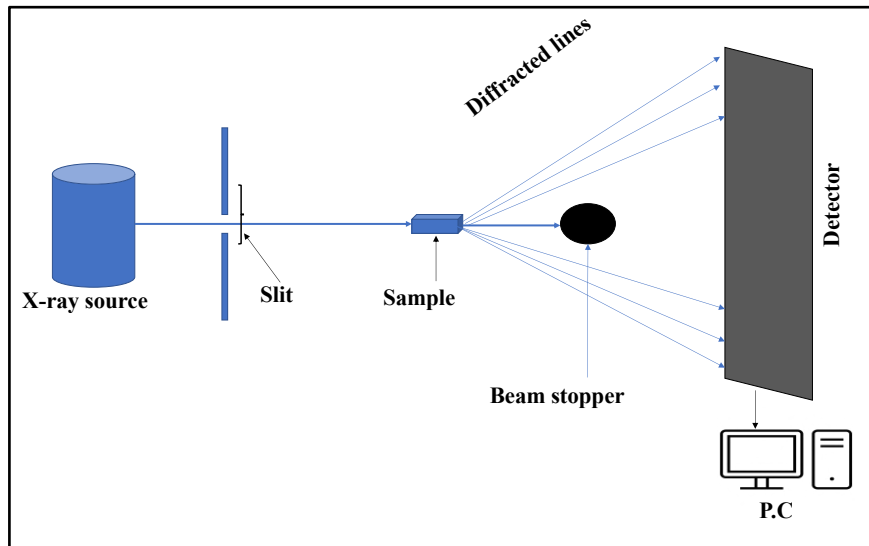
Figure 3.7. Demonstration of X-Ray Diffraction (XRD) spectroscopy

3.5. Preparation of nano-fuel blends (Doping)

The properties of nanoparticles prepared and characterized are listed in **Table 3.1.** The nano-fuels (diesel-biodiesel blend+NPs) were prepared by doping nanoparticles of alumina and MWCNT with the optimum diesel-biodiesel blend. The concentration of nanoparticles was varied in the range of 25-125 ppm. However, due to the smaller particle size, the mixing of nanoparticles inside the base fluid is a complex phenomenon. This can be related to the van der Waals forces between the atoms. Due to size ranging in nanometres, the nanoparticles have very low van der Waals forces, resulting in week bonding force. Thus, the particles show a higher tendency of agglomeration as soon as the temperature inside the medium changes.

In view of this, in the present study, the mixing of nanoparticles with the base fuel (diesel-biodiesel blend) was carried out by adopting the process of ultrasonication. This process makes

use of high-frequency ultrasonic waves to agitate nanoparticles in the sample. The advantage of using this process is that it has good control over the characteristics of the mixture.

Table 3.1. Specifications of Nanoparticles

Details	Alumina (Al$_2$O$_3$)	Multi-walled carbon nanotubes (MWCNT)
Preparation Method	Sol-gel	Thermal chemical vapour decomposition
Chemicals/Reagents	Disodium EDTA (Purity 99-101%), Aluminium Chloride (98%), Ethanol (95%)	Benzene, Iron nanoparticles, Nitrogen
Molecular weight	101.96	172.11
Average Particles size (nm)	20-100	10-30 (outer diameter)
Length, μm	-	1–10
Specific surface area, m^2/g	20	39
Purity	>99%	>93%
Appearance	White	Black

3.5.1. Ultrasonication

In the present research, BRANSON [Make: CPX-2800H] ultrasonicator equipped with the heater was used to achieve the colloidal mixing of alumina and MWCNT nanoparticles. It consists of a stainless-steel tank with 2.5ltr capacity and a maximum frequency of 40kHz. The operating temperature range of the heater installed inside the apparatus is 5°C to 40°C. The steel tank is filled with distilled water and the fuel samples were placed submerged inside the it. The photographic view of ultrasonic mixing is shown in **Plate 3.6.** The mixing of nanoparticles starts as soon as the transducer installed just below the steel tank radiates ultrasonic waves and generates high- and low-pressure waves in the water. The process of mixing is accomplished in two stages. First, the low-pressure waves create a large number of tiny bubbles inside the water, i.e., cavities or cavitation phenomena. In the second stage, these small bubbles collapse with each other and result in releasing an enormous amount of energy. The release of this energy is utilized for breakdown and homogenous mixing of nanoparticles in the base fuel.

Plate 3.6. Demonstration of ultrasonication process

3.5.2. Surfactant

Several researches conducted in the past have revealed that the effect of ultrasonic dispersion of nanoparticles in the base fluid starts diminishing with time and temperature. Therefore, settling down of nano-additives in the fuel might affect the engine working characteristics. Examining all these critical issues, and prevent the agglomeration of nano-additives, the surfactants were added in the nano-fuels. The addition of surface-active agents in the most effective method to improve the dispersion and particle aggregation in the nanofluid. Surfactant act as a stabilizing medium in the colloidal preparation of nano-fuel blends. It lowers the surface tension of the base fuel and enhances the suspension period of the nanoparticles. In the present study Sodium Dodecyl Sulfate (SDS), an anionic surfactant was used for dispersion of alumina and MWCNT nanoparticles in the diesel-biodiesel blend. The surfactant was added to the nano-fuels just before the start of the sonication process. Its concentration was varied in the range of 0.5-2% (by vol.).

Thus, on the whole, a total of ten nano-fuel samples were prepared in the present study for the investigation. These includes D80B20A/C25+S1, D80B20A/C50+S2, D80B20A/C75+S3, D80B20A/C100+S4 and D80B20A/C125+S5. The description regarding the nomenclature and composition of different nano-fuels is listed in **Table 3.2** and the photographic image is shown in **Plate 3.7.**

Some studies on nano-particles doped alternative fuels in Unmodified CI Engine

Table 3.2. Nomenclature and composition of different test fuel samples

Sample no.	Notation	Diesel (%) 'D'	Biodiesel (%) 'B'	NPs dosage (ppm) 'A/C*'	NPs to Surfactant (S) ratio
1.	D100	100	0	0	0
2.	B100	0	100	0	0
3.	D80B20	80	20	0	0
4.	D80B20A25S1	80	20	25	1:2
5.	D80B20A50S2	80	20	50	1:2.5
6.	D80B20A75S3	80	20	75	1:3
7.	D80B20A100S4	80	20	100	1:3.5
8.	D80B20A125S5	80	20	125	1:4
9.	D80B20C25S1	80	20	25	1:2
10.	D80B20C50S2	80	20	50	1:2.5
11.	D80B20C75S3	80	20	75	1:3
12.	D80B20C100S4	80	20	100	1:3.5
13.	D80B20C125S5	80	20	125	1:4

*A: Alumina nanoparticles, C: MWCNT nanoparticles

Plate 3.7. Prepared nano-fuel samples

Some studies on nano-particles doped alternative fuels in Unmodified CI Engine
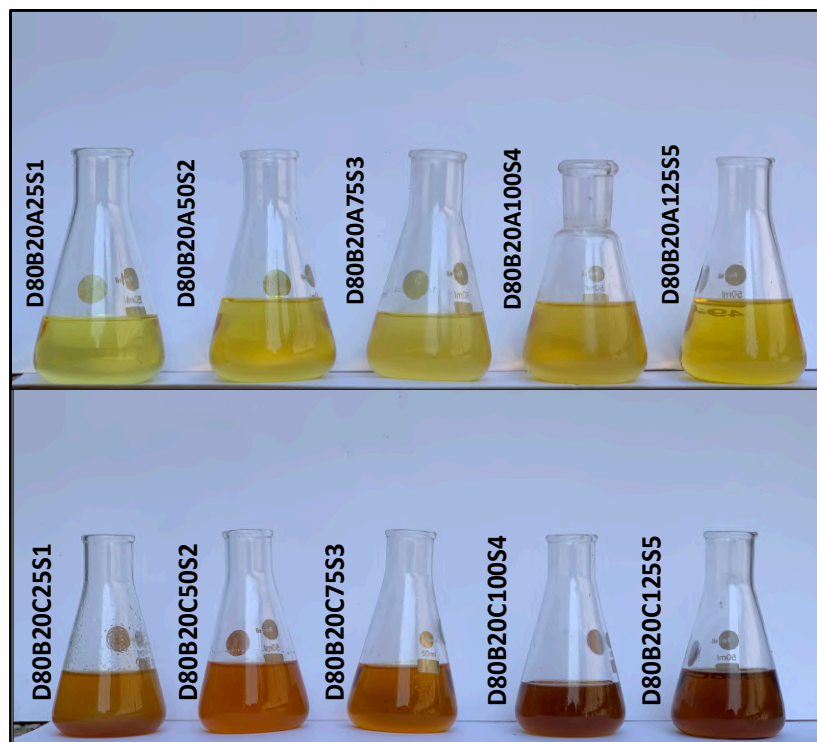
3.6. Stability analysis of the Nano-fuel blends

There are various factors which governs the nanoparticles stability starting from preparation to shape and size, types of base fluid in which particles are suspended, particle concentration, surfactant and mixing quality, etc. The stability of nanoparticles in the diesel-biodiesel blend is amongst the major technical challenge due to the higher tendency of agglomeration. The poor stability significantly influences the physico-chemical properties of the fuel which further affects the engine performance and emission characteristics. Therefore, in the present study the stability analysis of different nano-fuels prepared were analysed by using two different techniques:

3.6.1. Zeta potential analysis

Zeta potential or electro kinetic potential technique is used to suspect the aggregate formation of nanoparticles suspended in the diesel-biodiesel blend (base fluid). It is defined as the measure of potential difference between the layer of base fluid containing charged ion paired with nanoparticle surface and the oppositely charged layer of bulk fluid [213]. The magnitude of zeta potential gives the stability of nanoparticle in the base fluid. Higher is the magnitude of zeta potential (either positive or negative) higher will be the electrostatic repulsion and stability. In the present study, the zeta potential was determined by using Dynamic Light Scattering (DLS) based (Malvern Zetasizer Nano) instrument. The zeta potential was also carried out at a specific temperature ranges ($10^{\circ}C$, $25^{\circ}C$ and $40^{\circ}C$) which were considered according to the local weather conditions in different seasons.

3.6.2. Visual Inspection

In the visual inspection technique, the stability period of the different nano-fuels was analysed by keeping the ultrasonicated fuel samples in the conical flasks. It is one of the simplest methods in which sedimentation of supernatant particles is observed with time and atmospheric conditions. The phase separation event was noticed by capturing the photographs of the

sedimentation of nanoparticles in the different conical flasks. Each and every fuel samples were stored in different weather conditions (local) and regularly monitored over a period of total six-month duration to study the influence of storage time and temperature on nanoparticles stability. The room temperature in different seasons according to local weather conditions (10°C, 25°C and 40°C) were considered for the stability analysis.

3.7. Methods and procedures for physico-chemical properties evaluation

The performance, combustion rate and exhaust emissions are highly reliant on the physico-chemical properties of the fuel, operating the engine. In the present research, the nano-fuels prepared are the combination of diesel and biodiesel fuel plus additives (nanoparticles). Therefore, the amount of aromatic content in diesel, fatty acids composition in biodiesel and catalytic properties of nanoparticles and their dosage will play an influencing role on the fuel properties. Thus, it becomes necessary to examine and compare the physico-chemical properties of different nano-fuels with the baseline data of diesel, before conducting the engine trials. The subsequent sections provide a detailed explanation regarding the different methods, procedures and equipment's adopted for determining the fuel properties.

3.7.1. Kinematic Viscosity

The kinematic viscosity of the fuel samples was determined by using "Petrotest Viscometer". The measurements were carried out at 40°C temperature by following the ASTM D445 standard. There are couple of factors on which kinematic viscosity is strongly dependent. However, in the present study, the temperature of the medium, composition of the fuel and nanoparticles dosage in the base fuel are the key factors which affects the fuel viscosity. However, for better atomization and efficient fuel-air mixing during the combustion process, the viscosity should lie in an optimum range. The equipment used for measuring the kinematic viscosity is portrayed in the **Plate 3.8.** The setup consists of a u-shaped Ostwald type capillary

tube submerged inside the viscometer reservoir in a manner that upper and lower mark of the level bulb is dipped inside the water. The reservoir is filled with the distilled water. A measured quantity of the fuel is then injected in the bulb of the capillary tube with the help of syringe till it reaches the upper mark of the bulb. Therefore, time taken by the fuel sample to reach from upper mark to the lower mark of the capillary bulb is recorded and the viscosity value is determined by using the equation 3.6:

where ϑ= Kinematic viscosity, k= capillary constant of the tube and t= time consumed by the sample for travelling from upper mark to the lower mark.

$$\vartheta = k * t \tag{3.6}$$

3.7.2. Density

Density is another important fuel property which controls the spray characteristics, mass of fuel injected and other physiochemical properties such as calorific value and cetane number. Identical to viscosity, the density of the fuel is also desirable to be lower for better engine performance and combustion. In the present study, Anton Par make Density Meter, Model DMA 4500 shown in **Plate 3.9** was used for the measurement. The density of different fuel samples was obtained at a specified temperature value of 15°C according to the ASTM D4052. The density measurement is based on U-tube oscillating principle. The sample loaded U-tube is oscillated at a certain frequency according to the nature of the sample and the value of the density is determined by capturing the corresponding frequency. Thus, the procedure for the measurement is very simple. The primary step involves thorough cleaning of the U-tube pipeline with the help of 10 ml toluene injecting into it. Thereafter, the fuel sample is loaded for the density determination. To obtain more reliable data, each fuel sample were measured thrice and the average of the three was considered as the final value of the density.

3.7.3. Flash Point

Flash point of the fuel is the lowest temperature whereat the fuel or its vapours turns into ignitable mixture in the presence of air [214]. Although, the value of flash point doesn't significantly affect the engine performance, but it gives a clear indication about the inflammability of the fuel. Due to the low molecular weight and presence of long branched chain compounds, the flash point of neat diesel is significantly lower than biodiesel, thus signifying that diesel should be handle and stored with care. In the present study, the flash point of fuel samples was measured by automated controlled Pensky Martens flash point tester (Scavini) as shown in **Plate 3.10.** The test-setup consist of a cup-shaped sample holder with an opening at the top for pilot flame introduction and temperature sensor. The measurement was carried out in accordance to the ASTM D93 standard. The flame generated at regular temperature intervals by means of automatic feeder gives the value of flash point.

3.7.4. Cetane Index

It is the property of the petroleum diesel or diesel alike fuels which defines the quality of ignitibility in CI engines. Cetane index of the fuel plays a key role in satisfactory working of a diesel engine. It describes the quality of combustion process occurring inside the engine cylinder by providing information regarding the self-ignition pace of fuel when sprayed in the compressed air chamber. The lower is the value of cetane number, higher will be the chances of engine knocking. On the other side, very high value of cetane index results in improper mixing of fuel-air mixture and leads to poor engine operatability. Therefore, accurate measurement of cetane index is very necessary especially when comparison is to be made between different fuel samples.

In the present study, cetane index was calculated by following the ASTM D4737 standard. Thus, the value of cetane index was obtained by measuring the density and distillation curve of different fuel samples [215]. The apparatus used for determining the distillation

temperatures is shown in **Plate 3.11**. The correlation for estimated autoignition value of different fuels is given in equation (3.7):

$$ECI = 45.2 + (0.0892)(BT_{10A}) + [0.131 + (0.901)(X)][BT_{50A}] + [0.0523 -$$

$$(0.420)(X)][BT_{90A}] + [0.00049][(BT_{10A})^2 - (BT_{90A})^2](107X + 60X^2) \qquad \textbf{(3.7)}$$

where ECI= Estimated cetane index; X= $[e^{(-3.5)Z}] - 1$, Z= D-0.85, D= Density of the fuel; $BT_{10,50,90A}$= Recovery/Boiling temperature for obtaining 10%, 50% and 90% distilled fuel.
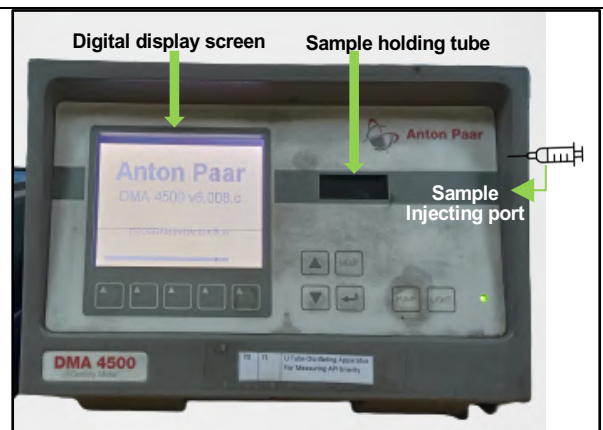
Plate 3.8. Viscometer	**Plate 3.9.** Density Meter
Plate 3.10. Flash point tester	**Plate 3.11.** Distillation setup
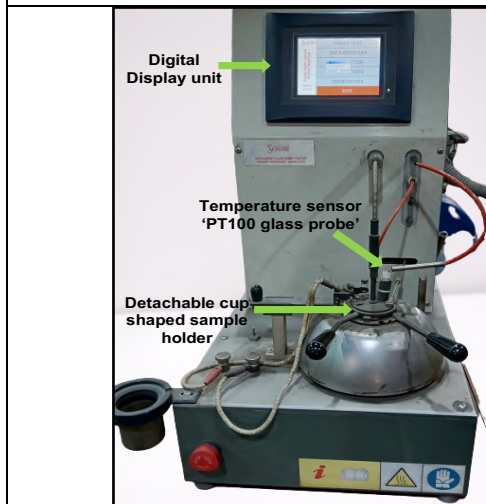
3.7.5. Calorific value

Calorific value or lower heating value is the amount of heat developed when 1 kg of the fuel is completely combusted in the presence of air. In the present study, the calorific value was

determined by using Anton Parr make 6100 Compensated Calorimeter as shown in **Plate 3.12.** The set-up operates in accordance with the ASTM standard D240. It consists of an automated computerized controlled electric arc generated system used for the charging the oxygen bomb. Moreover, the oxygen filling process is also automatic and controlled. The measured quantity of fuel sample is placed inside the sample holder which fits into the bomb. The electrode is fixed in a manner that its mid portion is dipped inside the fuel for igniting the mixture. Thus, as soon as the current is passed through the electrode, the hydrogen atoms present in the fuel react with the pressurized oxygen in the bomb and result in the formation of steam. The amount of heat released from the steam gives the estimate of calorific value of the fuel.

3.7.6. Oxygen Content (wt%)

The oxygen content present in the fuel plays a significant role on controlling the performance and emission characteristics of diesel engines. Higher is the amount of oxygen content in the fuel, more complete will be the combustion process and lower will be the harmful CO and UHC emissions. The addition of oxygen rich biodiesel and nanoparticles of different concentration especially aluminium oxide (Al_2O_3) can substantially alter the oxygen content of the diesel fuel. Therefore, investigation of oxygen content of different fuel sample prepared in the present research becomes inevitable.

The Euro EA make EA3000 series CHNS/O elemental analyzer as shown in **Plate 3.13** was used for the measurement of oxygen wt%. The equipment works on the ASTM D5373 standard. The method for measurement of oxygen gas is slightly different in comparison to setup used for carbon, hydrogen, nitrogen and sulphur elements. Unlike combustion reactor which uses oxygen for burning, the pyrolysis reactor with 5% hydrogen dissolved in helium was used in case of oxygen gas determination. The setup consists of a pyrolysis reactor equipped with unique nickelized carbon wool, a trapping mechanism for acidic gases and a gas chromatograph column for separating the gas mixture. The helium gas is circulated throughout

the setup for carrying the pyrolyzed products. In the initial step, the prepared sample is dropped into the pyrolysis reactor and heated upto 1080°C. Thereafter, resulting in breakdown of sample and release of oxygen gas. The oxygen gas reacts with nickel carbon wool to form carbon monoxide and nitrogen (if any present in sample). Further the pyrolyzed products formed are passed and separated to the GC separation column where the gases are distinguished and detected sequentially by the thermal conductivity detector (TCD). The TCD act as a medium which detects the gases and process them into a specific signals or elemental peaks. Thus, the elements peak is further read by the software which compares the peak and generates a report for each, and every element present in the sample.

3.7.7. Carbon Residual

It is the amount of carbon/deposit left after the combustion of the fuel. The carbon residual was determined by using Alcor make Micro Carbon Residue Tester (MCRT160) which works on ASTM D4530 standard for the measurement. **Plate 3.14** shows the photographic view of carbon residue tester. Firstly, the fuel sample weighed 5gm in small test tube is loaded inside the airtight crucible of MCRT160. Thereafter, the fuel sample is combusted slowly to 500°C at an interval of 10°C per min. The combustion of fuel is continued for 15 minutes. Thus, the second and the final stage involves cooling of the residual left after combustion by purging nitrogen gas inside the setup. The test-tube is than cooled to about 30°C and the residue or traces left inside it is weighed to calculate the amount of carbon residual left after combustion of fuel.

3.7.8. Copper strip Corrosion

Wide variety of acids and sulphur present in the fuel can lead to the corrosion of engine parts and cylinder linings. Thus, copper strip corrosion test bath determines the corrosive nature of the different fuel samples prepared in the present study. The photographic view of the test setup is displayed in **Plate 3.15.** The measurement was carried out by following the ASTM D130

standard test. The corrosivity was determined by dipping the copper strip in the fuel bath for a time period of 3 hrs. The temperature of the bath was kept constant at 50°C. After the completion of the specified time period, the copper strip was extracted out from the fuel bath. The final step includes comparison of the extracted strip with the standardized colour code charts. The chart has different colour codes varying from 1 to 4, thus giving the copper strip corrosion test result.
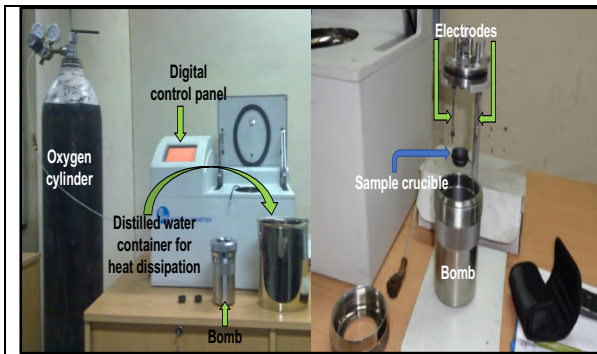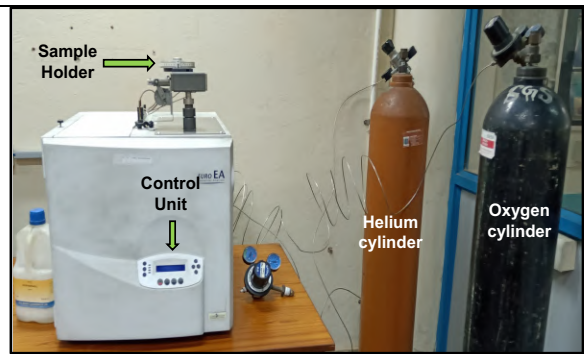
Plate 3.12. Bomb Calorimeter	Plate 3.13. CHNS/O Elemental Analyzer

Plate 3.14. Carbon Residue tester	Plate 3.15. Copper Strip Corrosion tester

3.7.9. Cold Flow Properties

The most important properties especially when the fuel is being used for the running the engines in the low temperature regions. The difficulties in starting of engine, filter plugging, chocking of injectors and emission of white smoke are some of the common cold starting issues which reflects the poor cold weather performance of the fuel. Therefore, cold flow properties

of different fuel samples were distinguished on determining their Cold Point (CP), Cold Filter Plugging Point (CFPP) and Pour Point (PP).

i. Cold Point & Pour Point

It is the lowest temperature at which white cloud shadow or wax crystals starts developing inside the fuel. Moving ahead, the pour point is the temperature at which fuel loses its flow properties. The measurement of cloud point and pour point test was conducted in accordance to the ASTM D2500 and D97, respectively. **Plate 3.16** shows the refrigerator used for determination of cloud and pour point. The rubber cork equipped test-tube filled with fuel sample is placed inside the opening provided on the top of the refrigerator. The cork has an opening in the middle for the insertion of RTD temperature sensor which gives the temperature reading of the fuel. The test-tube is extracted and visualized after every 3°C drop in temperature to visualize the cloud formation and pour point determination.

ii. Cold Filter Plugging Point

This is the point or condition of the fuel which lies in between the cloud and pour point. The temperature at which fuel starts gelling up in a manner that it still can pass through a standardized fuel filter within a stipulated period of time. The CFPP of the different fuel samples were determined by using Linetronic Technologies make CFPP setup as shown in **Plate 3.17.** It operates on ASTM D6371 standard for the measurement of cold filter plugging point of diesel or diesel like fuels. Firstly, the initial step involves, cooling the bath to -34°C temperature. As soon as the specified temperature range is reached, the metered amount of fuel is sucked inside the capillary by vacuum assisted mechanism. Thereafter, the sample is allowed to cool in the low temperature bath. The moment fuel fails to rise or fall through the standardized filter of 10 micron (equipped inside the test-setup) within a time limit of 1 minute is the recorded to be the CFPP of the fuel.

Plate 3.16. Cold filter plugging point apparatus	Plate 3.17. Cloud point and Pour point apparatus
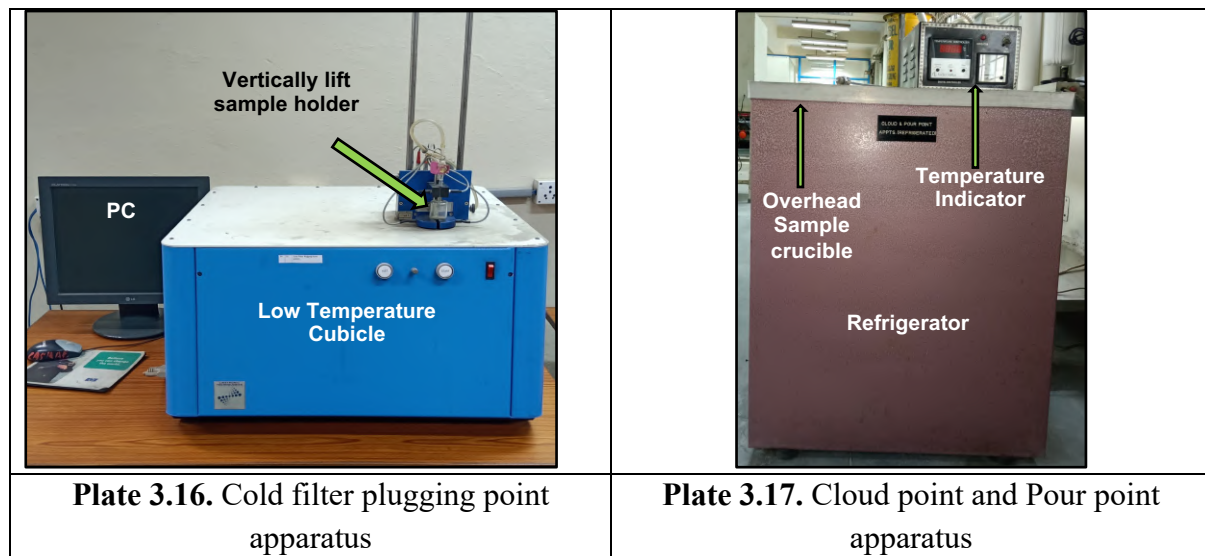
3.8. Experimental set-up to measure the hotplate Ignition characteristics

The evaporation rate and ignition probability of the fuel samples was evaluated by developing and conducting a hot-plate test. The test-setup consists of a fine polished stainless-steel (SS) plate of 8mm thickness and 152mm diameter. An electric heater controlled by a variac transformer was used to heat the surface of the plate. The temperature controller (PID 330) and K-type thermocouple were employed to control and measure the temperature of the surface. A glass pipette mounted firmly on an adjustable arm was used as a fuel discharge unit. The dropping of fuel onto the hot-surface is controlled by a solenoid valve mechanism connected to the nitrogen pressurized fuel reservoir. The test-setup is arranged in such a way that the SS plate is kept on the top of the heater coils. The outer periphery of the heater is insulated by glass wool to minimize the heat losses to the surroundings. The upper surface of the plate having direct contact with the fuel droplets had a concave cavity at its centre. The cavity acts as a collector for the droplets ejecting out from the pipette. To prevent the ignition of fuel inside the pipette and also to minimize the drop breakup chances while falling, the distance of the pipette nozzle is kept fixed at 20 mm from the hotplate. The fuel was supplied

by pressuring the nitrogen in the fuel reservoir at 0.13 bar above the ambient pressure. The schematic of the set-up is illustrated in **Figure 3.8.**

Five different trials at a specific set temperature value were conducted for the test fuels and the average value of the five trials was taken for the study. As the hot-plate temperature attains a predefined value, the solenoid valve pressurizes the fuel from the reservoir to the pipette and pushes the droplet onto the red-hot plate. The result obtained is recorded in the terms of ignition and non-ignition event. This complete process together constituted a single ejection event. Thus, ten consecutive ejection events at a predefined temperature value were carried out for every test fuel. The temperature range of 230-530°C with an increment of 20°C was chosen for conducting the ignition probability trials. The experiment was conducted in an air-tight room at about 25°C temperature and 1.013 bar pressure to avoid the interference of outer surroundings. Also, to get rid of any contamination, the surface of the SS plate is finished with a very fine 90 grit size sandpaper after every observation.
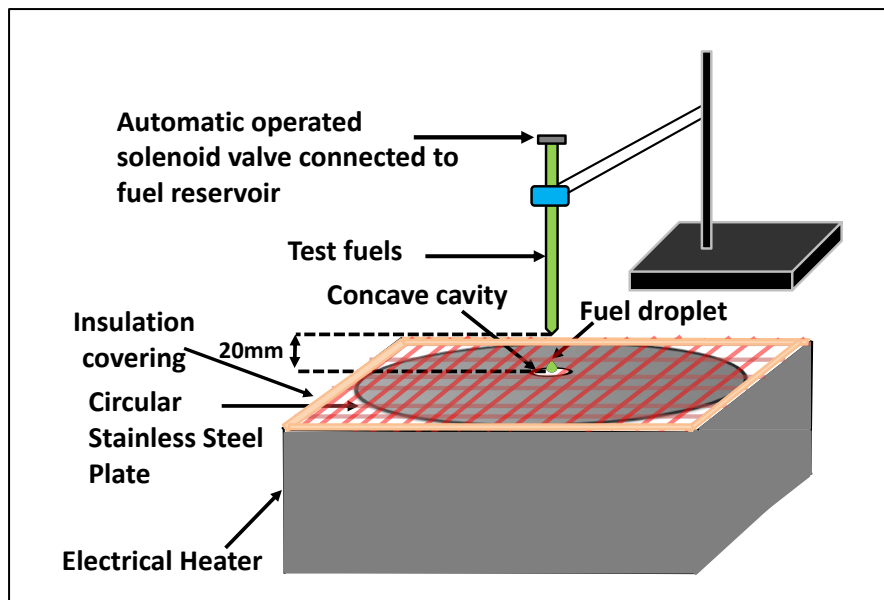
Figure 3.8. Schematic of the hot-surface Ignition experimental set-up [96]

3.9. Experimental setup to measure the fuel droplet size

The smaller is the fuel droplet size, better will be the atomization process and efficient will the rate of fuel-air mixing. Therefore, measurement of fuel droplet size plays an essential

role for the study of the combustion characteristics. The experiment was carried out on a laser diffraction-based Malvern spraytec apparatus. It utilizes a high-intensity laser beam to analyze the spray characteristics of macro/micro level and is designed in a manner that both the rapid and continuous events within 0.1 to 2000 μm size range are captured.

The setup consists of a common rail unit, which supplies fuel from high-pressure pump to the fuel injector, placed cross-sectional to the laser beam path. A single-holed, solenoid-controlled injector identical to that of injector installed in the engine (preferred for engine trials) was opted for the present analysis. The injection system used for delivering of fuel was set at a constant pressure of 220 bar. The reason behind setting the specific pressure range is that the injection system of farmland engine used for performing engine trials further, works on similar pressure value. Also, the droplet distribution is significantly affected by the distance between the injector nozzle and the laser beam. Therefore, the distance should be adjusted in a manner laser beam can capture the whole spray plume, to obtain more precise data. Taking this into consideration, the nozzle of the injector is set fixed at 5 cm away from the beam path. The schematic of the experimental setup is illustrated in **Figure 3.9.** Also, to minimize the uncertainty factor in the experiment, each test fuel was undergone five different trials and the final value was obtained by averaging the sum of trails. As it is well known that, in real-life conditions, the injection process sustains only for about 12ms; however, in the present analysis, the data was captured for 200ms to obtain more clearer picture of fuel spray distribution. The atomization process is pre-dominantly governed by the injector geometry, air density/pressure in which the fuel is sprayed and the fuel properties. Therefore, to analyze the effect of only fuel properties in major, the analysis was performed in a low luminance, stagnant atmosphere having ambient temperature and pressure conditions. Since, all other parameters are almost constant, the fuel properties are anticipated to grab the primary role in determining the spray characteristics.
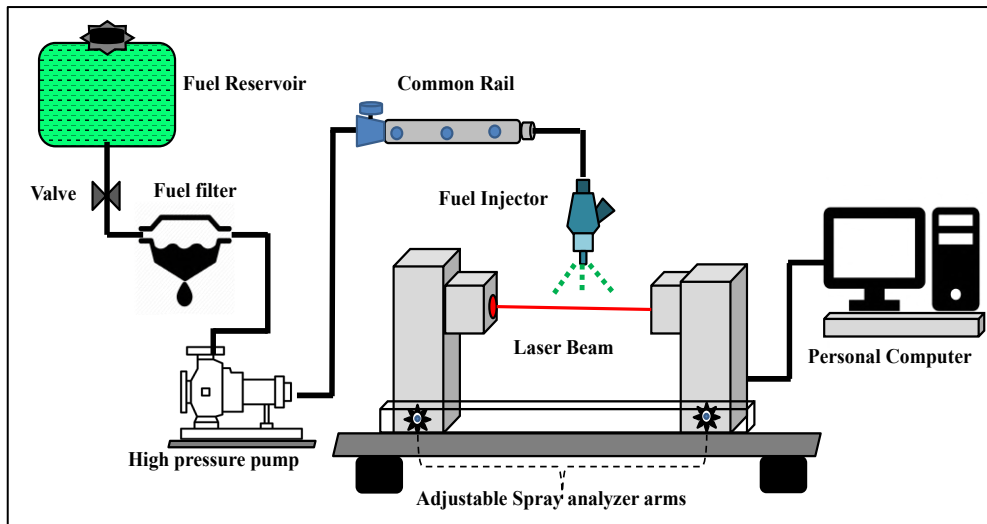
Figure 3.9. Schematic of fuel spray analyser setup [54]

3.10. Experimental set-up for conducting engine trials

As already discussed, the primary aim of the present study is to identify the potentials of nano-fuels, as a sustainable fuel for CI engines. Therefore, to determine the efficacy of different nano-fuels, the foremost step is the selection of appropriate diesel engine followed by investigation of performance, combustion and emission characteristics by conducting series of trials under different engine operating conditions.

3.10.1. Selection of appropriate CI engine

It is a well-known fact that agricultural sector is the engine of growth for the development of the world economy. It has already embarked noteworthy contributions to the vibrant economy of the advanced countries. Its impact on boosting up the growth of the developing countries are also prominent. There are millions of diesel engine which are revolutionizing the agriculture sector since the end of the second world war. Despite being a significant contributor to environmental pollution, diesel engines are still the technology of choice for running the farm and rural economy. Agriculture remains a major source of livelihoods for countries like India and Africa, where there are still more than 5 million light and medium-duty diesel engines [15]. Similarly, the situation is prevalent in advanced countries like the USA, where these engines provide 2/3rd of the energy for American farm machinery [16]. However, the

introduction of electric vehicle and fuel cell technology had offered some relief to the global transportation scenario. Still, its advancement in the rural and agricultural community requires more massive investment and replacement of existing infrastructure. The consequences of which might affect the world economy adversely.

In view of this, nano-fuels, a new advancement in the fuel reformulation techniques, will be a significant step ahead for improving the engine characteristics of millions of existing farmland engines. Thus, in the present study, the Kirloskar make medium-duty, four-stroke, single-cylinder stationary diesel engine was used for the engine trials in the present study. These engines are more commonly used in the agriculture farmlands for power generation and irrigation and other wide variety of works. Kirloskar farmland engines are robust and reliable prime mover having rigid structured cylinder block made up of cast iron. The cylinder liner is centrifugally casted with phosphorus mixed cast iron to provide good resistance to wear. The overhead camshaft driven by crankshaft equipped two pair of bevel gears controls the inlet and outlet valves opening. The fuel pump totally surrounded with the heat insulted chamber is designed for 220 bar injection pressure and is directed by the crankshaft. The engine is water cooled i.e., it is attached with cooling water tank and fan setup. The water-cooling arrangement assists in dissipation of heat generated during the operation of the engine and maintains the normal working temperature of the engine. Also, for the lubrication of different engine parts, wet sump design was used in the present chosen engine.

3.10.2. Assembling/Installation of Engine test-rig

Figure 3.10 shows the schematic layout and **Table 3.3** summarizes the detailed specification of the test setup developed for conducting the engine trails. The setup consist of a farmland purpose medium duty diesel engine which is further connected to an eddy current type dynamometer for measuring the torque and power supplied to the engine. A very precise (strain gauge) type load cell was attached to the dynamometer for accurate transmission of engine load

to the controlled unit as shown in **Plate 3.18 (B).** The principle of eddy current dynamometer loading is based on the variation in the magnetic flux (engine loading) of the rotor generated in the stator housing or coils. The eddy current generated in the rotor compels it attain a reverse force thus disturbing the rotational speed of the rotor and the engine, which is connected with a common shaft. However, the torque provided by the engine helps it to keep moving with the same speed. The value of torque applied by the engine is determined by the rpm sensor (magnetic pickup type) installed at the arm of the dynamometer as shown in **Plate 3.18 (B).** To maintain the constant supply of water from the coiling tank to engine block and dynamometer casing, the pump and two rotameters were installed along with the engine test-setup. The flow rate of cooling water for engine and the dynamometer was maintained at 350ltr./hr and 120ltr./hr, respectively.

Moreover, separate fuel tanks i.e. one dedicated tank for the neat diesel and other for the test fuels were connected with the engine test rig. The variation of cylinder pressure in every engine cycle was analysed by installing a Kistler make (6613CA) piezoelectric pressure transducer in the cylinder head and crank angle encoder at the free end of the crankshaft. The detailed specification of Kistler pressure sensor is given in **Appendix 1.** A K-type thermocouple was installed just before the inlet of the exhaust manifold of the engine to measure the temperature of the burned gases. The differential pressure sensor connected at the orifice plates at the back of the engine control panel unit determines the flow rate of air. Similarly, the measurement of fuel flow rate was determined by calibrated 20cc (by vol.) standard burette and stop watch. Also, to prevent the burette from overflowing and emptying, photoelectric sensors were employed. The photographic images of piezoelectric pressure sensor, airflow differential pressure sensor, fuel pump, and K-type thermocouple are shown in **Plate 3.18 (A,C,D).**
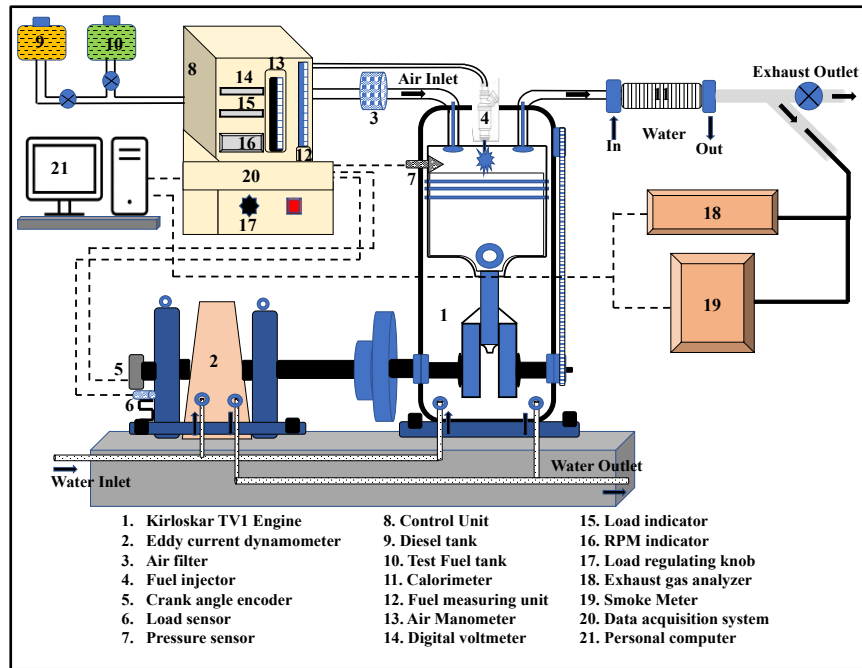
Figure 3.10. Schematic of engine trials-setup

1. Kirloskar TV1 Engine	8. Control Unit	15. Load indicator
2. Eddy current dynamometer	9. Diesel tank	16. RPM indicator
3. Air filter	10. Test Fuel tank	17. Load regulating knob
4. Fuel injector	11. Calorimeter	18. Exhaust gas analyzer
5. Crank angle encoder	12. Fuel measuring unit	19. Smoke Meter
6. Load sensor	13. Air Manometer	20. Data acquisition system
7. Pressure sensor	14. Digital voltmeter	21. Personal computer

Table 3.3. Specifications of the diesel engine test-setup

Description	Data
Manufacturer	Kirloskar
Model	TV1, Vertical, 4 strokes, water cooled, single cylinder, DI diesel engine
Rated Brake Power	3.5 kW @ 1500 rpm
Bore x Stroke (mm)	87.5 x 110
Displacement volume (cc)	661
BMEP at 1500 rpm	6.34 Kg/cm^2
Compression ratio	17.5:1
Loading type	Eddy current
Fuel tank capacity	6.5 Ltr.
Fuel injection pump	MICO inline, with mechanical governor and flange mounted
Fuel injection timing	23º bTDC
Injector holes	3(no.) x 0.288mm
Injection duration	18ºCA
Nozzle opening pressure	220 bar
Valve timing a) Inlet valve opening b) Inlet valve closes c) Exhaust valve opening d) Exhaust valve closes	 4.5º bTDC 35.5º aBDC 35.5º bBDC 4.5º aTDC
Lubrication system	Forced feed system
Lubrication pump	Plunger/gear type
Lube oil sump capacity	3.5 Ltr.
Filter type a) air filter b) fuel filter c) lube oil filter	 Dry type /oil bath type Paper element Bypass filter with paper element
Weight of standard engine (dry weight)	160 Kg

Some studies on nano-particles doped alternative fuels in Unmodified CI Engine

3.10.3. Engine test-rig control panel

The control panel is the heart of the engine test-rig which comprises of fuel and air measuring burette and u-tube manometer, voltage, load and rpm value indicators, load variation nob and USB based-data acquisition unit. After sensing or recording the wide variety of signals during the engine operation, the signals are further fed to the centralized unit known as data acquisition system. The (NI USB-6210) based acquisition unit receives, processes and transmits the signals to the software "Engine Soft" installed on the personal computer. Thus, the software transforms the signals into readable form. **Plate 3.18** shows the photographic view of complete engine test bench used for conducting engine trials in the present study.
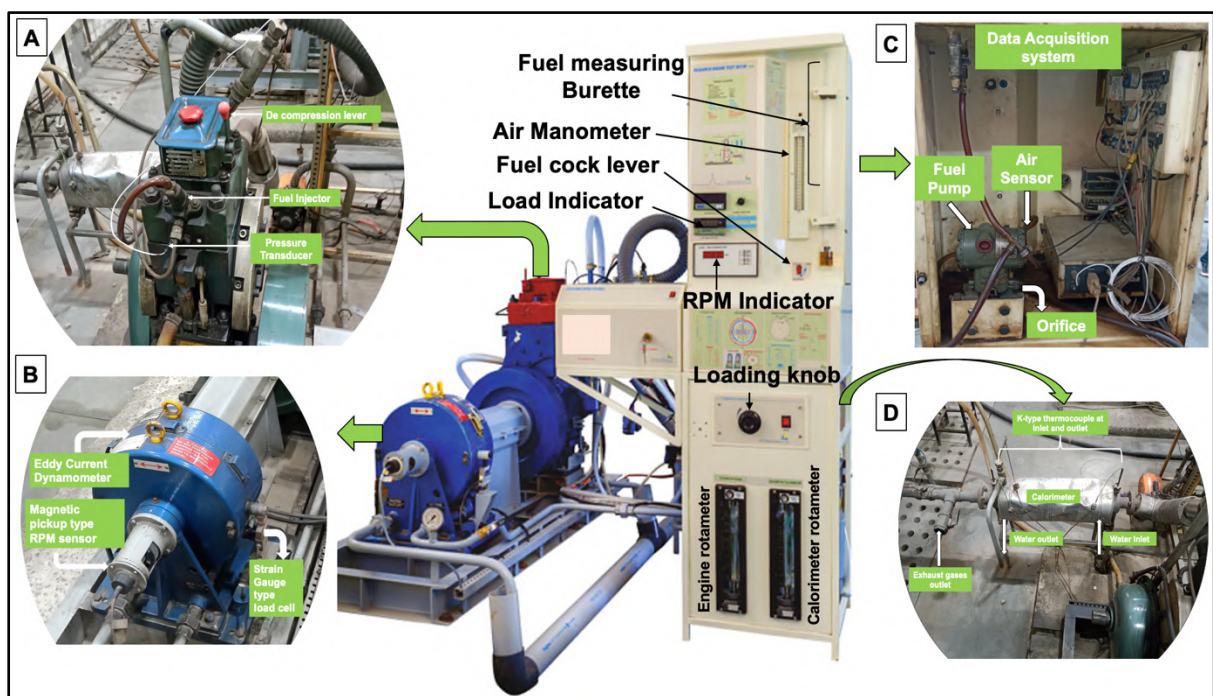
Plate 3.18. Actual representation of diesel engine test bench

3.10.4. Measurement of engine exhaust emission

The concentration of harmful pollutants such as carbon monoxide (CO), carbon dioxide (CO_2), unburnt hydrocarbon (UBHC) and nitrogen oxide (NO_x) released during the burning of different test fuels were measured by using AVL 1000 gas analyzer and smoke opacity by AVL DISMOKE 480 BT smokemeter. The physical appearance of gas analyzer and smoke meter

along with the probe is shown in **Plate 3.19.** Also, the detailed specifications are listed in **Appendix II.**
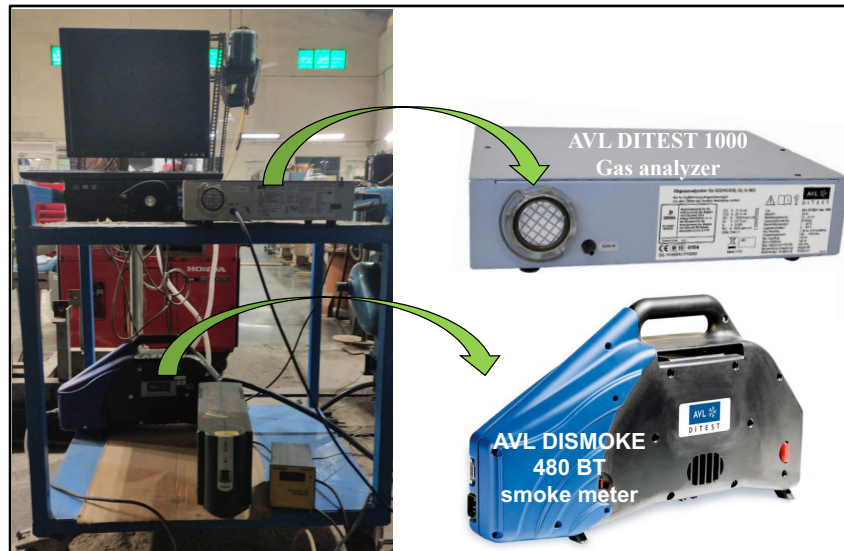
Plate 3.19. AVL Exhaust gas analyzer and smoke meter

i. Principle working of AVL DITEST 1000 gas analyzer

The AVL DITEST 1000 gas analyzer uses Non-dispersive Infrared Radiation Spectroscopy (NDIR) principle for the measuring the concentration of gaseous pollutants such as CO, HC, and CO_2, whereas for detection of O_2 and NO_x it uses electrochemical principle of measurement. Every gas has a unique property of absorbing infrared radiation of specific wavelength. Therefore, by emitting and transmitting IR source of specific wavelength, through a sample cell (exhaust gas) and reference cell (inert gas) the amount of different gases (CO, CO_2 and HC) is detected. However, the NO_x measurement technique is totally different, as it is based on electrochemistry principle. The NO_x sensor consists of Ag and AgCl electrode pairs. The product of NO_x, passing through a gas permeable membrane and electrolyte covered probe is oxidized on the NO_x sensor. The process of oxidation is initiated by creating a potential difference between the measuring and the reference electrodes which leads to the generation of redox current. Thus, the intensity of current is recorded and measured by an amplifier which is equivalent to the concentration of NO_x gas.

ii. Principle working of AVL DISMOKE 480 BT smoke meter

The AVL DISMOKE is based upon the principle of light beam scattering on a filter paper. The filter paper is exposed to the exhaust gases of stream which captures the soot or unburnt particles left behind during the combustion. Moving ahead, the filter paper filled with black carbon particles/soot is exposed to the light beam. The part of the incident light is transmitted back by the soot particles, which is sensed by the photocell by means of photoelectric current generated between the reference and main detector. Thus, the photoelectric current produced is the measure of the soot concentration or smoke opacity.

iii. Conversion of exhaust gases on 'brake specific' basis

The measurement of exhaust gases on the "brake specific" basis is much more significant than molar concentration basis especially when comparison is being made between several fuel samples of different compositions. Therefore, taking into consideration the fuel flexible composition, the exhaust emissions in the present study were converted into brake specific emissions i.e. mass flow rate of individual exhaust species divided by engine brake power. The formulas for conversion are specified below:

CO emission (g/kWh)$= [\{CO(\%vol.) * (10^{-6})\} * (m_{co}/m_a) * \{(A + F) * 1000\}]/(B.P)$ **(3.8)**

HC emission (g/kWh)$= [\{HC(ppm) * (10^{-6})\} * (m_{HC}/m_a) * \{(A + F) * 1000\}]/(B.P)$ **(3.9)**

NOₓ emission (g/kWh)$= [\{NOx(ppm) * (10^{-6})\} * (m_{NO}/m_a) * \{(A + F) * 1000\}]/(B.P)$ **(3.10)**

Where: m_a= molar weight of air i.e. 29g/mol

m_{co}= molar weight of CO emission i.e. 28g/mol

m_{UBHC}= molar weight of UBHC emission i.e. 78g/mol

m_{NO}= molar weight of NO emission i.e. 30g/mol

A= mass flow rate of air (Kg/hr)

F= mass flow rate of fuel (Kg/hr)

B.P = Engine brake power (kW)

Some studies on nano-particles doped alternative fuels in Unmodified CI Engine

3.11. Assessment of observed engine test parameters

3.11.1 Fuel flow measurement

The valuation of time required for the consumption of given volume of fuel gives the value of fuel flow or fuel consumed by an engine at different operating conditions. Further, the product of the volumetric fuel consumption and the density of the fuel gives the value of the mass of the fuel consumed. In the present engine test-setup, the volume of the fuel consumed can be determined both by automatically and manually. The fuel flow sensor located in the control panel of the engine test-rig helps in automatic calculation whereas for manual reading or in case the sensor data is to be validated, the fuel flow is determined by measuring the time consumed by a given volume of fuel filled inside the burette (20cc). However, in the present study, the fuel flow was calculated automatically after validating it with the manual method of measurement.

3.11.2. Air flow measurement

The flow of air is determined by the air sensor stored at the back of the engine test-rig control panel. The air sensor is nothing but an arrangement of turbine flow meter and magnetic pickup type sensor. The air from the pump enter inside the flow meter and strikes the rotor blades assembly. The blades are angled in a manner that the flow energy of air is converted into the rotational energy. Therefore, the speed of the rotation shaft is directly proportional to the air flow. Each blade of rotor is made up of fine shining metal which generates a special pulse when there is in the rotation of the blades. These pulses are sensed by the magnetic pickup type sensor which transmit the pulses to the control unit (data acquisition system) where the signals are processed and send further to the engine software.

3.11.3. Measurement of in-cylinder pressure

As discussed in the section 3.10.2. the variation in the cylinder pressure of different engine cycles was recorded by using the piezoelectric pressure transducer based Kistler (6613CA)

sensor. The pressure sensor is fitted inside the cylinder head as shown in **Plate 3.18(A).** It can measure the pressure value of upto 100 bar. The sensed signals from the transducer is transmitted to the charge amplifier which converts the signal into the analog voltage. Thereafter, the charge amplifier process the signals to the data acquisition system where the engine control module transforms the signals into digital form. In the present study, to obtain more accurate and precise data, the average of 60 cycles were considered for the combustion analysis.

3.11.4 Measurement of engine exhaust temperature and gases

The exhaust temperature was measured using a K-type 10 cm nickel-alumel thermocouple. The temperature sensor is installed just before the inlet of the engine exhaust as shown in **Plate 3.18(D).** The other end of the thermocouple is connected to a six-channel PID controller which shows the reading of the temperature and is installed at the control panel.

As discussed above, the concentration of gaseous pollutants was measured by inserting the probe of the gas analyzer and smoke meter inside the engine exhaust outlet. The emission analyzer are further connected to the personal computer which gives the measured value of different gases coming out of the exhaust during the engine operation **(Plate 3.19).**

3.12. Assessment of calculated engine test parameters

3.12.1. Calculation of Heat release rate (HRR)

The principle tool for the investigation of combustion characteristics in a diesel engine is the cylinder pressure versus crank angle (P-θ) curve. Due to the up-down movement of the piston, there is a significant change in the volume of the cylinder which affects the cylinder pressure and the heat transfer rate mechanism. In order to study the heat release rate, it becomes essential to analyse the pressure rise and drop of every cycle and split the combustion process from other effects. In the past, various models had been developed to study the heat release rate of the direct ignition CI engine. Therefore, in the present study, the Krieger and Borman [216] model

was adopted for the calculation of HRR. In this model cylinder pressure of combust gases are used to compute the overall heat release rate of the fuel burned. The combustion in diesel engine is heterogenous; however, in the present study (following the Sorenson method [217]), combustion contents were considered as homogenous i.e., fuel evaporation rate, pressure waves and temperature gradients and other non-uniform conditions are neglected. Thus, based on the first law of thermodynamics (eq 3.11):

$$Q_{(cyl+wall)} = U+W \qquad\qquad\qquad (3.11)$$

Where $Q_{(cyl+wall)}$= Combined heat release in the engine cylinder and exchange of heat across the walls; U=Internal energy of the combust gases (J/kg); W= Work done by the system to displace the system periphery.

$$U= Q_{(cyl+wall)}-W$$

$$mC_v \frac{dT}{d\theta} = Q_{(cyl+wall)}-P\frac{dV}{d\theta} \qquad\qquad\qquad (3.12)$$

Considering the combust gases as ideal and using PV=mRT to solve the eq. (2)

$$\frac{dT}{d\theta} = \frac{1}{mR}\left[P\frac{dV}{d\theta} + V\frac{dP}{d\theta}\right] \qquad\qquad\qquad (3.13)$$

Where T= temperature of the combust gas (K); R= gas constant; m= mass of the combust gas (Kg); P= cylinder pressure in bar; V= volume of the combust gases (m^3); θ= rotation of the crank (in degree)

Combining eq. (3.12) and eq. (3.13), the heat release rate is derived as:

$$Q_{(cyl+wall)} = \left[\frac{C_v}{R} + 1\right] P\frac{dV}{d\theta} + \frac{C_v}{R}V\frac{dP}{d\theta} \qquad\qquad\qquad (3.14)$$

Where C_v= specific heat of combust gases at constant volume (J/kgK)

$$Q_{(cyl+wall)} = \frac{\lambda}{\lambda-1}P\frac{dV}{d\theta} + \frac{\lambda}{\lambda-1}V\frac{dP}{d\theta} \qquad\qquad\qquad (3.15)$$

Where λ=Heat capacity ratio

3.12.2. Calculation of performance characteristics

i. Brake Power (kW)

The power produced at the output shaft of the engine is termed as brake power. The brake power of the engine can be calculated by referring the equation given below:

$$B.P(kW) = \frac{2\pi NT}{60,000} \qquad\qquad\qquad (3.16)$$

Where N=engine speed in rpm; T= engine torque in Nm and putting its value in **eq. (3.16)**

$$B.P(kW) = \frac{2\pi NFL}{60,000} \qquad\qquad\qquad (3.17)$$

Where F=Force applied on dynamometer (N); L= length of the dynamometer arm (meter).

In the present investigation, the engine chosen for the engine trials has rated power of 3.5 kW. Also, the dynamometer attached to the engine has an arm length of 0.185 meter. Therefore, the minimum (zero load) and maximum load (100% load) value calculated for the eddy current dynamometer used in the present study is 0.3Kg and 17.3Kg, respectively. Considering this, the load value was divided into 5 different intervals with 25% increase in each step i.e., 1.3Kg (0%), 3.3Kg (25%), 6.8Kg (50%), 10.4Kg (75%) and 13.8Kg (100%). Thus, all the performance, combustion and emission characteristics were obtained at the 6 different engine load values. The brake power values calculated corresponding to 0%, 25%, 50%, 75% and 100% were 0.5kW, 0.94kW, 1.93kW, 2.96kW and 3.98kW respectively.

ii. Brake Mean Effective Pressure (BMEP)

It is equal to the average pressure applied on the piston during the entire combustion cycle. It is calculated by measuring the torque on engine dynamometer, this is why it is termed as brake mean effective pressure (BMEP). Formula for calculation of BMEP is given below in equation 3.18.

$$BMEP = \frac{2\times60\times BP(kW)}{L\times A\times N\times101.325} \qquad\qquad (3.18)$$

Where: N= number of power stroke per min i.e. N/2 for 4-stroke and N for two stroke engines;
L= Length of stroke in meter; A= cross-sectional area of the piston (m^2).

The BMEP values calculated corresponding to 0.5kW, 0.94kW, 1.93kW, 2.96kW, 3.98kW and 4.71kW were 0.59 bar, .1.19 bar, 2.38 bar, 3.58 bar and 4.77 bar respectively.

iii. Brake Thermal Efficiency (BTE)

Brake thermal efficiency (η_{BTE}) indicates how efficiently an engine is converting the chemical energy of the fuel (burnt during combustion) into useful work. It is dependent on the brake power of the engine, fuel consumption and the calorific value of the fuel. The formula for calculation of BTE is mentioned in equation below:

$$\eta_{BTE}(\%) = \frac{B.P \times 100}{m_f \times C_v} \qquad (3.19)$$

Where: m_f= mass flow rate of the fuel consumed (Kg/s); C_v=Calorific value of the fuel (KJ/Kg)

iv. Brake Specific Energy Consumption (BSEC)

It reflects the amount of energy consumed for producing one unit of power output. The BSEC (MJ/kWh) is mainly dependent on the viscosity and calorific value of the fuel. The eq. (3.20) shows the relation for the calculation of brake specific energy consumption.

$$BSEC\left(\frac{MJ}{kWh}\right) = \frac{m_f \times C_v \times 3600}{B.P(kW)} \qquad (3.20)$$

3.13. Methodology for Engine trials

The foremost step of engine testing involves some routine checks, which are essential for the proper functioning and accuracy of the engine test-rig. Before cranking the engine in the present study, the level of fuel in the fuel tank or any air bubble in the fuel line was checked. In addition to this, the supply of cooling water to the test-setup, lubricant level in the sump and also engine at no-load condition were all verified and confirmed. Thereafter, the engine was started and allowed to run ideally for about 20-30 minutes. This was done to make sure that engine attains a steady state condition and also the exhaust gas temperature in accordance to that particular load get stabilizes. In the meantime, the data acquisition system (DAS) was activated by connecting it with the LabView based "EngineSoft" version 4.0 software installed in the personal computer. After the activation of the DAS, the sensors and transmitters fitted at different location in the engine test setup starts receiving the signals. The next step involves, adjusting the resolution of the sensors by creating a fresh file in the Enginesoft, according to

the requirement. In the present study, to obtain more precise data and minimize the error, the values of all the sensors were set to the minimum resolution. For combustion data, the average of total 60 cycles were opted whereas average of 10 datasets were chosen for performance and emission characteristics evaluation. As per the calibrated details provided by the engine manufacturer's, the engine trials were conducted at rated power of 3.5 kW and constant speed of 1500 rpm. Also, the trials were carried out by following the IS:10000 standards.

The engine characteristics were investigated thoroughly at different load settings i.e., no load, 25%, 50%, 75% and 100%. Also, to avoid any discrepancy in the results and obtain a robust set of data, the average of three different readings at a particular engine load value was taken. After every 25% increase in the load value, the engine was first allowed to reach to the steady state, before proceeding to the measurement. In parallel, the exhaust emission measurement process was also carried out by inserting the gas analyzer and smoke meter probe inside the engine exhaust. In analogous to the evaluation of engine performance and combustion, the average of sum of three different readings were considered for exhaust emissions calculation. All, the experiment was carried out in ambient temperature and pressure conditions. As mentioned above, firstly the tests were conducted on neat diesel to obtain the baseline data. Followed by the nano-fuels containing different dosage of alumina and MWCNT were tested and compared with the diesel-biodiesel blends and neat diesel (baseline).

3.14. Analysis of experimental accuracies and uncertainties

The instruments involved in the experiments have a certain level of accuracy associated with them, resulting in uncertainty during the measurement of any physical quantity, also referred to as error analysis. Besides, human involvement, improper calibration, inappropriate data entry, faults in experiment designing and random errors can also generate ambiguity in the experiments. Uncertainty analysis provides the difference between the measures and the true value. Although the experiments performed to fulfill the present research objective were

carried out with higher repeatability, still to showcase the robustness of the results obtained, uncertainty was conducted. **Table 3.4**. illustrates the range and accuracy of different instruments along with the uncertainties associated with various measurements.

Table 3.4. Measuring principle, range, accuracy and uncertainty of various instruments and calculated parameters

Measurements	Measurement Principle	Range	Accuracy	Uncertainty (%)
Engine speed	Magnetic pick up type	0-2000 rpm	±10 rpm	±0.1
Engine load	Strain gauge type load cell	0-25 kg	±0.1 kg	±0.2
Cylinder pressure	Piezoelectric pressure transducer	0–100 bar	±0.1 bar	±0.1
Crank angle encoder (CAD)	Optical	0-720º	±1º	±0.3
Time	Digital stop watch	---	±0.1 s	±0.3
Temperature	K-type thermocouple	0–1000 ºC	±1 ºC	±0.2
Fuel flow	Differential pressure transmitter	0-500 mm	±0.05 mm	±0.06
Sauter mean diameter (SMD)	Laser diffraction	0.1-2000 μm	± 0.1 μm	± 0.05
NO$_x$	Electrochemical	0-5000 ppm	±50 ppm	±1
CO	Non-dispersive infrared (NDIR)	0-10% vol.	±0.01%	±0.2
HC	Non-dispersive infrared (NDIR)	0-20000 ppm	±10 ppm	±0.15
Smoke density	Photochemical	0-100%	±1%	±1
Fuel consumption	Level sensor	---	---	±0.4
Air consumption	Turbine flow type	---	---	±0.3
HRR	Sorenson method	---	---	±0.25
B.P	---	---	---	±0.5
BTE	---	---	---	±0.4
BSEC	---	---	---	±0.5

*Note: The values of different physico-chemical properties such as viscosity, density, calorific value, etc., were measured thrice. The average of the three was considered the final value for obtaining more reliable and accurate results. Therefore, uncertainty values were found to be less than 0.1% and were neglected.

3.15. Optimization of nanoparticle concentration

The outcomes collected by conducting a series of engine trials on multiple nano-fuel blends containing 25-125 ppm dosage level of MWCNT nanoparticles highlighted that the nanoparticles incorporation could significantly improve the sustainability of the biodiesel economy. However, after analyzing the engine characteristics, the question arises as to what should be the optimum dosage level of MWCNT nanoparticles that can serve the role of 'cure-all' additive for diesel-biodiesel blend. In view of this, an RSM-based multi-objective

optimization model was constructed to identify the appropriate dosage level of MWCNT nanoparticles and engine loading condition (BMEP) at which optimum engine performance and emission results can be obtained.

It is a widely used statistical technique for modelling and analyzing the engineering-based problems affected by numerous independent variables. Its prime aim is to determine the connection between the complex input and response factors. The RSM approach helps in predicting the best possible outcome that can be obtained from the input resources by effective utilization of independent resources and also reducing the experimental time and money [218]. The flowchart shown in **Figure 3.11** provides a step-step overview of the RSM model designed and executed in the present research.
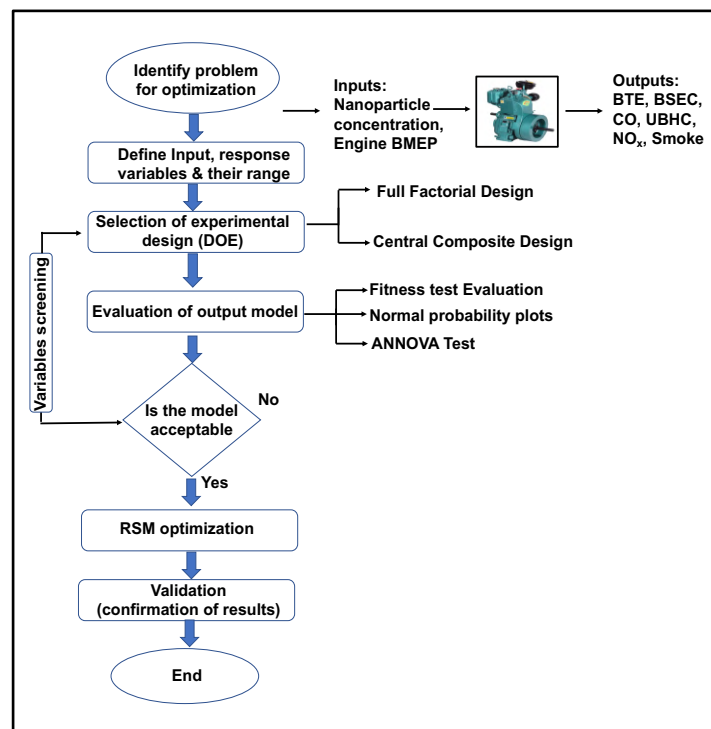
Figure 3.11 Flowchart of the response surface methodology approach (RSM)

3.15.1. Selection of Variables and designing of experiments

The initial step of RSM analysis involves the selection of the input and the output variables. The dosage level of MWCNT nanoparticles and engine load in terms of brake mean effective pressure was opted as input variables. Furthermore, the parameters significantly affected by

Input variables were considered as the output or responses. Thus, engine performance and emission parameters, including Brake thermal efficiency (BTE), Brake specific energy consumption (BSEC), NO_x, CO, UBHC and smoke opacity, were highly influenced by the inputs and were opted as the response/output parameters. The least affected parameters and uncontrolled parameters were not considered. Hence, the experimental range (lower and upper limits) of input variables are listed in **Table 3.5.**

Table 3.5. Experimental ranges and factor levels of variables applied in the experimental design

Input parameters:	-1	0	+1
Nanoparticles concentration (ppm)	25	75	125
Engine BMEP (bar)	0.59	2.68	4.77

After selecting variables, the next step includes designing experimental runs according to the appropriate statistical multivariate method. By taking the three different factors, including the accuracy in the prediction results, fewer experimental trials, and two input variables' requirements into priority, the Central Composite Design (CCD) was preferred in the present investigation. The CCD design is comprised of six-axis points, six center points and the mid-point. It is also known as face-centered CCD approach due to the star points' presence at the cubic portion's face on the design **(Figure 3.12).** It combines the 2-level full factorial and 2 types of points known as centre and factorial points. All the factor values are at midrange (or zero) value at centre points whereas at factorial points all the factor values are at corner points.
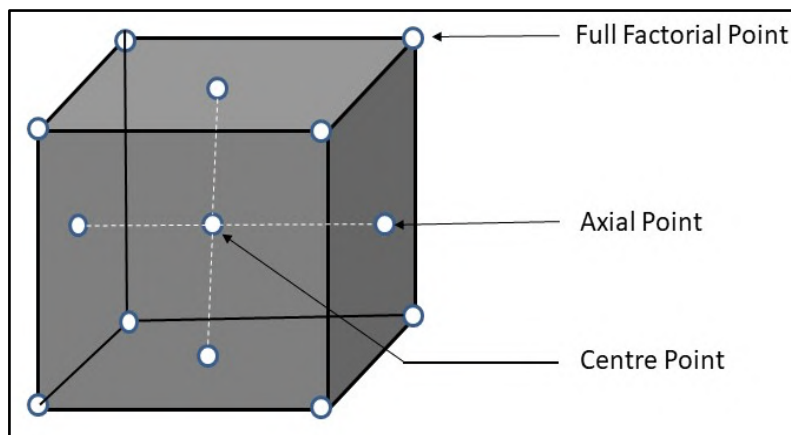
Figure 3.12. Layout of face centred central composite design

Some studies on nano-particles doped alternative fuels in Unmodified CI Engine

The CCD can screen the broad range of parameters on three different levels and include each variable's role. Therefore, it is a widely preferred model by researchers as it allows enough space for experimentation within the design points, where the cube points are located. Moreover, due to the presence of corner points, the quality of the regression models is also good. Also, the total no. of experimental runs are also reduced, so that effective information can be generated in a very less time. After analyzing each variable, the relation between input and the response variables are obtained by fitting them into the second order polynomial equations presented below:

$$Y = \beta_0 + \sum_{i=1}^{k} \beta_i x_i + \sum_{i=1}^{k} \sum_{j>1}^{k} \beta_{ij} x_i x_j + \alpha$$

Where

Y= predicted response, i= linear coefficient, j= quadratic coefficient, β = regression coefficient, k= number of factors, α = random error in the response.

The designing of experiment was performed with the help of MINITAB 17 software. A two-factor, two-level CCD scheme based on RSM modelling was applied. Hence, the total number experimental runs was obtained by using the equation (3.21) and design matrix is listed in

Table 3.6.

Total no. of runs = $2^m + 2m + q$ **(3.21)**

where, m is the number of independent variables, 2^m refers to the number of factorial points or corner points, 2m refers to the number of axial points and q is the number of replicated centre points.

Hence, total number of experimental runs = 13

Table 3.6. Design Matrix of experiments obtained after incorporating CCD

Experiment Run	Nanoparticle Con. (ppm)	Engine BMEP (bar)	BTE (%)	BSEC MJ/kWh	NO$_x$ (g/kWh)	CO (g/kWh)	UBHC (g/kWh)	Smoke opacity (%)
1	125	0.59	16.23	21.99	14.4	14.9	0.74	7.31
2	75	4.77	31.6	12.65	9.8	5.289	0.53	65.02
3	75	0.59	20.5	19.35	16.4	10.77	0.54	3.5
4	125	4.77	30.04	13.8	9.17	7.328	0.66	71.1
5	75	2.38	28.08	11.77	12.3	3.778	0.31	15.44

Some studies on nano-particles doped alternative fuels in Unmodified CI Engine

6	75	2.38	28.08	11.77	12.3	3.778	0.31	15.44
7	25	0.59	17.2	21.99	18.5	13.6	0.69	6.01
8	75	2.38	28.08	11.77	12.3	3.778	0.31	15.44
9	75	2.38	28.08	11.77	12.3	3.778	0.31	15.44
10	125	2.38	25.68	14.19	11	5.211	0.47	19.83
11	25	4.77	30.22	13.6	10.7	6.878	0.3	70.77
12	75	2.38	28.08	11.77	12.3	3.778	0.31	15.44
13	25	2.38	26.33	13.3	14.1	4.761	0.45	19.83

Some studies on nano-particles doped alternative fuels in Unmodified CI Engine

4.1. Introduction

In this chapter, the results of the investigations carried out in the present research have been discussed comprehensively. The compositions of saturated and unsaturated fatty acids present in *Schleichera oleosa* biodiesel, particle size and crystalline phases of nanoparticles synthesized are elaborated thoroughly. The findings gained from the phase stability study of nano-fuels stored under different environmental conditions are also shown. The effect of adding nanoparticles of different dosages on the physico-chemical properties, ignition characteristics and fuel droplet size of the diesel-biodiesel blend is also analyzed. Later in the subsequent section the engine trials conducted to examine the combustion, performance and emission characteristics on different nano-fuels are shown and results are compared with neat diesel, biodiesel and diesel-biodiesel blend. Lastly, the RSM based multi-objective model is discussed in the chapter to identify the optimum dosage of MWCNT nanoparticles in the base fuel at which optimal engine characteristics can be obtained.

4.2. Fatty acid structure of *Schleichera oleosa* biodiesel

Figure. 4.1 shows the GC-MS profile of *Schleichera oleosa methyl ester* (SOME) and the percentage composition of different saturated and unsaturated fatty acids present in it is listed in **Table 4.1.** The fatty acid composition plays a significant role on the physico-chemical properties of biodiesel. The review study conducted by Pinzi et al. [219] and Silitonga et al. [220] in search of ideal biodiesel feedstock showed that the presence of higher content of monounsaturated fatty acids (Elaidic, oleic and Palmitoleic acid) offers better ignition, cold flow properties and oxidation stability to the biodiesel. Therefore, amongst a wide variety of fatty acids present, the percentage of Elaidic acid (26.02%), Stearic acid (9.52%), Arachidic

acid (7.67%) and Palmitoleic acid (74.43%) is higher in SOME. Moreover, the longer carbon

chain ranging between C-11 to C-28 and the presence of higher saturated fatty acid content

(51.5%) certifies *S. oleosa* biodiesel a higher cetane index fuel. Overall, the results gained from

the GC-MS profile confirm *S. oleosa*, an ideal biodiesel feedstock for running the CI engine.
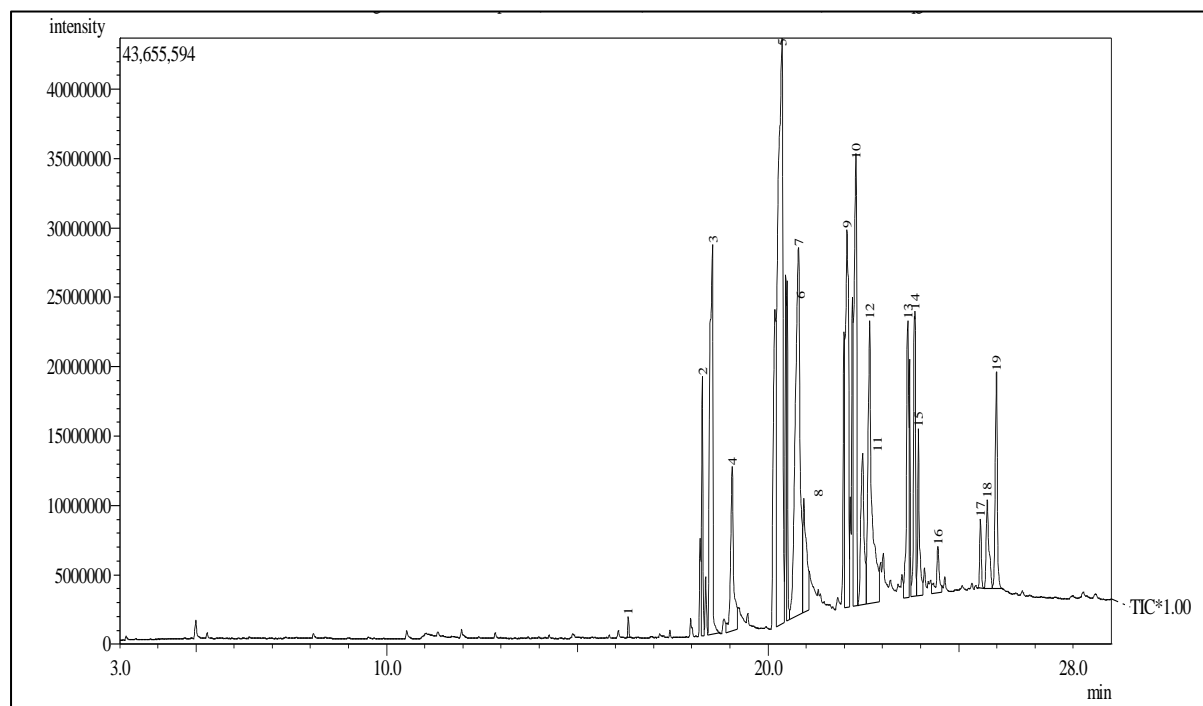
Figure 4.1. Gas-chromatogram of *Schleichera oleosa* Methyl Ester (SOME)

Table 4.1. List of different fatty acids and their composition present in *Schleichera oleosa* Methyl Ester (SOME)

Fatty acids (detected)	Systematic name	Structure (A:B)*	Composition (%)
Capric	Decanoic acid	11:0	0.03
Lauric	Dodecanoic acid	12:0	0.98
Tridecylic	Tridecanoic acid	13:0	2.02
Myristic	Tetradecanoic acid	14:0	1.30
Pentadecylic	Pentadecanoic acid	15:0	1.03
Myristoleate	9-Pentadecenoic acid	15:1	1.27
Palmitic	Hexadecanoic acid	16:0	5.41
Palmitoleic	9-Hexadecenoate acid	16:1	7.43
Margaric	Heptadecanoic acid	17:0	5.57
Palmitelaidic	7-Hexadecenoic acid	17:1	0.92
Stearic	Octadecanoic acid	18:0	9.52
Oleic	cis-9-Octadecenoic acid	18:1	5.50
Nonadecylic	Nonadecanoic acid	19:0	2.87
Elaidic	9-Octadecenoic acid	19:1	26.02
Arachidic	Eicosanoic acid	20:0	7.67
Heneicosylic	Heneicosanoic acid	21:0	6.85

Behenic	Docosanoic acid	22:0	1.54
Erucic	(Z)-Docos-13-enoic acid	22:1	3.37
Tricosylic	Tricosanoic acid	23:0	3.29
Brassidic	13-Docosenoic acid	23:1	2.95
Pentacosylic	Pentacosanoic acid	25:0	0.30
Selacholeic	15-Tetracosenoic acid	25:1	0.68
Cerotic	Hexacosanoic acid	26:0	0.96
Carboceric	Heptacosanoic acid	27:0	0.94
Montanic	Octacosanoic acid	28:0	1.24
Saturated fatty acids			**51.52**
Unsaturated fatty acids			**48.14**
Total			**99.66**

*A: Total number of carbon atoms, B: number of double bonds b/w carbon atoms

4.3. SEM and XRD spectroscopy of Alumina and MWCNT nanoparticles

The nanoparticles synthesized in the present research were characterized to identify their particle size and crystalline phases. The detailed procedure of the SEM and XRD spectroscopy is already provided in chapter 3 of the thesis. The topographical view and X-ray spectrum of aluminium oxide (al_2O_3) nanoparticles synthesized by the sol-gel technique are shown in **Figure. 4.2.** The average size of al_2O_3 np's are calculated by referring to the Scherer's equation is 30nm. On the other side, the crystallinity level was confirmed by three dominant peaks obtained at 37.05°, 45.80° and 66.6°. The results were identical to those obtained by Basha and Anand **[221].** Similarly, the sharp apex obtained at 2θ = 25.8° in **Figure. 4.3(B)** justifies the graphitized nature of MWCNT np's. Palanisamy and Kumar, in their investigation on MWCNT NPs also obtained a similar sharp peak in the 2θ range of 25-27°. The SEM images of MWCNT NPs @ (×50,000 magnification) are shown in **Figure 4.3(A)** and the average particle size calculated obtained by using the Scherer's equation is 15nm.
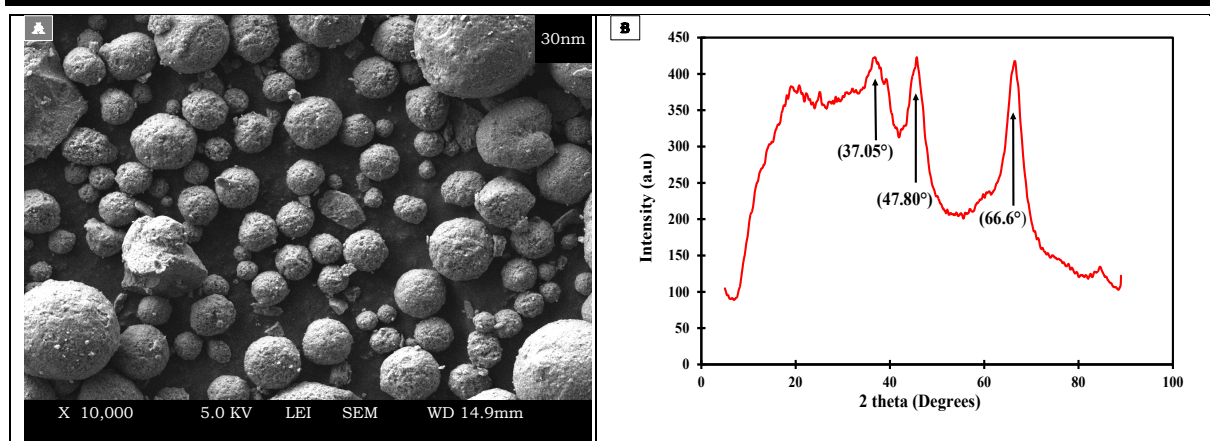
Figure 4.2. A: Scanning Electron Microscopy image (SEM); **B**: XRD pattern of alumina nanoparticles
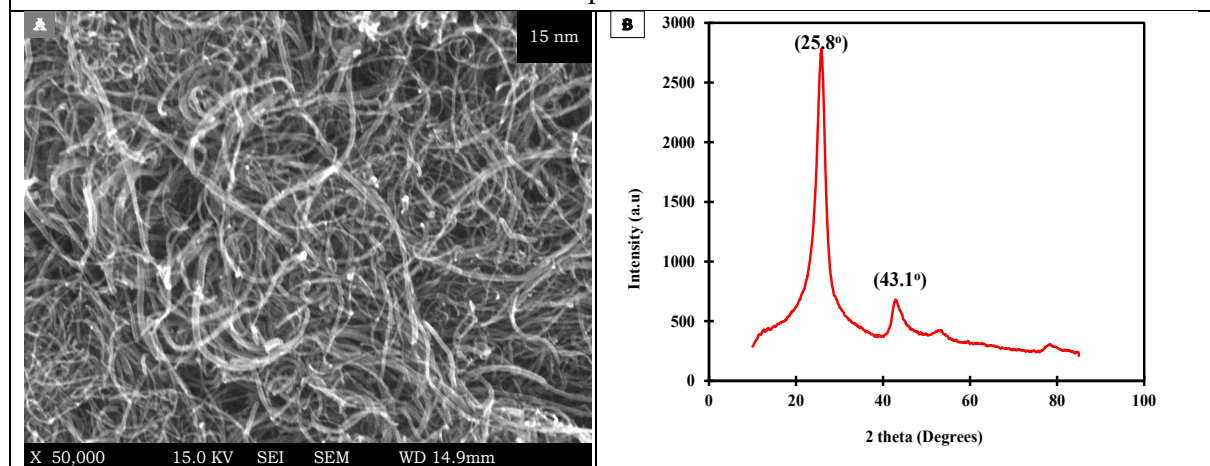
Figure 4.3. A: Scanning Electron Microscopy image (SEM); **B:** XRD pattern of MWCNT nanoparticles

4.4. Phase stability analysis of Nano-fuel blends

The phase stability of fuel blends with respect to time and temperature is an important aspect especially when engine trials have to be conducted on the blends of different composition. Therefore, to obtain the appropriate quantity of surfactant to be mixed with nanoparticles of different concentration the zeta potential of freshly prepared nano-fuel samples at different temperature limit i.e., 10, 25 and 40°C were measured and then later the phase stability was confirmed by performing the long-term visual inspection study.

4.4.1. Zeta Potential Analysis

The zeta potential measures the electrostatic repulsion offered by the surfactant coating over the suspended nanoparticles. Generally, the nanoparticle suspension having the value of zeta

potential above ± 30mV is considered to have good stability. In the present study, for measuring the zeta potential a series of nano-fuel blends in 250ml quantity were prepared. The ratio of biodiesel to diesel were kept fixed at 1:4 whereas the ratio of nanoparticles (alumina/MWCNT) to surfactant (SDS) ratio was varied as 1:2, 1:2.5, 1:3, 1:3.5 and 1:4 respectively. The variation of zeta potential value of different nano-fuel blends at the specified temperature limit is portrayed in **Figure 4.4.** It can be clearly observed that nano-fuel blends containing MWCNT nanoparticles showed higher value of zeta potential at all the temperature values in comparison to alumina dispersed fuels for the same nanoparticles and surfactant concentration. This can be attributed to the increasing in magnitude of repulsion forces which decreases the conglomeration tendency. Therefore, revealing the better colloidal stability of carbon-based nanoparticles in the diesel-biodiesel fuel blend.
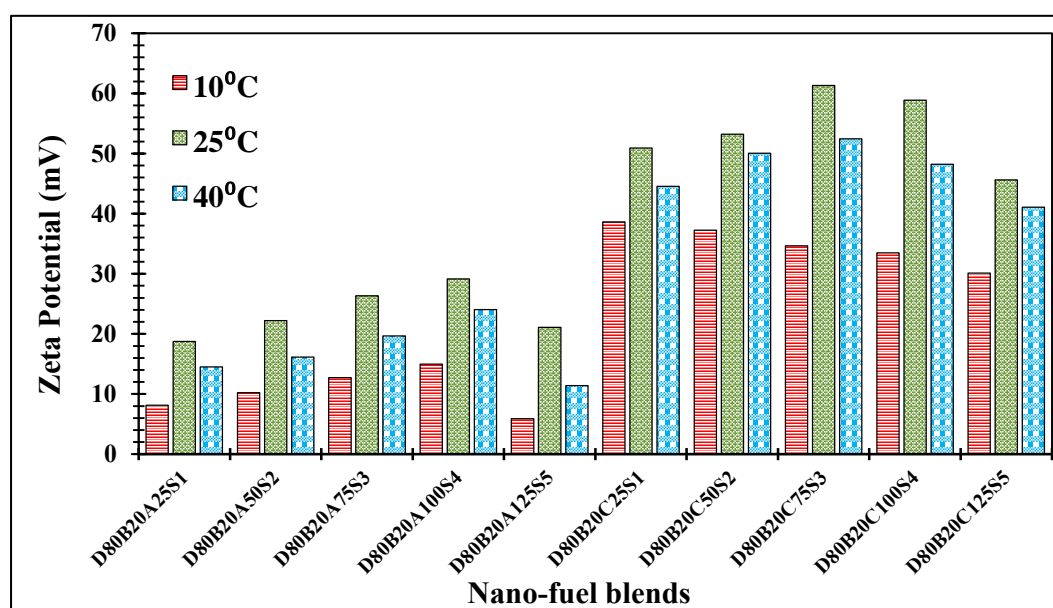
Figure 4.4. Variation in Zeta potential values of Nano-fuel blends at different temperature (10, 25 and 40°C) values

4.4.2. Visual Inspection Analysis

The results obtained from the zeta potential analysis showed that diesel-biodiesel blend combination containing MWCNT nanoparticles dosage in range of 25-125 ppm and nanoparticles to surfactant ratio as 1:3 and 1:3.5 are likely to be more stable and homogenous

for longer duration. Moreover, the stable and homogenous fuel blends will result in better engine characteristics as well. In view of this, alumina dispersed nano-fuel blends were not considered for visual inspection analysis and engine trials.

In the visual inspection test the samples were kept untouched in a clinical chamber to examine the effect of storage time and temperature on the phase stability. The storage time of six months and temperature range of 10°C, 25°C and 40°C were considered for the investigation. Taking into account the Indian temperature conditions, the particular temperature range was chosen. At a specified temperature range, every fuel samples were monitored for two months and separation were noticed visually by taking photographs at regular intervals. The phase stability in the present study is illustrated by taking photographs of the nanofuel samples as shown in **Plate 4.1.**
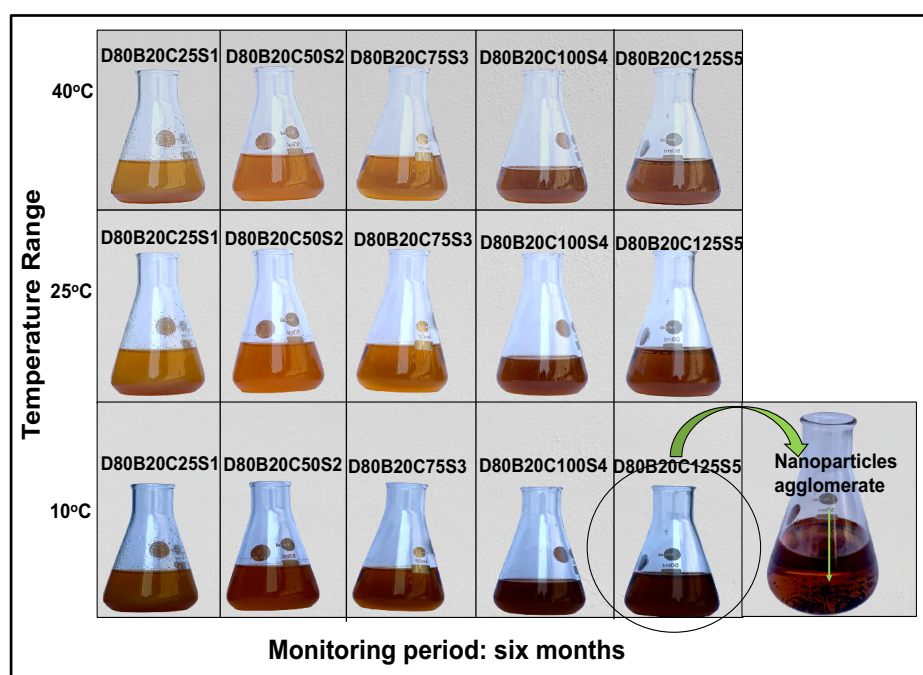
Plate 4.1. Visual Inspection of nano-fuel samples at different temperature ranges

4.5. Physico-chemical properties of Nano-fuel blends

The influence on physico-chemical properties such as viscosity, density, calorific value, cetane index, etc. of the neat diesel with the addition of *S. oleosa* biodiesel and nano-additives of different sizes and concentration were investigated in accordance to the ASTM D6751

Some studies on nano-particles doped alternative fuels in Unmodified CI Engine

standard (procedure discussed in Chapter 3). The properties were evaluated on the last day of the six-month duration time-period.

4.5.1. Variation of Kinematic Viscosity

It is an important fuel property that plays an influencing role in determining the fuel spray characteristics (droplet size and air-fuel ratio) sprayed out of the injector. Higher viscosity value might lead to poor fuel atomization, which could lead to higher fuel consumption, poor efficiency and severe issues of soot and engine deposit formation. The viscosity of the diesel-like fuels should lie in the range of 2-6cSt, according to the ASTM D6751 and EN 14214 standard. The value of viscosity lying below or above this specified range is undesirable. Due to the higher molecular mass, longer chain structure, the neat *S. oleosa* oil has higher viscosity content, i.e., ≈40.02 cSt @ 40°C and a higher viscosity index (185) [54]. The higher value of the viscosity index indicates a relatively slight variation in kinematic viscosity with respect to temperature. On the other side, due to the reduction of FFA content, the kinematic viscosity of *S. oleosa* methyl ester was significantly lower (5.75cSt) compared to triglycerides.

Figure 4.5. shows the variation in viscosity with the addition of biodiesel, MWCNT nanoparticles of 25-100ppm concentration to diesel fuel. It can be observed that the viscosity of D80B20 is quite comparable to diesel. However, with the increase in nanoparticles' dosage, the value of viscosity tends to rise slightly. This can be attributed to the resistance offered by the suspended particles to the base fuel (D80B20). Though, due to nano-size and efficient mixing quality, the change in the value is not much intense. The value of viscosity for D100, B100, D80B20, D80B20C25S1, D80B20C50S2, D80B20C75S3, D80B20C100S4 and D80B20C125S5 is 2.51, 5.75, 3.56, 3.67, 3.86, 3.88, 3.91 and 4.12cSt, respectively.
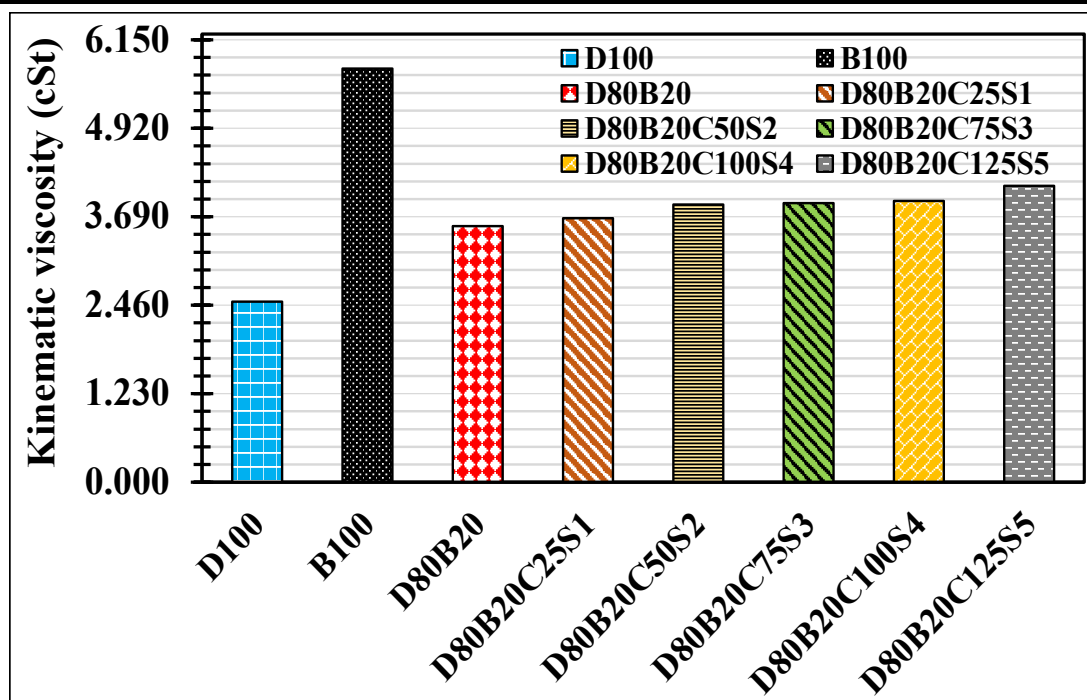
Figure 4.5. Kinematic viscosity trend of different test fuel samples

4.5.2. Variation of density

Density becomes a more important parameter, especially when the role of two or more fuel mixtures come into play. There shouldn't lie much difference in the density of the fuels for achieving a homogenous and stable fuel blend mixture. Besides, the density also plays a significant role during the combustion of the fuel. Therefore, according to the diesel fuel standard ASTM D6751 and EN 14214, the fuel's density to be blended with diesel should lie in the range of 0.820-0.900g/cc. The value lying outside the specified density range might result in poor fuel atomization, leading to incomplete combustion and carbon deposits inside the cylinder.

Figure 4.6 shows the density trend for different fuel samples. Due to the presence of long-chain carbon atoms, the density of *S. oleosa* biodiesel is higher than diesel and diesel-biodiesel blend. The addition of foreign substance (MWCNT nanoparticles) to the diesel-biodiesel blend results in an increase in the density value except for neat biodiesel (B100), which exhibits the highest density (0.896 gm/cc).
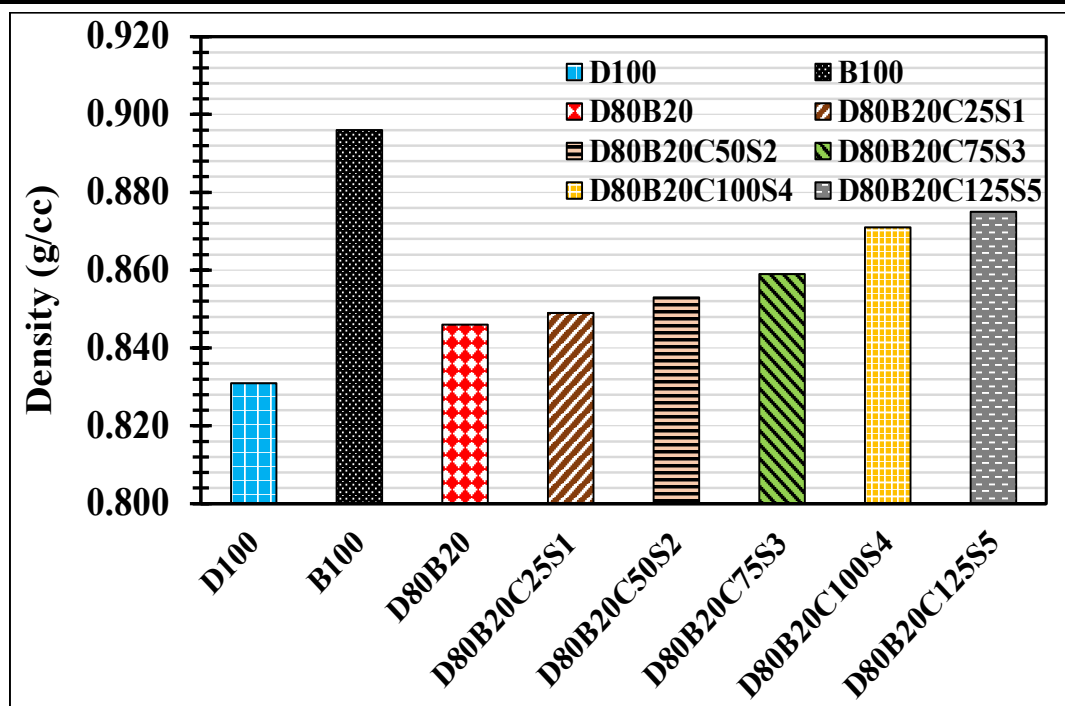
Figure 4.6. Density trend of different test fuel samples

4.5.3. Variation of Calorific value

The calorific value or lower heating value signifies the energy content present inside the fuel. As prescribed in EN 14213, for efficient engine performance, the fuel's heating value shouldn't lie below 35000KJ/kg. Higher is the calorific value better will be the engine brake thermal efficiency and lower is fuel consumption. Due to higher oxygen content, the calorific value of biodiesel is generally lower than diesel fuel. Thus, signifying that for the same amount of fuel, the energy content release during the burning biodiesel is lower than diesel fuel. **Figure 4.7** shows the change in the calorific value of the diesel fuel with the addition of biodiesel and MWCNT nanoparticles of different dosage levels. As can observe the increase in dosage of nanoparticles showed a positive influence on calorific value. This is due to nanoparticles' catalytic behavior, thus increasing the energy content during the burning of fuel [222]. Hence, an increment of about 7.9, 8.8, 9.5, 9.8, 9.9, 10% in calorific value of D80B20, D80B20C25S1, D80B20C50S2, D80B20C75S3, D80B20C100S4 and D80B20C125S5 was observed as

compared to neat biodiesel (B100), with neat diesel showing the highest calorific value i.e., 43690 KJ/kg.
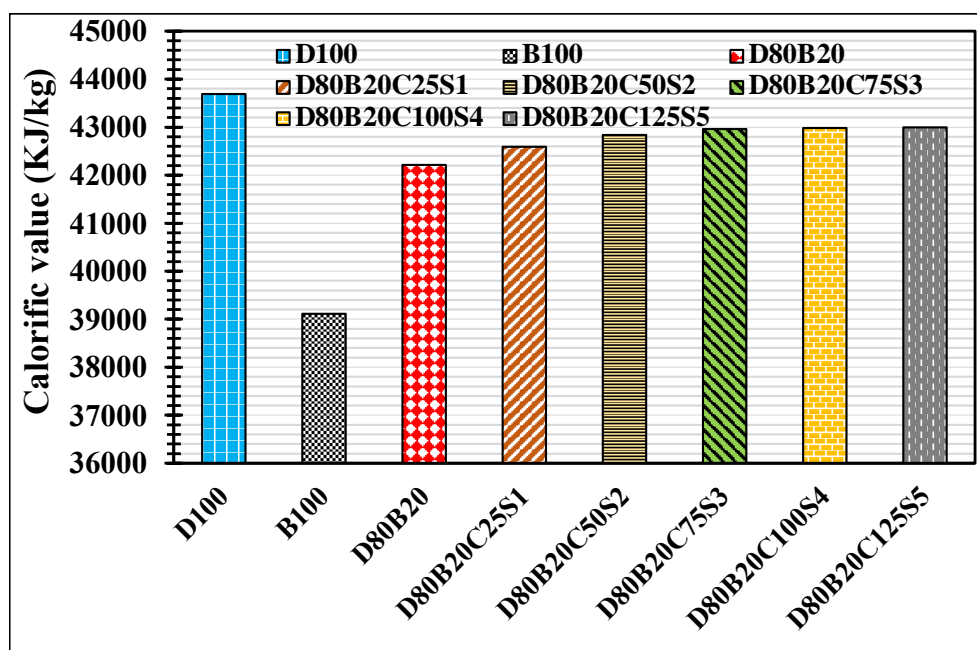
Figure 4.7. Calorific value trend of different test fuel samples

4.5.4. Variation of Cetane Index

The cetane index gives information regarding the ignition quality of the fuel. It is the measure of the fuel self-ignition after injecting it into the combustion chamber. The shorter is the delay in the ignition, the higher will be the cetane index. The cetane index value increases with the increase in the carbon chain length. However, with the increase in C-C double bonds, the cetane index tends to reduce. *S. oleosa* biodiesel has carbon atoms in the range of C-11 to C-28 and unsaturated fatty acids of monotype only. Therefore, the cetane index is observed to be highest in neat *S. oleosa* biodiesel among all the fuel samples, i.e., 60.2. In contrast to this addition of diesel fuel decreases the cetane index significantly, due to branch chained compounds in its structure. The cetane index of nano-fuel blends was observed to be higher as compared to the D80B20 blend. This can be attributed to improvement in the thermal properties of fuel blend with the addition of MWCNT nanoparticles, thus acting as a cetane enhancer for the diesel-biodiesel fuel blend. **Figure 4.8.** portrays the cetane index value of different fuel samples.
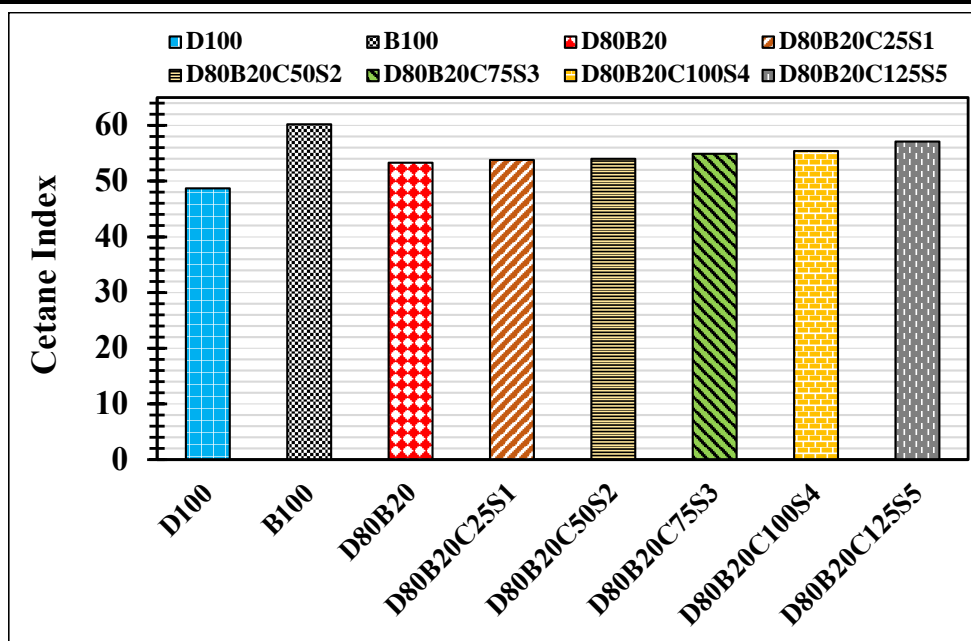
Figure 4.8. Cetane Index trend of different fuel samples

4.5.5. Variation of Flash point

The flash point role becomes vital, when it comes to the handling and long-term storage of the fuels. The value of flash point changes inversely with the fuel volatility. The flash point of biodiesel and diesel should lie in range of 100-185℃ and 55-66℃, according to the ASTM D6751 and D975 standards. **Figure 4.9.** shows the flash point value for different fuel samples. Neat Diesel having been less dense and more volatile showed lowest value of flash point. In contrast due to the lower volatility and poor flow properties of *S. oleosa* biodiesel, the value of flash point is observed to be maximum for B100 followed by D80B20. However, the addition of nanoparticles in the diesel-biodiesel blend showed slight improvement in the flash point value. This can be ascribed to the higher thermal conductivity of MWCNT nanoparticles, thus resulting in the increase in threshold value of the fuel operating temperature (flash point). Thus, among all the nanofuel blends D80B20C100S4 showed highest flash point temperature followed by D80B20C75S3, D80B20C125S5, D80B20S50S2 and D80B20S25S1 with the lowest value.
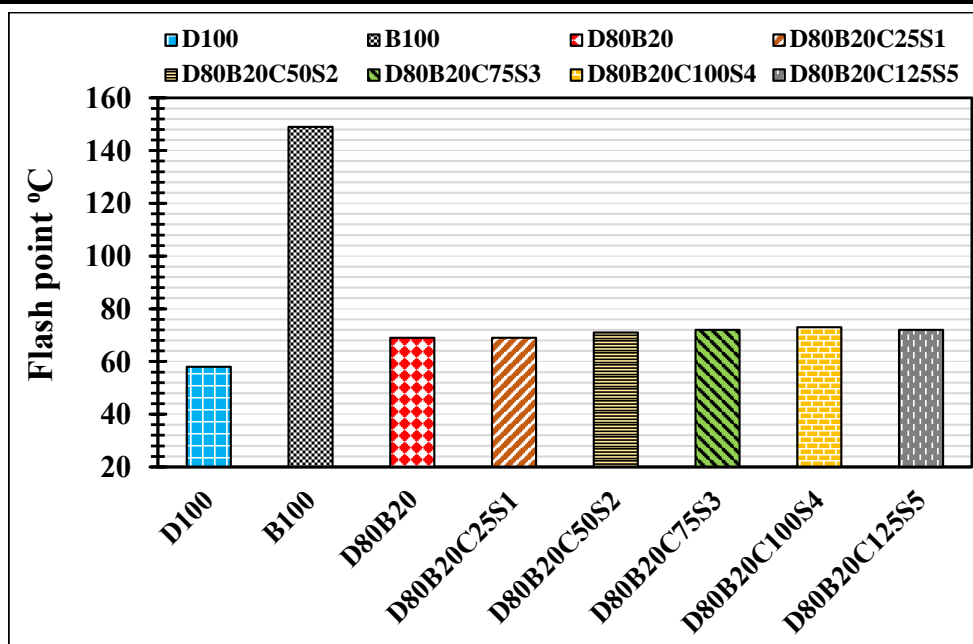
Figure 4.9. Flash point trend for different test fuel samples

4.5.6. Variation of Cold flow properties

The cold flow properties such as cloud point, pour point, and cold filter plugging point are essential parameters, primarily when the engine is operated in low-temperature regions. The petrodiesel comprising paraffin hydrocarbons and aromatic compounds tends to show good ignition characteristics at normal temperature ranges. However, due to paraffin hydrocarbons' wax crystal formation nature at low temperature, the diesel fuel shows poor cold-flow properties [223]. Hence, the low-temperature operability is significantly affected by the structure and composition of compounds present in the fuel. The biodiesel fuel usually has better cold flow properties due to the absence of paraffin and aromatic compounds compared to diesel. However, in some instances, the detrimental effect of higher viscosity, the cold-flow properties of biodiesel are considerably affected. In addition, the outcomes gathered from several studies conducted in the past also showed that there exists a trade-off relation between cold flow properties and oxidation stability [224]. A higher degree of C=C bond (unsaturated fatty acids) promotes cold flow properties and, at the same time, demotes the oxidation stability. Therefore, the biodiesel feedstock having higher monounsaturated fatty acids is the

optimum choice of selection. The variation in cold flow properties (C.P, CFPP and P.P) of different test fuels are highlighted in **Figure 4.10.**
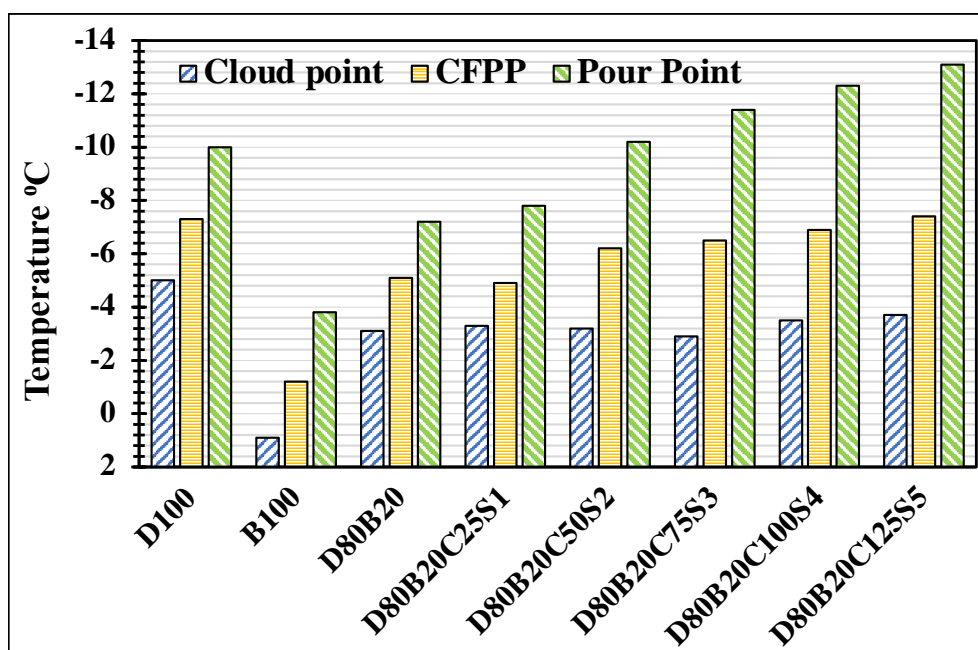
Figure 4.10. Cold flow properties trend of different test fuel samples

As can be observed that B100 i.e., neat *S. oleosa* biodiesel showed the lowest value of cloud point, pour point and CFFP among all the fuels despite of higher mono-unsaturated fatty acids in its structure (**refer Table 4.2**). This can be attributed to the lower viscosity value of *S. oleosa* biodiesel among all the test fuels. In contrast, the cold flow properties of neat diesel were observed to be highest due to the lower viscosity and higher volatility of the diesel fuel.

The addition of MWCNT nanoparticles to the diesel-biodiesel blend showed significant improvement especially in the pour point and CFPP value at higher dosing levels, i.e., (≥50ppm). However, the majority of studies conducted in the past on nano-fuels showed no significant effect of nanoparticles on cold-flow properties. In view of this profound investigation was conducted in the present study to identify how MWCNT nanoparticles addition improves the cold flow properties. Therefore, it was reported that due to the polymeric structure, the MWCNT nanoparticles have excellent mechanical strength, thermal stability and abrasive resistance over other nanoparticles, making it a potential pour point depressant for

diesel, biodiesel fuel. Therefore, the suspension of MWCNT in the D80B20 fuel blend modifies wax crystals' morphology by means of heterogenous nucleation resulting in slowing down the pace of wax precipitation [225].

4.5.7. Additional physico-chemical properties

Fuel properties such as oxygen content (wt%), carbon residue and copper strip corrosion test were also determined and are listed in **Table 4.2.** The details about the procedures and instruments are described in the previous chapter.

Table 4.2. Physico-chemical properties of neat diesel, biodiesel, diesel-biodiesel and nano-fuel blends

Properties	Test Fuels							
	D100	B100	D80B20	D80B20C25S1	D80B20C50S2	D80B20C75S3	D80B20C100S4	D80B20C125S5
Kinematic Viscosity (cSt) at 40ºC	2.51	5.75	3.56	3.67	3.86	3.88	3.91	4.12
Density (g/cc) at 15ºC	0.831	0.896	0.846	0.849	0.853	0.859	0.871	0.875
Calorific Value (KJ/kg)	43690	39112	42213	42591	42837	42960	42982	42995
Cetane Index	48.7	60.2	53.3	53.8	54	54.9	55.4	57.1
Flash point (ºC)	58	149	69	69	71	72	73	72
Cloud Point (ºC)	-5	0.9	-3.1	-3.3	-3.2	-2.9	-3.5	-3.7
CFPP (ºC)	-7.3	-1.2	-5.1	-4.9	-6.2	-6.5	-6.9	-7.4
Pour Point (ºC)	-10	-3.8	-7.2	-7.8	-10.2	-11.4	-12.3	-13.1
Oxygen content (wt%)	0.00	11.01	5.74	5.77	5.78	5.78	5.78	5.81
Carbon residue (% mass)	0.9	0.18	1.01	1.22	1.98	2.10	2.25	2.51
Copper Strip corrosion (Rating)	1a	1a	1a	1a	1a	1a	1a	1a

4.6. Ignition Characteristics of Nano-fuel blends

The Ignition characteristics of nano-fuel blends were investigated by conducting the hot-plate ignition probability test of different fuel samples. The evaporation time and ignition probability ignition are the critical parameters when combustion analysis of different nano-fuels inside the engine is studied. Moreover, the cetane index (refer **Table 4.2.)** also showed significant improvement in its value with nanoparticles' addition in the diesel-biodiesel blend. In view of this, the ignition characteristics were determined. The detailed explanation of the hot-plate experiment is given in chapter 3.

The evaporation time of different fuel samples under varying temperature ranges (200-500°C) is shown in **Figure 4.11.** As can be observed, nano-fuel blends have lower evaporation time throughout the temperature range as compared to other fuels, thus signifying the better evaporation rate. The comparative assessment of the evaporation time also predicted that there exists a specific surface temperature value for the test fuels where evaporation time is lowest also known as critical temperature (T_c). At this temperature, the fuel droplet disintegrates at once, as soon as substantial burning starts at liquid-hot surface interface, thus resulting in instantaneous evaporation of fuel droplet. The nano-fuel blends having excellent heat transfer properties showed lower value of critical surface temperature as compared to D80B20, D100 and B100 fuels. The T_c for D80B20C125S5, D80B20C100S4, D80B20C75S3, D80B20C50S2, D80B20C25S1, D80B20, D100 and B100 is 303, 307, 309, 311, 316, 321, 329 and 340°C, respectively. The rate of evaporation is directly proportional to the dosage of nanoparticles in the base fuel. However, after a certain temperature range, the evaporation rate starts decreasing. This is due to the occurrence of unusual burnt residue deposition phenomenon on the surface of the hot-plate (exposed to the fuel droplet) after subsequent burning, restricting the heat transfer between plate surface and fuel droplet. The burning of fuel droplets on a hot surface is

a probabilistic event that can be altered by various factors such as temperature, atmosphere, hot plate material, thermal conductivity, fuel droplet size, and distance between the plate surface and nozzle. Considering this, the ignition probability of the different fuel samples was investigated to get more reliable results.
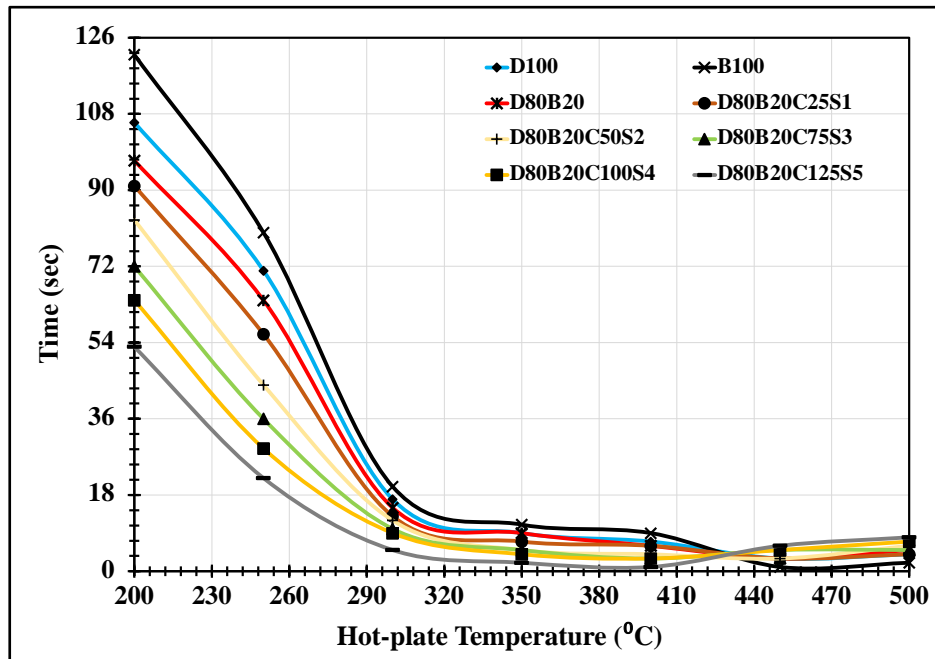
Figure 4.11. Evaporation time variation with the increasing hot-plate temperature

The variation in the ignition probability of fuel samples with respect to surface temperature is illustrated in **Figure 4.12.** The studies conducted in the past reveals that ignition probability is highest in the film boiling region [226,227]. This is because heat transfer in the film boiling region is governed by both conduction and radiation mechanism. In the present research, film boiling occurs in the temperature range of 230-530°C; therefore, ignition probability was investigated only in this specified temperature region. The moment surface temperature starts increasing, the radiation of heat through vapour film becomes more significant, increasing the ignition probability. It is clearly seen in the ignition probability curve that amongst all the fuel samples, test fuel containing 125ppm of MWCNT nanoparticles showed higher probability at all temperature ranges. The ignition probability reaches 100% at 430°C for D80B20C125S5 compared to D80B20, D100 and B100 which attains at 490°C, 510°C and 530°C, respectively.

The rest of the test fuels have values ranging in between the temperature range of 430°C and 530°C. Thus, putting the outcomes in a nutshell, blending of biodiesel and dispersion of nanoparticles showed a decrease in the autoignition temperature of the diesel fuel droplet. Mixing 20% by vol. of biodiesel showed a 3.92% decrease in autoignition temperature as compared to neat diesel, whereas a further reduction of upto 12.2% was noticed with the increasing dosage of MWCNT nanoparticles. Fuel chemistry also plays a significant role in ignition probability. The D80B20 fuel contains lower aromatic content as compared to neat diesel, which improves its cetane number, hence increasing the ignition probability. In comparison to other test fuels, the probability of ignition is significantly higher in nano-fuels. The key reason behind this is the higher surface area, which encourages larger electrons' accommodation on nanoparticles' surface, leading to a higher heat transfer rate. Secondly, higher thermal conductivity due to nanoparticles higher mobility with respect to temperature and shorter wavelengths of nanoparticles helps to ingest higher heat of radiation. This establishes the fact that the higher the dosage of nanoparticles in the fuel blend, the higher the ignition rate will be.
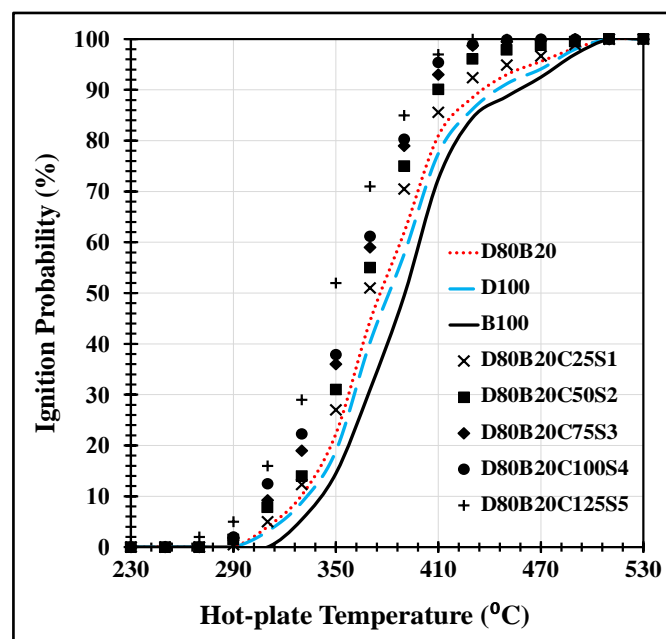
Figure 4.12. Ignition probability variation with increasing hot-plate temperature

4.7. Droplet Size of Nano-fuel blends

The nano-fuels' droplet size is examined to analyze the quality of atomization occurring inside the combustion chamber. Droplet size is distinguished based on the Sauter mean diameter. It is equal to the average diameter of fuel droplet having volume to surface area ratio equivalent to total spray injected out for a limited duration [50,51]. Fuels like biodiesel with high viscosity, density, and surface tension exhibit larger particle size, leading to poor fuel vaporization and ignition delay. On the other side, a very small particle size is also not desirable. This is because of poor fuel penetration of smaller particles, resulting in incomplete combustion and generation of rich fuel zones inside the engine cylinder. Therefore, in order to achieve efficient atomization, the droplet size should lie in an optimum range [41]. **Figure 4.13** shows the Sauter mean diameter variation of different test fuel samples. The lowest SMD value is observed for neat diesel, i.e., (14.4 μm), whereas the droplet size is largest for B100. The SMD of other test fuels lies in between these two values. Due to the higher viscosity of neat biodiesel, the molecules are closely packed, thus resisting fuel droplets' breakdown into smaller particles and resulting in higher SMD. However, with the decrease in biodiesel content in the D80B20 blend, the value of SMD starts decreasing. This can be attributed to a decrease in viscosity and higher volatility associated with diesel fuel.
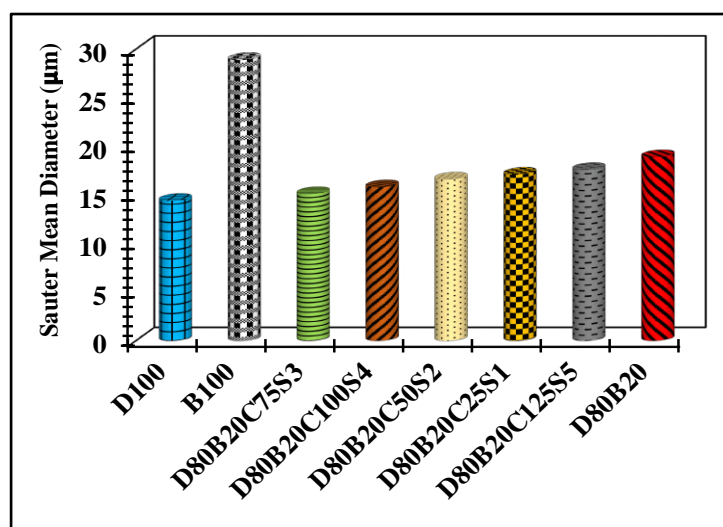
Figure 4.13. SMD values of neat diesel, biodiesel, diesel-biodiesel and nano-fuel blends

Interestingly, nanoparticles' addition triggers the atomization process and decreases SMD's value compared to the diesel-biodiesel (D80B20) blend. The mechanism behind this behavior is the higher collision force between nanoparticles initiated by the induced surfactant coating. The higher repulsion between the suspended nanoparticles facilitates droplets' breakdown by lowering the surface tension and viscosity, resulting in lower SMD. However, the decrease in SMD is maximum in range of 75-100ppm dosage level. This is because there exists a critical limit of surface tension above which it starts increasing again and particle disintegration becomes difficult due to less space and decrease in collision speed [228].

Hence, starting from the lowest value the SMD trend of different fuel samples is as follows:

D100<D80B20C75S3<D80B20C100S4<D80B20C50S2<D80B20C25S1<D80B20C125S5< D80B20 <B100.

4.8. Engine Combustion characteristics of Nano-fuel blends

The combustion of air-fuel mixture taking place inside the engine cylinder plays a decisive role on engine performance and emission characteristics. As already discussed in chapter 2, the phenomenon of combustion inside the CI engine occurs in four different phases i.e., (i) Ignition delay stage (ii) premixed/ uncontrolled combustion (iii) Diffusion/controlled combustion (iv) After burning/Late combustion. The flame front developed at the time of combustion reaction also plays a crucial role in diesel engine operation. In general, it is dependent on various factors such as quality of fuel, air-fuel mixing, combustion efficiency and compression ratio. Higher flame speed facilitates the combustion process and results in better engine performance, reduced CO, HC and soot emissions. However, NOx emissions will be higher, due to increased in-cylinder temperature. On the other side, very high flame speed is also not desirable, as it will lead to higher pressure, noise and detonation. Hence, flame speed should lie in an optimum range for better operation of the CI engine.

Nanoparticles having higher surface area to volume ratio, improved heat and mass transport properties can significantly boost the combustion kinetics of base fuel. Moreover, the improved physico-chemical properties, better ignition probability and fuel droplet size of nano-fuels in comparison to ordinary fuels can be breakthrough during the combustion process. Therefore, taking these factors into consideration, the investigation of important combustion characteristics such as in-cylinder pressure, heat release rate, mass fraction burnt, ignition delay and combustion duration of different fuel samples were carried out in the present research.

4.8.1. Heat release rate (HRR)

It is an important parameter that gives information about the rate of heat energy released at different crank angle positions during the burning of fuel in different combustion stages. The occurrence of ignition delay, start/end of combustion and mass fraction burnt is impossible to ascertain without analyzing the heat release rate curve. In the present thesis, the heat release rate was determined according to the Krieger and Borman equation (3.15), which is based on the Ist law of thermodynamics (refer chapter 3). The heat release rate in joules per degree crank angle (J/^{o}CA) at 100% engine load for different fuel samples is shown in **Figure 4.14.** Among all the fuels, the highest peak of heat release i.e., 66.8 J/$^\circ$CA was observed in neat diesel (D100). This can be attributed to higher calorific value and better fuel atomization via lower SMD. In contrast, the heat release rate is observed to be lowest i.e., 57.2 J/$^\circ$CA in D80B20 due to the inferior calorific value and flow properties.
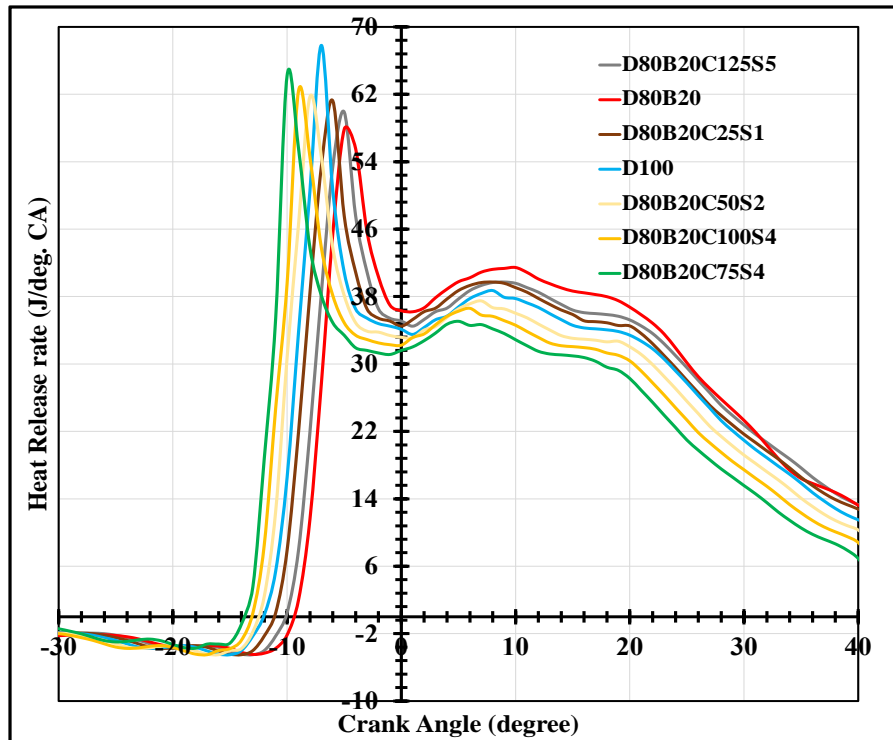
Figure 4.14. Variation of heat release rate with crank angle at full-load condition

Interestingly, the test fuel blends dispersed with MWCNT nanoparticles (D80B20C25S1, D80B20C50S2, D80B20C75S3, D80B20C100S4 and D80B20C125S5) showed significant improvement in heat release rate as compared to D80B20. Also, the rise in peak is more advanced in nano-fuels and therefore test fuel blend containing 75 ppm of MWCNT nanoparticles showed HRR nearly comparable to neat diesel i.e., 64.2 J/°CA. The increase in the dosage of nanoparticles in the diesel-biodiesel blend overcomes the detrimental effects (low calorific value and higher SMD) associated with the addition of biodiesel, which results in a higher rate of heat release.

4.8.2. In-cylinder pressure (P-Theta Curve)

It is considered the most significant parameter for diagnosing the combustion process occurring inside the engine cylinder. The pressure and temperature slope changes rapidly during the occurrence of different combustion phases and are required to be analyzed for optimizing the performance and emission characteristics of the CI engine. In general, at the end of the

compression stroke, when the piston is at the top dead center (TDC), the in-cylinder pressure is highest, representing the peak of premixed combustion. Subsequently, in the expansion stroke, which represents the diffusion phase, cylinder pressure starts decreasing and is lowest at the bottom dead center (BDC). The cylinder temperature follows a similar trend. The variation in-cylinder pressure at different crank angle positions is sensed by a pressure transducer device installed at the head the cylinder (refer chapter 3).

The in-cylinder pressure and temperature peaks of different fuel samples at full load are shown in **Figure 4.15**. The higher peaks of in-cylinder pressure indirectly signify the mixing quality of the fuel-air mixture. Among all the fuels, D100 having a lower viscosity, higher calorific value and volatility, smaller droplet size altogether, resulting in better fuel mixing and higher combustion rate shows the highest peak of in-cylinder pressure. On the other side, the addition of biodiesel in diesel fuel affects the fuel atomization phenomenon due to the larger droplet size. This is the reason D80B20 showed the lowest in-cylinder pressure peaks among all the fuels. The addition of MWCNT nanoparticles having a higher surface to volume ratio, enhanced thermal conductivity, higher heat transfer rates and repulsion forces among the particles act as a breakthrough in improving the ignition and spray characteristics of the diesel-biodiesel blend. Therefore, this is the reason higher in-cylinder pressure is observed as the dosage of MWCNT is increased in the D80B20 fuel blend, with D80B20C75S3 showing the highest peak among the nanofuel blends.
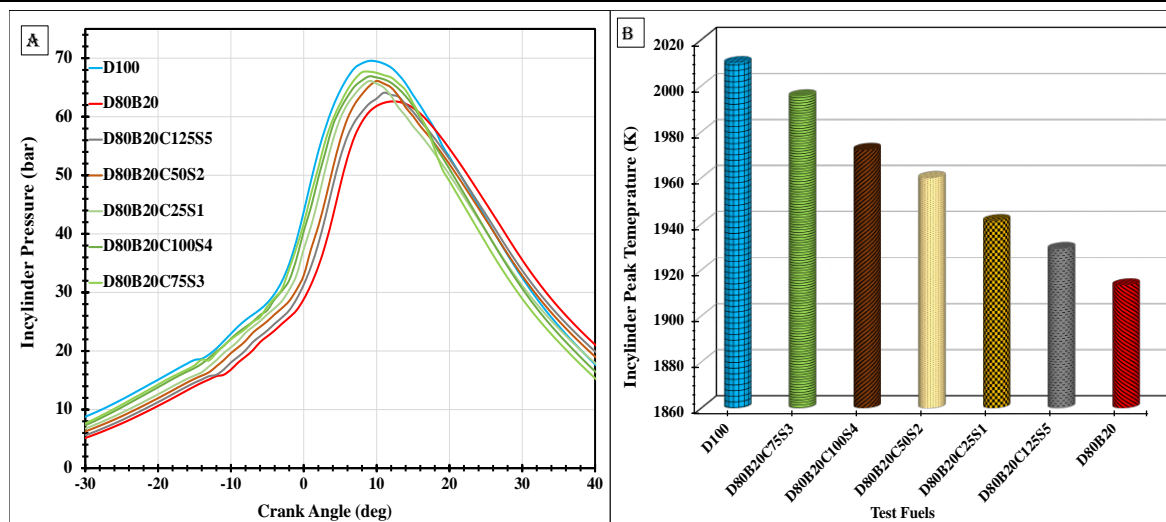
Figure 4.15. Variation of **A:** In-cylinder pressure and **B:** In-cylinder peak temperature with crank angle at full-load condition

4.8.3. Mass fraction burnt (MFB)

The Mass fraction burnt (MFB) analysis gives details about the fuel burnt amount and the fuel-burning rate at different crank angle degrees (CAD) during the combustion process. **Figure 4.16.** portrays the different percentages (CA10, 50, 90) of mass fraction burnt and their corresponding crank angle position for various fuel samples at peak load. In the present research, the crank angle corresponding to 10% of mass fraction burnt (CA10) was considered the start of combustion/premixed combustion, whereas CA50 was considered the end of premixed combustion followed by CA90, which corresponds to the end of combustion point. The difference between C10 and C50 was considered as the premixed combustion duration. The premixed combustion/rapid combustion period is the time period during which the initial combustion of the fuel-air mixture commences.

The CA10 for D100, D80B20, D80B20C25S1, D80B20C50S2, D80B20C75S3, D80B20C100S4 and D80B20C125S5 occurs at 11.3º, 9.45º, 10.8º, 11.7º, 12.7º, 12.3º and 10º bTDC, respectively. Interestingly, in spite of having higher value of cetane index, the rate of burning is observed to be lowest in D80B20 fuel. This can be clearly attributed to biodiesel's poor atomization property, leading to the longer ignition delay and slower burning. Moving

forward, the trend is similar for CA50 (highlighting the premixed phase), wherein the test fuel D80B20C75S3 showed highest burning rate due to combined effect of higher cetane index and efficient atomization. The result of efficient atomization leads to better fuel-air mixing competency resulting in burning of a larger amount of mixture in the premixed comparison period as compared to other fuel samples. The CA50 for D80B20C75S3 occurs at 4.2º bTDC. In contrast, the CA90, occurs earlier in neat diesel and nano-fuel blends except D80B20C25S1 and D80BC125S5 fuels which showed slightly higher crank angle value compared to neat diesel. This can be attributed to the burning of majority of mass fraction in earlier phase of combustion. However, in D80B20 due to higher delay and improper mixing quality the larger portion of the mixture is burnt in diffusion combustion period, thus resulting in higher value of CA90 i.e., 43.1º aTDC.
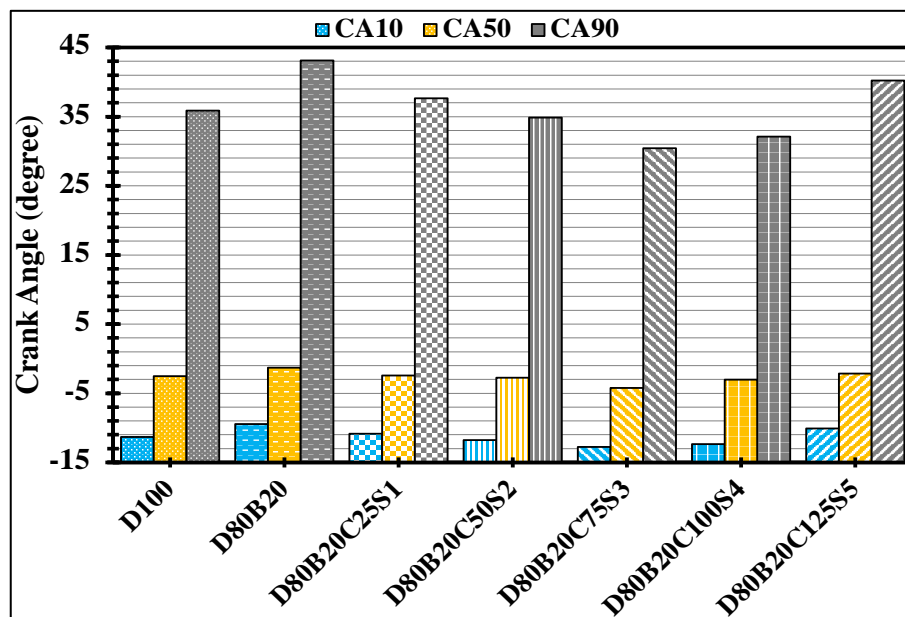
Figure 4.16. Mass fraction Vs. Crank angle at full-load condition

4.8.4. Ignition Delay (ID) & Combustion Duration (CD)

There exists a time lag between injection and commencement of combustion (ignition of the fuel-air mixture) inside the engine cylinder, which is termed as Ignition delay. The reason behind the delay in ignition is the cooling effect of fuel vaporization, the moment it is sprayed inside the combustion chamber. Therefore, the ignition of fuel will not occur until the exchange

of heat between the surrounding air and fuel overcomes the cooling effect. The ignition delay is primarily governed by two major parameters, i.e., cetane index and heat transfer coefficient. **Figure 4.17** shows the variation in ignition delay of different fuels at 100% engine load. Surprisingly, the most prolonged delay in ignition is observed for D80B20 besides having a higher cetane index value. In contrast, the delay is significantly reduced in nano-fuel blends with D80B20C75S3 showing the lowest value. The longer delay in biodiesel blend can be attributed to poor viscosity, lower volatility and poor fuel atomization induced by biodiesel fuel, diminishing the effect of higher cetane index. On the other side, MWCNT nanoparticles having a higher heat transfer coefficient than ordinary fuels and improved cetane index overcomes biodiesel's negative impact in the D80B20 blend, resulting in a decreased delay period. Therefore, the crank angle position at which ignition starts for D100, D80B20, D80B20C25S1, D80B20C50S2, D80B20C75S3, D80B20C100S4, D80B20C125S5 is 11.3º, 14.1º, 12.1º, 10.5º, 7.9º, 8.8º and 12.8º, respectively.
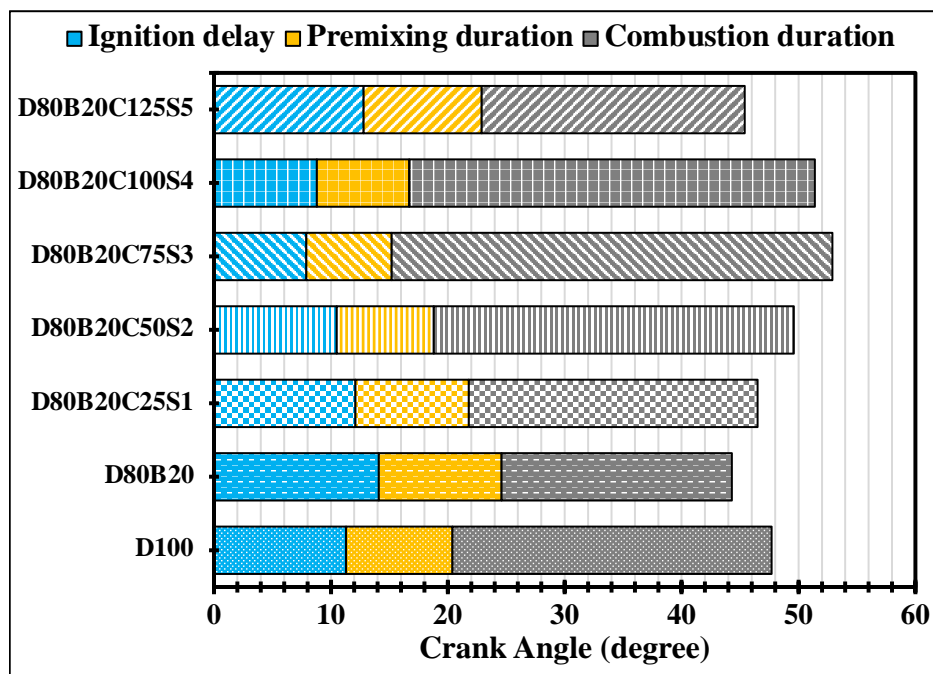
Figure 4.17. Variation in Ignition delay and combustion duration at full-load condition

As discussed in the previous section (Mass fraction burnt), the CA10 is marked as the start point and CA90 as the end of combustion. The difference between the C10 and CA90 is

recognized as the combustion duration. The combustion duration of different fuel samples at full load condition is illustrated in **Figure 4.17**. Due to the shorter delay and efficient atomization of the mixture, the combustion duration is observed to be higher in nano-fuel blends except D80B20C25S1 and D80B20C125S5 which showed slightly lower combustion duration compared to D100. On the other side, D80B20 showed lowest combustion duration due to the inefficient burning of fuel-air mixture. Moreover, the duration of combustion can also be interpreted on the basis of brake thermal efficiency trend shown in **Figure 4.20.** As can be observed, the BTE of the neat diesel (D100) is highest among all the fuel samples, signifying that the other fuel blends will require extra fuel supply for producing the same amount of power. The supply of extra fuel is proportional to the time required for burning, thus resulting in a longer combustion duration. Nautiyal et al. [229] also achieved the same trends while working on a similar specification engine with blends of *Spirulina platensis* biodiesel.

4.9. Engine Performance Characteristics of Nano-fuel blends

The influence of adding different dosage, i.e. (25-125 ppm) of MWCNT nanoparticles on the engine performance of diesel- *schleichera oleosa* biodiesel blend was examined and compared with neat diesel, biodiesel and diesel-biodiesel blends. The assessment was conducted by determining the air/fuel ratio, brake thermal efficiency (BTE), brake specific energy consumption (BSEC) and exhaust gas temperature (EGT) at different loading conditions, starting from no load to 100% engine load with a 25% increase in load after every interval.

4.9.1. Variation of Air/Fuel Ratio

Air/Fuel ratio signifies the mass flow rate of air to the fuel injected per cycle inside the cylinder at different engine loading conditions. It plays a crucial role on engine performance and on the formation of harmful exhaust emissions. Higher is the air-fuel ratio lower will be the overall

fuel consumption and better will be the engine brake thermal efficiency. Also, higher value of air-fuel ratio leads facilitates NOx emissions formation and on the other side suppress the growth of CO and unburnt hydrocarbon emission inside the diesel engine. The variation of air/fuel ratio with the change in brake mean effective pressure (BMEP) for different fuel samples is shown in **figure 4.18.** As can be observed due to increase in fuel supply rate, the air/fuel ratio tends, and the trend is similar for all the fuel samples. The highest air/fuel ratio is observed for neat diesel (D100), whereas biodiesel blend (D80B20) resulting in deficient combustion characteristics showed lowest value. Addition of MWCNT nanoparticles in the biodiesel blends leading to efficient combustion characteristics, showed improvement in the air-fuel ratio to a greater extent. Among all the nano-fuel blends, D80B20C75S3 blend showed upto 41.4% increase in air/fuel ratio compared to D80B20 at full load condition.
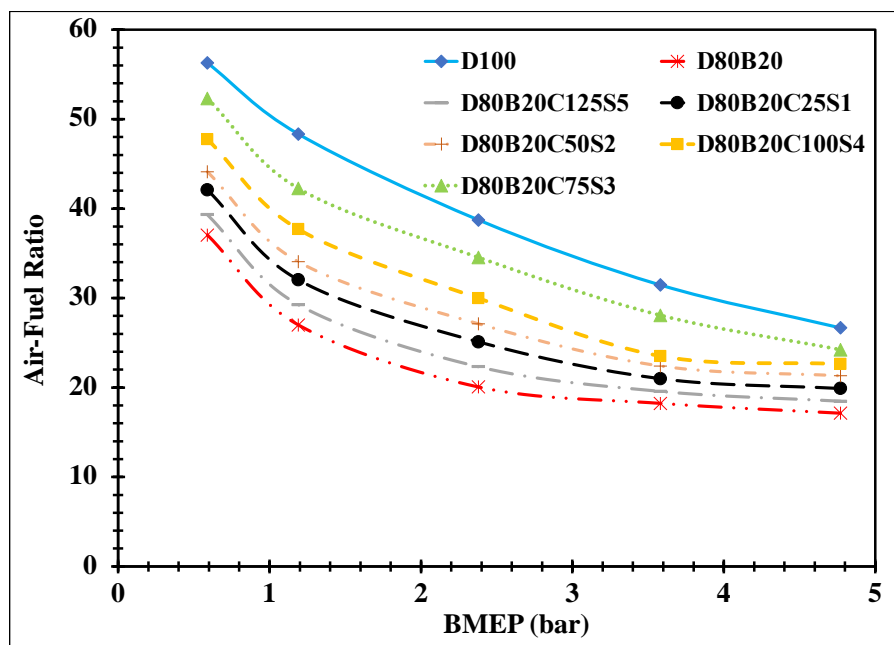
Figure 4.18. Variation of air-fuel ratio with brake mean effective pressure

4.9.2. Variation of Brake Specific Energy Consumption (BSEC)

BSEC is a critical performance parameter of the engine that demonstrates the amount of energy (volume basis) consumed by the fuel for developing one power output unit. The role of BSEC becomes more important, especially when blends contain fuels of different compositions,

calorific value and energy difference. In the present study, different test fuels containing *S. oleosa* biodiesel, MWCNT nanoparticles having dissimilar properties are blended with diesel fuel, therefore computing the BSEC in place of brake specific fuel consumption at different engine loading was considered the most reliable parameter.

Figure 4.19 shows the variation of brake specific energy consumption (BSEC) in MJ/kWh with brake mean effective pressure (BMEP) for different fuel samples. It stems from the fact that the fuel viscosity and calorific value mainly influence BSEC and there exists a trade-off between both the variables. As can be observed, BSEC decreases with the increase in load and the trend is similar for all the test fuels. However, due to the supply of rich mixture at peak load (100%), the BSEC tends to be slightly higher than the adjacent load (75%). Among all the fuel samples, biodiesel blend (D80B20) having higher viscosity, low volatility and lowest calorific value showed higher BSEC at all engine loading conditions. However, due to significantly higher calorific value and efficient fuel-air mixing rate (lower SMD), the BSEC was observed to be lowest i.e., 11.99MJ/kWh in D100 fuel at all the engine loads.

On the other hand, the addition of MWCNT nanoparticles showed substantial improvement in BSEC of the diesel-biodiesel (D80B20) blend. An overall decrement of 2.1%, 3.5%, 5.6%, 9.0% and 10.3% in the BSEC was observed for D80B20C125S5, D80B20C25S1, D80B20C50S2, D80B20C100S4 and D80B20C75S3, respectively. This can be attributed to the efficient combustion characteristics of nano-fuels compared to ordinary fuels, resulting in more complete combustion. Therefore, the result of which at a constant fuel supply, the power developed by nano-fuel blends will be more than the diesel-biodiesel blend, signifying lower energy consumption.
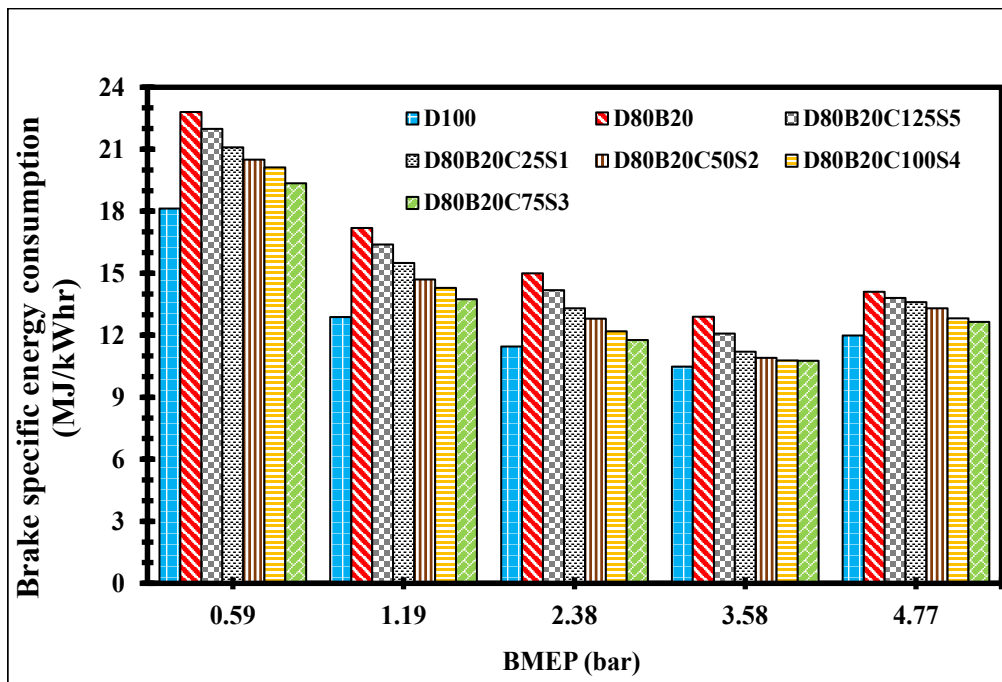
Figure 4.19. Variation of brake specific energy consumption with brake mean effective pressure

4.9.3. Variation of Brake Thermal Efficiency (BTE)

Brake Thermal Efficiency (BTE) represents how competently an engine transforms the fuel's chemical energy into useful work. The change in BTE with respect to BMEP for different test fuel samples is portrayed in **Figure 4.20.** As can be observed, the BTE tends to rise with the increase in engine load and is maximum at 75% engine load instead of peak load. The variation in BTE peaks with respect to BMEP is same of the test fuel samples. The degradation of BTE at peak load can be attributed to the supply of rich mixture, which perturbs the fuel burning rate and has a negative impact on BTE.

Among all the fuels, the highest BTE is observed for D100, whereas D80B20 showed the lowest value. The BTE for other nano-fuel blends lies in between these two fuels. With the addition of 20% by volume of biodiesel, the BTE tends to decrease gradually due to poor viscosity, higher SMD results associated with biodiesel fuel. At peak load (100%), the BTE for D80B20, D80B20C125S5, D80B20C25S1, D80B20C50S2, D80B20C100S4, D80B20C75S3 and D100 are 29.6%, 30.04%, 30.2%, 30.4%, 31.2%, 31.6% and 32.9%, respectively. The

introduction of nano-additives of different concentrations annul the biodiesel addition's adverse effect and thus improves the BTE. Nanoparticles act as a catalyst during the combustion reaction by enhancing the thermal conductivity, diffusivity and convective heat transfer coefficient. The efficient fuel atomization and higher evaporation rate resulting in shorter ignition delay of nano-fuels compensate with higher viscosity and lower calorific value. This improves the BTE of diesel-biodiesel blends. However, due to the higher calorific value and lowest SMD, the BTE of D100 is highest at all the engine loads.
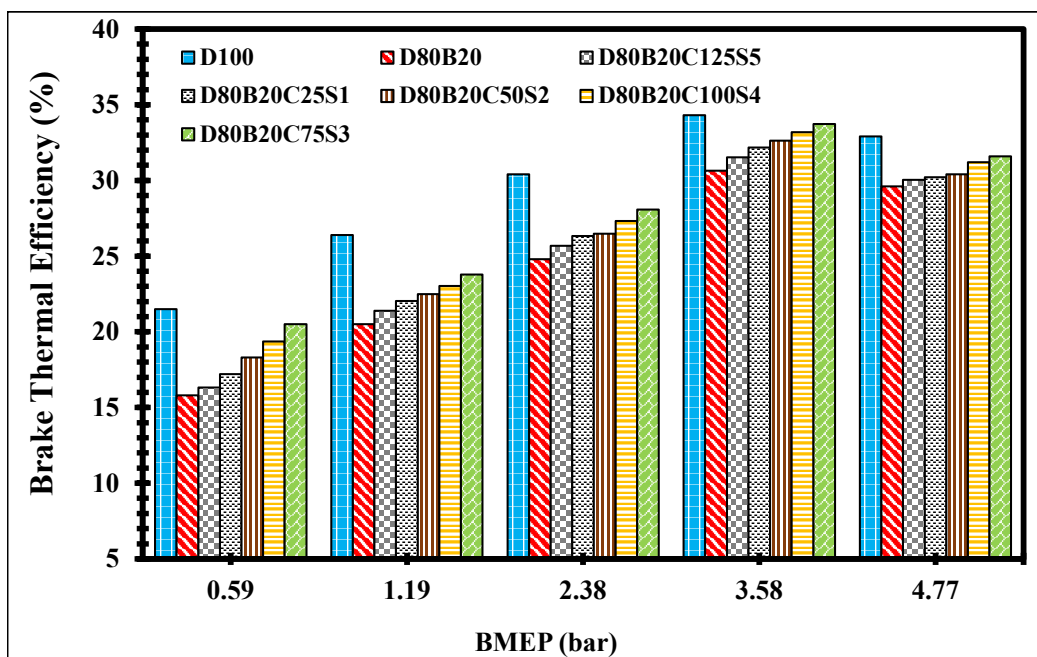
Figure 4.20. Variation of brake thermal efficiency with brake mean effective pressure

4.9.4. Variation in Exhaust Gas Temperature (EGT)

EGT is the most critical operating parameter of the CI engine, which significantly controls the emission of harmful gases liberated during combustion. The EGT trend for different fuel samples with the change in BMEP is shown in **Figure 4.21.** As can be observed; the EGT varies linearly with the rise in engine load. This can be attributed to the increase in the supply of fuel and higher combustion rates at higher loads.
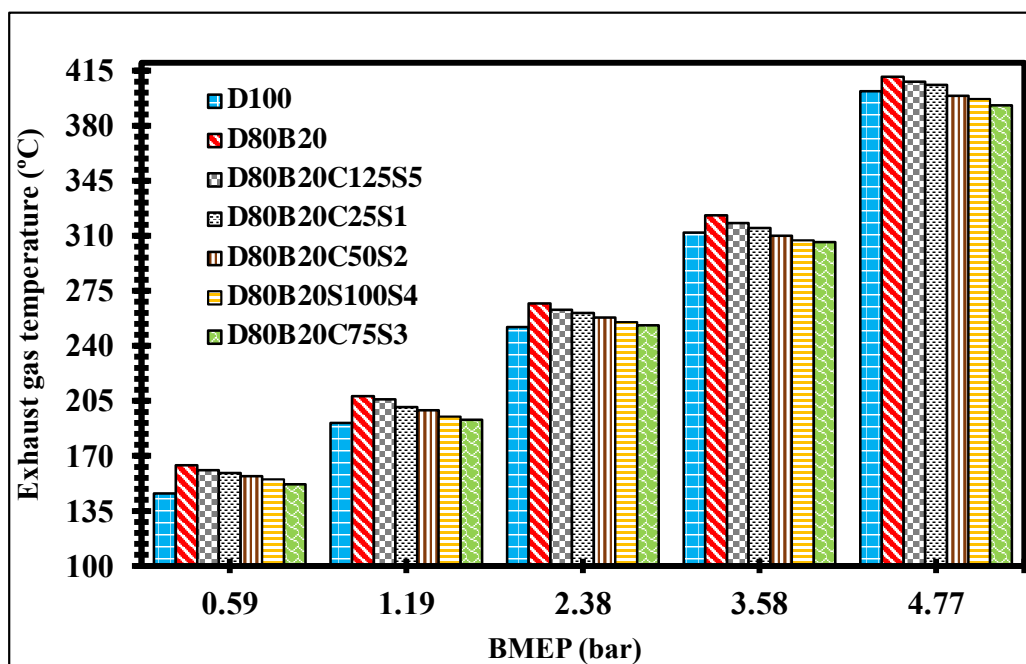
Figure 4.21. Variation of exhaust gas temperature with brake mean effective pressure

The engine operating on the 75ppm dosage of the nano-fuel blend showed the lowest EGT at all the engine loads, whereas EGT is highest for D80B20 test fuel. The higher EGT in diesel-biodiesel blend is closely associated with the larger portion of fuel mixture burning in the diffusion combustion phase compared to neat diesel. The truth of the matter is that the heat released during the diffusion combustion is not utilized for useful work and is treated as a waste, which further gets assembled in the exhaust and raises its temperature. However, in the case of neat diesel and nano-fuel blends, the maximum portion of the mixture is burnt in the earlier (premixed) combustion phase, resulting in lower EGT at all the engine loads. Besides the higher heat transfer rate of MWCNT nanoparticles also plays a significant role, thereby resulting in significant decrease in exhaust gas temperature. Therefore, at full load the EGT temperature of neat diesel, D80B20, D80B20C25S1, D80B20C50S2, D80B20C75S3 and D80B20C100S4 and D80B20C125S5 is 402, 411, 406, 399, 393, 397 and 408 °C, respectively.

4.10. Exhaust Emission characteristics of Nano-fuel blends

The present section illustrates the mechanism behind the generation of exhaust emissions in the CI engine and the influence of *S. oleosa* biodiesel and MWCNT nanoparticles dosage on

their formation and control. The exhaust gases such as Nitrogen Oxide (NO_x), Carbon Monoxide (CO), Unburnt Hydrocarbon (HC) and smoke opacity liberated during the combustion of different fuels were analyzed and compared by varying the engine loads from 0 to 100%. As already detailed in chapter 3, the engine exhaust emissions were captured by means of AVL gas analyzer and smoke meter installed at the engine exhaust and also the evaluation was made on brake specific (g/kWh)" basis by considering the flexible fuel composition.

4.10.1. Nitrogen Oxide (NO_x) emissions

The nitrogen oxide emission is amongst the most harmful pollutant associated with CI engine, which plays a significant role in causing severe health hazards to mankind and the environment. Long-time exposure to NO_x emission can adversely affect human health by causing serious respiratory and heart disease issues. Besides, the smog and brown clouds of NO_x is the major contributor to acid rain and the ozone layer constitution at ground level, damaging flora and fauna along with the ecosystem.

Broadly, the formation of NO_x during the combustion inside the CI engine is dependent on three mechanisms, including (i) Thermal NO_x, (ii) Fuel NO_x (iii) Prompt NO_x. The temperature of exhaust gases during the combustion is mainly responsible for the formation of thermal NO_x. The higher temperature in the exhaust can be attributed to the presence of oxygen availability, facilitating the combustion and residence time of high-temperature combustion reactions [67]. Nanoparticles having higher heat dissipation potentiality can play a decisive role in reducing the formation of thermal NO_x. On the other side, the nitrogen molecule bonded with the fuel is accountable for the fuel NO_x. The outgrowth of prompt NO_x is insuppressible, and it is the outcome of the reaction of nitrogen present in the atmosphere with the combust products in the fuel-rich zone [66]. However, in CI engines, the higher temperature chemical reactions play a dominant role in the NO_x formation (based on extended Zeldovich mechanism) [41].

The variation of NO_x emission with respect to BMEP for different fuel samples is shown in

Figure 4.22. As can be observed, the rise in engine loads results in decreased NO_x emissions

for all the fuels. Thus, signifying a potential trade-off between engine load and NO_x emissions.

This is due to the availability of lean mixture i.e., excess air at lower and part loads ($\leq$50%).

Therefore, excess air availability facilitates the combustion reaction, resulting in a substantial

rise in temperature and results in higher NO_x emission formation. In comparison to neat diesel,

the NO_x emission is considerably higher in D80B20 fuel. This can be attributed to the

availability of extra oxygen in biodiesel, facilitating the combustion process as well as the NO_x

emission.

It is interesting to note that the NO_x emission was significantly reduced in case of nano-fuel

blends, when comparison is made with D80B20 and D100 fuel. The results also highlighted

that increasing the dosage of MWCNT nanoparticles restricts the NO_x formation. This is why

despite of the presence of 20% by volume of biodiesel in nano-fuel blends, the NO_x emission

was reported to be lower than neat diesel fuel at all the engine loads. The reduction can be

attributed to the higher convective heat transfer co-efficient of MWCNT nanoparticles, making

it an excellent coolant for maintaining the combustion chamber temperature and resulting in

lower NO_x emission. Secondly, the excellent NO_x adsorption proneness of MWCNT

nanoparticles. It soaks up the NO_x emitted out during the combustion and further decomposed

it into nitrogen in the presence of reducing gases such as H_2, CO, or hydrocarbons [192].

Therefore, the NO_x emission value at peak load for D100, D80B20, D80B20C25S1,

D80B20C50S2, D80B20C75S3, D80B20C100S4 and D80B20C125S5 is 11.0, 11.8, 10.7,

10.1, 9.8, 9.6 and 9.1 g/kWh, respectively.
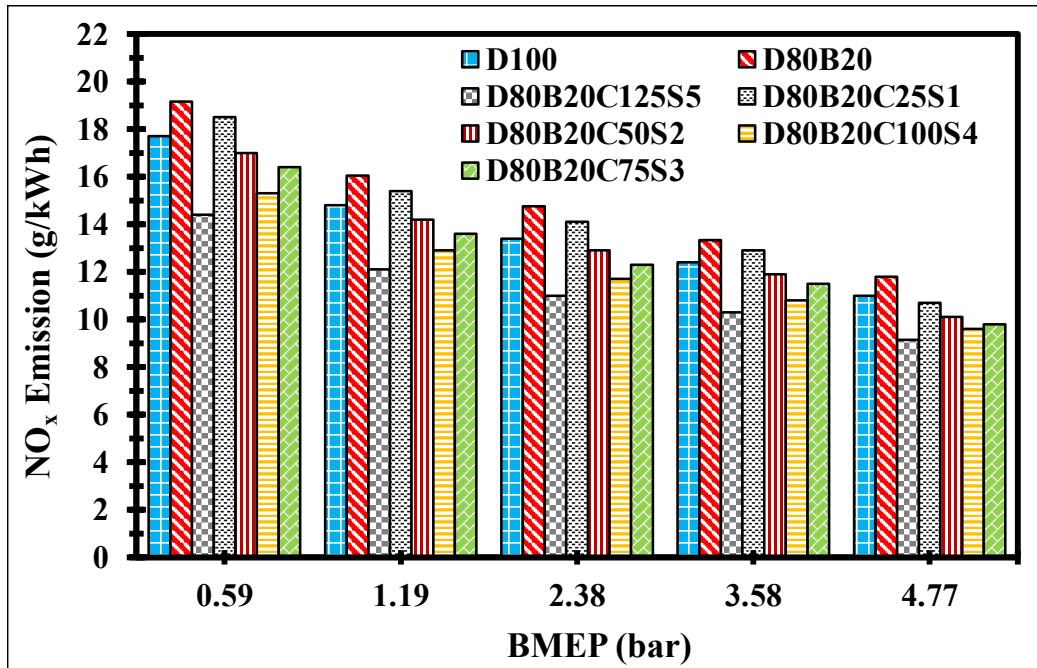
Figure 4.22. Variation of NO_x emissions with brake mean effective pressure

4.10.2. Carbon Monoxide (CO) emissions

Carbon Monoxide is the product of incomplete combustion of carbon-containing fuel in the combustion chamber. The majority of CO pollutants in the atmosphere come from vehicular exhaust. In comparison to other exhaust gases, the CO is very stable, and it can remain in the atmosphere for a longer duration, it is because it is a big threat to the environment.

Figure 4.23 portrays the variation of CO emission with BMEP for different test fuel blends, and neat diesel. The CO emission in the CI engine is governed by fuel-air equivalence ratio. As can be observed, with the rise in engine load upto 50%, the CO emissions tends to decrease and reaches to minimum. At low load, the fuel-air equivalence ratio is improper and oxidation rate is relatively slow due to the availability of excess air and lower cylinder temperature, thus resulting in higher CO emission. However, the availability of optimum fuel and air for proper combustion at part loads, supporting the oxidation of carbon and resulting in lower CO emissions. Furthermore, the interrupted supply of rich mixture at higher loads leads to partial oxidation and formation of higher CO emission. The supply of additional oxygen for the complete conversion of carbon molecules to carbon dioxide, the CO emissions were

significantly lower in biodiesel blend whereas neat diesel showed the highest emission at all the engine loads. On the other side the excellent oxygen donating tendency of nanoparticles from its lattice side during the chain reaction, facilitates the oxidation process and restricts the CO constitution. In addition, the improved ignition characteristics and better fuel atomization of nano-fuel blends improves the combustion efficiency and restricts the CO emissions to a greater extent. Therefore, the CO emissions at peak load is 9.0, 7.8, 6.8, 6.4, 5.2, 5.9 and 7.3 g/kWh for D100, D80B20, D80B20C25S1, D80B20C50S2, D80B20C75S3, D80B20C100S4 and D80B20C125S5, respectively.
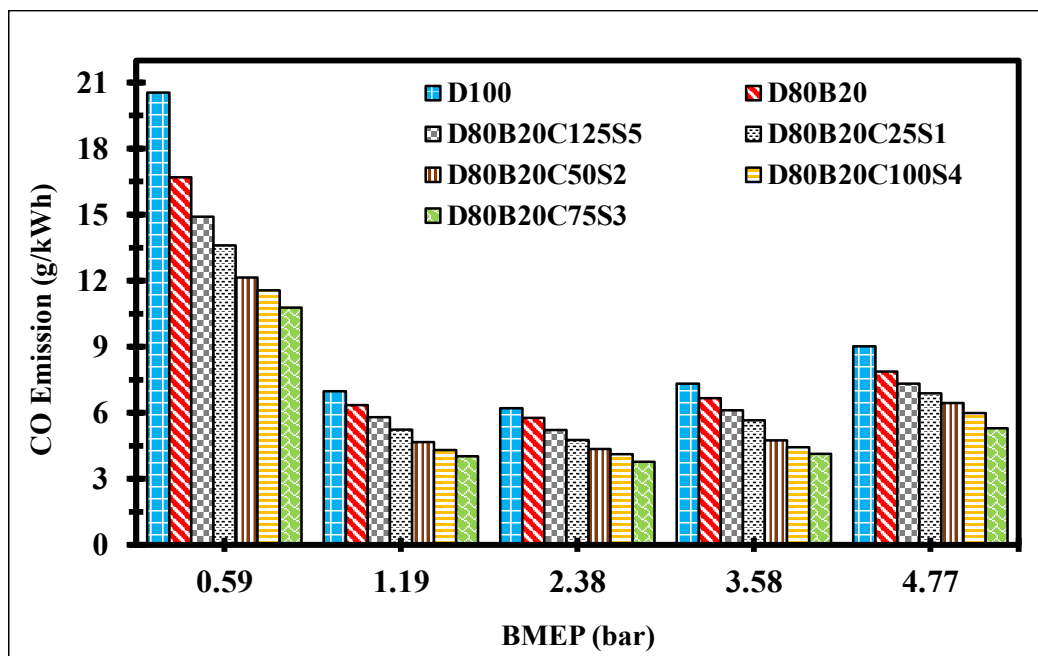
Figure 4.23. Variation in CO emissions with brake mean effective pressure

4.10.3. Unburnt Hydrocarbon (UBHC) emissions

The fuel particles that don't take part in the combustion reaction and leave the exhaust as unprocessed are unburnt hydrocarbon pollutants. Conversely, it wouldn't be wrong saying that the percentage of unburnt hydrocarbon emission represents the quality of combustion occurring inside the engine. There are certain factors such as composition of fuel, combustion temperature, cylinder crevices, availability of oxygen, combustion reaction time, engine

configuration etc. which can facilitate the formation of UBHC emission in the diesel engine [52].

Figure 4.24. shows the variation of UBHC emission of different fuels with BMEP. Due to lower in-cylinder temperature and distorted flame speed resulting in improper propagation, the emission is higher at low loads. With the engine load increase, the emissions were found to decrease and are minimum at 75% engine load. However, due to rich mixture availability at peak load, the UBHC emissions were slightly higher than the adjacent load. The trend is similar to the fuel samples. Among all the fuels, the neat diesel with higher ignition delay and insufficient oxygen availability showed the highest UBHC emission peaks at all the engine loads. The emissions are significantly lower in biodiesel blend due to sufficient oxygen content leading to complete combustion. In comparison to D100, at full load the decrease of 7.8%, 39.2% and 23.5% in the value of UBHC emission was observed for D80B20, D80B20C25S1 and D80B20C50S2. The UBHC emissions are significantly lower in nano-fuel blends except for D80B20C75S3, D80B20C100S4 and D80B20C125S5 which showed slightly higher emissions i.e., 3.9%, 11.7% and 29.4%, respectively at peak engine load than the neat diesel. The decrease in UBHC emission with the addition of lower dosage (25 and 50 ppm) MWCNT nanoparticles can be attributed to catalytic behaviour, improved thermal conductivity and efficient heat and mass transfer property efficient, promoting the complete combustion of carbon particles. On the other side, the presence of rich carbon availability in MWCNT structure comes into play, due to which the emission is slightly increased at higher loads.
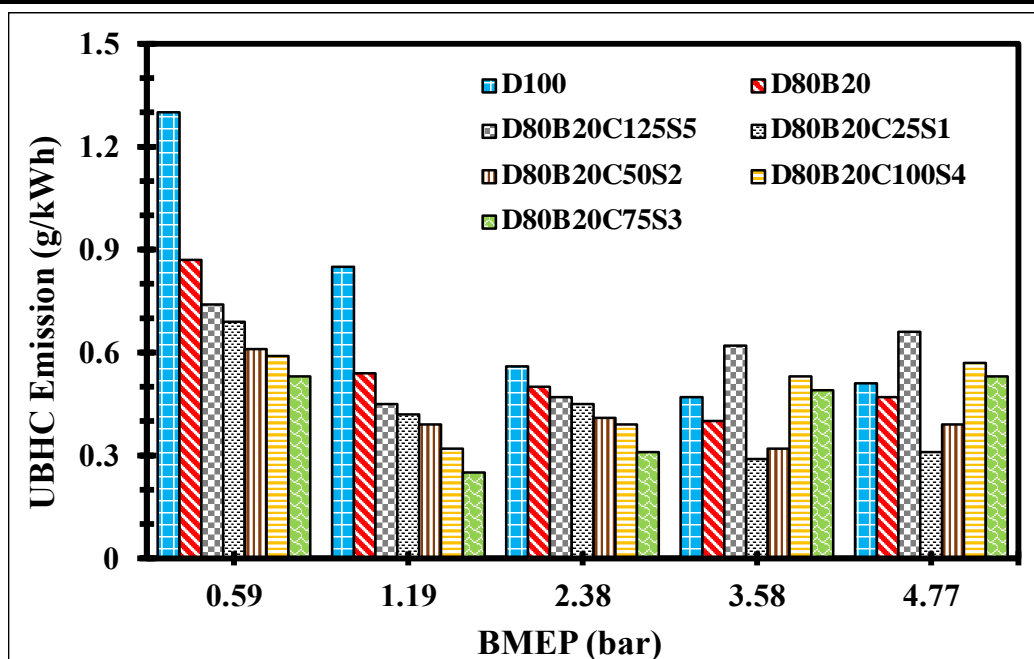
Figure 4.24. Variation in UBHC emissions with brake mean effective pressure

4.10.4. Smoke Opacity (%)

The smoke opacity indirectly signifies the amount of soot present in the engine exhaust emission and to be more specific soot is the dominating component in the particulate matter composition. The soot formation is the result of the thermal cracking of long branch chained hydrocarbon in the oxygen-deficient atmosphere [230]. Therefore, a decrease in the air-fuel ratio promotes the smoke opacity in the diesel engine.

The variation of smoke opacity with respect to BMEP is shown in **Figure 4.25.** The increase in fuel supply at higher engine loads facilitates the smoke opacity and, therefore, is maximum at peak load. A similar trend is observed for all the fuel samples. Smoke is mainly the result of rich fuel zones present inside the combustion chamber. Among all the fuel samples, the smoke opacity is higher in neat diesel due to the deficiency of oxygen, delay in the ignition and higher aromatic content. With the addition of oxygenated biodiesel fuel, the smoke opacity was observed to be significantly reduced. At full load, the percentage of smoke opacity for D100, D80B20, D80B20C25S1, D80B20C50S2, D80B20C75S3 and D80B20C100S4 and D80B20C125S5 is 74%, 71.8%, 70.7%, 69.4%, 65%, 66% and 71.1% respectively.

Moreover, the soot formation in nano-fuel blends is substantially lower than diesel, biodiesel, and its blend. This can be attributed to the higher heat transfer characteristics minimizing the fuel-rich zones and efficient fuel-air mixing initiated with MWCNT nanoparticles' addition in the diesel-biodiesel blend.
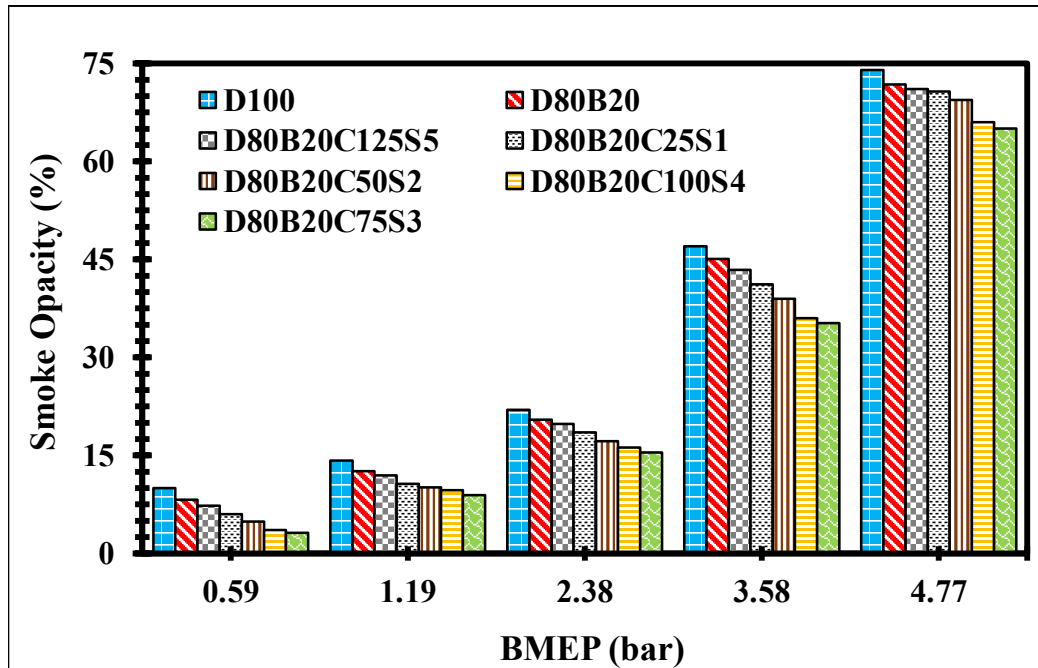
Figure 4.25. Variation in smoke opacity (%) with brake mean effective pressure

4.11. Evaluation of RSM Model (ANNOVA Analysis)

The relation between the input and the response variables considered for RSM approach were predicted in terms of coded factors which are nothing but just a non-dimensional second order polynomial equations **(refer APPENDIX 4)**. These equations help in predicting the response factors and are only valid if the value of input lies in between the particular limits i.e. nanoparticle concentration (25-125 ppm) and engine BMEP (0.59-4.77 bar).

The validation of the model chosen and implemented was carried out by performing the ANOVA test. The ANOVA is a statistical method which verifies the significance of the responses derived from the hypothesis constructed. In simple words, it is helpful in examining whether or not multiple correlation fit approach is statistically important for the entire quadratic model. The analysis of variance (ANOVA) for different response factors considered are listed

in **Table 4.3, 4.4 and 4.5.** The statistical relevant values of the each independent factors and their interrelationship with the each other are also determined in terms of calculating the SS, F and P values. The significance of all the models were confirmed at a confidence level of 95%. Also, if the p-value is less than 0.05 for any given input factor, it denotes the factor effect are significant at 95% confidence level i.e. weightage of that particular input is higher in comparison to the other. As can be observed both the input variables have significant effect on the given responses. The value of R^2 (Coefficient of determination) in **Table 4.6.** is the indicator of fitness. In simple words its percentage value signifies the model chosen and applied for the given analysis is highly accurate when compared is made with the experimental results. The significance of adjusted R^2 comes into play when any there is any modification in the model i.e. it counterbalances the effect of addition or subtraction of new variable. Larger is the value of adjusted R^2, better is the accuracy of the model. However, on the other side, the predicted R^2 value denotes the prediction quality of the model i.e., what extent the model predicts the new set of data.

Table 4.3. ANOVA (Analysis of variance) for BTE and BSEC

Source	BTE			BSEC		
	*SS	*F-value	*P-value	SS	F-value	P-value
Model	286.806	209.90	0.01	178.063	233.30	0.000
Linear						
A: Nanoparticle (ppm)	0.457	437.46	0.00	0.201	1.31	0.0185
B: Engine BMEP (bar)	238.644	1.67	0.237	90.326	591.72	0.000
Interaction						
AB	0.126	0.46	0.519	0.004	0.03	0.878
Square						
A²	15.005	54.91	0.00	10.099	66.16	0.000
B²	27.861	101.95	0.00	61.061	400.01	0.000
Error	0.0321			0.0213		
Total	288.719			179.131		

Table 4.4. ANOVA (Analysis of variance) for CO and UBHC

Source	CO			UBHC		
	*SS	*F-value	*P-value	SS	F-value	P-value
Model	180.046	103.67	0.00	0.2897	13.12	0.002
Linear						
A: Nanoparticle (ppm)	0.762	2.19	0.0351	0.0341	7.73	0.027

Some studies on nano-particles doped alternative fuels in Unmodified CI Engine

B: Engine BMEP (bar)	65.175	187.63	0.00	0.0384	8.69	0.021
Interaction						
AB	0.163	0.47	0.516	0.0266	6.04	0.044
Square						
A^2	9.999	28.79	0.001	0.0320	7.26	0.031
B^2	80.351	231.32	0.00	0.1032	23.37	0.002
Error	0.0115			1.0012		
Total	182.478			0.3207		

Table 4.5. ANOVA (Analysis of variance) for NO_x and Smoke opacity

Source	NO_x			Smoke opacity		
	*SS	*F-value	*P-value	SS	F-value	P-value
Model	80.70	4941.62	0.000	7456.84	4716.57	0.000
Linear						
A: Nanoparticle (ppm)	12.12	3713.14	0.003	0.45	1.42	0.273
B: Engine BMEP (bar)	64.22	19663.01	0.000	6038.85	19098.38	0.000
Interaction						
AB	1.67	0.33	0.585	0.17	0.53	0.492
Square						
A^2	0.0836	25.59	0.001	56.86	179.82	0.000
B^2	3.89	1193.37	0.000	554.67	1754.18	0.000
Error	0.000			0.000		
Total	80.72			7459.05		

Table 4.6. Evaluation of Model

Model	BTE (%)	CO (g/kW/h)	UBHC (g/kW/h)	Smoke Opacity (%)	BSEC (MJ/kW/h)	NO (g/kW/h)
R^2 (%)	99.34	98.67	90.36	99.97	99.40	99.97
Adjusted R^2 (%)	98.86	97.72	89.47	99.95	98.98	99.95
Predicted R^2 (%)	93.84	90.44	85.04	99.68	93.73	99.80

4.12. 3D-Surface and Contour plots for input and output variables

By taking into consideration the fitted models of different responses, the contour and surface plots were developed to analyze the collective effect of input variables (nanoparticle concentration and engine load) on the engine performance and emission characteristics.

Some studies on nano-particles doped alternative fuels in Unmodified CI Engine
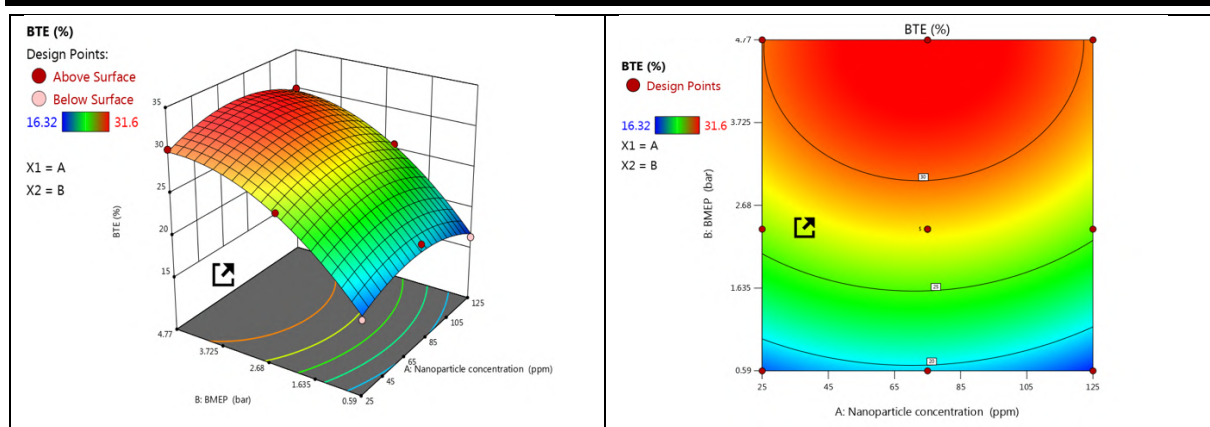
Figure 4.26. 3D-Surface and contour plots of BTE vs. nanoparticle concentration and engine BMEP
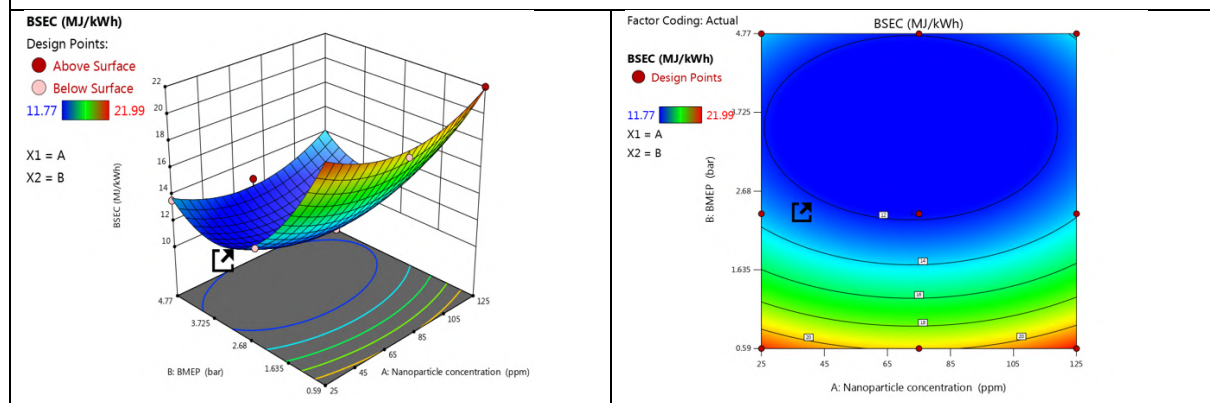
Figure 4.27. 3D-Surface and contour plots of BSEC vs. nanoparticle concentration and engine BMEP

The plots in **Figure 4.26** clearly portrays that as the nanoparticle concentration increases in the fuel blend, the BTE first increases and reaches its maximum values and then starts decreasing. This can be attributed to the poor fuel atomization resulting in improper fuel-air mixing. Whereas, due to increase in supply of rich mixture at higher engine BMEP, the BTE is observed to be lower. Thus, there exists a critical value of BTE and which lies in the nanoparticle concentration range of 65-85ppm and moderate engine BMEP of ≈3 bar.

In contrast to BTE, the surface and contour plot of BSEC (**Figure 4.27)** showed decreasing trend, when the nanoparticle concentration and engine load value reaches to a moderate limit. However, with further increase in any of the input variable, the BSEC starts rising and is maximum at nanoparticle dosage of 125ppm and engine BMEP 4.77 bar.

Figure 4.28. 3D-Surface and contour plots of CO vs. nanoparticle concentration and engine BMEP
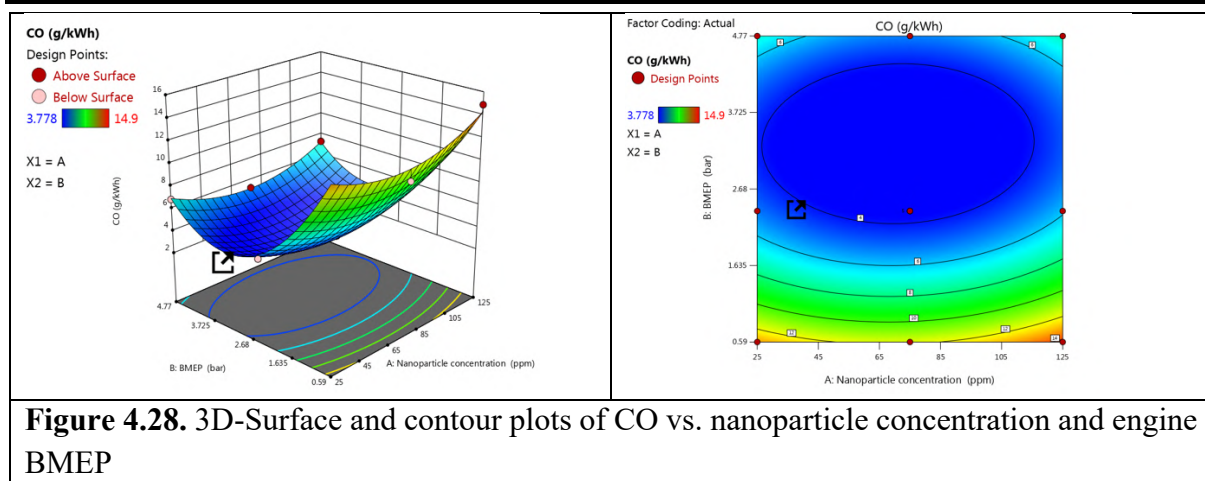
Figure 4.28, 4.29, 4.30 and 4.31 shows the interaction of nanoparticle concentration and engine loading condition on exhaust emissions (CO, UBHC, NO_x and Smoke opacity). The CO and UBHC emissions curves showed decreasing trend, as soon as the concentration of MWCNT nanoparticle is increased and at the same time engine BMEP is kept constant. However, after reaching the concentration at higher levels i.e. ($\approx$<85ppm) dosage level, the emissions start increasing again. This can be attributed to the ineffective atomization rate offered by increase in the dosage of nanoparticles. Also, the nature of CO and UBHC emissions plot are observed comparable, when the condition is reversed i.e., nanoparticle concentration level is kept constant and at the same time the engine BMEP is increased from (0.59-4.77) bar. This can be justified due to the sufficient availability of air-fuel mixture at moderate engine loads, thus facilitating the oxidation of carbon monoxide and reducing the UBHC emissions.

As a whole, the plots highlighted that increasing the nanoparticle concentration, the exhaust emissions showed decreasing trend upto 85 ppm dosage level, however, with any further increase in the nanoparticle concentration, the emissions are significantly higher except for smoke opacity on which the effect is not much intense. Similarly, the change in CO, UBHC and NO_x emissions are observed to be similar with the increase in engine BMEP.

Figure 4.29 shows that keeping the nanoparticle concentration level in between 65 to 85ppm and at the same time engine operating in range of 2.5-3 bar BMEP, the CO emission is observed to be optimum i.e., in range of (2.054-3.256 g/kWh) amongst all the other combinations.
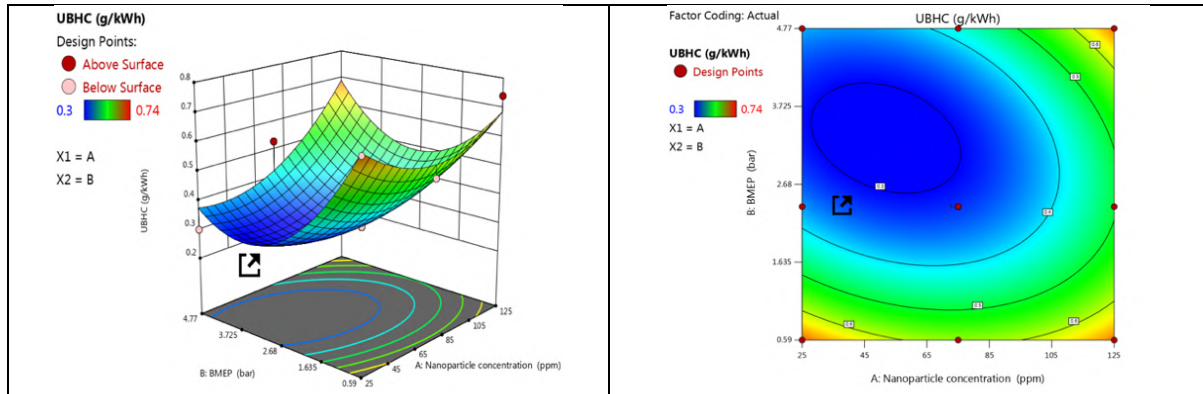
Figure 4.29. 3D-Surface and contour plots of UBHC vs. nanoparticle concentration and engine BMEP

Similarly, the collective effect of input variables on UBHC emissions is shown in **figure 4.29.** The UBHC emissions i.e. in range of (0.2317-0.3672 g/kWh) can be obtained at a nanoparticle concentration limit of 65-85 ppm and engine BMEP of 2.5-3 bar.
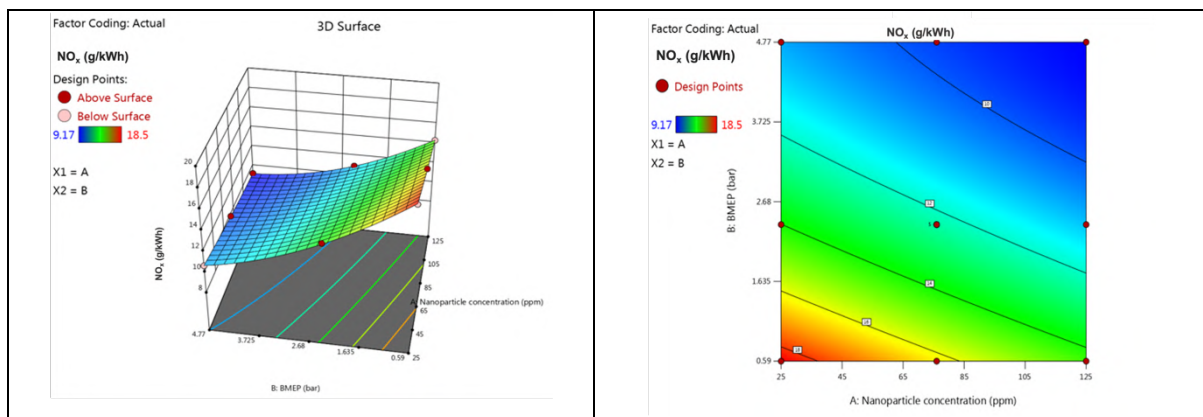
Figure 4.30. 3D-Surface and contour plots of NO_x vs. nanoparticle concentration and engine BMEP

Figure 4.30 shows the relationship between input variables and NO_x emissions. The plots clearly highlight that keeping the BMEP value constant and increasing the nanoparticle concentration showed lower emissions of NO_x. However, on the contrary keeping the nanoparticle dosage level constant and increasing the BMEP showed very slight decrease in the value, thus highlighting the dominating nature of MWCNT nanoparticles on NO_x

emissions. The combined effect of input variables on smoke opacity is also shown in **Figure 4.31.** Smoke opacity showed exponential rise with the increase in BMEP and the value is maximum at full engine load. However, increasing nanoparticles concentration showed decreasing trend and the smoke opacity is minimum in between (65 to 85ppm) dosage level, subsequently, the emission starts increasing again.

Figure 4.31. 3D-Surface and contour plots of smoke opacity vs. nanoparticle concentration and engine BMEP
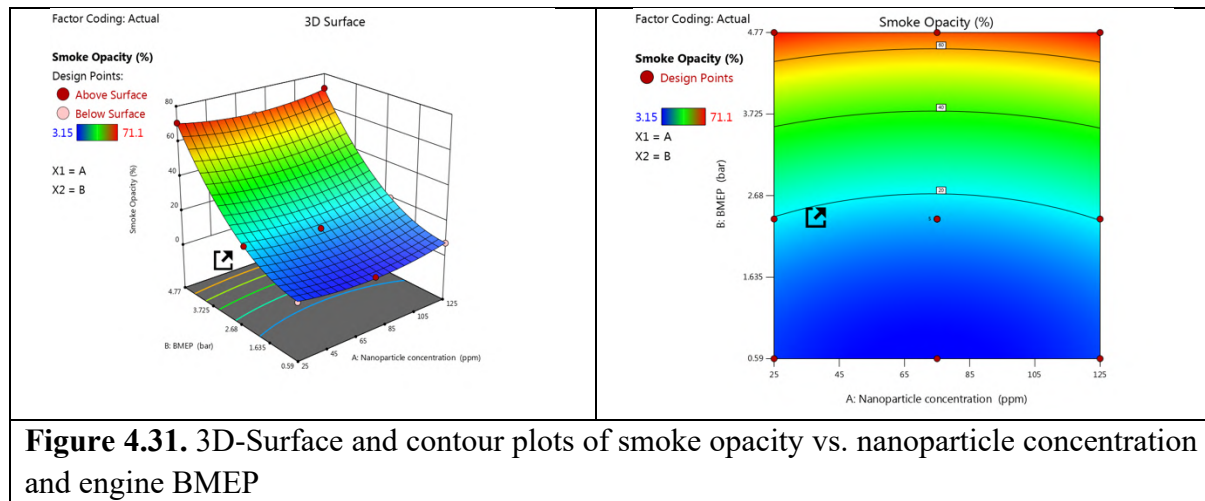
4.12.1. Optimization & Validation test

RSM optimizer tool generally working on the desirability function approach was used to obtain the optimized values. Desirability is measured on the scale of 0 to 1, with the value close to 1 represent the closeness of output value to ideal and 0 corresponds to the unacceptable interval. The objective of employing the RSM based multi-optimization technique in the present research is to identify the appropriate concentration level of MWCNT nanoparticle (ppm) and engine operating condition (BMEP) to preserve the time and experimentation cost. The analysis was done by giving the input and the output values similar weightage and significance. Also, the goal is to obtain the higher engine efficiency and lower emissions. Therefore, the performance parameters were kept in criterion of maximum whereas the minimum criterion was assigned to engine exhaust emissions parameters. It is also worth to mention that input variable brake specific energy consumption was not considered for the optimization, as RSM optimizer can accommodate only five response variables at a time. **Table 4.7** highlights the

details of the optimization principle adopted and **Figure 4.32** shows the output of the RSM optimizer tool. Therefore, engine operating at BMEP of 2.99 bar and test fuel containing nanoparticle concentration of 75.5 ppm are the ideal parameters at which engine delivers optimum output i.e., 30.0% BTE, 11.3 g/kWh NO_x, 2.62 g/kWh CO, 0.299 g/kWh UBHC and 24.7% smoke opacity.

Table 4.7. Optimization principles

| Factors | Boundaries | | Weight | Significance | Criterion |
	Lower	Upper			
Nanoparticles Concentration (ppm)	25	125	1	3	In range
Engine BMEP (bar)	0.59	4.77	1	3	In range
BTE (%)	16.3	31.6	1	3	Maximum
BSEC (MJ/kWh)	11.7	21.9	1	3	Maximum
CO (g/kWh)	3.77	14.9	1	3	Minimum
UBHC (g/kWh)	0.31	0.74	1	3	Minimum
NO_x (g/kWh)	9.15	18.5	1	3	Minimum
Smoke opacity (%)	3.15	71.1	1	3	Minimum
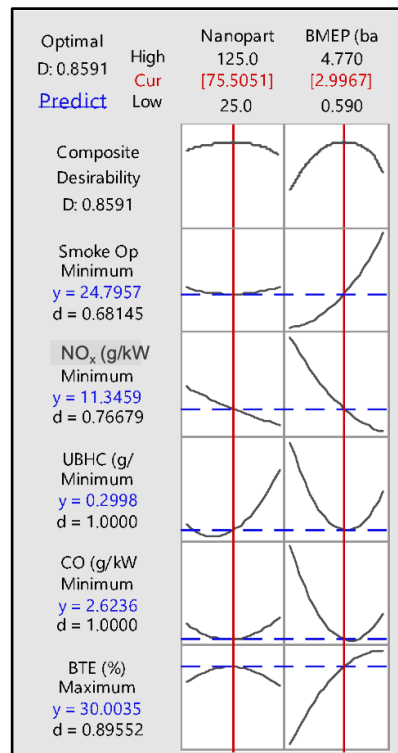
Figure 4.32 Optimization plot: Effect of input parameters on various responses

Moreover, the validation test was performed to measure the effectiveness of the RSM model applied. The effectiveness of the model signifies its ability to deliver the desired output. The

predicted results obtained from the RSM optimizer tool was validated by carrying out the actual

engine trials by taking into consideration the obtained optimized inputs. **Table 4.8.** gives the

effectiveness of the model which is equal to the difference(residual) between the predicted and

experimental values. The residual percentage obtained for different responses are well within

the acceptable range. Hence, the regression models developed for the optimization of

nanoparticle concentration and engine BMEP value is useful in successfully predicting the

experimental data with a fair accuracy of 90%.

Table 4.8. Validation test

Fuel Blend	Engine BMEP (bar)		BTE (%)	CO g/kWh	UBHC g/kWh	NO$_x$ g/kWh	Smoke opacity (%)
D80B20C75.5S3	2.99	Predicted	30.0	2.62	0.299	11.34	24.7
		Experimental	29.58	2.87	0.32	12.06	25.8
		Residual (%)	1.4	9.8	7.3	6.4	4.8

CONCLUSION AND FUTURE SCOPE

5.1. Conclusions

The present research work explores the feasibility of two different nanoparticles with an objective to enhance the sustainability of underutilized inedible *Schleichera oleosa* oil biodiesel. Various nano-fuel blends containing different concentration levels of alumina and MWCNT nanoparticles dispersed in the diesel-biodiesel blend were prepared and their results were compared with neat diesel, biodiesel and diesel-biodiesel blend. The economical routes of nanoparticle synthesis, characterization techniques and long-term stability aspects of nano-fuels their physico-chemical properties were evaluated as per ASTM standards.

The experimentation on ignition probability and fuel droplet size of nano-fuel blends were also investigated profoundly by developing a hot-plate and fuel-spray analyzer set-up. Subsequently, the combustion, performance and emission characteristics were investigated by operating a farmland diesel engine fuelled with nano-fuel blends and comparing the outcomes with diesel (D100), biodiesel (B100) and its blend (D80B20). Eventually, an RSM based multi-objective optimization model was designed with the purpose to determine the most optimum concentration level of nanoparticle and engine load at which the appropriate engine characteristics can be obtained.

The following conclusions are drawn based on comprehensive research carried out:

1. The presence of (0.03-0.05%) of cyanolipids, more than 40% of unsaturated fatty acids and higher oil content (35-40%), *Schleichera oleosa* oil can be a promising inedible feedstock for biodiesel production, especially for India and Southeast Asia.

2. Nano-fuels, exhibiting unique catalytic, higher thermal conductivity and enhanced radiative and convective heat & mass transfer properties, proven to be a potential fuel reformulation concept for millions of existing CI engines.

3. Diesel-biodiesel blend containing nanoparticles (Alumina and MWCNT) to surfactant (SDS) in ratio 1:3 and 1:3.5 showed higher zeta potential value. Thus, signifying the more extended stability and homogeneity of nanoparticles suspension. Also, as a whole compared to alumina, MWCNT dispersed fuels showed higher zeta potential values at all the dosage level.

4. The visual inspection tests showed that 100 ppm is the critical concentration of MWCNT nanoparticles beyond which the agglomeration witnesses when nano-fuel blends were kept stored at a temperature range of 10°C for 60 days.

5. As compared to diesel-biodiesel blend, the physico-chemical properties such as cetane index, calorific value and flash point of nano-fuel blends were significantly improved, except viscosity and density which were slightly higher. Also, the polymeric structure, of MWCNT NPs makes it an excellent pour point depressant for diesel-biodiesel blend.

6. Due to higher radiative, heat and mass transfer characteristics, the increase in MWCNT nanoparticles' dosage in the diesel-biodiesel blend showed higher ignition probability with D80B20C125S5 fuel blend attaining 100% at 430°C.

7. The fuel droplet size found for D80B20C75S3 is 15.1μm, which is almost comparable with neat diesel (14.4 μm) and much better than D80B20 (18.9 μm), thereby indicating better atomization of nano-fuel blends in the engine.

8. Nano-fuel blend containing 75ppm of MWCNT showed HRR nearly comparable to D100 i.e., 64.2 J/°CA. The tendency of donating extra oxygen atom present in its lattice site, nanoparticles act as an exceptional catalyst in the combustion reaction. Therefore,

diminishing the effect of low calorific value and poor atomization effect of biodiesel and improving the combustion efficiency.

9. Due to the higher evaporation rate offered by MWCNT NPs, the ignition delay is lowest in nano-fuel blends. In contrast, the burning of a larger portion of the mixture in the diffusion phase, the combustion duration, is also more prolonged in nano-fuel blends.

10. The engine performance and emissions characteristics with nano-fuel blends were significantly improved as compared to D80B20. However, D100 showed the highest value of BTE and lowest BSEC among all the fuel samples. At peak load, the D80B20C75S3 blend showed 6.7% increase in BTE and 10.3% reduction in BSEC as compared to D80B20.

11. Substantial reduction in harmful exhaust emissions (CO, UBHC, and smoke opacity) was also noticed when the engine was operated with nano-fuels. At peak load, maximum reduction of 42.2% in CO emission & 12.1% in smoke opacity was reported in D80B20C75S3 fuel, whereas D80B20C25S1 showed maximum reduction of 39.2% in UBHC emission as compared to D100.

12. Most importantly, the NO_x emission (a major contradicts of diesel, biodiesel blends) was also significantly reduced with the usage of nano-fuels. The maximum reduction of 17.2% & 22.8% was observed in D80B20C125S5, compared to D100 & D80B20 fuel, due to the excellent NO absorbent tendency of MWCNT nanoparticles.

13. The RSM-optimizer result showed that fuel blend containing 75.5ppm concertation of MWCNT NPs and engine operating with BMEP of 2.9 bar are the appropriate input conditions at which optimum engine output can be achieved.

5.2. Scope of Future Work

1. In the present work, biodiesel's blending ratio is limited to 20% by volume in the diesel. However, to explore a new window of opportunity, the investigation can be further extended by investigating higher blends or 100% *schleichera oleosa* biodiesel.

2. The properties of MWCNT nanoparticles as a fuel additive are utilized in the present study. Research efforts are required to be invested in other unexplored nanoparticles such as Iron, silicon, boron having higher heating value (in terms of volume) and the capability to resist agglomeration when suspended in the base fluid.

3. Efforts can also be deployed to study the effect of nanoparticles addition on soot and PM exhaust emissions.

4. The spray characteristics such as cone angle of spray plume angle, secondary atomization, breakup length and ambient pressure conditions of nano-fuels are still not penetrated to its full-depth. The numerical study can be conducted by analyzing the spray models under different conditions using computational fluid dynamics.

5. The risk assessments related to the release of unburnt nanoparticles after combustion into the atmosphere still lack profound research and can be a delicate issue that requires extensive attention.

REFERENCES

[1] Diesel Technology Forum Annual Report **2019**, https://www.die-selforum.org/files/dmfile/2019-annual-report-pages-FINAL.pdf.

[2] Agarwal, A.K., Gupta, J.G., and Dhar, A., "Potential and challenges for large-scale application of biodiesel in automotive sector," *Prog. Energy Combust. Sci.* 61:113–149, **2017**, doi:10.1016/j.pecs.2017.03.002.

[3] IEA, World Energy Outlook **2019**, https://webstore.iea.org/download/summary/2467?fileName=1.English-Summary-WEO2019.pdf.

[4] BP Statistical Review of World Energy **2020**, https://www.bp.com/content/dam/bp/business-sites/en/global/corporate/pdfs/energy-economics/statistical-review/bp-stats-review-2020-full-report.pdf.

[5] Gebremariam, S.N. and Marchetti, J.M., "Economics of biodiesel production: Review," Energy Convers. Manag. 168(April):74–84, **2018**, doi:10.1016/j.enconman.2018.05.002.

[6] Sommer, A., "Burning Fossil Fuels: Impact of Climate Change on Health," Int. J. Health Serv. 46(1):48–52, **2016**, doi:10.1177/0020731415625253.

[7] Halder, D. and Gupta, A., "Application of Portfolio Approach towards Energy Security: A Case Study of Japan and Implications for India," J. Econ. Manag. Trade 23(6):1–12, **2019**, doi:10.9734/jemt/2019/v23i630151.

[8] Ramkumar, M., Santosh, M., Mathew, M.J., and Siddiqui, N.A., "India at crossroads for energy," Geosci. Front. (October), **2019**, doi:10.1016/j.gsf.2019.10.006.

[9] Shanmugam, J.C.M.V.P., "Impact of Crude Oil Price on the Socio-Political Environment of Global Countries," Soc. Sci. Res. Netw. (9):198–208, **2019**, doi:10.26643/rb.v118i3.7635.

[10] Kumar, S., Pradhan, A.K., Tiwari, A.K., and Kang, S.H., "Correlations and volatility spillovers between oil, natural gas, and stock prices in India," Resour. Policy 62(April):282–291, **2019**, doi:10.1016/j.resourpol.2019.04.004.

[11] BP Statistical Review of World Energy **2018**, https://www.bp.com/content/dam/bp/business-sites/en/global/corporate/pdfs/energy-economics/statistical-review/bp-stats-review-2018-full-report.pdf.

[12] IQAir, "World Air Quality Report," 2019 World Air Qual. Rep. 1–35, **2019**.

[13] Kumar, A., Kumar, P., Mishra, R.K., and Shukla, A., "Study of Air and Noise Pollution in Mega Cities of India," in: Singh, V. P., Yadav, S., and Yadava, R. N., eds.,

Environmental Pollution, Springer Singapore, Singapore, ISBN 978-981-10-5792-2: 77–84, **2018**.

[14] Lloyd, A.C. and Cackette, T.A., "Diesel Engines: Environmental Impact and Control," J. Air Waste Manag. Assoc. 51(6):809–847, **2001**, doi:10.1080/10473289.2001.10464315.

[15] Akinci, B., Kassebaum, P.G., Fitch, J. V., and Thompson, R.W., "The role of bio-fuels in satisfying US transportation fuel demands," Energy Policy 36(9):3485–3491, **2008**, doi:10.1016/j.enpol.2008.05.021.

[16] Mehta, C.R., Jena, P.C., Chandel, N.S., and Jha, A., "Indian agriculture counting on farm mechanization," AMA, Agric. Mech. Asia, Africa Lat. Am. 50(1):84–89, **2019**.

[17] IBEF, Indian Agriculture and Allied Industries Report (September **2020**), https://www.ibef.org/download/IBEF-Theme-1-15-updated-low.pdf.

[18] Greim, H., "Diesel engine emissions: are they no longer tolerable?," Arch. Toxicol. 93(9):2483–2490, **2019**, doi:10.1007/s00204-019-02531-5.

[19] Bharj, R.S., Kumar, R., and Singh, G.N., "On-Board Post-Combustion Emission Control Strategies for Diesel Engine in India to Meet Bharat Stage VI Norms," in: Agarwal, A. K., Gupta, J. G., Sharma, N., and Singh, A. P., eds., Advanced Engine Diagnostics, Springer Singapore, Singapore, ISBN 978-981-13-3275-3: 105–125, **2019**, doi:10.1007/978-981-13-3275-3_6.

[20] Lion, S., Vlaskos, I., and Taccani, R., "A review of emissions reduction technologies for low and medium speed marine Diesel engines and their potential for waste heat recovery," Energy Convers. Manag. 207(September 2019):112553, **2020**, doi:10.1016/j.enconman.2020.112553.

[21] Bergthorson, J.M. and Thomson, M.J., "A review of the combustion and emissions properties of advanced transportation biofuels and their impact on existing and future engines," Renew. Sustain. Energy Rev. 42:1393–1417, **2015**, doi:10.1016/j.rser.2014.10.034.

[22] Knecht, W., "Diesel engine development in view of reduced emission standards," Energy 33(2):264–271, **2008**, doi:10.1016/j.energy.2007.10.003.

[23] Das, H.S., Rahman, M.M., Li, S., and Tan, C.W., "Electric vehicles standards, charging infrastructure, and impact on grid integration: A technological review," Renew. Sustain. Energy Rev. 120(February), **2020**, doi:10.1016/j.rser.2019.109618.

[24] Gandoman, F.H., Jaguemont, J., Goutam, S., Gopalakrishnan, R., Firouz, Y., Kalogiannis, T., Omar, N., and Mierlo, J. Van, "Concept of reliability and safety assessment of lithium-ion batteries in electric vehicles: Basics, progress, and challenges," Appl. Energy 251(January):113343, **2019**, doi:10.1016/j.apenergy.2019.113343.

[25] Mahmoudzadeh Andwari, A., Pesiridis, A., Rajoo, S., Martinez-Botas, R., and Esfahanian, V., "A review of Battery Electric Vehicle technology and readiness levels," Renew. Sustain. Energy Rev. 78(May):414–430, **2017**, doi:10.1016/j.rser.2017.03.138.

[26] Ã, A.D., "Importance of biodiesel as transportation fuel," 35:4661–4670, **2007**, doi:10.1016/j.enpol.2007.04.003.

[27] Atadashi, I.M., Aroua, M.K., and Aziz, A.A., "High quality biodiesel and its diesel engine application: A review," Renew. Sustain. Energy Rev. 14(7):1999–2008, **2010**, doi:10.1016/j.rser.2010.03.020.

[28] Bukljaš Skočibušić, M., Jolić, N., and Bukljaš, Z., "Economic and Social Aspects of Applying Biodiesel Fuel in Road Transport," in: Mikulski, J., ed., Transport Systems Telematics, Springer Berlin Heidelberg, Berlin, Heidelberg, ISBN 978-3-642-16472-9: 243–252, **2010**.

[29] United States Environmental Protection Agency, "Renewable Fuel Standard Program under Energy Independence and Security Act of **2007**," https://www.epa.gov/renewable-fuel-standard-program/overview-renewable-fuel-standard#structure, 2007.

[30] IEA, "India 2020 Policy Energy Review," Www.Iea.Org 1–304, **2020**.

[31] Mustard, A. and Aradhey, A., "India Biofuels Annual 2019," USDA Foreign Agric. Serv. 15:1–16, **2019**.

[32] Lin, L., Cunshan, Z., Vittayapadung, S., Xiangqian, S., and Mingdong, D., "Opportunities and challenges for biodiesel fuel," Appl. Energy 88(4):1020–1031, **2011**, doi:10.1016/j.apenergy.2010.09.029.

[33] Mirhashemi, F.S. and Sadrnia, H., "NOX emissions of compression ignition engines fueled with various biodiesel blends: A review," J. Energy Inst. 93(1):129–151, **2020**, doi:10.1016/j.joei.2019.04.003.

[34] Kumar, A. and Sharma, S., "Potential non-edible oil resources as biodiesel feedstock: An Indian perspective," Renew. Sustain. Energy Rev. 15(4):1791–1800, **2011**, doi:10.1016/j.rser.2010.11.020.

[35] Demirbas, A., Bafail, A., Ahmad, W., and Sheikh, M., "Biodiesel production from non-edible plant oils," Energy Explor. Exploit. 34(2):290–318, **2016**, doi:10.1177/0144598716630166.

[36] Sreenivas, C., Rao, A.B., and Patwardhan, A., "Critical Evaluation of Biodiesel Production Initiatives in India," in: Kumar, A., Ogita, S., and Yau, Y.-Y., eds., Biofuels: Greenhouse Gas Mitigation and Global Warming: Next Generation Biofuels and Role of Biotechnology, Springer India, New Delhi, ISBN 978-81-322-3763-1: 155–176, **2018**, doi:10.1007/978-81-322-3763-1_9.

[37] Ramalingam, S., Rajendran, S., and Ganesan, P., "Performance improvement and exhaust emissions reduction in biodiesel operated diesel engine through the use of operating parameters and catalytic converter: A review," Renew. Sustain. Energy Rev. 81(July 2017):3215–3222, **2018**, doi:10.1016/j.rser.2017.08.069.

[38] Wang, X., Zhang, J., MA, Y., Wang, G., Han, J.P., Dai, M., and Sun, Z.Y., "A comprehensive review on the properties of nanofluid fuel and its additive effects to compression ignition engines," Appl. Surf. Sci. 504(October 2019), **2020**, doi:10.1016/j.apsusc.2019.144581.

[39] Hatami, M., Hasanpour, M., and Jing, D., "Recent developments of nanoparticles additives to the consumables liquids in internal combustion engines: Part I: Nano-fuels," J. Mol. Liq. 318:114250, **2020**, doi:10.1016/j.molliq.2020.114250.

[40] Kegl, T., Kovač Kralj, A., Kegl, M., and Kegl, B., "Practical Viability of Nanofuels Usage in Diesel Engines," Nanomaterials for Environmental Application: Fuel Additives for Diesel Engines, Springer International Publishing, Cham, ISBN 978-3-030-54708-0: 159–175, **2020**, doi:10.1007/978-3-030-54708-0_6.

[41] Heywood, J.B., "Internal Combustion Engine Fundamentals, Second Edition," 2nd Editio, McGraw-Hill Education, ISBN 978-1-26-011610-6, **2018**.

[42] Kamimoto, T. and Kobayashi, H., "Combustion processes in diesel engines," Prog. Energy Combust. Sci. 17(2):163–189, **1991**, doi:10.1016/0360-1285(91)90019-J.

[43] Management, D.E., "Diesel Engine Management," Diesel Engine Manag. 60–71, **2014**, doi:10.1007/978-3-658-03981-3.

[44] Mohamed Shameer, P., Ramesh, K., Sakthivel, R., and Purnachandran, R., "Effects of fuel injection parameters on emission characteristics of diesel engines operating on various biodiesel: A review," Renew. Sustain. Energy Rev. 67(3):1267–1281, **2017**, doi:10.1016/j.rser.2016.09.117.

[45] Murayama, T., "Effects of Fuel Properties in Combustion Systems," in: Someya, T., ed., Advanced Combustion Science, Springer Japan, Tokyo, ISBN 978-4-431-68228-8: 245–272, **1993**, doi:10.1007/978-4-431-68228-8_7.

[46] Mueller, C.J., Cannella, W.J., and Kalghatgi, G.T., "Fuels for Engines and the Impact of Fuel Composition on Engine Performance," Encycl. Automot. Eng. 1–27, **2014**, doi:10.1002/9781118354179.auto125.

[47] Raeie, N., Emami, S., and Karimi Sadaghiyani, O., "Effects of injection timing, before and after top dead center on the propulsion and power in a diesel engine," Propuls. Power Res. 3(2):59–67, **2014**, doi:10.1016/j.jppr.2014.06.001.

[48] Rao, D.C.K., Karmakar, S., and Basu, S., "Atomization characteristics and instabilities in the combustion of multi-component fuel droplets with high volatility differential," Sci. Rep. 7(1):1–15, **2017**, doi:10.1038/s41598-017-09663-7.

[49] Zhao, H. and Liu, H., "Breakup Morphology and Mechanisms of Liquid Atomization," in: Agarwal, R. K., ed., Environmental Impact of Aviation and Sustainable Solutions, IntechOpen, Rijeka, **2020**, doi:10.5772/intechopen.84998.

[50] Chen, P.C., Wang, W.C., Roberts, W.L., and Fang, T., "Spray and atomization of diesel fuel and its alternatives from a single-hole injector using a common rail fuel injection system," Fuel 103(10):850–861, **2013**, doi:10.1016/j.fuel.2012.08.013.

[51] Danov, S.N. and Gupta, A.K., "Effect of sauter mean diameter on the combustion related parameters in a large-bore marine diesel engine," SAE Tech. Pap. 16(6), 1999, doi:10.4271/1999-01-0224.

[52] Alozie, N.S. and Ganippa, L.C., "Diesel Exhaust Emissions and Mitigations," in: Viskup, R., ed., Introduction to Diesel Emissions, IntechOpen, Rijeka, **2020**, doi:10.5772/intechopen.85248.

[53] Schöttke, G., Finger, H., and Schwarz, V., "The analysis of the diesel engine heat release," MTZ Worldw. 64(11):32–35, 2003, doi:10.1007/BF03227634.

[54] Tomar, M. and Kumar, N., "Effect of multi-walled carbon nanotubes and alumina nano-additives in a light duty diesel engine fuelled with schleichera oleosa biodiesel blends," Sustain. Energy Technol. Assessments 42(June):100833, **2020**, doi:10.1016/j.seta.2020.100833.

[55] Agarwal, A.K., Dhar, A., Gupta, J.G., Kim, W. Il, Choi, K., Lee, C.S., and Park, S., "Effect of fuel injection pressure and injection timing of Karanja biodiesel blends on

fuel spray, engine performance, emissions and combustion characteristics," Energy Convers. Manag. 91:302–314, **2015**, doi:10.1016/j.enconman.2014.12.004.

[56] AGARWAL, A.K., GUPTA, P., and DHAR, A., "Combustion, performance and emissions characteristics of a newly developed CRDI single cylinder diesel engine," Sadhana 40(6):1937–1954, **2015**, doi:10.1007/s12046-015-0428-9.

[57] Olivier, J.G.J. and Peters, J.A.H.W., "Trends in Global CO2 and Total Greenhouse Gas Emissions:Report **2019**. PBL Netherlands Environmental Assessment Agency The Hague," 2020(4068):70, 2020.

[58] Jackson, R.B., Quéré, C. Le, Andrew, R.M., Canadell, J.G., Korsbakken, J.I., Liu, Z., Peters, G.P., and Zheng, B., "Global energy growth is outpacing decarbonization," Environ. Res. Lett. 13(12), **2018**, doi:10.1088/1748-9326/aaf303.

[59] Sharma, S. and Saraf, M.R., "Source Apportionment of PM2.5 & PM10 Concentrations of Delhi NCR for Identification of Major Sources," TERI ARAI (August):30, **2018**.

[60] Reşitoɬlu, I.A., Altinişik, K., and Keskin, A., The pollutant emissions from diesel-engine vehicles and exhaust aftertreatment systems, Clean Technol. Environ. Policy 17(1):15–27, 2015, doi:10.1007/s10098-014-0793-9.

[61] Maji, K.J., Dikshit, A.K., and Deshpande, A., "Disability-adjusted life years and economic cost assessment of the health effects related to PM 2.5 and PM 10 pollution in Mumbai and Delhi, in India from 1991 to 2015," 4709–4730, **2017**, doi:10.1007/s11356-016-8164-1.

[62] Initiative, B. and Pollution, A., "Articles The impact of air pollution on deaths, disease burden, and life expectancy across the states of India: the Global Burden of Disease Study 2017," Lancet Planet Heal. 26–39, **2019**, doi:10.1016/S2542-5196(18)30261-4.

[63] Manisalidis, I., Stavropoulou, E., Stavropoulos, A., and Bezirtzoglou, E., "Environmental and Health Impacts of Air Pollution: A Review," Front. Public Heal. 8(February):1–13, **2020**, doi:10.3389/fpubh.2020.00014.

[64] Kampa, M. and Castanas, E., "Human health effects of air pollution," Environ. Pollut. 151(2):362–367, **2008**, doi:10.1016/j.envpol.2007.06.012.

[65] Rößler, M., Velji, A., Janzer, C., Koch, T., and Olzmann, M., "Formation of Engine Internal NO2: Measures to Control the NO_2/NOX Ratio for Enhanced Exhaust After Treatment," SAE Int. J. Engines 10(4), **2017**, doi:10.4271/2017-01-1017.

[66] Environmental Protection Agency (EPA), "Nitrogen oxides (NOx), why and how they are controlled," Epa-456/F-99-006R (November):48, **1999**.

[67] Semakula, M. and Inambao, P.F., "The Formation, Effects and Control of Oxides of Nitrogen in Diesel Engines," Int. J. Appl. Eng. Res. 13(6):3200–3209, **2018**.

[68] Brückner, C., Kyrtatos, P., and Boulouchos, K., "NOx emissions in direct injection diesel engines: Part 2: model performance for conventional, prolonged ignition delay, and premixed charge compression ignition operating conditions," Int. J. Engine Res. 19(5):528–541, **2018**, doi:10.1177/1468087417721558.

[69] Thangaraja, J. and Kannan, C., "Effect of exhaust gas recirculation on advanced diesel combustion and alternate fuels - A review," Appl. Energy 180:169–184, **2016**, doi:10.1016/j.apenergy.2016.07.096.

[70] Mendez, S., Kashdan, J.T., Bruneaux, G., Thirouard, B., and Vangraefschepe, F., "Formation of unburned hydrocarbons in low temperature diesel combustion," SAE Int. J. Engines 2(2):205–225, **2010**, doi:10.4271/2009-01-2729.

[71] Xi, J. and Zhong, B.J., "Soot in diesel combustion systems," Chem. Eng. Technol. 29(6):665–673, **2006**, doi:10.1002/ceat.200600016.

[72] Oppenauer, K.S. and Alberer, D., "Soot formation and oxidation mechanisms during diesel combustion: Analysis and modeling impacts," Int. J. Engine Res. 15(8):954–964, **2014**, doi:10.1177/1468087413502661.

[73] Agarwal, A.K., "Biofuels (alcohols and biodiesel) applications as fuels for internal combustion engines," Prog. Energy Combust. Sci. 33(3):233–271, **2007**, doi:10.1016/j.pecs.2006.08.003.

[74] Kumar, N., Sonthalia, A., Pali, H.S., and Sidharth, "Alternative Fuels for Diesel Engines: New Frontiers," in: Viskup, R., ed., Diesel and Gasoline Engines, IntechOpen, Rijeka, **2020**, doi:10.5772/intechopen.80614.

[75] Devan, P.K. and Mahalakshmi, N. V., "Performance, emission and combustion characteristics of poon oil and its diesel blends in a DI diesel engine," Fuel 88(5):861–867, **2009**, doi:10.1016/j.fuel.2008.11.005.

[76] Ruhul, A.M., Kalam, M.A., Masjuki, H.H., Shahir, S.A., Alabdulkarem, A., Teoh, Y.H., How, H.G., and Reham, S.S., "Evaluating combustion, performance and emission characteristics of Millettia pinnata and Croton megalocarpus biodiesel blends in a diesel engine," Energy 141:2362–2376, **2017**, doi:10.1016/j.energy.2017.11.096.

[77] Ong, H.C., Masjuki, H.H., Mahlia, T.M.I., Silitonga, A.S., Chong, W.T., and Yusaf, T., "Engine performance and emissions using Jatropha curcas, Ceiba pentandra and

Calophyllum inophyllum biodiesel in a CI diesel engine," Energy 69:427–445, **2014**, doi:10.1016/j.energy.2014.03.035.

[78] Atabani, A.E., Mahlia, T.M.I., Masjuki, H.H., Badruddin, I.A., Yussof, H.W., Chong, W.T., and Lee, K.T., "A comparative evaluation of physical and chemical properties of biodiesel synthesized from edible and non-edible oils and study on the effect of bio-diesel blending," Energy 58:296–304, 2013, doi:10.1016/j.energy.2013.05.040.

[79] Silitonga, A.S., Masjuki, H.H., Ong, H.C., Kusumo, F., Mahlia, T.M.I., and Bahar, A.H., "Pilot-scale production and the physicochemical properties of palm and Calophyllum inophyllum biodiesels and their blends," J. Clean. Prod. 126:654–666, **2016**, doi:10.1016/j.jclepro.2016.03.057.

[80] How, H.G., Masjuki, H.H., Kalam, M.A., Teoh, Y.H., and Chuah, H.G., "Effect of Calophyllum Inophyllum biodiesel-diesel blends on combustion, performance, exhaust particulate matter and gaseous emissions in a multi-cylinder diesel engine," Fuel 227(April):154–164, **2018**, doi:10.1016/j.fuel.2018.04.075.

[81] Jamaluddin, N.A.M., Riayatsyah, T.M.I., Silitonga, A.S., Mofijur, M., Shamsuddin, A.H., Ong, H.C., Mahlia, T.M.I., and Rahman, S.M.A., "Techno-economic analysis and physicochemical properties of Ceiba pentandra as second-generation biodiesel based on ASTM D6751 and EN 14214," Processes 7(9):1–21, **2019**, doi:10.3390/pr7090636.

[82] Silitonga, A.S., Ong, H.C., Mahlia, T.M.I., Masjuki, H.H., and Chong, W.T., "Biodiesel conversion from high FFA crude jatropha curcas, calophyllum inophyllum and ceiba pentandra oil," Energy Procedia 61:480–483, **2014**, doi:10.1016/j.egypro.2014.11.1153.

[83] Yunus Khan, T.M., Atabani, A.E., Badruddin, I.A., Ankalgi, R.F., Mainuddin Khan, T.K., and Badarudin, A., "Ceiba pentandra, Nigella sativa and their blend as prospective feedstocks for biodiesel," Ind. Crops Prod. 65:367–373, 2015, doi:10.1016/j.indcrop.2014.11.013.

[84] Esmaeili, H., Yeganeh, G., and Esmaeilzadeh, F., "Optimization of biodiesel produc-tion from Moringa oleifera seeds oil in the presence of nano-MgO using Taguchi method," Int. Nano Lett. 9(3):257–263, **2019**, doi:10.1007/s40089-019-0278-2.

[85] Wakil, M.A., Kalam, M.A., Masjuki, H.H., Rizwanul Fattah, I.M., and Masum, B.M., "Evaluation of rice bran, sesame and moringa oils as feasible sources of biodiesel and

the effect of blending on their physicochemical properties," RSC Adv. 4(100):56984–56991, **2014**, doi:10.1039/c4ra09199j.

[86] Rashed, M.M., Kalam, M.A., Masjuki, H.H., Mofijur, M., Rasul, M.G., and Zulkifli, N.W.M., "Performance and emission characteristics of a diesel engine fueled with palm, jatropha, and moringa oil methyl ester," Ind. Crops Prod. 79:70–76, **2016**, doi:10.1016/j.indcrop.2015.10.046.

[87] Teoh, Y.H., How, H.G., Masjuki, H.H., Nguyen, H.T., Kalam, M.A., and Alabdulka-rem, A., "Investigation on particulate emissions and combustion characteristics of a common-rail diesel engine fueled with Moringa oleifera biodiesel-diesel blends," Re-new. Energy 136:521–534, **2019**, doi:10.1016/j.renene.2018.12.110.

[88] Mazumdar, P., Borugadda, V.B., Goud, V. V., and Sahoo, L., "Physico-chemical char-acteristics of Jatropha curcas L. of North East India for exploration of biodiesel," Bio-mass and Bioenergy 46:546–554, **2012**, doi:10.1016/j.biombioe.2012.07.005.

[89] Kouame, S.D.B., "Comparative characterization of Jatropha, soybean and commercial biodiesel," Ranliao Huaxue Xuebao/Journal Fuel Chem. Technol. 39(4):258–264, **2011**, doi:10.1016/s1872-5813(11)60020-0.

[90] Rajak, U., Chaurasiya, P.K., Nashine, P., Verma, M., Reddy Kota, T., and Verma, T.N., "Financial assessment, performance and emission analysis of Moringa oleifera and Jatropha curcas methyl ester fuel blends in a single-cylinder diesel engine," Energy Convers. Manag. 224(X):113362, **2020**, doi:10.1016/j.enconman.2020.113362.

[91] Sahoo, P.K. and Das, L.M., "Combustion analysis of Jatropha, Karanja and Polanga based biodiesel as fuel in a diesel engine," Fuel 88(6):994–999, **2009**, doi:10.1016/j.fuel.2008.11.012.

[92] Dhawane, S.H., Bora, A.P., Kumar, T., and Halder, G., "Parametric optimization of biodiesel synthesis from rubber seed oil using iron doped carbon catalyst by Taguchi approach," Renew. Energy 105:616–624, **2017**, doi:10.1016/j.renene.2016.12.096.

[93] Morshed, M., Ferdous, K., Khan, M.R., Mazumder, M.S.I., Islam, M.A., and Uddin, M.T., "Rubber seed oil as a potential source for biodiesel production in Bangladesh," Fuel 90(10):2981–2986, **2011**, doi:10.1016/j.fuel.2011.05.020.

[94] Devi, V.N.M., Prasad, P.N., Syndia, L.A.M., Rajakohila, M., and Ariharan, V.N., "Physico-Chemical Characterization of Rubber Seed Oil (Hevea Brasiliensis) - A Promising Feedstock for Biodiesel Production," Int. J. Chem. Anal. Sci. 3(5):1402–1404, **2012**.

[95] Vishal, D., Dubey, S., Goyal, R., Dwivedi, G., Baredar, P., and Chhabra, M., "Optimization of alkali-catalyzed transesterification of rubber oil for biodiesel production & its impact on engine performance," Renew. Energy 158:167–180, **2020**, doi:10.1016/j.renene.2020.05.136.

[96] Kumar, N. and Tomar, M., "Influence of nanoadditives on ignition characteristics of Kusum (Schleichera oleosa) biodiesel," Int. J. Energy Res. 43(8):3223–3236, **2019**, doi:10.1002/er.4446.

[97] Yadav, A.K., Khan, M.E., Dubey, A.M., and Pal, A., "Performance and emission characteristics of a transportation diesel engine operated with non-edible vegetable oils biodiesel," Case Stud. Therm. Eng. 8:236–244, **2016**, doi:10.1016/j.csite.2016.08.001.

[98] Yadav, M. and Sharma, Y.C., "Process optimization and catalyst poisoning study of biodiesel production from kusum oil using potassium aluminum oxide as efficient and reusable heterogeneous catalyst," J. Clean. Prod. 199:593–602, **2018**, doi:10.1016/j.jclepro.2018.07.052.

[99] Pali, H.S. and Kumar, N., "Comparative assessment of sal and kusum biodiesel properties," Energy Sources, Part A Recover. Util. Environ. Eff. 38(22):3391–3396, **2016**, doi:10.1080/15567036.2015.1136974.

[100] Shukla, P.C., Gupta, T., Labhsetwar, N.K., and Agarwal, A.K., "Physico-chemical speciation of particulates emanating from Karanja biodiesel fuelled automotive engine," Fuel 162(August):84–90, **2015**, doi:10.1016/j.fuel.2015.07.076.

[101] Venkatesh Kamath, H., Regupathi, I., and Saidutta, M.B., "Optimization of two step karanja biodiesel synthesis under microwave irradiation," Fuel Process. Technol. 92(1):100–105, **2011**, doi:10.1016/j.fuproc.2010.09.003.

[102] Shrivastava, P., Verma, T.N., David Samuel, O., and Pugazhendhi, A., "An experimental investigation on engine characteristics, cost and energy analysis of CI engine fuelled with Roselle, Karanja biodiesel and its blends," Fuel 275(April):117891, **2020**, doi:10.1016/j.fuel.2020.117891.

[103] Demirbas, A., "Production of biodiesel fuels from linseed oil using methanol and ethanol in non-catalytic SCF conditions," Biomass and Bioenergy 33(1):113–118, **2009**, doi:10.1016/j.biombioe.2008.04.018.

[104] Puhan, S., Saravanan, N., Nagarajan, G., and Vedaraman, N., "Effect of biodiesel unsaturated fatty acid on combustion characteristics of a DI compression ignition engine," Biomass and Bioenergy 34(8):1079–1088, **2010**, doi:10.1016/j.biombioe.2010.02.017.

[105] Veinblat, M., Baibikov, V., Katoshevski, D., Wiesman, Z., and Tartakovsky, L., "Impact of various blends of linseed oil-derived biodiesel on combustion and particle emissions of a compression ignition engine – A comparison with diesel and soybean fuels," Energy Convers. Manag. 178(October):178–189, **2018**, doi:10.1016/j.enconman.2018.10.028.

[106] Dharmaraja, J., Duc, D., Shobana, S., and Dattatrya, G., "Engine performance , emission and bio characteristics of rice bran oil derived biodiesel blends," Fuel 239(October 2018):153–161, **2019**, doi:10.1016/j.fuel.2018.10.123.

[107] MohamedMusthafa, M., Sivapirakasam, S.P., and Udayakumar, M., "Comparative studies on fly ash coated low heat rejection diesel engine on performance and emission characteristics fueled by rice bran and pongamia methyl ester and their blend with diesel," Energy 36(5):2343–2351, **2011**, doi:10.1016/j.energy.2010.12.047.

[108] Ahmad, M., Samuel, S., Zafar, M., Khan, M.A., Tariq, M., Ali, S., and Sultana, S., "Physicochemical characterization of Eco-friendly rice Bran oil biodiesel," Energy Sources, Part A Recover. Util. Environ. Eff. 33(14):1386–1397, **2011**, doi:10.1080/15567036.2010.511428.

[109] Das, M., Sarkar, M., Datta, A., and Santra, A.K., "Study on viscosity and surface tension properties of biodiesel-diesel blends and their effects on spray parameters for CI engines," Fuel 220(February):769–779, **2018**, doi:10.1016/j.fuel.2018.02.021.

[110] Kannan, M., Sathish Babu, R., and Sathish, S., "Experimental investigations on the performance and emission characteristics of CI engine fuelled with biodiesel from neem oil," Int. J. Ambient Energy 0(0):1–19, **2020**, doi:10.1080/01430750.2020.1726812.

[111] Kattimani, V., Radhika, R., Venkatesha, B., and Ananda, S., "Studies on fuel properties of neem oil methyl ester and its conventional diesel and kerosene blends," Int. J. Eng. Res. Gen. Sci. 3(1):291–296, **2015**.

[112] Yilmaz, N., Atmanli, A., and Trujillo, M., "Influence of 1-pentanol additive on the performance of a diesel engine fueled with waste oil methyl ester and diesel fuel," Fuel 207:461–469, **2017**, doi:10.1016/j.fuel.2017.06.093.

[113] Vieira da Silva, M.A., Lagnier Gil Ferreira, B., Costa Marques, L.G. da, Lamare Soares Murta, A., and Vasconcelos de Freitas, M.A., "Comparative study of NOx emissions of biodiesel-diesel blends from soybean, palm and waste frying oils using methyl and ethyl transesterification routes," Fuel 194:144–156, **2017**, doi:10.1016/j.fuel.2016.12.084.

Some studies on nano-particles doped alternative fuels in Unmodified CI Engine

[114] Yildizhan, Ş., Uludamar, E., Çalık, A., Dede, G., and Özcanlı, M., "Fuel properties, performance and emission characterization of waste cooking oil (WCO) in a variable compression ratio (VCR) diesel engine," Eur. Mech. Sci. 1(2):56–62, **2017**, doi:10.26701/ems.321789.

[115] Das, M., Sarkar, M., Datta, A., and Santra, A.K., "An experimental study on the combustion, performance and emission characteristics of a diesel engine fuelled with diesel-castor oil biodiesel blends," Renew. Energy 119:174–184, **2018**, doi:10.1016/j.renene.2017.12.014.

[116] Lahane, S. and Subramanian, K.A., "Effect of different percentages of biodiesel-diesel blends on injection, spray, combustion, performance, and emission characteristics of a diesel engine," Fuel 139:537–545, **2015**, doi:10.1016/j.fuel.2014.09.036.

[117] Anand, K., Sharma, R.P., and Mehta, P.S., "Experimental investigations on combustion, performance, and emissions characteristics of a neat biodiesel-fuelled, turbocharged, direct injection diesel engine," Proc. Inst. Mech. Eng. Part D J. Automob. Eng. 224(5):661–679, **2010**, doi:10.1243/09544070JAUTO1342.

[118] Jose, T.K. and Anand, K., "Effects of biodiesel composition on its long term storage stability," Fuel 177:190–196, **2016**, doi:10.1016/j.fuel.2016.03.007.

[119] Raman, L.A., Deepanraj, B., Rajakumar, S., and Sivasubramanian, V., "Experimental investigation on performance, combustion and emission analysis of a direct injection diesel engine fuelled with rapeseed oil biodiesel," Fuel 246(March 2018):69–74, **2019**, doi:10.1016/j.fuel.2019.02.106.

[120] Yadav, A.K., Khan, M.E., Pal, A., and Dubey, A.M., "Experimental Investigations of Performance and Emissions Characteristics of Kusum (Schleichera Oleosa) Biodiesel in a Multi-Cylinder Transportation Diesel Engine," Waste and Biomass Valorization 8(4):1331–1341, **2017**, doi:10.1007/s12649-016-9658-2.

[121] Pali, H.S., Kumar, N., and Mishra, C., "Some experimental studies on combustion, emission and performance characteristics of an agricultural diesel engine fueled with blends of kusum oil methyl ester and diesel," SAE Technical Papers, SAE International, **2014**, doi:10.4271/2014-01-1952.

[122] Pipitone, E. and Costanza, A., "An experimental investigation on the long-term compatibility of preheated crude palm oil in a large compression ignition diesel engine," Biofuel Res. J. 5(4):900–908, **2018**, doi:10.18331/BRJ2018.5.4.5.

[123] Mahmudul, H.M., Hagos, F.Y., Mamat, R., Adam, A.A., Ishak, W.F.W., and Alenezi, R., "Production, characterization and performance of biodiesel as an alternative fuel in diesel engines – A review," Renew. Sustain. Energy Rev. 72(November 2016):497–509, **2017**, doi:10.1016/j.rser.2017.01.001.

[124] Rajaeifar, M.A., Tabatabaei, M., Aghbashlo, M., Nizami, A.S., and Heidrich, O., "Emissions from urban bus fleets running on biodiesel blends under real-world operating conditions: Implications for designing future case studies," Renew. Sustain. Energy Rev. 111(April):276–292, **2019**, doi:10.1016/j.rser.2019.05.004.

[125] Kousoulidou, M., Fontaras, G., Ntziachristos, L., and Samaras, Z., "Biodiesel blend effects on common-rail diesel combustion and emissions," Fuel 89(11):3442–3449, **2010**, doi:10.1016/j.fuel.2010.06.034.

[126] Chen, H., Xie, B., Ma, J., and Chen, Y., "NOx emission of biodiesel compared to diesel: Higher or lower?," Appl. Therm. Eng. 137(February):584–593, **2018**, doi:10.1016/j.applthermaleng.2018.04.022.

[127] Haseeb, A.S.M.A., Fazal, M.A., Jahirul, M.I., and Masjuki, H.H., "Compatibility of automotive materials in biodiesel: A review," Fuel 90(3):922–931, **2011**, doi:10.1016/j.fuel.2010.10.042.

[128] Dhar, A. and Agarwal, A.K., "Effect of Karanja biodiesel blend on engine wear in a diesel engine," Fuel 134:81–89, **2014**, doi:10.1016/j.fuel.2014.05.039.

[129] Imdadul, H.K., Masjuki, H.H., Kalam, M.A., Zulkifli, N.W.M., Rashed, M.M., Rashedul, H.K., Monirul, I.M., and Mosarof, M.H., "A comprehensive review on the assessment of fuel additive effects on combustion behavior in CI engine fuelled with diesel biodiesel blends," RSC Adv. 5(83):67541–67567, **2015**, doi:10.1039/c5ra09563h.

[130] Shah, P.R. and Ganesh, A., "A comparative study on influence of fuel additives with edible and non-edible vegetable oil based on fuel characterization and engine characteristics of diesel engine," Appl. Therm. Eng. 102:800–812, **2016**, doi:10.1016/j.applthermaleng.2016.03.128.

[131] Rashedul, H.K., Masjuki, H.H., Kalam, M.A., Ashraful, A.M., Ashrafur Rahman, S.M., and Shahir, S.A., "The effect of additives on properties, performance and emission of biodiesel fuelled compression ignition engine," Energy Convers. Manag. 88:348–364, **2014**, doi:10.1016/j.enconman.2014.08.034.

[132] Lü, X.C., Yang, J.G., Zhang, W.G., and Huang, Z., "Improving the combustion and emissions of direct injection compression ignition engines using oxygenated fuel additives combined with a cetane number improver," Energy and Fuels 19(5):1879–1888, **2005**, doi:10.1021/ef0500179.

[133] Abe, M., Hirata, S., Komatsu, H., Yamagiwa, K., and Tajima, H., "Thermodynamic selection of effective additives to improve the cloud point of biodiesel fuels," Fuel 171(December):94–100, **2015**, doi:10.1016/j.fuel.2015.12.053.

[134] Madiwale, S., Karthikeyan, A., and Bhojwani, V., "A Comprehensive Review of Effect of Biodiesel Additives on Properties, Performance, and Emission," IOP Conf. Ser. Mater. Sci. Eng. 197(1), **2017**, doi:10.1088/1757-899X/197/1/012015.

[135] Ali, O.M., Mamat, R., and Faizal, C.K.M., "Review of the effects of additives on biodiesel properties, performance, and emission features," J. Renew. Sustain. Energy 5(1), **2013**, doi:10.1063/1.4792846.

[136] Danilov, A.M., "Progress in research on fuel additives (review)," Pet. Chem. 55(3):169–179, **2015**, doi:10.1134/S0965544115030020.

[137] Borsato, D., Cini, J.R.D.M., Silva, H.C. Da, Coppo, R.L., Angilelli, K.G., Moreira, I., and Maia, E.C.R., "Oxidation kinetics of biodiesel from soybean mixed with synthetic antioxidants BHA, BHT and TBHQ: Determination of activation energy," Fuel Process. Technol. 127:111–116, **2014**, doi:10.1016/j.fuproc.2014.05.033.

[138] Sindhi, V., Gupta, V., Sharma, K., Bhatnagar, S., Kumari, R., and Dhaka, N., "Potential applications of antioxidants – A review," J. Pharm. Res. 7(9):828–835, **2013**, doi:10.1016/j.jopr.2013.10.001.

[139] Sorate, K.A. and Bhale, P. V., "Biodiesel properties and automotive system compatibility issues," Renew. Sustain. Energy Rev. 41:777–798, **2015**, doi:10.1016/j.rser.2014.08.079.

[140] Srivyas, P.D. and Charoo, M.S., "Effect of lubricants additive: Use and benefit," Mater. Today Proc. 18:4773–4781, **2019**, doi:10.1016/j.matpr.2019.07.465.

[141] Fangsuwannarak, K., Wanriko, P., and Fangsuwannarak, T., "Effect of Bio-polymer Additive on the Fuel Properties of Palm Biodiesel and on Engine Performance Analysis and Exhaust Emission," Energy Procedia 100(September):227–236, **2016**, doi:10.1016/j.egypro.2016.10.170.

[142] Lawan, I., Zhou, W., Garba, Z.N., Zhang, M., Yuan, Z., and Chen, L., "Critical insights into the effects of bio-based additives on biodiesels properties," Renew. Sustain. Energy Rev. 102(May 2018):83–95, **2019**, doi:10.1016/j.rser.2018.12.008.

[143] Gürü, M., Koca, A., Can, Ö., Çinar, C., and Şahin, F., "Biodiesel production from waste chicken fat based sources and evaluation with Mg based additive in a diesel engine," Renew. Energy 35(3):637–643, **2010**, doi:10.1016/j.renene.2009.08.011.

[144] Cao, L., Wang, J., Liu, C., Chen, Y., Liu, K., and Han, S., "Ethylene vinyl acetate co-polymer: A bio-based cold flow improver for waste cooking oil derived biodiesel blends," Appl. Energy 132:163–167, **2014**, doi:10.1016/j.apenergy.2014.06.085.

[145] Bhale, P.V., Deshpande, N. V., and Thombre, S.B., "Improving the low temperature properties of biodiesel fuel," Renew. Energy 34(3):794–800, **2009**, doi:10.1016/j.renene.2008.04.037.

[146] Joshi, H., Moser, B.R., Toler, J., Smith, W.F., and Walker, T., "Ethyl levulinate: A potential bio-based diluent for biodiesel which improves cold flow properties," Biomass and Bioenergy 35(7):3262–3266, **2011**, doi:10.1016/j.biombioe.2011.04.020.

[147] Sivalakshmi, S. and Balusamy, T., "Influence of ethanol addition on a diesel engine fuelled with neem oil methyl ester," Int. J. Green Energy 9(3):218–228, **2012**, doi:10.1080/15435075.2011.621477.

[148] Kivevele, T.T., Kristóf, L., Bereczky, Á., and Mbarawa, M.M., "Engine performance, exhaust emissions and combustion characteristics of a CI engine fuelled with croton megalocarpus methyl ester with antioxidant," Fuel 90(8):2782–2789, **2011**, doi:10.1016/j.fuel.2011.03.048.

[149] Musthafa, M.M., Kumar, T.A., Mohanraj, T., and Chandramouli, R., "A comparative study on performance, combustion and emission characteristics of diesel engine fuelled by biodiesel blends with and without an additive," Fuel 225(March):343–348, **2018**, doi:10.1016/j.fuel.2018.03.147.

[150] Sathiyamoorthi, R. and Sankaranarayanan, G., "Effect of antioxidant additives on the performance and emission characteristics of a DICI engine using neat lemongrass oil-diesel blend," Fuel 174(February):89–96, **2016**, doi:10.1016/j.fuel.2016.01.076.

[151] Calder, J., Roy, M.M., and Wang, W., "Performance and emissions of a diesel engine fueled by biodiesel-diesel blends with recycled expanded polystyrene and fuel stabilizing additive," Energy 149:204–212, **2018**, doi:10.1016/j.energy.2018.02.065.

[152] Srivastava, S.P. and Hancsók, J., "Fuels and Fuel-Additives," John Wiley & Sons, Inc., Hoboken, New Jersey, ISBN 9781118796214, **2014**, doi:10.1002/9781118796214.

[153] Danilov, A.M., "Progress in research on fuel additives (review)," Pet. Chem. 55(3):169–179, **2015**, doi:10.1134/S0965544115030020.

[154] Mahmudul, H.M., Hagos, F.Y., Mamat, R., and Abdullah, A.A., "Impact of oxygenated additives to diesel-biodiesel blends in the context of performance and emissions characteristics of a CI engine," IOP Conf. Ser. Mater. Sci. Eng. 160(1):1–12, **2016**, doi:10.1088/1757-899X/160/1/012060.

[155] Kumar, C., Rana, K.B., Tripathi, B., and Nayyar, A., "Properties and effects of organic additives on performance and emission characteristics of diesel engine: a comprehensive review," Environ. Sci. Pollut. Res. 25(23):22475–22498, **2018**, doi:10.1007/s11356-018-2537-6.

[156] Ileri, E. and Koçar, G., "Experimental investigation of the effect of antioxidant additives on NOx emissions of a diesel engine using biodiesel," Fuel 125(x):44–49, **2014**, doi:10.1016/j.fuel.2014.02.007.

[157] Kuzhiyil, N. and Kong, S.C., "Energy recovery from waste plastics by using blends of biodiesel and polystyrene in diesel engines," Energy and Fuels 23(6):3246–3253, **2009**, doi:10.1021/ef801110j.

[158] Bedford, F., Rutland, C., Dittrich, P., Raab, A., and Wirbeleit, F., "Effects of direct water injection on di diesel engine combustion," SAE Tech. Pap. (724), **2000**, doi:10.4271/2000-01-2938.

[159] Porras, M., Solans, C., González, C., and Gutiérrez, J.M., "Properties of water-in-oil (W/O) nano-emulsions prepared by a low-energy emulsification method," Colloids Surfaces A Physicochem. Eng. Asp. 324(1–3):181–188, **2008**, doi:10.1016/j.colsurfa.2008.04.012.

[160] Radhakrishnan, S., Munuswamy, D.B., Devarajan, Y., Arunkumar, T., and Mahalingam, A., "Effect of nanoparticle on emission and performance characteristics of a diesel engine fueled with cashew nut shell biodiesel," Energy Sources, Part A Recover. Util. Environ. Eff. 40(20):2485–2493, **2018**, doi:10.1080/15567036.2018.1502848.

[161] Venu, H. and Madhavan, V., "Effect of Al2O3 nanoparticles in biodiesel-diesel-ethanol blends at various injection strategies: Performance, combustion and emission characteristics," Fuel 186:176–189, **2016**, doi:10.1016/j.fuel.2016.08.046.

[162]   Kumar, H. and Sangwan, P., "Synthesis and Characterization of Cobalt Oxide Nano-particles by Sol-Gel Method," Int. J. Adv. Res. Sci. Eng. 7:632–9, **2018**.

[163]   Li, J., Wu, Q., and Wu, J., "Synthesis of Nanoparticles via Solvothermal and Hydro-thermal Methods," in: Aliofkhazraei, M., ed., Handbook of Nanoparticles, Springer International Publishing, Cham, ISBN 978-3-319-13188-7: 1–28, **2015**, doi:10.1007/978-3-319-13188-7_17-1.

[164]   Ettefaghi, E., Ghobadian, B., Rashidi, A., Najafi, G., Khoshtaghaza, M.H., Rashtchi, M., and Sadeghian, S., "A novel bio-nano emulsion fuel based on biodegradable nano-particles to improve diesel engines performance and reduce exhaust emissions," Renew. Energy 125:64–72, **2018**, doi:10.1016/j.renene.2018.01.086.

[165]   Vairamuthu, G., Sundarapandian, S., Kailasanathan, C., and Thangagiri, B., "Experimental investigation on the effects of cerium oxide nanoparticle on Calophyllum inophyllum (Punnai) biodiesel blended with diesel fuel in DI diesel engine modified by nozzle geometry," J. Energy Inst. 89(4):668–682, **2016**, doi:10.1016/j.joei.2015.05.005.

[166]   Abdollahifar, M., Hidaryan, M., and Jafari, P., "The role anions on the synthesis of AlOOH nanoparticles using simple solvothermal method," Bol. La Soc. Esp. Ceram. y Vidr. 57(2):66–72, **2018**, doi:10.1016/j.bsecv.2017.06.002.

[167]   Phiwdang, K., Suphankij, S., Mekprasart, W., and Pecharapa, W., "Synthesis of CuO nanoparticles by precipitation method using different precursors," Energy Procedia 34:740–745, **2013**, doi:10.1016/j.egypro.2013.06.808.

[168]   Rane, A.V., Kanny, K., Abitha, V.K., and Thomas, S., "Methods for Synthesis of Nanoparticles and Fabrication of Nanocomposites," Elsevier Ltd., ISBN 9780081019757, **2018**, doi:10.1016/b978-0-08-101975-7.00005-1.

[169]   José-Yacamán, M., Miki-Yoshida, M., Rendón, L., and Santiesteban, J.G., "Catalytic growth of carbon microtubules with fullerene structure," Appl. Phys. Lett. 62(2):202–204, **1993**, doi:10.1063/1.109315.

[170]   Plata, D.L., Meshot, E.R., Reddy, C.M., Hart, A.J., and Gschwend, P.M., "Multiple alkynes react with ethylene to enhance carbon nanotube synthesis, suggesting a polymerization-like formation mechanism," ACS Nano 4(12):7185–7192, **2010**, doi:10.1021/nn101842g.

[171] Hata, K., Futaba, D.N., Mizuno, K., Namai, T., Yumura, M., and Iijima, S., "Water-Assisted Highly Efficient Synthesis of Impurity-Free Single-Walled Carbon Nanotubes," Science (80-.). 306(5700):1362–1364, **2004**, doi:10.1126/science.1104962.

[172] Teoh, W.Y., Amal, R., and Mädler, L., "Flame spray pyrolysis: An enabling technology for nanoparticles design and fabrication," Nanoscale 2(8):1324–1347, **2010**, doi:10.1039/C0NR00017E.

[173] Jolly, B.M. and Bhattacharya, S.S., "Synthesis of nanocrystalline alumina (Al_2O_3) particles from an aqueous precursor by flame-assisted spray pyrolysis," Mater. Today Proc. 5(3):10023–10027, **2018**, doi:10.1016/j.matpr.2017.10.201.

[174] 1. Ando, Y., Zhao, X., Sugai, T., and Kumar, M., "Growing carbon nanotubes," Mater. Today 7(9):22–29, 2004, doi:10.1016/s1369-7021(04)00446-8.

[175] Camargo, P.H.C., Satyanarayana, K.G., and Wypych, F., "Nanocomposites: Synthesis, structure, properties and new application opportunities," Mater. Res. 12(1):1–39, **2009**, doi:10.1590/S1516-14392009000100002.

[176] Alizadeh, M., Sharifianjazi, F., Haghshenasjazi, E., Aghakhani, M., and Rajabi, L., "Production of Nanosized Boron Oxide Powder by High-Energy Ball Milling," Synth. React. Inorganic, Met. Nano-Metal Chem. 45(1):11–14, **2015**, doi:10.1080/15533174.2013.797438.

[177] León, V., Quintana, M., Herrero, M.A., Fierro, J.L.G., Hoz, A. de la, Prato, M., and Vázquez, E., "Few-layer graphenes from ball-milling of graphite with melamine," Chem. Commun. 47(39):10936–10938, **2011**, doi:10.1039/C1CC14595A.

[178] Tomar, M. and Kumar, N., "Influence of nanoadditives on the performance and emission characteristics of a CI engine fuelled with diesel, biodiesel, and blends – a review," Energy Sources, Part A Recover. Util. Environ. Eff. 0(0):1–18, **2019**, doi:10.1080/15567036.2019.1623347.

[179] Aalam, C.S., Saravanan, C.G., and Kannan, M., "Experimental investigations on a CRDI system assisted diesel engine fuelled with aluminium oxide nanoparticles blended biodiesel," Alexandria Eng. J. 54(3):351–358, **2015**, doi:10.1016/j.aej.2015.04.009.

[180] Sajith, V., Sobhan, C.B., and Peterson, G.P., "Experimental Investigations on the Effects of Cerium Oxide Nanoparticle Fuel Additives on Biodiesel," **2010**, doi:10.1155/2010/581407.

[181] Prabu, A., "Nanoparticles as additive in biodiesel on the working characteristics of a DI diesel engine," Ain Shams Eng. J., **2017**, doi:10.1016/j.asej.2017.04.004.

[182] Somandepalli, V., Kelly, S., and Davis, S., "Hot surface ignition of ethanol-blended fuels and biodiesel," SAE Tech. Pap. 2008(724), **2008**, doi:10.4271/2008-01-0402.

[183] Shams, Z. and Moghiman, M., "Effect of metal oxide nanoparticles on the ignition characteristics of diesel fuel droplets: an experimental study," J. Brazilian Soc. Mech. Sci. Eng. 40(2):1–10, **2018**, doi:10.1007/s40430-018-1010-2.

[184] Khond, V.W. and Kriplani, V.M., "Experimental investigation and modeling of the evaporation rate of carbon nanotube blended emulsified Neem biodiesel," Biofuels 0(0):1–7, **2017**, doi:10.1080/17597269.2017.1323322.

[185] Roy, S., Parsi, P.K., Kotha, R.S., Barman, S., Vinayak, K., Roy, M.M., and Banerjee, R., "Effective utilisation of waste cooking oil in a single-cylinder diesel engine using alumina nanoparticles," Sustain. Energy Fuels 4(2):571–581, **2020**, doi:10.1039/C9SE00393B.

[186] Chandrasekaran, V., Arthanarisamy, M., Nachiappan, P., Dhanakotti, S., and Moorthy, B., "The role of nano additives for biodiesel and diesel blended transportation fuels," Transp. Res. Part D Transp. Environ. 46:145–156, **2016**, doi:10.1016/j.trd.2016.03.015.

[187] Nayak, S., Shet, V.B., Rao, C.V., and Joshi, K., "Performance Evaluation and Emission Characteristics of a 4 Stroke Diesel Engine Using Green Synthesized Silver Nanoparticles Blended Biodiesel," Mater. Today Proc. 5(2):7889–7897, **2018**, doi:10.1016/j.matpr.2017.11.470.

[188] Anchupogu, P., Rao, L.N., and Banavathu, B., "Effect of alumina nano additives into biodiesel-diesel blends on the combustion performance and emission characteristics of a diesel engine with exhaust gas recirculation," Environ. Sci. Pollut. Res. 25(23):23294–23306, **2018**, doi:10.1007/s11356-018-2366-7.

[189] Devarajan, Y., Munuswamy, D.B., and Mahalingam, A., "Performance, combustion and emission analysis on the effect of ferrofluid on neat biodiesel," Process Saf. Environ. Prot. 111:283–291, **2017**, doi:10.1016/j.psep.2017.07.021.

[190] Nagaraja, S., Dsilva Winfred Rufuss, D., and Hossain, A.K., "Microscopic characteristics of biodiesel – Graphene oxide nanoparticle blends and their Utilisation in a compression ignition engine," Renew. Energy 160:830–841, **2020**, doi:10.1016/j.renene.2020.07.032.

[191] Elwardany, A.E., Marei, M.N., Eldrainy, Y., Ali, R.M., Ismail, M., and El-kassaby, M.M., "Improving performance and emissions characteristics of compression ignition engine: Effect of ferrocene nanoparticles to diesel-biodiesel blend," Fuel 270(October 2019):117574, **2020**, doi:10.1016/j.fuel.2020.117574.

[192] Long, R.Q. and Yang, R.T., "Carbon nanotubes as a superior sorbent for nitrogen oxides," Ind. Eng. Chem. Res. 40(20):4288–4291, **2001**, doi:10.1021/ie000976k.

[193] Lu, C., Bai, H., Wu, B., Su, F., and Hwang, J.F., "Comparative study of CO2 capture by carbon nanotubes, activated carbons, and zeolites," Energy and Fuels 22(5):3050–3056, **2008**, doi:10.1021/ef8000086.

[194] El-Seesy, A.I., Abdel-Rahman, A.K., Bady, M., and Ookawara, S., "Performance, combustion, and emission characteristics of a diesel engine fueled by biodiesel-diesel mixtures with multi-walled carbon nanotubes additives," Energy Convers. Manag. 135:373–393, **2017**, doi:10.1016/j.enconman.2016.12.090.

[195] Sadhik Basha, J. and Anand, R.B., "Role of nanoadditive blended biodiesel emulsion fuel on the working characteristics of a diesel engine," J. Renew. Sustain. Energy 3(2), **2011**, doi:10.1063/1.3575169.

[196] Rizwanul Fattah, I.M., Masjuki, H.H., Kalam, M.A., Wakil, M.A., Rashedul, H.K., and Abedin, M.J., "Performance and emission characteristics of a CI engine fueled with Cocos nucifera and Jatropha curcas B20 blends accompanying antioxidants," Ind. Crops Prod. 57:132–140, **2014**, doi:10.1016/j.indcrop.2014.03.022.

[197] Kivevele, T.T., Kristóf, L., Bereczky, Á., and Mbarawa, M.M., "Engine performance, exhaust emissions and combustion characteristics of a CI engine fuelled with croton megalocarpus methyl ester with antioxidant," Fuel 90(8):2782–2789, **2011**, doi:10.1016/j.fuel.2011.03.048.

[198] Varatharajan, K. and Cheralathan, M., "Effect of aromatic amine antioxidants on NOx emissions from a soybean biodiesel powered di diesel engine," Fuel Process. Technol. 106(x):526–532, **2013**, doi:10.1016/j.fuproc.2012.09.023.

[199] Kuzhiyil, N. and Kong, S.C., "Energy recovery from waste plastics by using blends of biodiesel and polystyrene in diesel engines," Energy and Fuels 23(6):3246–3253, **2009**, doi:10.1021/ef801110j.

[200] Debnath, B.K., Sahoo, N., and Saha, U.K., "Adjusting the operating characteristics to improve the performance of an emulsified palm oil methyl ester run diesel engine," Energy Convers. Manag. 69:191–198, **2013**, doi:10.1016/j.enconman.2013.01.031.

[201] Lin, C.Y. and Lin, H.A., "Engine performance and emission characteristics of a three-phase emulsion of biodiesel produced by peroxidation," Fuel Process. Technol. 88(1):35–41, **2007**, doi:10.1016/j.fuproc.2006.07.008.

[202] Ryu, K., "Effect of antioxidants on the oxidative stability and combustion characteristics of biodiesel fuels in an indirect-injection (IDI) diesel engine," J. Mech. Sci. Technol. 23(11):3105–3113, **2009**, doi:10.1007/s12206-009-0902-6.

[203] Ramalingam, S., Rajendran, S., and Ganesan, P., "Improving the performance is better and emission reductions from Annona biodiesel operated diesel engine using 1,4-dioxane fuel additive," Fuel 185:804–809, **2016**, doi:10.1016/j.fuel.2016.08.049.

[204] Kannan, G.R., Karvembu, R., and Anand, R., "Effect of metal based additive on performance emission and combustion characteristics of diesel engine fuelled with biodiesel," Appl. Energy 88(11):3694–3703, **2011**, doi:10.1016/j.apenergy.2011.04.043.

[205] Dhinesh, B., Niruban Bharathi, R., Isaac JoshuaRamesh Lalvani, J., Parthasarathy, M., and Annamalai, K., "An experimental analysis on the influence of fuel borne additives on the single cylinder diesel engine powered by Cymbopogon flexuosus biofuel," J. Energy Inst. 90(4):634–645, **2017**, doi:10.1016/j.joei.2016.04.010.

[206] Nanthagopal, K., Ashok, B., Tamilarasu, A., Johny, A., and Mohan, A., "Influence on the effect of zinc oxide and titanium dioxide nanoparticles as an additive with Calophyllum inophyllum methyl ester in a CI engine," Energy Convers. Manag. 146:8–19, **2017**, doi:10.1016/j.enconman.2017.05.021.

[207] Balaji, G. and Cheralathan, M., "Effect of CNT as additive with biodiesel on the performance and emission characteristics of a DI diesel engine," Int. J. ChemTech Res. 7(3):1230–1236, **2014**.

[208] Zhang, Z., Lu, Y., Wang, Y., Yu, X., Smallbone, A., Dong, C., and Roskilly, A.P., "Comparative study of using multi-wall carbon nanotube and two different sizes of cerium oxide nanopowders as fuel additives under various diesel engine conditions," Fuel 256(October 2018):115904, **2019**, doi:10.1016/j.fuel.2019.115904.

[209] Mikolajczak, K.L. and Smith, C.R., "Cyanolipids of kusum (schleichera trijuga) seed oil," Lipids 6(5):349–350, **1971**, doi:10.1007/BF02531827.

[210] Sharma, Y.C. and Singh, B., "An ideal feedstock, kusum (Schleichera triguga) for preparation of biodiesel: Optimization of parameters," Fuel 89(7):1470–1474, 2010, doi:10.1016/j.fuel.2009.10.013.

[211] Balat, M. and Balat, H., "A critical review of bio-diesel as a vehicular fuel," Energy Convers. Manag. 49(10):2727–2741, **2008**, doi:10.1016/j.enconman.2008.03.016.

[212] Alleman, Teresa L., McCormick, Robert L., Christensen, Earl D., Fioroni, Gina, Moriarty, Kristi, and Yanowitz, Janet. Tue. "Biodiesel Handling and Use Guide, **2016** (Fifth Edition)". United States. https://www.osti.gov/servlets/purl/1347103.

[213] Choudhary, R., Khurana, D., Kumar, A., and Subudhi, S., "Stability analysis of Al2O3/water nanofluids," J. Exp. Nanosci. 12(1):140–151, **2017**, doi:10.1080/17458080.2017.1285445.

[214] Isac-García, J., Dobado, J.A., Calvo-Flores, F.G., and Martínez-García, H., "Determining Physical and Spectroscopic Properties," Exp. Org. Chem. 145–175, **2016**, doi:10.1016/b978-0-12-803893-2.50005-x.

[215] Aleme, H.G. and Barbeira, P.J.S., "Determination of flash point and cetane index in diesel using distillation curves and multivariate calibration," Fuel 102:129–134, **2012**, doi:10.1016/j.fuel.2012.06.015.

[216] R. Kriger G. Borman The Computation of Applied Heat Release for Internal Combustion Engines ASME Paper **1966** 66-WA/DGP-4.

[217] Ying, W., Li, H., Jie, Z., and Longbao, Z., "Study of HCCI-DI combustion and emissions in a DME engine," Fuel 88(11):2255–2261, **2009**, doi:10.1016/j.fuel.2009.05.008.

[218] Yusri, I.M., Abdul Majeed, A.P.P., Mamat, R., Ghazali, M.F., Awad, O.I., and Azmi, W.H., "A review on the application of response surface method and artificial neural network in engine performance and exhaust emissions characteristics in alternative fuel," Renew. Sustain. Energy Rev. 90(March):665–686, 2018, doi:10.1016/j.rser.2018.03.095.

[219] Pinzi, S., Redel-Macías, M.D., Leiva-Candia, D.E., Soriano, J.A., and Dorado, M.P., "Influence of ethanol/diesel fuel and propanol/diesel fuel blends over exhaust and noise emissions," Energy Procedia 142:849–854, **2017**, doi:10.1016/j.egypro.2017.12.136.

[220] Silitonga, A.S., Masjuki, H.H., Mahlia, T.M.I., Ong, H.C., Chong, W.T., and Boosroh, M.H., "Overview properties of biodiesel diesel blends from edible and non-edible feedstock," Renew. Sustain. Energy Rev. 22:346–360, **2013**, doi:10.1016/j.rser.2013.01.055.

[221] Sadhik Basha, J. and Anand, R.B., "Effects of nanoparticle additive in the water-diesel emulsion fuel on the performance, emission and combustion characteristics of a diesel engine," Int. J. Veh. Des. 59(2–3):164–181, **2012**, doi:10.1504/IJVD.2012.048692.

[222] Tomar, M. and Kumar, N., "Influence of nanoadditives on the performance and emission characteristics of a CI engine fuelled with diesel, biodiesel, and blends–a review," Energy Sources, Part A Recover. Util. Environ. Eff. 42(23):2944–2961, **2019**, doi:10.1080/15567036.2019.1623347.

[223] Dabelstein, W., Reglitzky, A., Schütze, A., and Reders, K., "Automotive Fuels," Ullmann's Encyclopedia of Industrial Chemistry, American Cancer Society, ISBN 9783527306732, **2007**, doi:10.1002/14356007.a16_719.pub2.

[224] Soriano, N.U. and Narani, A., "Evaluation of biodiesel derived from camelina sativa oil," JAOCS, J. Am. Oil Chem. Soc. 89(5):917–923, **2012**, doi:10.1007/s11746-011-1970-1.

[225] Zhen, Z., Jing, G., Sun, Z., and Zheng, C., "Nano-composite pour point depressants in improving the rheology of waxy crude oil," Pet. Sci. Technol. 36(17):1325–1331, **2018**, doi:10.1080/10916466.2018.1479421.

[226] Shams, Z. and Moghiman, M., "Effect of metal oxide nanoparticles on the ignition characteristics of diesel fuel droplets: an experimental study," J. Brazilian Soc. Mech. Sci. Eng. 40(2):1–10, **2018**, doi:10.1007/s40430-018-1010-2.

[227] Arifin, Y.M. and Arai, M., "The effect of hot surface temperature on diesel fuel deposit formation," Fuel 89(5):934–942, **2010**, doi:10.1016/j.fuel.2009.07.014.

[228] Tanvir, S. and Qiao, L., "Surface tension of nanofluid-type fuels containing suspended nanomaterials," West. States Sect. Combust. Inst. Spring Tech. Meet. **2012** 551–573, 2012.

[229] Nautiyal, P., Subramanian, K.A., Dastidar, M.G., and Kumar, A., "Experimental assessment of performance, combustion and emissions of a compression ignition engine fuelled with Spirulina platensis biodiesel," Energy 193:116861, **2020**, doi:10.1016/j.energy.2019.116861.

[230] Pischinger, F., Lepperhoff, G., and Houben, M., "Soot Formation and Oxidation in Diesel Engines," in: Bockhorn, H., ed., Soot Formation in Combustion: Mechanisms and Models, Springer Berlin Heidelberg, Berlin, Heidelberg, ISBN 978-3-642-85167-4: 382–395, **1994**, doi:10.1007/978-3-642-85167-4_22.

Some studies on nano-particles doped alternative fuels in Unmodified CI Engine

DYNAMOMETER TECHNICAL SPECIFICATIONS

DESCRIPTION	DATA
Make	Benz Systems, Pune, India
Model	ECB-70
Type	Eddy Current Dynamometer
Maximum Power	70PS @ 5000RPM
Maximum Torque	95Nm @ 5000 RPM
W(PAN) MAX	30Kg
W(IND)	W(PAN)Å~5
DYN.CONST	7026
BHP	W(IND)Å~RPM/DYN.CONST
Excitation coil Voltage	0 - 6 0 V D C @ 5A
Rotation	Bi-directional
Cooling	Water cooled
Water flow requirement	25 LPM @ 0.5 Kgcm^2
Dynamometer Controller	
Input	230VAC
Output	0-60VDC @5A
Adjustment	60VDC Adjustment is done by Autotransformer
Control	Open loop Control
Load Cell with Indicator	
Capacity	10kg, Precision grade, Universal type
Accuracy	± 0.1% fsd
Output	2.0mV/V
Temperature drift	0.005 % /0C of fsd
Excitation Voltage	5/10V
Display	3.5 digit 7 segment LED display

AVL DITEST 1000 GAS ANALYZER TECHNICAL SPECIFICATIONS

DESCRIPTION	DATA
Make	AVL
Model	AVL DITEST MDS 205 (Modular Diagnostic system)
Weight	2.2 Kg
Dimensions	344 x 252 x 85 (W x H x D)
Humidity	10-90 % non-condensing
Warm-up Time	Approx. 2 min
Operating Temperature	5- 40 °C
Storage Temperature	0-50°C
Interfaces	USB, Bluetooth Class 1, RS 232 (AK Protokoll)
Voltage Supply	11-25 V DC
Power Consumption	Approx. 20 VA
Measured Gas	CO, CO_2, HC, NO, O_2
Measurement Ranges CO CO_2 HC NO_x O_2	0-15% vol. 0-20% vol. 0–30000 ppm 0-5000 ppm 0-25% vol.
Accuracy CO CO_2 HC NO_x O_2	$\pm$ 0.01% $\pm$ 0.2% $\pm$ 10 ppm $\pm$ 50 ppm $\pm$ 1%
Resolution CO CO_2 HC NO_x O_2	0.01 % vol. 0.1 % vol. 1 ppm 1 ppm 0.01% vol.

AVL DISMOKE 480 BT SMOKE METER TECHNICAL SPECIFICATIONS

DESCRIPTION	DATA
Make	**AVL**
Model	AVL DITEST MDS 205 (Modular Diagnostic system)
Weight	3.2 Kg
Dimensions	395 x 285 x 136 (W x H x D)
Humidity	max. < 90 %, non-condensing
Interfaces	RS232; Bluetooth Class1
Power Consumption	approx. 78 VA (incl. heating)
Chamber Heating	100°C
Measuring principle	Light Extinction Measurement
Light source	Halogen bulb 12 V / 5W
Detector	Selenium Photocell, dia 45mm
Range	0-99%
Accuracy	0.1%
Max. Emission Temperature	200 °C
Measurement Length	215 mm ± 2 mm

OPTIMIZATION DATA
NON-DIMENSIONLESS SECOND ORDER POLYNOMIAL EQUATIONS

Response	Equation
BTE (%)	= 11.191 + 0.1298 [Nanoparticle concentration(ppm)] + 6.889 [BMEP (bar)] - 0.000932[Nanoparticle concentration(ppm)] * [Nanoparticle concentration(ppm)]- 0.7459 [BMEP (bar)] * [BMEP (bar)] + 0.00169 [Nanoparticle concentration(ppm)] * [BMEP (bar)]
BSEC (MJ/kWh)	= 28.125 - 0.1119 [Nanoparticle concentration(ppm)] -7.798 [BMEP (bar)] + 0.000765 [Nanoparticle concentration(ppm)] * [Nanoparticle concentration(ppm)] + 1.1043 [BMEP (bar)] * [BMEP (bar)] + 0.00030 [Nanoparticle concentration(ppm)] * [BMEP (bar)]
CO (g/kWh)	= 19.676 - 0.1019 [Nanoparticle concentration(ppm)] - 8.223 [BMEP (bar)] + 0.000761 [Nanoparticle concentration(ppm)] * [Nanoparticle concentration(ppm)] + 1.2667 [BMEP (bar)] * [BMEP (bar)] - 0.00192 [Nanoparticle concentration(ppm)] * [BMEP (bar)]
UBHC (g/kWh)	= 1.021 - 0.00704 [Nanoparticle concentration(ppm) - 0.3400 [BMEP (bar)] + 0.000043 [Nanoparticle concentration(ppm)] * [Nanoparticle concentration(ppm)] + 0.04540 [BMEP (bar)] * [BMEP (bar)] + 0.000779 [Nanoparticle concentration(ppm)] * [BMEP (bar)]
NO_x (g/kWh)	= 21.7942 - 0.05546 [Nanoparticle concentration(ppm) - 3.5237 [BMEP (bar)] + 0.000070 [Nanoparticle concentration(ppm)] * [Nanoparticle concentration(ppm)] + 0.27900 [BMEP (bar)] * [BMEP (bar)] + 0.006171 [Nanoparticle concentration(ppm)] * [BMEP (bar)]
Smoke opacity (%)	= 12.283 - 0.2615 [Nanoparticle concentration(ppm)] - 2.514 [BMEP (bar)] + 0.001815 [Nanoparticle concentration(ppm)] * [Nanoparticle concentration(ppm) + 3.3282 [BMEP (bar)] * [BMEP (bar)] - 0.00195 [Nanoparticle concentration(ppm)] * [BMEP (bar)]

LIST OF PUBLICATIONS

International Journals

1. **Mukul Tomar** and Naveen Kumar "Effects of multi-walled carbon nanotubes and alumina nano-additives in a light duty diesel engine fuelled with *schleichera oleosa* biodiesel blends", ***Sustainable Energy Technologies and Assessment***, **2020** (DOI: 10.1016/j.seta.2020.100833).
2. **Mukul Tomar** and Naveen Kumar "Influence of nanoadditives on the performance and emission characteristics of a CI engine fuelled with diesel, biodiesel, and blends—a review", ***Energy Source Part A: Recovery, Utilization and Environmental Effects***, **2019** (DOI: 10.1080/15567036.2019.1623347).
3. Naveen Kumar and **Mukul Tomar** "Influence of nanoadditives on Ignition characteristics of Kusum (*Schleichera oleosa*) biodiesel", ***International Journal of Energy Research*, 2019** (DOI: 10.1002/er.4446).

International Conferences

1. **Mukul Tomar** and Naveen Kumar **"**Impact of doping alumina nanoparticles on spray characteristics of diesel-biodiesel fuel blends", ***IOP Conference Series: Materials Science and Engineering*** 804 (1), 012007.
2. **Mukul Tomar** and Naveen Kumar **"**Hot-plate ignition probability test of nanoparticles blended waste cooking oil biodiesel", ***8th International Symposium on the fusion Science & Technologies (ISFT2020)***, ISBN No. 978-93-5396-516-7.

A Brief Biographical Sketch

Mukul Tomar was born on 30 April 1993 in Baraut, Uttar Pradesh, India. He did his B.Tech in Mechanical Engineering from Graphic Era Hill University Dehradun in the year 2015; M.Tech with major in Thermal Engineering from Gautam Buddha University, Gautam Buddh Nagar (U.P), India in the year 2017. He later joined the Delhi Technological University as a Ph.D. Scholar in the Centre for Advanced Studies and Research in Automotive Engineering at Mechanical Engineering Department.

Mr. Mukul is conducting research in alternative fuels with special emphasis on cleaner combustion techniques. His Ph.D. work is focused on state-of-the-art fuel reformulation technique, which aims to utilize the exclusive properties of nanoparticles as a fuel-borne additive for diesel, biodiesel and their blends. His research interests also include waste/biomass valorization, heat transfer and flow characterization. The wider goal of his research is to improve the sustainability of emerging alternative fuels. He has published thirteen scientific research papers in Scopus/SCI-indexed journals and conferences of repute. Besides, he has written two collaborative book chapters for well-known publishers such as Springer and Taylor & Francis. He also serves as a reviewer for many journals published by SAE, Taylor & Francis, Wiley, etc.

During his stay in Ph.D., Mr. Mukul earned good overseas exposure as well. In the year 2018, he got the opportunity to attend SAE World Congress & ASME (IMECE) 2018, held in the USA where he presented his research findings and interacted with fellow researchers, attendees and experts from similar areas across the world. In recognition of his excellent research contribution, he has also been awarded the DTU Research Excellence award for executing commendable research work in the year 2019 and 2020.

Aside from academics he also acquired good leadership and management skills. He was the chief organizer of the 8th International Symposium on the fusion Science & Technologies (ISFT2020) held in JCBUST, YMCA, Faridabad, India from January 6-10, 2020 and New Frontiers in Engineering, Science and Technology (NFEST-2018) held in New Delhi, India from January 8-12, 2018.

Curriculum Vitae

Personal Details:

Surname, First name:	Tomar, Mukul
Father's name:	Surendra Singh Tomar
Mother's name:	Bimlesh Tomar
Nationality	Indian
Date of Birth	30th April 1993
Languages known:	English & Hindi
Permanent Address:	20/339, Subhash Nagar Gali no. 3, Baraut, Dist. Baghpat (U.P), 250611, India
Contact No.:	+91-9808453137
Email Id:	mukultomar007@gmail.com
Research Gate:	www.researchgate.net/profile/Mukul_Tomar

Education:

Degree	Specialization/ Major	Year	Board/University	Marks percentage/CGPA
Ph.D.	Mechanical Engineering	2017- 2021	Delhi Technological University, Delhi	NA
M.Tech	Thermal Engineering	2015-2017	Gautam Buddha University, Gautam Buddh Nagar	8.17
B.Tech	Mechanical Engineering	2011-2015	Graphic Era Hill University, Dehradun	7.8

Research Focusses/Title of Dissertation:

- Biodiesel: Production, characterization & Utilization, IC engine combustion & emission control, Biomass valorization, fuel-reformulation techniques, Thermo-fluids Heat transfer.
- Some studies on nano-particles doped alternative fuels in Unmodified CI engine

Academic Projects:

- Testing of biogas as a potential biofuel on a single cylinder, 2-stroke, 98cc Spark Ignition engine.
- Designing and development of a prototype of "An automated convertible all weather two-wheeler vehicle" as a final year project in undergraduate studies.
- Numerical investigation of Unsteady state natural convection in a square enclosure using ANSYS Fluent.
- Designing and development of a Hot plate Ignition probability test rig model to investigate the ignition properties of different alternative/conventional fuel samples.

Publications:

International Journals:

1. A. Sonthalia, N. Kumar, **M. Tomar**, V.E. Geo, S.Thiyagarajan and A. Pugazhendhi, "Moving ahead from Hydrogen to Methanol Economy: Scope and challenges", ***Clean Technologies and Environmental Policy,*** 2021 (Accepted), <u>doi: 10.21203/rs.3.rs-280230/v1.</u>

2. **M. Tomar** and N. Kumar, "Effects of multi-walled carbon nanotubes and alumina nano-additives in a light duty diesel engine fuelled with *schleichera oleosa* biodiesel blends", ***Sustainable Energy Technologies and Assessment***, 42, 100833; 2020, <u>doi: 10.1016/j.seta.2020.100833.</u>

3. N. Kumar, A. Sonthalia, **M. Tomar** and R. Koul, "An Experimental Investigation on Spray, Performance and Emission of Hydrotreated Waste Cooking Blends in an Agricultural Engine", ***Int. J. of Engine Research***, 2020, <u>doi: 10.1177/1468087420928734.</u>

4. **M. Tomar,** A. Sonthalia, N. Kumar and H. Dewal, "Waste glycerol derived bio-propanol as a potential extender fuel for compressed ignition engine", ***Environmental Progress and Sustainable Energy***, 40 (2); 2020, <u>doi: 10.1002/ep.13526.</u>

5. **M. Tomar**, H. Dewal, A. Sonthalia and N. Kumar, "Optimization of SI Engine characteristics fuelled with oxygenated bio-additive (Triacetin) using Response Surface Methodology", ***Proc. Of IMechE, Part E: J. of Process Mechanical Engineering,*** 2020, <u>doi: 10.1177/0954408920971110.</u>

6. **M. Tomar,** A. Jain, P.C. Pujari, H. Dewal and N. Kumar, "Potentials of waste plastic pyrolysis oil as an extender fuel for diesel engine", ***Arabian J. Geoscience,*** 13 (504); 2020, <u>doi: 10.1007/s12517-020-05574-6.</u>

7. **M. Tomar** and N. Kumar, "Influence of nanoadditives on the performance and emission characteristics of a CI engine fuelled with diesel, biodiesel, and blends—a review", ***Energy Source Part A: Recovery, Utilization and Environmental Effects***, 42(23); 2019, <u>doi: 10.1080/15567036.2019.1623347.</u>

8. N. Kumar and **M. Tomar**, "Influence of nanoadditves on Ignition characteristics of Kusum (*Schleichera oleosa*) biodiesel", ***Int. J. of Energy Research***, 43 (8); 2019, <u>doi: 10.1002/er.4446.</u>

Peer Reviewed International Conferences:

1. **M. Tomar**, M. Choudhary and D. Jain "Performance analysis and economic feasibility of fuel cell vehicles: A perspective review", ***SAE Powertrain, Fuels & Lubricants Meetings 2020***, <u>doi: 10.4271/2020-01-2256.</u>

2. A. Malhotra, M. Yadav, **M. Tomar**, Shikhar Jain and Naveen Kumar "Effect of Using Exhaust Gas Recirculation (EGR) on The Emission Characteristics of the CI Engine Fuelled by Acetone-Butanol-Ethanol (ABE) Diesel Blends", ***SAE World Congress 2019***, <u>doi: 10.4271/2019-01-0748.</u>

3. N. Kumar, S. Jain, A. Bagla, S. Sharma and **M. Tomar** "Study of performance and emission characteristics of 2-propanol and gasoline fuel blends in unmodified spark ignition engine", *SAE World Congress 2019*, doi: 10.4271/2019-01-0793.

4. S. Mishra, **M. Tomar**, A. Ahmad, S. Jain and N. Kumar "Numerical Study of Forced Convection in Different Fluids from Stationary Heated Cylinders in a Square Enclosure", *The American Society of Mechanical Engineers Volume 8A: Heat Transfer and Thermal Engineering,* **2018**, doi: 10.1115/IMECE2018-87032.

5. **M. Tomar**, N. Kumar, A. Malhotra "Transient analysis of natural convection around a pair of circular cylinders inside a square enclosure", *SAE World Congress 2018*, doi: 10.4271/2018-01-0776

Book Chapters:

1. N. Kumar, **M. Tomar**, A. Sonthalia, Sidharth, P. Kumar, H.S. Pali and D. Mishra "**Methanol-Based Economy: A Way Forward to Hydrogen**", **Sustainable Development for Energy, Power, and Propulsion**, Green Energy and Technology. *Springer*, Singapore, **2020** (DOI: 10.1007/978-981-15-5667-8_23)

2. **M. Tomar**, H. Dewal, L. Kumar, N. Kumar, and N. Bharadvaja, "*Biodiesel Additives: Status and Perspectives*", Handbook of Biodiesel and Petrodiesel Fuels: Science, Technology, Health, and Environment Volume 1. *CRC Press, Taylor & Francis, 2021* (ISBN 9780367456146).

Reviewer:

- Energy Source Part A: Recovery, Utilization and Environmental Effects (Taylor & Francis)
- Environmental Progress and Sustainable Energy (Wiley)
- SAE International
- Journal of Mechanical Engineering and Sciences
- Groundwater for Sustainable Development (Elsevier)

International Conferences Attended/Organized

- **Chief Organizer, 8th International Symposium on the fusion Science & Technologies (ISFT2020)** held in JCBUST, YMCA, Faridabad, India from January 6-10, **2020**. 20 Keynote Speakers and more than 500 delegates from 20 countries across 5 continents will attended the conference.

- **Chief Organizer,** International Conference on **New Frontiers in Engineering, Science and Technology (NFEST-2018)** held in New Delhi, India from January 8-12, **2018**. 21 Keynote Speakers and more than 500 delegates from 22 countries across 6 continents attended the conference.

- **Presented/Attended, International Mechanical Engineering Congress & Exposition (IMECE2018)** hosted by The American Society of Mechanical Engineers, held in Pittsburgh, PA, USA from November 9-15, **2018**.
- **Presented/Attended, SAE World Congress and Exhibition 2018** hosted by Society of Automotive Engineers, held in Detroit, Michigan, USA from April 9-12, **2018**.
- **Presented/Attended, 7th International Symposium on the fusion Science & Technologies (ISFT2018)** held in Thailand, Bangkok from December 16-20, **2018**.
- **Attended, International Workshop on Sustainable Energy, Power and Propulsion (ISEPP2018)** held in NIT Kurukshetra from March 18-22, **2018**.

Technical Skills

- Experience of product design via. Solid Edge, Solid Works, Pro-E and CATIA softwares.
- Good hands on optimization softwares such as Minitab, Design Experts, DWSIM and MATLAB.
- Well conversant with simulation software including ANSYS (Fluent), Diesel-RK, GT-Power & Converge.
- Basic Knowledge of C, C++, Blue java.
- Experience in operating analytical instruments such as GC/MS, TGA, FTIR, XRD, FESEM, Flame Spray Pyrolysis System, AVL DITEST MDS 205, KiBoX Kistler Combustion. Analyzer.

Awards/Funding

- Received Delhi Technological University (DTU), Teaching and Research Fellowship, awarded by DTU for pursuing full-time Ph.D.
- Received DTU funding for attending SAE World Congress 2018 held in Detroit, Michigan, USA.
- Awarded the DTU Research Excellence Award for commendable Research in the academic year 2018-19, 2019-20.

References

- Dr. Naveen Kumar,
  Professor,
  Mechanical Eng. Dept,
  Delhi Technological University, India
  naveenkumardce@gmail.com

- Dr. Harishchandra Thakur,
  Assistant Professor,
  School of Engineering,
  Gautam Buddha University, India
  harish@gbu.ac.in

I hereby declare that the information furnished above is true to the best of my knowledge and belief.

Place: Delhi   (Mukul Tomar)